The Phanerozoic $\delta^{88/86}Sr$ Record of Marine Carbonates

Implications for Seawater Chemistry

Dissertation

Zur Erlangung des Doktorgrades

Dr. rer. nat.

Der Mathematisch-Naturwissenschaftlichen Fakultät

der Christian-Albrechts-Universität zu Kiel

vorgelegt von

Hauke Vollstaedt

Kiel, 2012

Referent:	Prof. Dr. Anton Eisenhauer
Korreferent:	Prof. Dr. Klaus Wallmann
Tag der mündlichen Prüfung:	29.10.2012

Zum Druck genehmigt:

Der Dekan

Hiermit erkläre ich, dass ich die vorliegende Doktorarbeit selbstständig und ohne Zuhilfenahme unerlaubter Hilfsmittel erstellt habe. Weder diese noch eine ähnliche Arbeit wurde an einer anderen Abteilung oder Hochschule im Rahmen eines Prüfungsverfahrens vorgelegt, veröffentlicht oder zur Veröffentlichung vorgelegt. Ferner versichere ich, dass die Arbeit unter Einhaltung der Regeln guter wissenschaftlicher Praxis der Deutschen Forschungsgemeinschaft entstanden ist.

Kiel, den

Hauke Vollstaedt

Abstract

In the light of increasing interest in the role of the world's oceans in future global change, it is important to understand the underlying processes that were responsible for paleoceanographic changes in the geological past. Previous studies working on the geochemistry of ancient marine deposits agree that the seawater chemistry must have been changed throughout the Phanerozoic Eon. In particular, concurrent long-term changes in radiogenic and stable isotope systems, element ratios and concentrations and their correlation with sea-level changes, climate reconstructions, and global mass extinctions suggests common causative mechanisms. However, the geological processes being responsible for the observed changes are still being debated. Specifically, the role of mid ocean spreading rates, dolomitization and sea-level changes are thought to play a major role in paleo-seawater chemistry of major and trace elements. Within this study the first Phanerozoic stable strontium (Sr) isotope seawater record ($\delta^{88/86}Sr_{sw}$) is reconstructed, which is sensitive to imbalances in the Sr input and output fluxes. In a consequent model approach, the radiogenic Sr isotope record ($^{87}Sr/^{86}Sr)_{sw}$ and $\delta^{88/86}Sr_{sw}$ are used to constrain the marine Phanerozoic Sr budget. On long timescales (~200Myr periodicity), $\delta^{88/86}Sr_{sw}$ and modelled Sr carbonate burial rates $(F(Sr)_{carb})$ follow times of proposed „aragonite seas" and „calcite seas", implying that the dominant carbonate mineralogy has an important effect on Sr burial rates. On shorter timescales, minima and maxima in $F(Sr)_{carb}$ are partly correlated to ocean anoxia and glaciations and related sea-level low stands, implying the importance of continental carbonate shelf weathering to the marine Sr budget. In particular, enduring high carbonate burial rates for ~21Myr could be related to seawater anoxia during the end-Permian mass extinctions. Here, bacterial sulphate reduction rates led to toxic and high alkaline deep waters that were intermittently upwelled to the surface ocean, causing massive carbonate precipitation on the seafloor as well as the largest biogeochemical crisis in the Phanerozoic

Eon. Ultimately, insights from changes in $\delta^{88/86}Sr_{sw}$ significantly improved our understanding of long-term changes in seawater chemistry and the relation of carbonate-related Sr fluxes to sea-level changes, mass extinctions, and global anoxia.

Kurzzusammenfassung

In Anbetracht des zunehmenden Interesses an der Rolle der Weltmeere im zukünftigen globalen Wandel, ist es wichtig die zugrunde liegenden Prozesse für die paläozeanographischen Veränderungen der geologischen Vergangenheit zu verstehen. Die bisherigen geochemischen Arbeiten an alten marinen Ablagerungen stimmen dabei überein, dass sich die Meerwasserchemie im Phanerozoikum geändert haben muss. Insbesondere die langfristigen Veränderungen in radiogenen und stabilen Isotopensystemen, Element-verhältnissen und –konzentrationen, sowie deren Korrelation mit Meeresspiegeländerungen, Klimarekonstruktionen und globalen Massenaussterbeereignissen weisen auf gemeinsame kausale Mechanismen hin. Allerdings sind die dafür verantwortlichen geologischen Prozesse noch in der Diskussion. Insbesondere die Prozesse der Ozeankrustenproduktion an mittelozeanischen Rücken, der Dolomitisierung und Meeresspiegeländerungen werden in Betracht gezogen, eine wichtige Rolle in der Paläo-Meerwasserchemie der Haupt- und Spurenelementen zu spielen. Im Rahmen dieser Studie wurde der erste phanerozoische stabile Strontium (Sr)-Isotopen Datensatz des Meerwassers ($\delta^{88/86}Sr_{sw}$) erstellt, welcher empfindlich auf Ungleichgewichte zwischen den Sr Quellen und Senken reagiert. In einem darauf folgenden Modell-Ansatz wurden die radiogenen ($^{87}Sr/^{86}Sr$) und stabilen ($\delta^{88/86}Sr_{sw}$) Daten verwendet, um das marine phanerozoische Sr Budget zu bilanzieren. Auf langen Zeitskalen (~ 200Mio. Jahre Periodizität) folgen $\delta^{88/86}Sr_{sw}$ und die modellierten Sr Sedimentationsflüsse ($F(Sr)_{carb}$) den Perioden von „Aragonit Meeren“ und „Calcit Meeren“, was bedeutet, dass die dominante Karbonatmineralogie einen wichtigen Einfluss auf die Sr Sedimentation hat. Auf kürzeren Zeitskalen sind Minima und Maxima in $F(Sr)_{carb}$ teilweise mit marinen Anoxien sowie Vereisungen und den damit verbundenen Meeresspiegeländerungen korreliert, welches die Bedeutung der kontinentalen Karbonatschelfverwitterung für das Sr Budget anzeigt. Insbesondere die ~21Mio. Jahre

anhaltendenden hohen Karbonatsedimentationsraten am Ende des Perms konnten zur Meerwasseranoxie während der Massenaussterbens in Bezug gesetzt werden. Hier führte die bakterielle Sulfatreduktion zu giftigen und stark alkalischen Tiefengewässern, die zeitweise zur Meeresoberfläche aufgetrieben wurden, was zu einer massiven Karbonatausfällung auf dem Meeresboden, sowie zur bisher größten biogeochemischen Krise im Phanerozoikum geführt hat. Letztendlich haben die Erkenntnisse aus den Veränderungen im $\delta^{88/86}Sr_{sw}$ unser Verständnis von langfristigen Veränderungen in der Meerwasserchemie, sowie den Zusammenhang zwischen marine Karbonatflüssen zu Meeresspiegeländerungen, Massenaussterben und globaler Anoxie, deutlich verbessert.

Acknowledgements

First of all, I would like to thank my supervisor Prof. Dr. Anton Eisenhauer for giving me the opportunity to carry out this PhD thesis and for giving me the best support I could imagine. I always profited from the ideas you brought into our discussions. I also appreciate that you gave me the greatest trust and space to develop my own ideas.

Further, I would like to thank my second supervisor Prof. Dr. Klaus Wallmann for continuative support and discussions on numerical modelling and marine biogeochemical cycles. I really profited from your competence to abstract complex processes.

Special thanks go out to Jan, Volker, Florian, and André! I benefited a lot from our joint discussions and your support during lab work! I also really appreciate that your door was always open for me to discuss every concern or problem I had!

I also would like to express my gratefulness to Prof. Dr. Ján Veizer, Juraj, and Chris for their support and fruitful discussions, especially on scientific meetings!

I would like to thank all the people who accompanied me during my studies and PhD thesis. In particular, my friends and Wulfsbrook flat mates Jan and Jacek, my close friend from Göttingen Magdalena, the other working group members including Agnes, the "good soul" Ana, Isabelle, Noa, Nico, Nico, Rashid, and Steffi, my colleagues and friends at GEOMAR including Andres, Wolf-Christian Dullo, Christine, Claudia, Clauschi, David, David, Dirk, Ed, Florian, Folkmar, Janett, Joana, Julia, Kristin, Lorenzo, Mark, Martin, Moritz, Nabil, Patricia, Roland, Sascha, my meeting companion Stefan, Stefan, Steffi, Sven, Thor, Torben, and the "Real Granit" football team are thanked for support and a great time!

My close friends Daniel, Moritz, Lars, Freddy, Mareike, Jannes, Agnes, Karin, Marcel, Seb, Mareike, Fabi, and Fredi are thanked for their support and many sights to behold!

Finally, I would like to thank my family and Mareike for their love, support, and being there for me! Without them this work would never have been realized!

Contents

List of Figures

VI. Chapter

List of Tables

List of Abbreviations

$(^{87}Sr/^{86}Sr)_{sw}$	Radiogenic Strontium Isotope Composition of Seawater
$(Sr/Ca)_{sw}$	Strontium to Calcium Ratio of Seawater
$[Ca]_{sw}$	Calcium Concentration in Seawater
$[Sr]_{sw}$	Strontium Concentration in Seawater
ACC	Amorphous Calcium Carbonate
BSR	Bacterial Sulfate Reduction
CC	Calcium Sarbonate
COC	Center of Calcification
CTD	Conductivity, Temperature, Depth
$D(F)_{Sr}$	Sr and Ca carbonate-related Output Flux Ratio Relative to $(Sr/Ca)_{sw}$
DS	Double Spike
D_{Sr}	Sr/Ca Partition Coefficient
$F(Sr)_{alt}$	Sr Output Flux into the Altered Oceanic Crust
$F(Sr)_{carb}$	Carbonate-related Sr flux
$F(Sr)_{hyd(in)}$	Sr Input Flux from Hydrothermal Fluids
$F(Sr)_{wc}$	Carbonate Weathering Sr Flux
$F(Sr)_{weath}$	Continental Weathering Sr Flux
$F(Sr)_{ws}$	Silicate Weathering Sr Flux
Fe-Mn	Ferromanganese
Gyr	Giga years (10^9 years)
GZG	Geowissenschaftliches Zentrum Göttingen
kyr	Kilo years (10^3 years)
Ma	Million years Before Present
MOR	Mid Ocean Ridge
Myr	Million years (10^6 years)
NIST	National Institute of Standards and Technology
OAE	Ocean Anoxic Event
ppm	Parts per million
RSD	Relative Standard Deviation
S	Salinity
SD or s.d.	Standard Deviation
SEM	Standard Error of the Mean
SIS	Strontium Isotope Stratigraphy
T	Temperature
TIMS	Thermo Ionization Mass Spectrometer
$\delta^{34}S_{CAS}$	Sulfur isotope composition of carbonate associated sulfates
$\delta^{44/40}Ca_{sw}$	Calcium isotope composition of seawater
$\delta^{88/86}Sr_{sw}$	Stable strontium isotope composition of seawater
$\Delta^{88/86}Sr_{sw\text{-}cc}$	Sr Fractionation Factor between Seawater and Calcium Carbonate

I. Chapter

Introduction to the Geologic History

of Phanerozoic Seawater

I.1. Motivation

The oceans play an important role in the functioning of the earth system, including the deposition of sediments derived from the continents, CO_2 exchange with the atmosphere, as well as carbon storage in marine carbonate deposits. The global ocean is supplied by elements transported by streams, wind, hydrothermal fluids, and glaciers which control the chemical composition of seawater.

The Phanerozoic is the current geological Eon and dates back to the beginning of the Cambrian period ~541Ma (Million years before present) where nearly all of the today's phyla evolved. The Phanerozoic derives its name from the Greek words "φανερός" and "ζωή" which could be translated as *visible life*. This is ascribed to the adaptive radiation of hard-shelled marine invertebrates, having a rigid skeleton composed of e.g. carbonate or silicate (STANLEY, 2001). The similarity in paleofaunal communitities and resembling mineralogical composition of sediments throughout the Phanerozoic led many authors to the conclusion that the seawater composition must have been relatively constant since ~541Ma (HOLLAND, 2010). However, with the investigation of several isotope and element proxies in marine carbonates as well as element concentrations in fluid inclusions, distinct changes in Phanerozoic seawater chemistry have been observed. These changes have been attributed to imbalances between the input and output fluxes of major and trace elements to the ocean. (e.g. (PETERMAN et al., 1970; BURKE et al., 1982; ZHU and MACDOUGALL, 1998; STOLL et al., 1999; VEIZER et al., 1999; DE LA ROCHA and DEPAOLO, 2000; LOWENSTEIN et al., 2001; HORITA et al., 2002; STEUBER and VEIZER, 2002; BRENNAN et al., 2004; KAMPSCHULTE and STRAUSS, 2004; FANTLE and DEPAOLO, 2005; LOWENSTEIN et al., 2005; FARKAŠ et al., 2007a; PROKOPH et al., 2008; PAYNE et al., 2010; RIES, 2010; MISRA and FROELICH, 2012)).

The main motivation for Phanerozoic research is to identify the causative mechanisms for these changing environmental conditions. In particular, their impact on life on earth and the coupling and feed back with other processes is of major scientific interest. These findings could then be transferred to the modern ocean and further to predict future environmental changes. For example, Ocean Anoxic Events (OAEs) and the highly productive carbonate burial under high atmospheric CO_2 concentrations in the Cretaceous period are taken as analogues to investigate modern oxygen minimum zones and ocean acidification, respectively. These fundamental questions are tried to be answered by defining changes in the occurrences of marine deposits, major element seawater concentrations, seawater isotopic composition, and their relationship to plate tectonics and biological evolution (HOLLAND, 2010; VEIZER and MACKENZIE, 2010).

This chapter aims to summarize the state of the art of research on Phanerozoic seawater chemistry. First, the main marine sedimentary archives and their relative proportions through Earth's history will be investigated (section I.2). Second, the most important results from studies working on isotopes, element concentrations and ratios, and model simulations will be presented (sections I.3 and I.4). Finally, the state of the art of Phanerozoic seawater research will be summarized followed by the outline of this study (sections I.5 and I.6).

I.2. Sedimentary archives

To investigate the geological history of seawater it is crucial to find sedimentary archives which record information about past marine environmental conditions. In particular, these archives have to resist diagenetic alteration caused by chemical reactions with pore waters and/or thermal alteration processes. Traditional archives to investigate paleo-seawater chemistry are marine carbonates and evaporites. Fluid inclusions trapped in marine halites were recently identified as additional archives for seawater chemistry reconstructions

(LOWENSTEIN et al., 2001; HORITA et al., 2002; BRENNAN et al., 2004; LOWENSTEIN et al., 2005). Further, marine barites and phosphates (conodonts or fish teeth enamel), ferromanganese crusts, cherts, hydrocarbons or biogenic silica were used as a recording phase of ancient seawater (e.g. (KNAUTH and EPSTEIN, 1976; KOLODNY and EPSTEIN, 1976; KARHU and EPSTEIN, 1986; PAYTAN et al., 1993; DIENER et al., 1996; EBNETH et al., 1997; ISOZAKI, 1997; WENZEL et al., 2000; FRANK, 2002; JOACHIMSKI et al., 2004; WALTHER and THORROLD, 2006; ANBAR and ROUXEL, 2007; GORJAN and KAIHO, 2007; GRIFFITH et al., 2008; TURCHYN et al., 2009; YOUNG et al., 2009; FANTLE, 2010; VEIZER and MACKENZIE, 2010; KOZUR and WEEMS, 2011; BOITEAU et al., 2012; DEBOND et al., 2012; HINOJOSA et al., 2012)). Within this section the most important sedimentary archives are summarized.

Marine carbonates

Marine carbonates are the most established archive to investigate time-dependent changes in seawater chemistry. Their advantage is their overall abundance in the modern oceans and their continuity in the geological record throughout the Phanerozoic. Further, marine carbonates contain abundant quantities of major and minor chemical and isotopic tracers (VEIZER and MACKENZIE, 2010). Marine carbonates can be subdivided into inorganically precipitated carbonates and biogenic skeletal carbonates. The relative proportions of these carbonate deposits in the geological record itself provide an important constraint to reconstruct changes in ocean chemistry throughout the Phanerozoic. For example, the amount of neritic and pelagic carbonates is related to plate tectonic activity which, in turn, modulates global sea level and extend of shelf areas (HOLLAND, 2010). Further, the occurrence of dolostones might be related to changes in sea-level (VEIZER and MACKENZIE, 2010). The Phanerozoic temporal trend in non-skeletal carbonate mineralogy brought (SANDBERG, 1983) to the classification of "calcite seas" and "aragonite seas" which were considered to be driven by plate-tectonically forces and their influence on atmospheric pCO_2

and $(Mg/Ca)_{sw}$ (see also section I.3.3 and 1.10) (SANDBERG, 1983; STEUBER and VEIZER, 2002; MORSE et al., 2007; VEIZER and MACKENZIE, 2010).

The main limitation of a carbonate recording phase is its variable degree of fidelity to retain the original seawater signal. Smalley et al. (1994) separated different carbonate archives into three types of reliability. Highly reliable archives are belemnites, non-luminescent brachiopods, well-preserved foraminifers from deep-sea sedimentary rocks, red algae, and rudist bivalves. Medium reliable archives are luminescent brachiopods, thick-shelled bivalves, and conodonts with low colour alteration index (relationship of conodont colour to diagenetic burial history (EPSTEIN et al., 1977)). Less reliable archives are conodonts with a high colour alteration index, thin-shelled bivalves, fish teeth, echinoids, ammonoids, foraminifers from deeply buried sandstones, and whole-rock limestone and chalk (SMALLEY et al., 1994). Therefore, studies on Paleozoic seawater chemistry mostly used brachiopod shells as they are highly reliable and furthermore one of the most abundant species in carbonate rocks. Studies on the Mesozoic seawater evolution used belemnites, foraminifera, bivalve rudists, brachiopods, but also calcium carbonate veins in Mid Ocean Ridge (MOR) basalts (e.g. (JONES et al., 1994; VEIZER et al., 1999; STEUBER and VEIZER, 2002; FARKAŠ et al., 2007a; COGGON et al., 2010; MISRA and FROELICH, 2012)). Similarly, this study used brachiopod samples for the Paleozoic and Early Mesozoic Eon which are complemented by Mesozoic belemnite samples. The temporal correlation of carbonates from different sites is based on biostratigraphy (biozones) or chemostratigraphy. These methods yield an uncertainty of ~1Myr for the Cenozoic and <~3Myr for the early Paleozoic as a result of the duration of biozones (See Fig. I.1 for an example) (VEIZER et al., 1999).

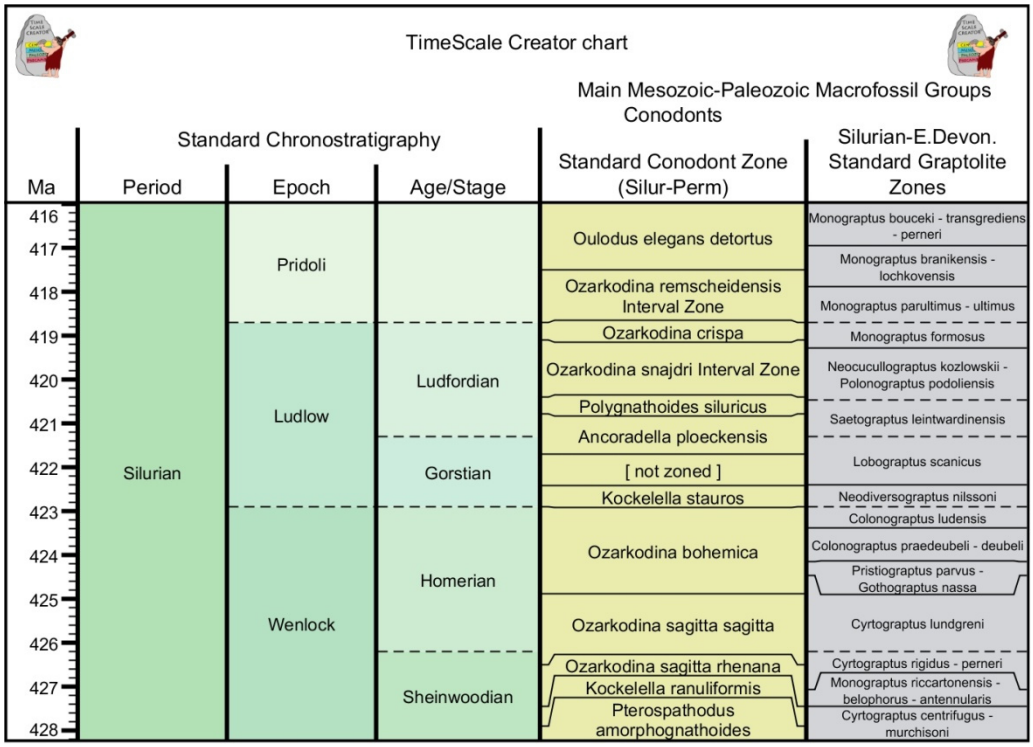

FIGURE I.1 – Stratigraphic chart for the upper Silurian period. Biostratigraphy is based on conodont and graptolite biozones. The uncertainty of this relative dating method depends on the duration of biozones, which is not more than 3Myr for the Early Paleozoic (source: Time Scale Creator Version 5.4, website: https://engineering.purdue.edu/Stratigraphy/tscreator/index/index.php).

Marine evaporites

Marine evaporites are chemical sediments that formed during the ongoing evaporation of seawater as a consequence of oversaturation with respect to specific evaporitic minerals. The least soluble minerals in a "seawater evaporation sequence" are carbonate minerals (calcite and dolomite) and sulphates (gypsum and anhydrite) and these represent the major part of evaporate sequences in the geological record. They are followed in the seawater evaporation sequence by halides and K-Mg-rich salts. The relative occurrence of evaporite deposits has been used to reconstruct the salinity of the Phanerozoic ocean, which is thought to have decreased from ~50‰ in the Early Paleozoic to modern values of ~35‰ (HAY et al., 2006). Changes in salinity were related to the radiation and extinction of marine organisms, e.g. to the end-Permian extinctions or the radiation of planktonic foraminifera and calcareous nannoplankton in the Early Mesozoic (HAY et al., 2006).

However, marine evaporites are also a carrier phase of important geochemical information. Several studies focussed on brine inclusions found in halite or carbonate cements to reconstruct changes in seawater major cations (Ca, K, Mg, SO_4, see section I.3.3). Fluid inclusions are considered as the most direct archive to investigate in past seawater chemistry as they represent brines from ancient seawater (LOWENSTEIN et al., 2001; HORITA et al., 2002; BRENNAN et al., 2004; LOWENSTEIN et al., 2005; HOLLAND, 2010). Further, marine evaporites are rich in sulphur which facilitates the analysis of sulphur isotopes (section I.2.3.2.). However, the episodic occurrence and uncertain chronology of evaporites possibly lead to the large spread in coeval sulphur isotopes (VEIZER and MACKENZIE, 2010) so that carbonate-associated sulphates provide an archive with a much higher temporal resolution and reliability (KAMPSCHULTE and STRAUSS, 2004).

Ferromanganese crusts

Ferromanganese (Fe-Mn) crusts grow directly from ambient seawater on a hard substrate at low local sedimentation rates. Under oxygenated conditions, these crusts can preserve their chemical signatures and thus may be used for paleoceanographic applications. Growth rates of Fe-Mn crusts vary in between 1 and 15mm Myr^{-1} resulting in a low temporal resolution. On the other hand, secular changes in the isotopic composition of trace metals in paleo-seawater can be assessed by investigating the continuous record of a single Fe-Mn crust. Another advantage is the high concentration of trace metals which is up to ten orders of magnitude with respect to seawater (FRANK, 2002). For many elemental and isotope systems like Neodymium (Nd), Beryllium (Be), Osmium (Os), Lead (Pb), Hafnium (Hf), and possibly also Magnesium (Mg), it has been shown that surfaces of Fe-Mn crusts record the isotope signal of the ambient seawater (FRANK, 2002; ROSE-KOGA and ALBARÈDE, 2010). The samples are usually dated by uranium series or depth profiles of the beryllium isotope ^{10}Be, which are restricted to 0.4Ma and 10Ma, respectively. Beyond this age, there are no other reliable dating

methods available (FRANK, 2002). Long-term records of particle-reactive metals like Nd, Pb, Hf, and Os are considered to be reliable, whereas less particle reactive elements like U and Sr are affected by post-depositional seawater exchange processes (FRANK, 2002).

I.3. Proxies for changes in Phanerozoic seawater chemistry

This section summarizes the main radiogenic and stable isotope systems and element proxies which have been investigated in the course of this study. In particular, this study measured stable and radiogenic strontium isotopes and the results are compared with osmium, carbon, oxygen, and sulphur isotopes. As a consequence of different ocean residence times, each isotope system allows the investigation of processes that occur on specific timescales. Hereby, it is focused on long-term changes of element and isotope systems to reconstruct changes in past seawater chemistry that occur on geological timescales.

Radiogenic isotope systems

Radiogenic isotope ratios vary due to the ingrowth of a daughter isotope by the radioactive decay of the parent isotope. For example, regarding the radiogenic isotope ratio $^{87}Sr/^{86}Sr$, the radiogenic isotope ^{87}Sr grows due to the radioactive decay of the parent isotope ^{87}Rb. Therefore, the $^{87}Sr/^{86}Sr$ ratio of Rb-bearing minerals (e.g. biotite, olivine, and pyroxene) depends on the initial Rb/Sr ratio and the age of the mineral. Incompatible elements with radioactive isotopes like Rb, K, U, Th, and Re are enriched within the Earth's crust compared to their daughter isotopes (FAURE and MENSING, 2005).

Radiogenic isotope ratios are used for geochronometry and for investigating mixing processes, e.g. for distinguishing types of sediments within a depositional basin or mixing of water masses in a stream or within the ocean (FAURE and MENSING, 2005).

The most radiogenic isotope ratios like Sr, Nd, Hf, and Os are normalized to a fixed stable isotope ratio of the respective element (when two stable isotopes exist) to correct for mass-dependent fractionation during the measurement. A consequence of this normalization is the neglect of isotope fractionation processes in the radiogenic isotope systematic. However, this makes seawater radiogenic isotope ratios a sensitive tracer for changes in the ratio of different input fluxes with distinct isotope signatures. On the other hand, seawater radiogenic isotope ratios cannot provide any information about the respective output fluxes in the ocean e.g. precipitation, evaporation, and/or uptake/release by organisms, as these processes do not discriminate the radiogenic isotopes. Within this chapter the most investigated Phanerozoic radiogenic isotope systems, strontium and osmium, are reviewed. Both isotope systems are used to constrain continental weathering rates in the past.

Strontium

The Rb/Sr ratios of common igneous rocks vary in the range between 0.06 (basalt) and 1.7 (granite), depending on the differentiation grade of the rock (FAURE and MENSING, 2005). This is a consequence of preferred Sr incorporation into plagioclase during fractional crystallization, leading to increased Rb/Sr ratios in highly evolved magmas. The half-life of ^{87}Rb is ~$5x10^{10}$ years, making the Rb-Sr method suitable for dating igneous, metamorphic, and sedimentary rocks and minerals (FAURE and MENSING, 2005).

In seawater, strontium is a trace element with a modern concentration of 7.74ppm (mg/kg seawater), a residence time of ~2.5Myr, and a radiogenic isotope composition of 0.709175 (HODELL et al., 1990; MCARTHUR, 1994; FAURE and MENSING, 2005). The marine budget of Sr is similar to that of Ca (see section I.3.2.4.) with its major sources coming from silicate and carbonate weathering and hydrothermal venting. The most important sink is the burial of marine carbonates and to a lesser extent the alteration of the oceanic crust (HART et al., 1974; KRABBENHÖFT et al., 2010). Secular variations in seawater $^{87}Sr/^{86}Sr$ are controlled by the

balance between Sr fluxes coming from continental weathering ($^{87}Sr/^{86}Sr_{weath}$ = 0.712) and hydrothermal fluids ($^{87}Sr/^{86}Sr_{hyd}$ = 0.7025) and their respective isotope compositions (SPOONER, 1976; PALMER and EDMOND, 1989; DAVIS et al., 2003). Nevertheless, the Sr isotopic composition of the modern continental rivers varies from 0.703 to 0.730, depending on the lithology of the catchment areas (VEIZER and MACKENZIE, 2010). The weathering of continental silicate rocks is the most important sink for atmospheric CO_2 and therefore one of the major processes that control climate on Earth on geological timescales (GAILLARDET et al., 1999). Therefore, seawater $^{87}Sr/^{86}Sr$ ratios are a powerful tool to obtain information about past dynamics of continental weathering and its effects on atmospheric pCO_2.

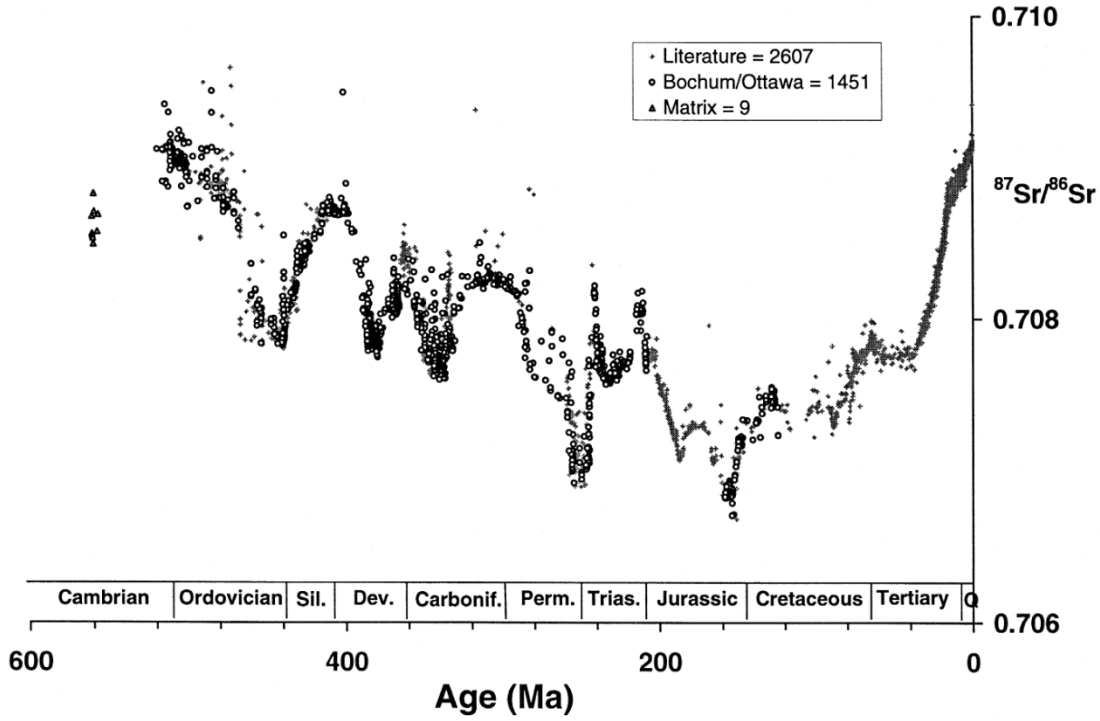

FIGURE I.2 – The Phanerozoic $^{87}Sr/^{86}Sr$ record of marine carbonates as compiled by (VEIZER et al., 1999). Geological periods and timescale from (HARLAND et al., 1990).

The trend in strontium isotopes during the last 4Gyr could be classified in three orders. The primary control on the seawater strontium isotope composition of the first order (billion years trend) will be exercised by the growth pattern of the continental crust (VEIZER and COMPSTON, 1976; VEIZER et al., 1983; VEIZER, 1989; VEIZER et al., 1989a; VEIZER et al., 1989b; VEIZER et al., 1990; VEIZER et al., 1992; MIROTA and VEIZER, 1994; HALL and VEIZER, 1996;

SHIELDS and VEIZER, 2002). A second order Phanerozoic decreasing trend from the Cambrian (~0.709) to the Jurassic period (~0.7065) is observed, which is followed by a subsequent increase to modern values (Fig. I.2, see Veizer et al. (1999)). Superimposed are third order cycles with a frequency of ~50Myr (PROKOPH et al., 2008). The observed $^{87}Sr/^{86}Sr$ oscillations must be caused by changes in the continental weathering flux and its isotopic composition because seafloor spreading rates are relatively sluggish and the strontium isotope ratio of the hydrothermal flux is relatively constant at ~0.7025 (ROWLEY, 2002; DAVIS et al., 2003; VEIZER and MACKENZIE, 2010). This record has been used to constrain continental weathering effects and its relationship to i) mass extinctions, ii) the diversification of organisms, iii) ocean anoxia, iv) plate tectonics, and v) strontium isotope stratigraphy (SIS) (DEPAOLO and INGRAM, 1985; ELDERFIELD, 1986; BERNER and CANFIELD, 1989; HODELL et al., 1989; BERNER, 1991; KRAMM and WEDEPOHL, 1991; EDMOND, 1992; BERNER, 1994; MCARTHUR, 1994; SMALLEY et al., 1994; DIENER et al., 1996; VEIZER et al., 1997; BERNER and KOTHAVALA, 2001; MCARTHUR et al., 2001; WALLMANN, 2001a; HANSEN and WALLMANN, 2003; KORTE et al., 2003; WALLMANN, 2004; FAURE and MENSING, 2005; HEUSER et al., 2005; ARVIDSON et al., 2006; BERNER, 2006; FARKAŠ et al., 2007a; AZMY et al., 2009; BERNER, 2009; SCHNEIDER et al., 2009; JENKYNS, 2010).

Specifically, SIS is a suitable method for indirect dating of marine carbonates especially when index fossils are lacking or their amount is too small. The precision of this method is limited to the age model reconstructed from biostratigraphy and is <0.15Myr - 2Myr in most cases (MCARTHUR, 1994; MCARTHUR et al., 2001). The stratigraphic resolution of SIS is limited by the slope of the $(^{87}Sr/^{86}Sr)_{sw}$ curve. Furthermore, $^{87}Sr/^{86}Sr$-ratios differ between distinct biozones leading to a global geological reproducibility not better than $5x10^{-5}$ (DIENER et al., 1996). Therefore the seawater Sr isotope curve can only be resolved as a band, due to the uncertainties in biostratigraphy, geochronology, and uncertainties in $^{87}Sr/^{86}Sr$ determinations due to preservation of sample material (VEIZER et al., 1997).

Osmium

Both Rhenium (Re) and Osmium (Os) are siderophile elements. The chemical properties of Re^{4+} are similar to that of Molybdenum (Mo^{4+}) resulting in high Re concentrations in Mo-bearing minerals. The radioactive isotope ^{187}Re decays to the stable isotope ^{187}Os with a halflife of ~$4x10^{10}$yr. Os is a member of the platinum (Pt) group (VIII, see figure 1-8) and thus found together with Pt group elements in iron-bearing minerals. Re/Os ratios vary globally between ~0.1 in ultramafic rocks and ~10 in granites (FAURE and MENSING, 2005). These differences are a consequence of the fractionation of Re and Os during the formation of the continental crust with high Re/Os ratios in highly evolved rocks (FAURE and MENSING, 2005). The Os isotopic composition of modern seawater ($(^{187}Os/^{188}Os)_{sw}$ = 1.06) is controlled by the relative contributions of Os input fluxes from continental weathering (70% of the total Os supply to the oceans), alteration of abyssal peridotites (16%), and aeolian dusts (14%) (FRANK, 2002). The Os isotopic composition of the input varies in the range between radiogenic values as high as 1.54 (upper continental crust) to more unradiogenic values of ~0.126 (peridotites and cosmic dust) (FRANK, 2002). The only sinks for Os in the ocean are sediments in reducing environments, located beneath major upwelling regions (FRANK, 2002). The modern residence time of Os in the ocean is in between 6.5 – 15kyrs implying a homogeneous distribution of Os ($[Os]_{sw}$ = 10.86ppm) and its isotopic composition. This allows to trace short-term fluctuations in seawater composition, as for example those caused by glacial/interglacial cycles which are difficult to replicate by the buffered Sr isotope system (VANCE et al., 2009; VEIZER and MACKENZIE, 2010).

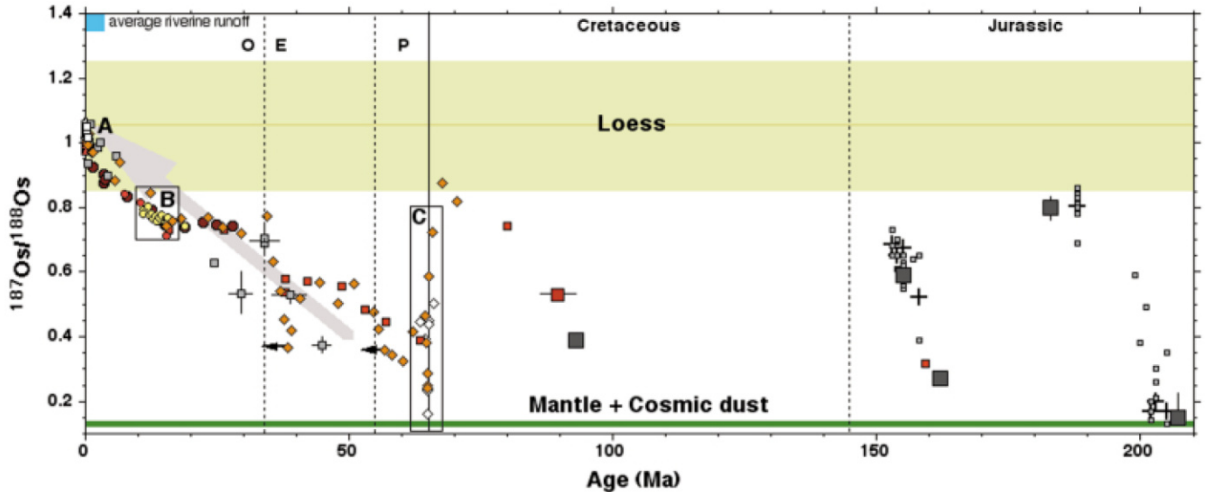

FIGURE I.3 – The marine Osmium record for the last 210Myr as compiled by (PEUCKER-EHRENBRINK and RAVIZZA, 2000). Different symbols and colours represent different proxy archives, including metalliferous pelagic clays, sediments, carbonates and organic-rich sediments and mudstones. Also indicated is the modern average runoff (blue square) as well as isotopic compositions for loess, mantle and cosmic dust Os inputs (For particular literature sources and additional information see (PEUCKER-EHRENBRINK and RAVIZZA, 2000) and references therein).

The seawater Os isotopic composition through time is recorded in metalliferous sediments, e.g. ferromanganese crusts. Over the last 200Myr the $^{187}Os/^{188}Os$ ratio of seawater varies between 0.17 and 1.06 (Fig. I.3). During the last ~65Myr a general increase is observed which is in similarity to Sr and Li isotopes (EDMOND, 1992; GALY et al., 1999; VEIZER et al., 1999; MISRA and FROELICH, 2012). Seawater Os isotopes have been used to determine changes in weathering rates and detecting impacts of extraterrestrial bodies or intense volcanic activity in the past (PEUCKER-EHRENBRINK and RAVIZZA, 2000; JENKYNS, 2010). In particular, the combined use of radiogenic Sr and Os isotopes may help to discriminate between high-frequency and low-frequency tectonic forcing (PEUCKER-EHRENBRINK and RAVIZZA, 2000).

Stable isotope systems

The stable isotopes are, in contrast to radiogenic isotopes (section I.2), highly sensitive to environmental and biological factors. For example, oxygen isotopes in marine carbonates are influenced by water temperature, water depth, salinity, pH, and species-specific physiological ("vital") effects. As a consequence, the stable isotopic composition of a given

element in a marine biogenic carbonate is influenced by the temporal variability of the seawater signal, but also by variations in habitat and organism-specific isotope fractionation parameters (PROKOPH et al., 2008).

The partition of isotopes between two phases is known as isotope fractionation. This partitioning can be caused by i) isotope exchange reactions (equilibrium isotope fractionation) or ii) kinetic processes (kinetic isotope fractionation). For equilibrium fractionation, isotope effects are predominantly caused by the dependence of the equilibrium constant on temperatures. In particular, isotope fractionation tends to become zero at high temperatures (Hoefs, 2009). Kinetic isotope fractionation is always associated with incomplete and unidirectional processes, e.g. evaporation, dissociation reactions, or biologically mediated reactions like precipitation of carbonate minerals. Here, the partitioning of isotopes is related to isotope specific reaction rates of molecules. In particular, unidirectional chemical reactions always produce a relative enrichment of the light isotope in the reaction product as its molecule has a higher reaction rate (ANBAR and ROUXEL, 2007; HOEFS, 2009).

Variations in stable isotope compositions are used e.g. as geothermometers, for the detection and quantification of kinetic processes, to provide information about elemental biogeochemical cycling, as proxies for ocean oxygenation, and as a tracer of mixing processes, especially for systems with endmembers that have a different isotope signatures due to biological mediated processes (e.g. (ANBAR and ROUXEL, 2007; HOEFS, 2009; EISENHAUER et al., 2011; MISRA and FROELICH, 2012)).

By now, variations in isotopic compositions of ~30 elements have been detected (Fig I.4). Besides variations in the traditional light stable isotope systems of hydrogen, carbon, nitrogen, oxygen and sulphur, research also shifted to the new non-traditional stable isotopes within the last two decades. This section summarizes the main findings of long-term

changes (>1Myr) in seawater stable isotope composition of elements that have been studied most extensively so far.

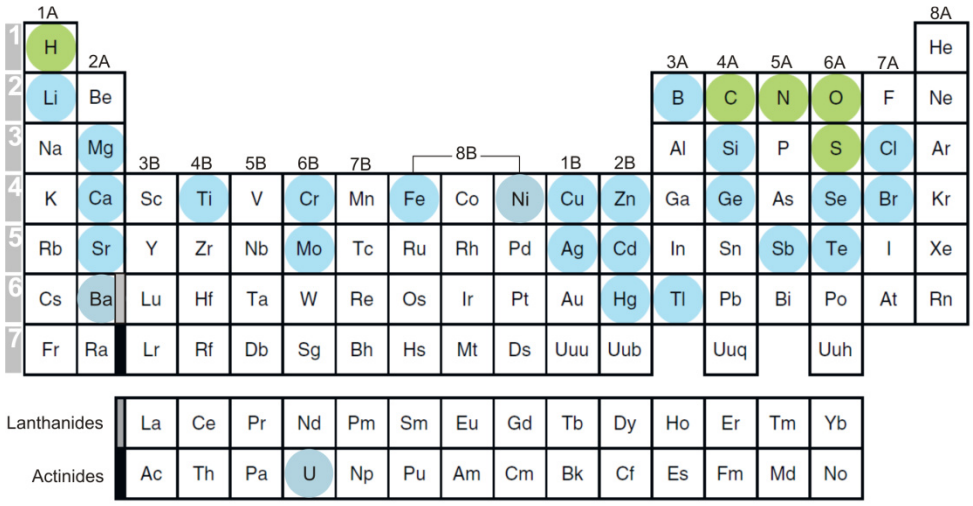

FIGURE I.4 – The periodic table of elements, showing the stable isotope systems (modified after (ANBAR and ROUXEL, 2007)). The traditional (green) and non-traditional (blue) stable isotope systems are indicated.

Carbon

Changes in the carbon isotope composition of seawater have been recorded in marine carbonates. Carbon isotopes are notated in the common delta-notation relative to the Pee Dee Belemnite (PDB) standard (HOEFS, 2009):

$$\delta^{13}C_{sample} = \left(\frac{\left({}^{13}C/{}^{12}C \right)_{sample}}{\left({}^{13}C/{}^{12}C \right)_{PDB}} - 1 \right) \times 1000 \qquad [I.1]$$

The $\delta^{13}C$ composition of marine carbonates is closely related to the $\delta^{13}C$ of seawater bicarbonate which reflects its carbon source. This $\delta^{13}C$ record has been used for chemostratigraphy (e.g. (KORTE and KOZUR, 2010)) and reconstructions of the global carbon cycle.

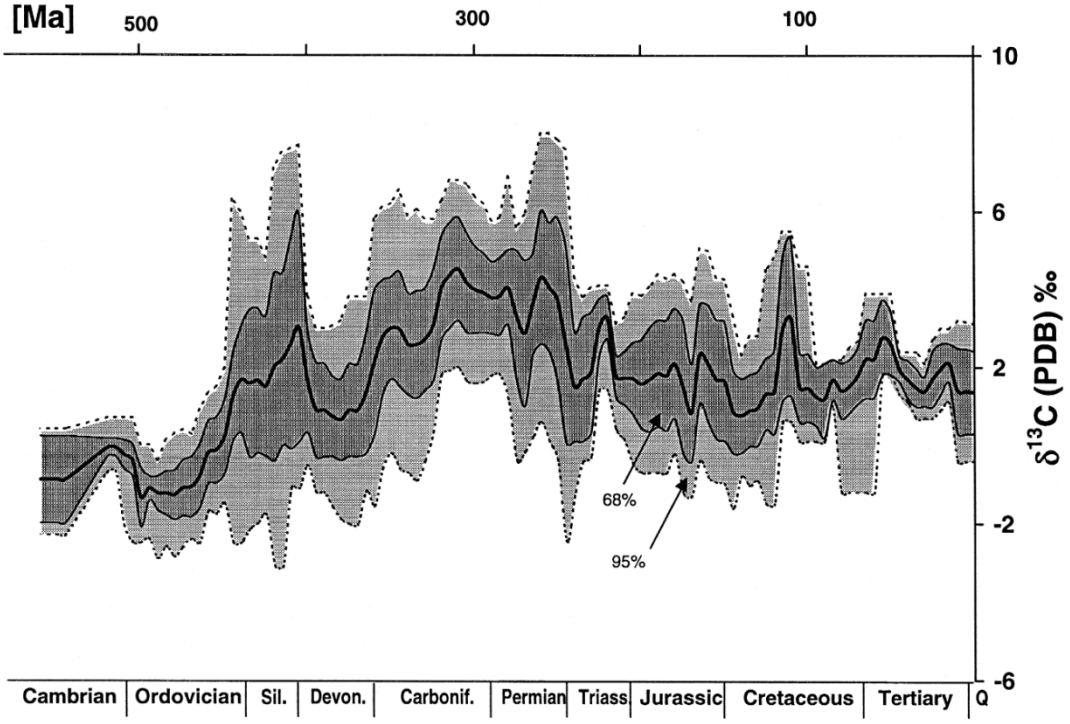

FIGURE I.5 – The Phanerozoic $\delta^{13}C$ record of marine carbonates as compiled by (VEIZER et al., 1999). The grey shaded areas around the running mean include 68% (1 s.d.) and 95% (2 s.d.) of all data. Timescale from (HARLAND et al., 1990).

In general, increasing $\delta^{13}C$ reflect an increase in the burial of organic matter, as it preferably incorporates the lighter carbon isotope. For the Proterozoic, these $\delta^{13}C$ excursions are correlated with interglacials and associated efficient burial of organic matter (SHIELDS and VEIZER, 2002). Concerning the Phanerozoic (Fig. I.5), there is no agreement on the driving forces for the $\delta^{13}C$ trend (VEIZER and MACKENZIE, 2010). Model simulations of (KUMP and ARTHUR, 1999) indicate that the burial of organic carbon, the atmospheric pCO_2 influence on the fractionation factor between carbon from organic matter and CO_2, and changes in the ratio of carbonate/silicate continental weathering rates have a significant influence on $\delta^{13}C$ of marine carbonates. However, the relation between the carbon cycle and climate is still being debated. In particular, modelled atmospheric pCO_2 (BERNER and KOTHAVALA, 2001; ROTHMAN, 2002; WALLMANN, 2004), based on $\delta^{13}C$, and reconstructed paleo-climate from proxy data show an inconsistency in some cases (VEIZER et al., 2000; BOUCOT and GRAY, 2001; ROYER, 2006; ROYER et al., 2007). Therefore, the roles of atmospheric pCO_2 and

astronomical mechanisms, e.g. galactic rays, will be investigated in future research (VEIZER et al., 2000; ROYER et al., 2007).

Oxygen

The oxygen cycle of the ocean is strongly coupled to the water cycle. The oxygen isotope composition in the last ~3Myr is mainly influenced by changes in global ice volume. However, there are considerable changes of $\delta^{18}O$ in marine carbonates of ~10‰ over the Phanerozoic which are controversial and a yet not completely understood (VEIZER et al., 1999) (Fig. 1.6). For low-temperature studies on carbonates, $^{18}O/^{16}O$ ratios are given in the delta-notation (compare Eq. I.1) relative to the PDB standard (HOEFS, 2009).

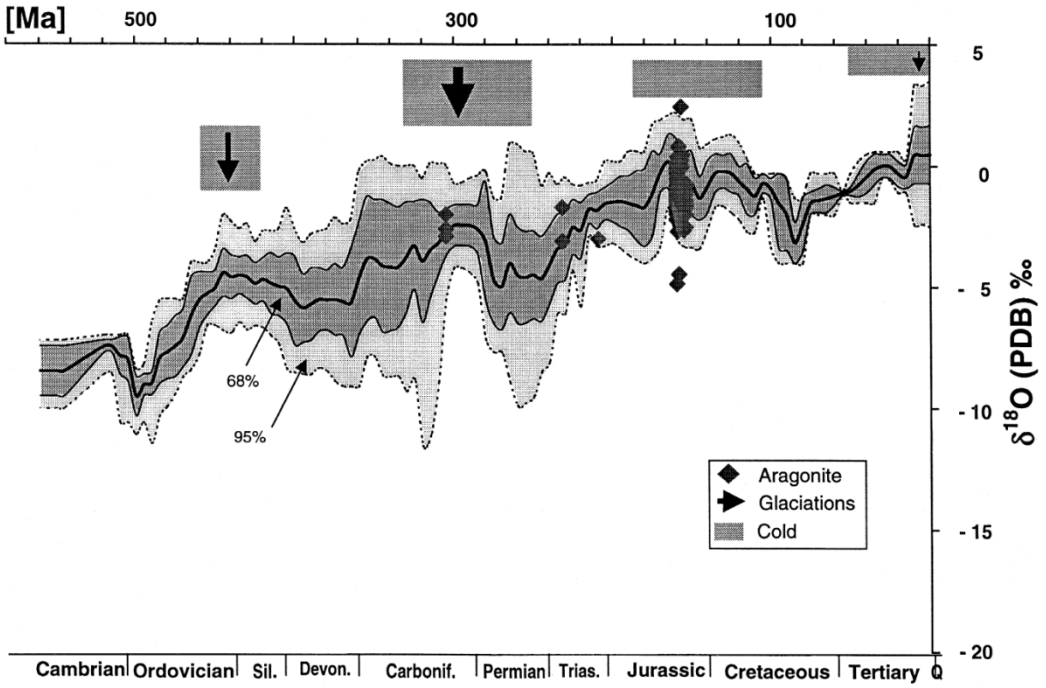

FIGURE I.6 – The Phanerozoic $\delta^{18}O$ record of marine carbonates as shown and compiled in (VEIZER et al., 1999). The grey shaded areas around the running mean include 68% (1 s.d.) and 95% (2 s.d.) of all data. Grey boxes mark time of cold climate and glaciations (arrows) which correlate with high $\delta^{18}O$ values. Timescale from (HARLAND et al., 1990).

The $\delta^{18}O$ record reveals a long-term increase of ~10‰ from the Cambrian to Quaternary period with superimposed short-term variations (Fig. I.6). The reason for the long-term increase in $\delta^{18}O$ is yet not fully understood. In particular, the ratio between low-temperature

and high-temperature alteration of the oceanic crust, and changes in seawater temperature are still being debated (HOEFS, 2009; HOLLAND, 2010).

While (VEIZER et al., 1999) proposed a tectonic process that controls both $\delta^{18}O$ and $^{87}Sr/^{86}Sr$ similarly, (WALLMANN, 2001b) related the long-term $\delta^{18}O$ increase to a progressive loss of light oxygen as structurally bound water into the mantle. This overall subduction into the mantle exceeds the H_2O release rate at mid ocean ridges, resulting in decreasing sea-levels and increasing $\delta^{18}O$ of seawater (WALLMANN, 2001b). This general trend is superimposed by a cyclic $\delta^{18}O$ pattern that has been interpreted to reflect changes in i) paleo-T controlled by galactic orbital modulation of climate due to the impact of cosmic ray on cloud cover, ii) climate caused by changing atmospheric pCO_2 and related changes in seawater pH, or iii) by a combination of these processes, implying that global climate swings were not restricted to higher latitudes but also occurred in equatorial regions (BERNER and KOTHAVALA, 2001; WALLMANN, 2004; ROYER et al., 2007; PROKOPH et al., 2008; VEIZER and MACKENZIE, 2010).

Sulphur

The oceanic sulphur reservoir, which is almost entirely in the form of dissolved sulphate, is more than ten times larger than the marine pool of bicarbonate (WALKER, 1986). Sulphur is supplied to the oceans by weathering and dissolution of S-bearing minerals and the volcanic release of sulphur. The sum of these input fluxes is about ten times smaller than the C input fluxes, resulting in an oceanic residence time of ~14Myr (WALKER, 1986). Sulphur is removed from seawater via precipitation of evaporites and by pyrite burial in marine sediments. The sulphur isotope ratio $^{34}S/^{32}S$ is reported in the delta-notation (compare Eq. I.1) relative to the Canyon Diablo Troilite (CDT) standard (e.g. (KAMPSCHULTE and STRAUSS, 2004)).

While the S isotope composition of evaporite minerals is quite similar to that of seawater sulphate, there is a large fractionation factor between reduced sulphide and sulphate (WALKER, 1986). This is a consequence of a strong isotope fractionation induced by

dissimilatory bacterial reduction to sulphate, where large fractionation factors in between +4‰ and <-46‰ have been observed (NAKAI and JENSEN, 1964; CANFIELD and THAMDRUP, 1994; HABICHT and CANFIELD, 1996; CANFIELD, 2001; VEIZER and MACKENZIE, 2010). Therefore, changes in the sulphur isotope composition of seawater are interpreted as changes in Sulphate Reduction Rates (BSR) by bacteria. In particular, increasing $\delta^{34}S$ of seawater sulphate are indicative for pyrite burial rates that exceed pyrite weathering on the continents.

$$2C(H_2O) + SO_4^{2-} \xrightarrow{BSR} 2HCO_3^- + H_2S \quad [I.2]$$

The BSR reaction takes place in anoxic environments where oxygen is absent and organic matter ($2C(H_2O)$) is preferentially oxidized by bacteria while reducing sulphate to hydrogen sulphide (Eq. I.2). H_2S likely forms metal sulphides in the water, which are stored (mostly as pyrite FeS_2) in marine sediments.

The sulfur isotope composition of seawater is recorded in evaporates, barites, carbonates (as carbonate associated sulphates (CAS)), and sulfide minerals. Since evaporates are not continuously recorded through geological time and additionally show a larger scatter in coeval $\delta^{34}S$, they are not considered as a robust archive (HOEFS, 2009). Similar observations were made for pyrite (Fe_2S) minerals that show a larger scatter in coeval data, which was interpreted to reflect local redox conditions within the sediment. Therefore, sulfide minerals are also not considered to reflect the seawater $\delta^{34}S$ composition (HOEFS, 2009).

The Phanerozoic $\delta^{34}S$ record which is based on isotope measurements on marine carbonates and barites is supposed to reflect changes in seawater $\delta^{34}S$ isotope composition (Fig I.7). In general, $\delta^{34}S$ are decreasing from the Cambrian period (~30‰) to the Permian period (~10%) and slowly increasing afterwards up to the modern value of ~20%. From this general trend it has been concluded that pyrite burial must have been as twice as large as today during the Early Paleozoic. Furthermore, the Phanerozoic carbon isotope composition mirrors that of sulfur, implying that there might be redox balance between $\delta^{13}C$ and $\delta^{34}S$ on these timescales

(VEIZER et al., 1999; PROKOPH et al., 2008; VEIZER and MACKENZIE, 2010). However, there is no consensus about a physical geologic scenario for this coupling (HOLLAND, 2010; VEIZER and MACKENZIE, 2010).

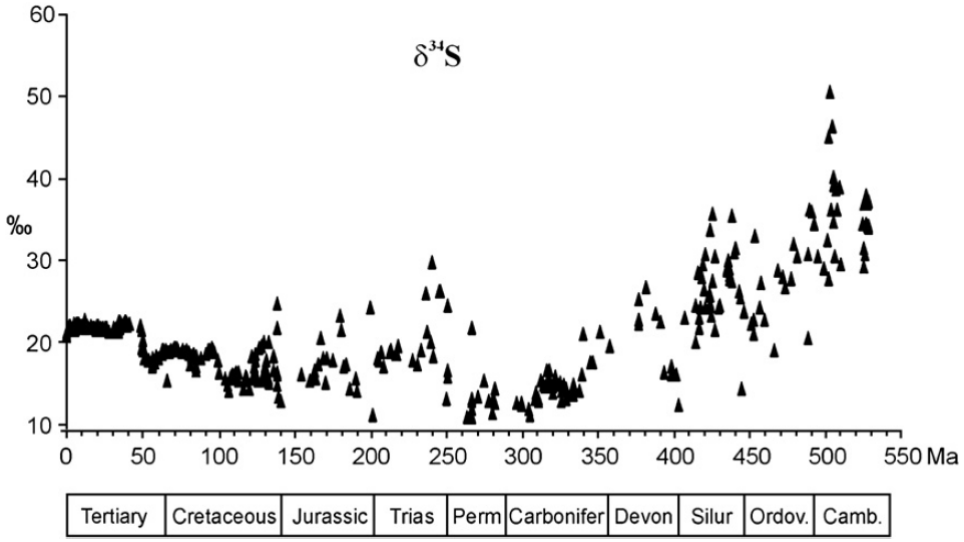

FIGURE I.7 - The Phanerozoic $\delta^{34}S$ record of carbonate associated sulphates (CAS) and marine barites as shown and compiled in (PROKOPH et al., 2008). Timescale from GTS 2004 (GRADSTEIN et al., 2005).

Calcium

The oceanic calcium cycle is closely linked to the global carbon cycle via continental weathering of carbonate and silicate rocks. Modern Ca and its isotopes are homogenously distributed within the ocean due to its long residence time (0.5 – 1.0Myr) (Blättler et al., 2012). Therefore, long-term isotope studies provide useful insights into the evolution of past seawater Ca concentrations and ultimately the past global carbon cycle (ZHU and MACDOUGALL, 1998; DE LA ROCHA and DEPAOLO, 2000; HEUSER et al., 2005; FARKAŠ et al., 2007a). In particular, seawater Ca concentrations are an important factor to reconstruct the carbon dioxide system in the ocean within model simulations (Berner et al., 1983; Wallmann, 2004). These results contribute to our understanding of the relationship between atmospheric CO_2 and global climate (WALLMANN, 2004; KASEMANN et al., 2005). The calcium isotope

composition is reported in the delta-notation (compare Eq. I.1), relative to the standard NIST SRM 915a (EISENHAUER et al., 2004).

Results from Ca isotopes measured in marine calcium carbonates reveal significant variations that were interpreted as changes in seawater Ca isotope composition ($\delta^{44/40}Ca_{sw}$, Fig. I.8), reflecting imbalances in the Ca input and output fluxes (ZHU and MACDOUGALL, 1998; DE LA ROCHA and DEPAOLO, 2000; FANTLE and DEPAOLO, 2005; HEUSER et al., 2005; KASEMANN et al., 2005; FARKAŠ et al., 2007a; EISENHAUER et al., 2009; PAYNE et al., 2010; BLÄTTLER et al., 2011; HINOJOSA et al., 2012).

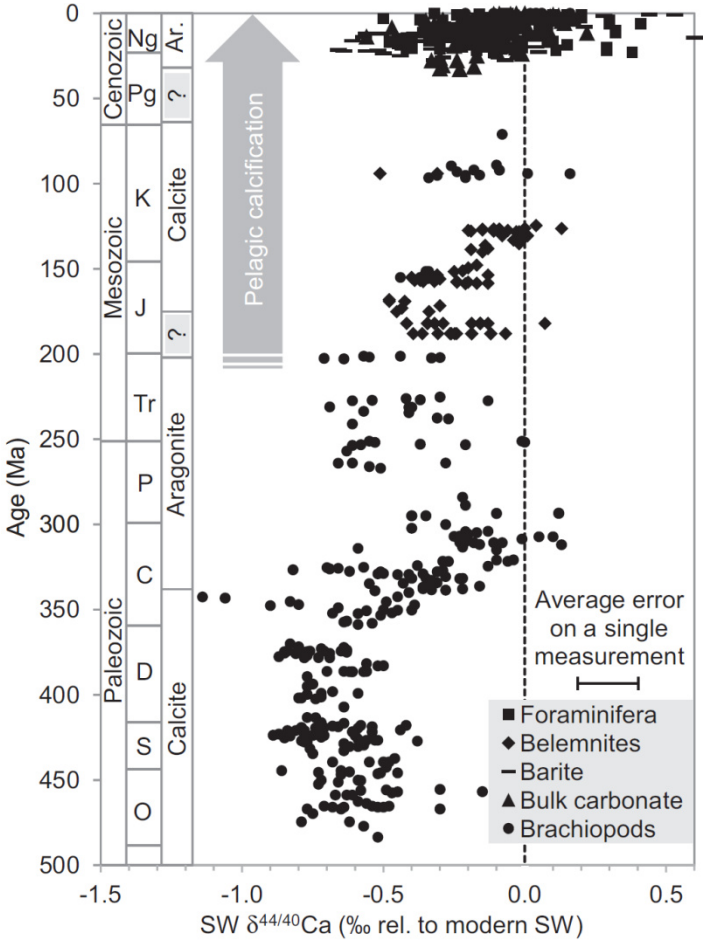

FIGURE I.8 - The Phanerozoic $\delta^{44/40}Ca$ record of seawater as compiled in (Blättler et al., 2012). The majority of data are from diagenetically screened brachiopods and belemnites (Farkaš et al., 2007a; Farkaš et al., 2007b). Cenozoic data is based on foraminifera, bulk carbonates and marine barites (FANTLE and DEPAOLO, 2005; HEUSER et al., 2005; FANTLE and DEPAOLO, 2007; GRIFFITH et al., 2008). Timescale from (Ogg et al., 2008). Time of aragonite and calcite seas from (Sandberg, 1983). Ng = Neogene, Pg = Paleogene, K = Cretaceous, J = Jurassic, Tr = Triassic, P = Permian, C = Carboniferous, D = Devonian, S = Silurian, O = Ordovician.

However, the Ca isotope signals in marine carbonates may be superimposed by i) changes in the dominant carbonate mineralogy, ii) temperature, iii) dolomitization rates and, v) changes in seawater carbonate ion concentration (DE LA ROCHA and DEPAOLO, 2000; NÄGLER et al., 2000; GUSSONE et al., 2003; GUSSONE et al., 2005; HIPPLER et al., 2006; FARKAŠ et al., 2007a; FANTLE, 2010; PAYNE et al., 2010; BLÄTTLER et al., 2012; HINOJOSA et al., 2012). In particular, a recent study of (BLÄTTLER et al., 2012) supports the conclusion of (FARKAŠ et al., 2007a) that secular changes in $\delta^{44/40}Ca_{sw}$ are primarily caused by changes in the dominant carbonate mineralogy and related changes in fractionation factors. Further, short-term changes in $\delta^{44/40}Ca_{sw}$ were interpreted to be a result of changing carbonate sedimentation (De La Rocha and DePaolo, 2000), ocean acidification (PAYNE et al., 2010; HINOJOSA et al., 2012), and changes in the flux or isotope composition of continental weathering (GRIFFITH et al., 2008; FANTLE, 2010; BLÄTTLER et al., 2011).

Strontium

The geochemistry of strontium is introduced in section 2.1.1.. The stable strontium isotope composition is given in the common delta-notation (compare Eq. I.1) relative to the $SrCO_3$ standard NIST SRM987 (FIETZKE and EISENHAUER, 2006).

The marine budget of Sr is similar that of Ca with its major sources coming from silicate and carbonate weathering and hydrothermal fluids. The most important sink is the burial of marine carbonates and to a lesser extent the alteration of the oceanic crust (HART et al., 1974; ELDERFIELD and SCHULTZ, 1996; ALLÈGRE et al., 2010; KRABBENHÖFT et al., 2010). The precipitation of marine carbonates is associated with an isotope offset to seawater ($\Delta^{88/86}Sr_{sw\text{-}cc}$, Eq. I.3) which is for modern marine carbonates in the range of -0.12‰ to -0.37‰ with a mean of ~0.21‰ (FIETZKE and EISENHAUER, 2006; RÜGGEBERG et al., 2008; KRABBENHÖFT et al., 2010; BÖHM et al., 2012).

$$\Delta^{88/86}Sr_{sw-cc} = \delta^{88/86}Sr_{cc} - \delta^{88/86}Sr_{sw} \quad [I.3]$$

To reconstruct changes in $\delta^{88/86}Sr_{sw}$, it is crucial to find an archive that has a constant $\Delta^{88/86}Sr_{sw-cc}$, independent of the environmental conditions. For the warm-water coral *Pavona clavus* it has been shown that a temperature-dependent isotope fractionation is associated with the Sr incorporation into the carbonate (FIETZKE and EISENHAUER, 2006). Accordingly, *Pavona clavus* is not an applicable archive to investigate in seawater $\delta^{88/86}Sr$ changes. However, the requirement of a temperature independency was shown for the cold-water coral *Lophelia pertusa* (RADDATZ, personal communication), although these results are different to the findings of (RÜGGEBERG et al., 2008) who found a temperature-dependent $\delta^{88/86}Sr$ fractionation in the same samples applying the less precise bracketing standard technique. Nevertheless, changes in carbonate burial rates should have a significant effect on the temporal evolution of $\delta^{88/86}Sr_{sw}$. For the modern ocean, it has been shown that the Sr budget is out of steady state with Sr output fluxes exceeding 2-3 times the Sr input fluxes (VANCE et al., 2009; KRABBENHÖFT et al., 2010). Accordingly, the reconstruction of Phanerozoic $\delta^{88/86}Sr_{sw}$ will give additional constraints to the marine carbonate budget of geological timescales (section 1.6 and chapters 4 and 5).

Element concentrations and ratios

Beside the large and growing number of isotope systems which are used to investigate in changes in seawater chemistry, there is also some evidence from fluid inclusions for changes in element concentrations of seawater. Further evidence comes from element ratios in marine carbonates, such as Sr/Ca or Mg/Ca. These proxies may be used to find common causative mechanisms for covariant sedimentary and isotope evolution.

The use of the mineralogy of marine evaporites and of the composition of fluid inclusions trapped in marine halite is not free of difficulties (HORITA et al., 2002). Nevertheless, there is an overall agree that at least magnesium, calcium, and strontium concentrations have been

variable throughout the Phanerozoic (e.g. (LOWENSTEIN et al., 2001; HORITA et al., 2002; BRENNAN et al., 2004; LOWENSTEIN et al., 2005)).

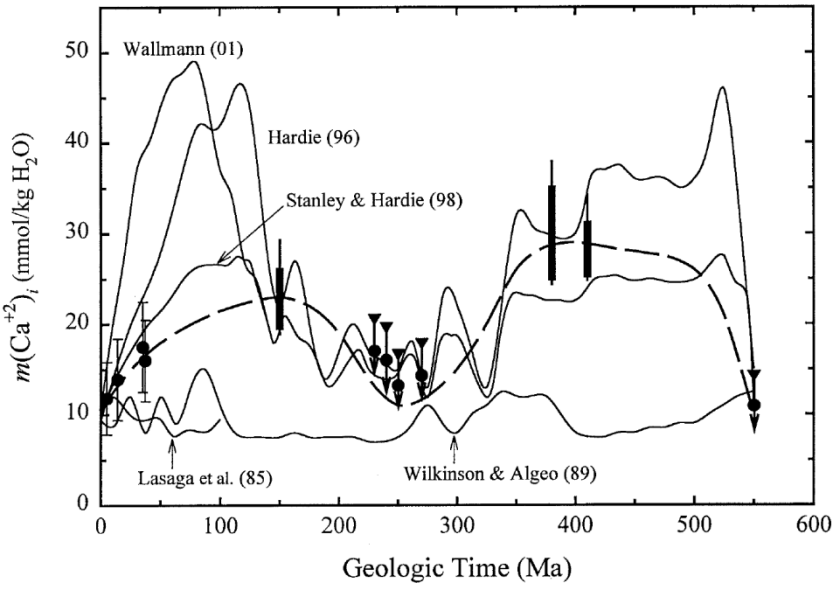

FIGURE I.9 – The Ca concentration based on fluid inclusions of marine halite (solid symbols) are shown together with results from different model studies (HORITA et al., 2002).

The results of the experimental studies agree that the seawater chemistry of the Permian period must be similar to the modern ocean, but concentrations of Ca, Mg, and SO_4 changed by factor 2-4 within the Phanerozoic (Fig. I.9). Interestingly, despite the large variations of the mentioned ions in seawater, the seawater K concentrations remained constant through time (HORITA et al., 2002).

Other studies investigated secular changes of element ratios like Sr/Ca and Mg/Ca in skeletal carbonates (STEUBER and VEIZER, 2002; LEAR et al., 2003; RIES, 2010) (Fig. I.10). These secular changes might be superimposed to some extent in some biogenic skeletal carbonates (especially corals) by effects of [CO_3^{2-}], T, S, growth rate, photosynthesis, and biomineralization processes on the Sr/Ca and Mg/Ca distribution coefficient (D_{Sr} and D_{Mg}) (CORRÉGE, 2006; ROSENTHAL, 2007). However, both element ratios correlate well with times of "aragonite seas" and "calcite seas" as proposed by (SANDBERG, 1983) and changes in KCl and $MgSO_4$ evaporite deposits (HARDIE, 1996).

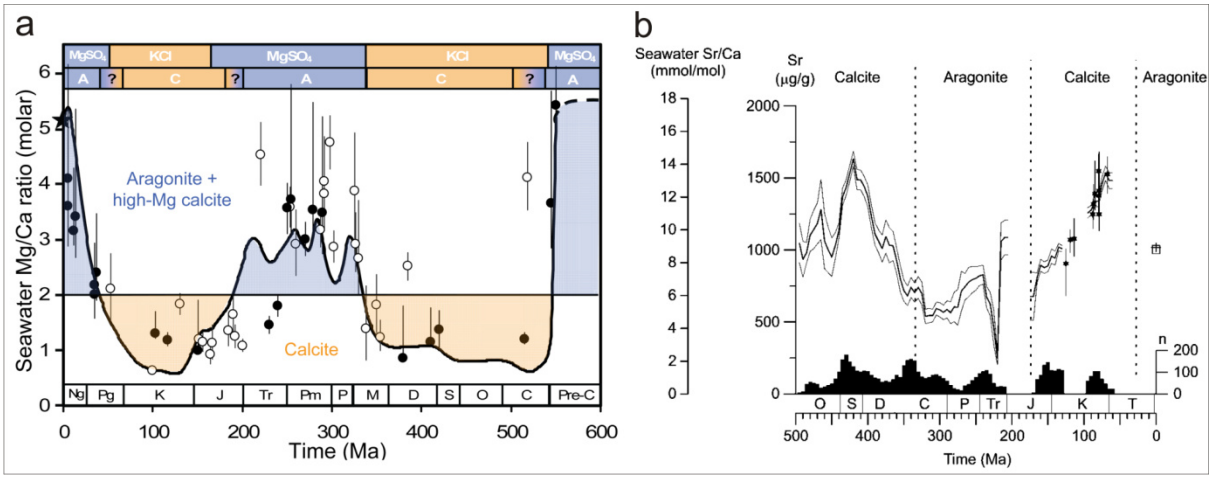

FIGURE I.10 – a: Phanerozoic seawater Mg/Ca ratios estimated from fluid inclusions (closed circles) and fossil echinoids (opencircles) are shown together with model estimations. The horizontal lines divides calcite (Mg/Ca<2) and aragonite (Mg/Ca>2) nucleation fields in seawater, which correlate well with intervals of primary aragonitic (A) and calcitic (C) abiotic precipitates from (SANDBERG, 1983) and KCl and $MgSO_4$ evaporites (HARDIE, 1996) (source (RIES, 2010)). b: The Phanerozoic seawater Sr/Ca reconstructed from marine brachiopods and bivalve rudists is shown together with intervals of primary aragonitic (A) and calcitic (C) abiotic precipitates from (SANDBERG, 1983) (source (STEUBER and VEIZER, 2002)).

The data suggest that periodic changes between high Mg/Ca, low Sr/Ca and aragonite mineralogy on the one hand and low Mg/Ca, high Sr/Ca, and calcite mineralogy on the other hand occurred during the Phanerozoic. In particular, three times of "aragonite seas" and two times of "calcite seas" are observed (Fig 1.10) (SANDBERG, 1983; HARDIE, 1996; STANLEY and HARDIE, 1998). Therefore, the composition of seawater must have changed significantly over the Phanerozoic (HOLLAND, 2010; VEIZER and MACKENZIE, 2010). However, the primary mechanism for changing seawater Mg/Ca ratios remains unclear. Some authors argued for the role of MOR spreading rates that changed considerably through time and therefore must have changed the composition of major cations in the ocean (GAFFIN, 1987; HARDIE, 1996; RIES, 2010). However, more recent studies showed that ocean crust formation were nearly constant for the last 180Myr (ROWLEY, 2002) which questions the relationship between sea-level and oceanic crust production rates as proposed by (GAFFIN, 1987). Another explanation is the role of sea-level changes and its influence on dolomitization rates. In particular, high sea-levels may have led to the flooding of continents and dolomitization, which is favored in

warm, shallow evaporate settings which may explain the correlation of the Mg and SO_4 concentration of seawater (HOLLAND, 2010). Future studies on the Phanerozoic magnesium isotope composition of seawater might help to explain these competing hypotheses for the explanation of long-term changes in major ion composition of Phanerozoic seawater.

Proxies in developmental stages

During the last decade there are a large and growing number of isotope and element proxies that are not discussed in the last section. Especially, redox-sensitive isotope and element ratio proxies are predominantly investigated and might help in clarifying the relationship between the Phanerozoic marine sulphur and carbon isotope curve and the role of anoxia on mass extinctions. Here, the isotope systems of molybdenum (Mo), uranium (U), and chromium (Cr) as well as the element ratios of iodine/calcium (I/Ca) and uranium/calcium (U/Ca) are promising tools to reconstruct oxygen concentrations in the geological past (e.g. (CRUSE and LYONS, 2004; ANBAR and ROUXEL, 2007; VOEGELIN et al., 2009; JENKYNS, 2010; LU et al., 2010; BRENNECKA et al., 2011; BOITEAU et al., 2012)). It has been shown that these proxies are sensitive to changes in the redox state of the aqueous solutions. First applications investigated OAEs in the Cretaceous period and the Permian/Triassic boundary (VOEGELIN et al., 2009; ZHOU et al., 2009; LU et al., 2010; BRENNECKA et al., 2011; BOITEAU et al., 2012).

Furthermore, boron isotopes ($\delta^{11}B$) have been investigated to reconstruct changes in paleo-seawater pH (KASEMANN et al., 2005; HÖNISCH et al., 2008; RAE et al., 2011; MCCULLOCH et al., 2012). These investigations have been successfully applied for last 400kyr, but long-term reconstructions of seawater pH were unsuccessful (LEMARCHAND et al., 2000; JOACHIMSKI et al., 2005; HÖNISCH et al., 2008). In particular, secular changes in $\delta^{11}B_{sw}$ were better explained by changes in the rate and isotopic composition of the boron continental weathering flux (LEMARCHAND et al., 2000; JOACHIMSKI et al., 2005).

I.4. Model simulations of Phanerozoic seawater chemistry

The proxy-derived investigations (section I.3) were enhanced by model approaches on seawater chemistry (HARDIE, 1996; DEMICCO et al., 2005). Here, changes in seawater composition are modelled by i) variable input of river waters ii) variable rates of high-temperature alteration of the oceanic crust at MOR, iii) variable rates of low-temperature alteration of the oceanic, and iv) variable rates of $CaCO_3$ production to sustain a constant saturation state. Generally, these studies are based on secular variations in MOR spreading rates, which are based on changes in global sea-levels (GAFFIN, 1987). The model results are in agreement with data from fluid inclusions, including near-constant seawater K concentrations throughout the Phanerozoic, which require variable rates of high-T and low-T alteration of the oceanic crust (DEMICCO et al., 2005). Therefore, it is concluded that variable rates of seawater cycling through the oceanic crust are the most important parameter that controls seawater chemistry on Phanerozoic timescales (DEMICCO et al., 2005). However, the model did not account for changing carbonate mineralogy, dolomitization rates, and furthermore relies on oceanic crust production curve which was questioned by (ROWLEY, 2002) who found nearly invariable oceanic crust production rates during the last 180Myr.

Another attempt to investigate in changing ocean chemistry was made by (WALLMANN, 2001a) and later refined by (HANSEN and WALLMANN, 2003; WALLMANN, 2004; HEUSER et al., 2005; FARKAŠ et al., 2007a) who modelled coupled carbon/calcium/strontium/magnesium cycles from a set of proxy-derived forcing parameters, including seawater $\delta^{18}O$, $\delta^{13}C$, $\delta^{44/40}Ca$, $(Sr/Ca)_{sw}$, $^{87}Sr/^{86}Sr$, and $(Mg/Ca)_{sw}$ ratios with first implications to seawater pH, surface temperature, atmospheric pCO_2, and dolomitization rates (Fig I.11).

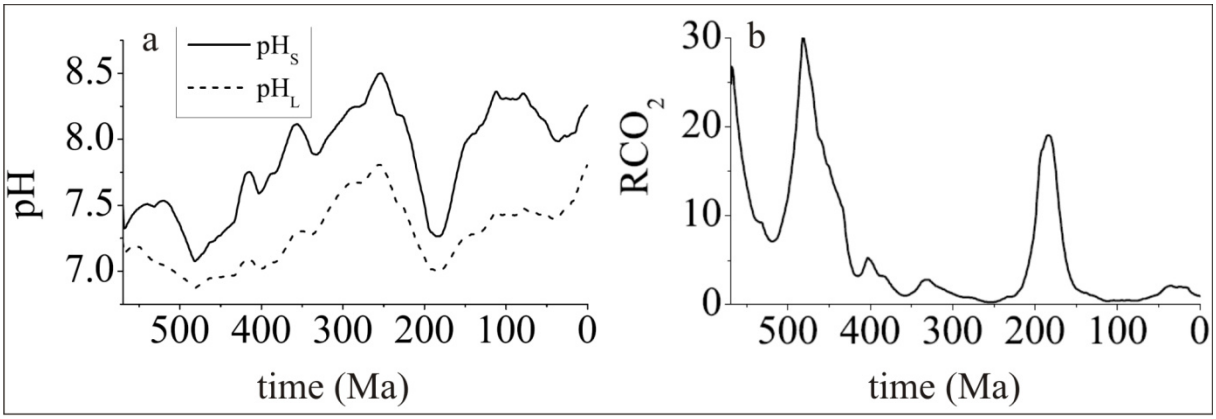

FIGURE I.11 – a: Changes in modelled seawater pH values in surface water (pH_S) and at the calcite saturation depth (pH_L). b: Changes in modelled atmospheric RCO_2 (atmospheric pCO_2 relative to the modern value) (source (WALLMANN, 2004)).

The model results are in agreement with climate predictions from the geological record and predict warm climate phases during Cambrian, Devonian, Triassic, and Cretaceous period, while colder climate and glaciations are modelled in the Carboniferous to Early Permian and in the Late Cenozoic (WALLMANN, 2004). The modelled atmospheric CO_2 concentrations are also in general agreement with proxy data from (ROYER et al., 2007) but differ on short-term timescales. The later refinement of (FARKAŠ et al., 2007a) provided evidence that secular variations in $\delta^{44/40}Ca_{sw}$ follow time of proposed "aragonite seas" and "calcite seas", because of different isotope fractionation factors for Ca in the two calcium carbonate polymorphs. However, these models are based on the assumption that seawater calcite saturation is sustained by carbonate sedimentation. However, this was probably not the case in the unbuffered neritic Paleozoic Ocean due to the lack of pelagic carbonates and associated carbonate compensation. Furthermore, the modelled Sr cycle has to rely on uncertain $(Sr/Ca)_{sw}$ ratios measured in marine carbonates (STEUBER and VEIZER, 2002; LEAR et al., 2003) which are known to be very susceptible to diagenetic alteration. New proxy data are therefore needed to validate these numerical models. In particular, changes in seawater pH reconstructed by e.g. boron isotopes, carbonate burial rates constraint by stable strontium

isotopes, and changes in the redox state of the ocean by Mo, U, and Cr isotopes as well as I/Ca ratios will significantly contribute to our understanding of seawater chemistry.

A similar approach was made by (ARVIDSON et al., 2006) who set-up a dynamical model for elemental cycling of sodium, potassium, calcium, magnesium, chloride, oxygen, iron, sulphur, and phosphorous in the Phanerozoic ocean. In similarity to (WALLMANN, 2001a), their model is based on i) chemical weathering fluxes reconstructed by time-dependent changes in paleogeography, atmospheric pCO_2, exposed lithology, land area, runoff, relief, and agency of plants, ii) formation of sedimentary carbonate minerals, iii) hydrothermal and magmatic fluxes, and iv) production, sequestration, and oxidation of organic matter. However, contrastly, (ARVIDSON et al., 2006) did not include isotope constraints from $\delta^{13}C$, $^{87}Sr/^{86}Sr$, $\delta^{34}S$, and $\delta^{44/40}Ca$.

The model results of (ARVIDSON et al., 2006) reveal that Phanerozoic $(Mg/Ca)_{sw}$ reflect the transfer of magnesium between the carbonate and silicate reservoirs. This is probably mediated by changes in seafloor spreading rates which influences dolomite formation rates, seawater alkalinity, and ultimately $(Mg/Ca)_{sw}$. Modelled atmospheric O_2 concentrations include a general increase during the Phanerozoic which was related to a increasing phosphorous availability resulting from progressive increase in continental apatite ($Ca_5(PO)_4(F,Cl,OH)$) weathering.

The isotope records of carbon, sulphur, and radiogenic strontium were also used for reconstructing Phanerozoic oxygen and carbon dioxide levels by combined carbon and sulphur biogeochemical cycles (BERNER and CANFIELD, 1989; BERNER, 1991; BERNER, 1994; BERNER and KOTHAVALA, 2001; BERNER, 2006; BERNER, 2009). These results are partly in disagreement with model estimates of Wallmann (2004), particularly in the Early Paleozoic and Cretaceous period.

Ultimately the model results for Phanerozoic seawater chemistry, which are based on different forcing parameters, show similar long-term trends in major ion composition and

atmospheric pCO_2. However, there are significant differences in the amplitude of short-term variations (e.g. Fig. 1.9). Therefore, more proxy and model data are needed to gain a better understanding of the coupling and feed back of mechanisms as well as their impact on the environmental conditions.

I.5. Summary

Constraints on changes in Phanerozoic ocean chemistry have been gained by the relative abundance of marine sediments, isotope studies in marine sediments, element ratios in marine carbonates, and element concentrations in fluid inclusions. There is an overall agreement that Phanerozoic ocean chemistry was not constant through time, although faunal assemblages and mineral precipitates are quite similar throughout the last ~541Myr. These time-dependent changes can be subdivided in secular changes with a periodicity of ~200Myr, superimposed by cycles with a frequency of 50Myr. Similar patterns for the main calcium carbonate polymorphs, seawater Mg/Ca, Sr/Ca, Ca and SO_4^{2-}, $\delta^{44/40}Ca_{sw}$, sea-level, atmospheric pCO_2, and correlations to mass extinctions suggest a common causative relationship. Specifically, earlier studies suggested changes in MOR spreading rates and therefore changing alteration rates of the oceanic crust as the main reason for the observed changes. However, oceanic crust production rates have been found to be very constant throughout the last 180Myr, therefore questioning large variations in MOR spreading rates throughout the Phanerozoic (ROWLEY, 2002). An alternative explanation for the observed changes is a secular change dolomitization rates which are linked to changes in sea-level. Future studies on the Mg isotope composition of seawater and more analysis of fluid inclusions will probably clarify this issue. Nevertheless, the observed correlation of parameters suggests a relation to changes in the atmosphere-hydrosphere conditions that are probably driven by tectonic forces. Another open question is the geological mechanism

behind the inverse correlation between carbon and sulphur isotopes on Phanerozoic timescales. It has been proposed that the two systems are connected by a shift of oxygen between the two reservoirs. Future studies on redox-sensitive proxies like Mo, Cr, and U isotopes as well as I/Ca, and U/Ca ratios will give additional constraints to the answer of this question. Model reconstructions of the Phanerozoic carbonate system are presently based on different assumptions for the marine carbonate system. Therefore, additional constraints for changes in seawater alkalinity and/or carbonate sedimentation rates are needed. Later might be constraint with the stable strontium isotope composition of paleo-seawater.

I.6. Thesis outline

This PhD-thesis focuses on the reconstruction of a Phanerozoic $\delta^{88/86}Sr$ record in marine carbonates. We used brachiopod shells and belemnites as archives, being very resistant to diagenetic alteration. The proxy-derived data are further enhanced with a consequent numerical modelling study. In particular, a complete constraint of the marine Sr budget will enhance previous model approaches (WALLMANN, 2001a; WALLMANN, 2004; HEUSER et al., 2005; FARKAŠ et al., 2007a). Herewith, first time implications for the marine carbonate budget including carbonate burial rates and changes in seawater alkalinity will be made on geological timescales. In particular, first reconstruction of carbonate burial rates with associated changes in seawater alkalinity will be presented. The results will be used to make additional constraints to mass extinctions and secular variations in seawater chemistry. The impetus for this work was given by the earlier work of (KRABBENHÖFT et al., 2010) who reconstructed the modern marine Sr budget with first implications to carbonate weathering on glacial/interglacial timescales. The Sr double spike method for accurate determinations of $^{88}Sr/^{86}Sr$ ratios in natural samples was earlier published by (KRABBENHÖFT et al., 2009). This work is divided into seven chapters:

Chapter I: Gives a general overview about changes in seawater chemistry on Phanerozoic timescales. In particular, it reviews the state of the art of proxy and model approaches.

Chapter II: This chapter represents a detailed description of the development of the Sr double spike technique combined with Thermal Ionization Mass Spectrometry (TIMS). This chapter was published as a technical note in the *Journal of Analytical Atomic Spectroscopy* (Krabbenhöft et al., 2009).

Chapter III: This chapter represents the first application of the Sr double spike technique to natural samples coming from seawater, hydrothermal fluids, river waters, and marine carbonates. Within a model approach these data were used to constrain the modern marine carbonate budget. The results indicate that the modern Sr budget is out of equilibrium conditions with respect to its input and output fluxes. This chapter was published in the Journal *Geochimica and Cosmoschimica Acta* (KRABBENHÖFT et al., 2010).

Chapter IV: This chapter represents the first reconstruction of paleo-seawater $\delta^{88/86}Sr$ values to investigate changes in the carbonate budget at the end-Permian mass extinctions. In particular, long-term high carbonate burial rates were explained by additional alkalinity coming from BSR in deep anoxic waters. The combination of long-term seawater anoxia and intermittent overturn of anoxic and toxic deep waters to the surface are considered to be responsible for the largest mass extinction within the Phanerozoic Eon. This chapter is currently submitted to the Journal *Geology* and still in review.

Chapter V: This chapter represents the updated Phanerozoic $\delta^{88/86}Sr$ record of seawater. The results are compared with other proxy data like $(^{87}Sr/^{86}Sr)_{sw}$ and $\delta^{44/40}Ca_{sw}$ to infer common

causative mechanisms. In a consequent model approach, the Phanerozoic marine Sr budget, including changes in seawater Sr concentrations and Sr carbonate burial rates is constraint. Long-term changes in Sr carbonate burial follow times of "aragonite seas" and "calcite seas", whereas short-term maxima and minima in Sr carbonate burial could be partly related to ocean anoxia and glaciations, respectively. This chapter is intended to be submitted to *Geochimica and Cosmochimica Acta*.

Chapter VI: This chapter investigates environmental influences on $\delta^{88/86}$Sr, Sr/Ca, Mg/Ca, Li/Ca, and Mg/Li in the scleractinian cold-water coral *Lophelia pertusa*. The results indicate that water temperature has a significant influence on Sr/Ca, Li/Ca, and Mg/Li but not on $\delta^{88/86}$Sr. In particular, highly sensitive Mg/Li might serve as a new paleotemperature proxy whereas results for $\delta^{88/86}$Sr indicate the general applicability of *Lophelia pertusa* as an archive for $\delta^{88/86}Sr_{sw}$. This chapter is already submitted to *Earth and Planetary Science Letters* and still in review.

Chapter VII: This chapter provides a synthesis of the results obtained in the frame of this work and gives an outlook on future research perspectives.

Appendix: Within the appendix, the abstracts submitted to scientific meetings that I attended during the course of my PhD are presented. Further it provides a manual for data reduction of TIMS-derived Sr isotope data.

I.7. References

Allègre, C. J., Louvat, P., Gaillardet, J., Meynadier, L., Rad, S., and Capmas, F., 2010. The fundamental role of island arc weathering in the oceanic Sr isotope budget. *Earth Planet. Sci. Lett.* **292**, 51-56.

Anbar, A. D. and Rouxel, O., 2007. Metal stable isotopes in paleoceanography, *Annu. Rev. Earth Planet. Sci.* Annual Reviews, Palo Alto.

Arvidson, R. S., Mackenzie, F. T., and Guidry, M., 2006. MAGic: A Phanerozoic Model for the Geochemical Cycling of Major Rock-Forming Components. *Am. J. Sci.* **306**, 135-190.

Azmy, K., Poty, E., and Brand, U., 2009. High-resolution isotope stratigraphy of the Devonian-Carboniferous boundary in the Namur-Dinant Basin, Belgium. *Sediment. Geol.* **216**, 117-124.

Berner, R. A., 1991. A model for atmospheric CO_2 over Phanerozoic time. *Am J Sci* **291**, 339-376.

Berner, R. A., 1994. GEOCARB II; a revised model of atmospheric CO_2 over Phanerozoic time. *Am J Sci* **294**, 56-91.

Berner, R. A., 2006. GEOCARBSULF: A combined model for Phanerozoic atmospheric O_2 and CO_2. *Geochim. Cosmochim. Acta* **70**, 5653-5664.

Berner, R. A., 2009. Phanerozoic atmospheric oxygen: New results using the GEOCARBSULF model. *Am J Sci* **309**, 603-606.

Berner, R. A. and Canfield, D. E., 1989. A new model for atmospheric oxygen over Phanerozoic time. *Am J Sci* **289**, 333-361.

Berner, R. A. and Kothavala, Z., 2001. Geocarb III: A Revised Model of Atmospheric CO2 over Phanerozoic Time. *Am J Sci* **301**, 182-204.

Berner, R. A., Lasaga, A. C., and Garrels, R. M., 1983. The carbonate-silicate geochemical cycle and its effect on atmospheric carbon dioxide over the past 100 million years. *Am. J. Sci.* **283**, 641-683.

Blättler, C. L., Henderson, G. M., and Jenkyns, H. C., 2012. Explaining the Phanerozoic Ca isotope history of seawater. *Geology* **40**, 843-846.

Blättler, C. L., Jenkyns, H. C., Reynard, L. M., and Henderson, G. M., 2011. Significant increases in global weathering during Oceanic Anoxic Events 1a and 2 indicated by calcium isotopes. *Earth Planet. Sci. Lett.* **309**, 77-88.

Böhm, F., Eisenhauer, A., Tang, J., Dietzel, M., Krabbenhöft, A., Kisakürek, B., and Horn, C., 2012. Strontium isotope fractionation of planktic foraminifera and inorganic calcite. *Geochim. Cosmochim. Acta*.

Boiteau, R., Greaves, M., and Elderfield, H., 2012. Authigenic uranium in foraminiferal coatings: A proxy for ocean redox chemistry. *Paleoceanography* **27**, PA3227.

Boucot, A. J. and Gray, J., 2001. A critique of Phanerozoic climatic models involving changes in the CO2 content of the atmosphere. *Earth-Science Reviews* **56**, 1-159.

Brennan, S. T., Lowenstein, T. K., and Horita, J., 2004. Seawater chemistry and the advent of biocalcification. *Geology* **32**, 473-476.

Brennecka, G. A., Herrmann, A. D., Algeo, T. J., and Anbar, A. D., 2011. Rapid expansion of oceanic anoxia immediately before the end-Permian mass extinction. *Proceedings of the National Academy of Sciences* **108**, 17631-17634.

Burke, W. H., Denison, R. E., Hetherington, E. A., Koepnick, R. B., Nelson, H. F., and Otto, J. B., 1982. Variation of Sea-Water $^{87}Sr/^{86}Sr$ Throughout Phanerozoic Time. *Geology* **10**, 516-519.

Canfield, D. and Thamdrup, B., 1994. The production of ^{34}S-depleted sulfide during bacterial disproportionation of elemental sulfur. *Science* **266**, 1973-1975.

Canfield, D. E., 2001. Isotope fractionation by natural populations of sulfate-reducing bacteria. *Geochim. Cosmochim. Acta* **65**, 1117-1124.

Coggon, R. M., Teagle, D. A. H., Smith-Duque, C. E., Alt, J. C., and Cooper, M. J., 2010. Reconstructing Past Seawater Mg/Ca and Sr/Ca from Mid-Ocean Ridge Flank Calcium Carbonate Veins. *Science* **327**, 1114-1117.

Corrége, T., 2006. Sea surface temperature and salinity reconstruction from coral geochemical tracers. *Palaeogeography, Palaeoclimatology, Palaeoecology* **232**, 408-428.

Cruse, A. M. and Lyons, T. W., 2004. Trace metal records of regional paleoenvironmental variability in Pennsylvanian (Upper Carboniferous) black shales. *Chem. Geol.* **206**, 319-345.

Davis, A. C., Bickle, M. J., and Teagle, D. A. H., 2003. Imbalance in the oceanic strontium budget. *Earth Planet. Sci. Lett.* **211**, 173-187.

De La Rocha, C. L. and DePaolo, D. J., 2000. Isotopic Evidence for Variations in the Marine Calcium Cycle Over the Cenozoic. *Science* **289**, 1176-1178.

DeBond, N., Oakes, R. L., Paytan, A., and Wortmann, U. G., 2012. Early Aptian carbon and sulphur isotope signatures at ODP Site 765. *Isotopes in Environmental and Health Studies* **48**, 180-194.

Demicco, R. V., Lowenstein, T. K., Hardie, L. A., and Spencer, R. J., 2005. Model of seawater composition for the Phanerozoic. *Geology* **33**, 877-880.

DePaolo, D. J. and Ingram, B. L., 1985. High-Resolution Stratigraphy with Strontium Isotopes. *Science* **227**, 938-941.

Diener, A., Ebneth, S., Veizer, J., and Buhl, D., 1996. Strontium isotope stratigraphy of the Middle Devonian: Brachiopods and conodonts. *Geochim. Cosmochim. Acta* **60**, 639-652.

Ebneth, S., Diener, A., Buhl, D., and Veizer, J., 1997. Strontium isotope systematics of conodonts: Middle Devonian, Eifel Mountains, Germany. *Palaeogeography, Palaeoclimatology, Palaeoecology* **132**, 79-96.

Edmond, J. M., 1992. Himalayan Tectonics, Weathering Processes, and the Strontium Isotope Record in Marine Limestones. *Science* **258**, 1594-1597.

Eisenhauer, A., Böhm, F., Vollstaedt, H., Krabbenhöft, A., Liebetrau, V., Fietzke, J., Kisakürek, B., and Erez, J., 2011. Strontium isotope fractionation and its application in earth system sciences*Goldschmidt 2011*, Prague, Czech Republic.

Eisenhauer, A., Kisakürek, B., and Böhm, F., 2009. Marine Calcification: An Alkali Earth Metal Isotope Perspective. *ELEMENTS* **5**, 365-368.

Eisenhauer, A., Nägler, T. F., Stille, P., Kramers, J., Gussone, N., Bock, B., Fietzke, J., Hippler, D., and Schmitt, A.-D., 2004. Proposal for International Agreement on Ca Notation Resulting from Discussions at Workshops on Stable Isotope Measurements Held in Davos (Goldschmidt 2002) and Nice (EGS-AGU-EUG 2003). *Geostandards and Geoanalytical Research* **28**, 149-151.

Elderfield, H., 1986. Strontium Isotope Stratigraphy. *Paleogeogr. Paleoclimatol. Paleoecol.* **57**, 71-90.

Elderfield, H. and Schultz, A., 1996. Mid-ocean ridge hydrothermal fluxes and the chemical composition of the ocean. *Annu. Rev. Earth Planet. Sci.* **24**, 191-224.

Epstein, A. G., Epstein, J. B., and Harris, L. D., 1977. Conodont color alteration; an index to organic metamorphism. *USGS Professional Paper* **995**.

Fantle, M. S., 2010. Evaluating the Ca isotope proxy. *Am J Sci* **310**, 194-230.

Fantle, M. S. and DePaolo, D. J., 2005. Variations in the marine Ca cycle over the past 20 million years. *Earth Planet. Sci. Lett.* **237**, 102-117.

Fantle, M. S. and DePaolo, D. J., 2007. Ca isotopes in carbonate sediment and pore fluid from ODP Site 807A: The Ca^{2+}(aq)–calcite equilibrium fractionation factor and calcite recrystallization rates in Pleistocene sediments. *Geochim. Cosmochim. Acta* **71**, 2524-2546.

Farkaš, J., Böhm, F., Wallmann, K., Blenkinsop, J., Eisenhauer, A., van Geldern, R., Munnecke, A., Voigt, S., and Veizer, J., 2007a. Calcium isotope record of Phanerozoic oceans: Implications for chemical evolution of seawater and its causative mechanisms. *Geochim. Cosmochim. Acta* **71**, 5117-5134.

Farkaš, J., Buhl, D., Blenkinsop, J., and Veizer, J., 2007b. Evolution of the oceanic calcium cycle during the late Mesozoic: Evidence from $\delta^{44/40}$Ca of marine skeletal carbonates. *Earth Planet. Sci. Lett.* **253**, 96-111.

Faure, G. and Mensing, T. M., 2005. *Isotopes - Principles and applications*. John Wiley & Sons Inc., Hoboken, New Jersey.

Fietzke, J. and Eisenhauer, A., 2006. Determination of temperature-dependent stable strontium isotope (^{88}Sr/^{86}Sr) fractionation via bracketing standard MC-ICP-MS. *Geochem. Geophys. Geosyst.* **7**.

Frank, M., 2002. Radiogenic isotopes: Tracers of past ocean circulation and erosional input. *Rev. Geophys.* **40**, 1001.

Gaffin, S., 1987. Ridge volume dependence on sea-floor generation rate and inversion using long-term sealevel change. *Am. J. Sci.* **287**, 596-611.

Gaillardet, J., Dupré, B., Louvat, P., and Allègre, C. J., 1999. Global silicate weathering and CO_2 consumption rates deduced from the chemistry of large rivers. *Chem. Geol.* **159**, 3-30.

Galy, A., France-Lanord, C., and Derry, L. A., 1999. The strontium isotopic budget of Himalayan rivers in Nepal and Bangladesh. *Geochim. Cosmochim. Acta* **63**, 1905-1925.

Gorjan, P. and Kaiho, K., 2007. Correlation and comparison of seawater $\delta^{34}S_{CAS}$ records at the Permian-Triassic transition. *Chem. Geol.* **243**, 275-285.

Gradstein, F. M., Ogg, J. G., and Smith, A. G., 2005. *A Geologic Time Scale 2004*. Cambrudge University Press, Cambridge.

Griffith, E. M., Paytan, A., Caldeira, K., Bullen, T. D., and Thomas, E., 2008. A Dynamic Marine Calcium Cycle During the Past 28 Million Years. *Science* **322**, 1671-1674.

Gussone, N., Böhm, F., Eisenhauer, A., Dietzel, M., Heuser, A., Teichert, B. M. A., Reitner, J., Wörheide, G., and Dullo, W.-C., 2005. Calcium isotope fractionation in calcite and aragonite. *Geochim. Cosmochim. Acta* **69**, 4485-4494.

Gussone, N., Eisenhauer, A., Heuser, A., Dietzel, M., Bock, B., Böhm, F., Spero, H. J., Lea, D. W., Bijma, J., and Nägler, T. F., 2003. Model for kinetic effects on calcium isotope fractionation (δ^{44}Ca) in inorganic aragonite and cultured planktonic foraminifera. *Geochim. Cosmochim. Acta* **67**, 1375-1382.

Habicht, K. S. and Canfield, D. E., 1996. Sulphur isotope fractionation in modern microbial mats and the evolution of the sulphur cycle. *Nature* **382**, 342-343.

Hall, S. M. and Veizer, J., 1996. Geochemistry of Precambrian carbonates: VII. Belt supergroup, Montana and Idaho, USA. *Geochim. Cosmochim. Acta* **60**, 667-677.

Hansen, K. W. and Wallmann, K., 2003. Cretaceous and Cenozoic evolution of seawater composition, atmospheric O_2 and CO_2: A model perspective. *Am J Sci* **303**, 94-148.

Hardie, L. A., 1996. Secular variation in seawater chemistry: An explanation for the coupled secular variation in the mineralogies of marine limestones and potash evaporites over the past 600 m.y. *Geology* **24**, 279-283.

Harland, W. B., Armstrong, R. L., Cox, A. V., Craig, L. E., Smith, A. G., and Smith, D. G., 1990. A geologic time scale 1989. Cambridge University Press, Cambridge.

Hart, S. R., Erlank, A. J., and Kable, E. J. D., 1974. Sea floor basalt alteration: Some chemical and Sr isotopic effects. *Contributions to Mineralogy and Petrology* **44**, 219-230.

Hay, W. W., Migdisov, A., Balukhovsky, A. N., Wold, C. N., Flögel, S., and Söding, E., 2006. Evaporites and the salinity of the ocean during the Phanerozoic: Implications for climate, ocean circulation and life. *Palaeogeography, Palaeoclimatology, Palaeoecology* **240**, 3-46.

Heuser, A., Eisenhauer, A., Bohm, F., Wallmann, K., Gussone, N., Pearson, P. N., Nagler, T. F., and Dullo, W. C., 2005. Calcium isotope ($\delta^{44/40}$Ca) variations of Neogene planktonic foraminifera. *Paleoceanography* **20**, 13.

Hinojosa, J. L., Brown, S. T., Chen, J., DePaolo, D. J., Paytan, A., Shen, S.-z., and Payne, J. L., 2012. Evidence for end-Permian ocean acidification from calcium isotopes in biogenic apatite. *Geology*.

Hippler, D., Eisenhauer, A., and Nägler, T. F., 2006. Tropical Atlantic SST history inferred from Ca isotope thermometry over the last 140ka. *Geochim. Cosmochim. Acta* **70**, 90-100.

Hodell, D. A., Mead, G. A., and Mueller, P. A., 1990. Variation in the strontium isotopic composition of seawater (8 Ma to present) : Implications for chemical weathering rates and dissolved fluxes to the oceans. *Chemical Geology: Isotope Geoscience section* **80**, 291-307.

Hodell, D. A., Mueller, P. A., McKenzie, J. A., and Mead, G. A., 1989. Strontium isotope stratigraphy and geochemistry of the late Neogene ocean. *Earth Planet. Sci. Lett.* **92**, 165-178.

Hoefs, J., 2009. *Stable Isotope Geochemistry*. Springer-Verlag, Berlin Heidelberg.

Holland, H. D., 2010. The Geologic History of Seawater. In: Holland, H. D. and Turekian, K. K. Eds.), *Readings from the Treatise of Geochemistry*. Elsevier.

Hönisch, B., Bickert, T., and Hemming, N. G., 2008. Modern and Pleistocene boron isotope composition of the benthic foraminifer Cibicidoides wuellerstorfi. *Earth Planet. Sci. Lett.* **272**, 309-318.

Horita, J., Zimmermann, H., and Holland, H. D., 2002. Chemical evolution of seawater during the Phanerozoic: Implications from the record of marine evaporites. *Geochim. Cosmochim. Acta* **66**, 3733-3756.

Isozaki, Y., 1997. Permo-Triassic boundary superanoxia and stratified superocean: Records from lost deep sea. *Science* **276**, 235-238.

Jenkyns, H. C., 2010. Geochemistry of oceanic anoxic events. *Geochem. Geophys. Geosyst.* **11**, Q03004.

Joachimski, M. M., Simon, L., van Geldern, R., and Lécuyer, C., 2005. Boron isotope geochemistry of Paleozoic brachiopod calcite: Implications for a secular change in the boron isotope geochemistry of seawater over the Phanerozoic. *Geochim. Cosmochim. Acta* **69**, 4035-4044.

Joachimski, M. M., van Geldern, R., Breisig, S., Buggisch, W., and Day, J., 2004. Oxygen isotope evolution of biogenic calcite and apatite during the Middle and Late Devonian. *International Journal of Earth Sciences* **93**, 542-553.

Jones, C. E., Jenkyns, H. C., Coe, A. L., and Stephen, H. P., 1994. Strontium isotopic variations in Jurassic and Cretaceous seawater. *Geochim. Cosmochim. Acta* **58**, 3061-3074.

Kampschulte, A. and Strauss, H., 2004. The sulfur isotopic evolution of Phanerozoic seawater based on the analysis of structurally substituted sulfate in carbonates. *Chem. Geol.* **204**, 255-286.

Karhu, J. and Epstein, S., 1986. The implication of the oxygen isotope records in coexisting cherts and phosphates. *Geochim. Cosmochim. Acta* **50**, 1745-1756.

Kasemann, S. A., Hawkesworth, C. J., Prave, A. R., Fallick, A. E., and Pearson, P. N., 2005. Boron and calcium isotope composition in Neoproterozoic carbonate rocks from Namibia: evidence for extreme environmental change. *Earth Planet. Sci. Lett.* **231**, 73-86.

Knauth, L. P. and Epstein, S., 1976. Hydrogen and oxygen isotope ratios in nodular and bedded cherts. *Geochim. Cosmochim. Acta* **40**, 1095-1108.

Kolodny, Y. and Epstein, S., 1976. Stable isotope geochemistry of deep sea cherts. *Geochim. Cosmochim. Acta* **40**, 1195-1209.

Korte, C. and Kozur, H. W., 2010. Carbon-isotope stratigraphy across the Permian-Triassic boundary: A review. *Journal of Asian Earth Sciences* **39**, 215-235.

Korte, C., Kozur, H. W., Bruckschen, P., and Veizer, J., 2003. Strontium isotope evolution of Late Permian and Triassic seawater. *Geochim. Cosmochim. Acta* **67**, 47-62.

Kozur, H. W. and Weems, R. E., 2011. Detailed correlation and age of continental late Changhsingian and earliest Triassic beds: Implications for the role of the Siberian Trap in the Permian-Triassic biotic crisis. *Palaeogeography, Palaeoclimatology, Palaeoecology* **308**, 22-40.

Krabbenhöft, A., Eisenhauer, A., Böhm, F., Vollstaedt, H., Fietzke, J., Liebetrau, V., Augustin, N., Peucker-Ehrenbrink, B., Hansen, B. T., Nolte, N., and Wallmann, K., 2010. Constraining the marine strontium budget with natural strontium isotope fractionations ($^{87}Sr/^{86}Sr^{*}$-$\delta^{88/86}Sr$) of carbonates, hydrothermal solutions and river waters. *Geochim. Cosmochim. Acta* **74**, 4097-4109.

Krabbenhöft, A., Fietzke, J., Eisenhauer, A., Liebetrau, V., Böhm, F., and Vollstaedt, H., 2009. Determination of radiogenic and stable strontium isotope ratios ($^{87}Sr/^{86}Sr$; $\delta^{88/86}Sr$) by thermal ionization mass spectrometry applying an $^{87}Sr/^{84}Sr$ double spike. *J. Anal. At. Spectrom.* **24**, 1267-1271.

Kramm, U. and Wedepohl, K. H., 1991. The isotopic composition of strontium and sulfur in seawater of Late Permian (Zechstein) age. *Chem. Geol.* **90**, 253-262.

Kump, L. R. and Arthur, M. A., 1999. Interpreting carbon-isotope excursions: carbonates and organic matter. *Chem. Geol.* **161**, 181-198.

Lear, C. H., Elderfield, H., and Wilson, P. A., 2003. A Cenozoic seawater Sr/Ca record from benthic foraminiferal calcite and its application in determining global weathering fluxes. *Earth Planet. Sci. Lett.* **208**, 69-84.

Lemarchand, D., Gaillardet, J., Lewin, E., and Allègre, C. J., 2000. The influence of rivers on marine boron isotopes and implications for reconstructing past ocean pH. *Nature* **408**, 951-954.

Lowenstein, T. K., Timofeeff, M. N., Brennan, S. T., Hardie, L. A., and Demicco, R. V., 2001. Oscillations in Phanerozoic Seawater Chemistry: Evidence from Fluid Inclusions. *Science* **294**, 1086-1088.

Lowenstein, T. K., Timofeeff, M. N., Kovalevych, V. M., and Horita, J., 2005. The major-ion composition of Permian seawater. *Geochim. Cosmochim. Acta* **69**, 1701-1719.

Lu, Z., Jenkyns, H. C., and Rickaby, R. E. M., 2010. Iodine to calcium ratios in marine carbonate as a paleo-redox proxy during oceanic anoxic events. *Geology* **38**, 1107-1110.

McArthur, J. M., 1994. Recent Trends in Strontium Isotope Stratigraphy. *Terr. Nova* **6**, 331-358.

McArthur, J. M., Howarth, R. J., and Bailey, T. R., 2001. Strontium Isotope Stratigraphy: LOWESS version 3: Best fit to the marine Sr-isotope curve for 0-509 Ma and accompanying look-up table for deriving numerical age. *The Journal of Geology* **109**, 155-170.

McCulloch, M., Trotter, J., Montagna, P., Falter, J., Dunbar, R., Freiwald, A., Försterra, G., López Correa, M., Maier, C., Rüggeberg, A., and Taviani, M., 2012. Resilience of cold-water scleractinian corals to ocean acidification: Boron isotopic systematics of pH and saturation state up-regulation. *Geochim. Cosmochim. Acta* **87**, 21-34.

Mirota, M. D. and Veizer, J., 1994. Geochemistry of precambrian carbonates: VI. Aphebian albanel formations, Quebec, Canada. *Geochim. Cosmochim. Acta* **58**, 1735-1745.

Misra, S. and Froelich, P. N., 2012. Lithium Isotope History of Cenozoic Seawater: Changes in Silicate Weathering and Reverse Weathering. *Science* **335**, 818-823.

Morse, J. W., Arvidson, R. S., and Luttge, A., 2007. Calcium Carbonate Formation and Dissolution. *Chemical Reviews* **107**, 342-381.

Nägler, T. F., Eisenhauer, A., Müller, A., Hemleben, C., and Kramers, J., 2000. The δ^{44}Ca-temperature calibration on fossil and cultured Globigerinoides sacculifer: New tool for reconstruction of past sea surface temperatures. *Geochem. Geophys. Geosyst.* **1**.

Nakai, N. and Jensen, M. L., 1964. The kinetic isotope effect in the bacterial reduction and oxidation of sulfur. *Geochim. Cosmochim. Acta* **28**, 1893-1912.

Ogg, J. G., Ogg, G., and Gradstein, F. M., 2008. *The concise geologic time scale*. Cambridge University Press.

Palmer, M. R. and Edmond, J. M., 1989. The strontium isotope budget of the modern ocean. *Earth Planet. Sci. Lett.* **92**, 11-26.

Payne, J. L., Turchyn, A. V., Paytan, A., DePaolo, D. J., Lehrmann, D. J., Yu, M., and Wei, J., 2010. Calcium isotope constraints on the end-Permian mass extinction. *Proceedings of the National Academy of Sciences* **107**, 8543-8548.

Paytan, A., Kastner, M., Martin, E. E., Macdougall, J. D., and Herbert, T., 1993. Marine barite as a monitor of seawater strontium isotope composition. *Nature* **366**, 445-449.

Peterman, Z. E., Hedge, C. E., and Tourtelot, H. A., 1970. Isotopic composition of strontium in sea water throughout Phanerozoic time. *Geochim. Cosmochim. Acta* **34**, 105-120.

Peucker-Ehrenbrink, B. and Ravizza, G., 2000. The marine osmium isotope record. *Terr. Nova* **12**, 205-219.

Prokoph, A., Shields, G. A., and Veizer, J., 2008. Compilation and time-series analysis of a marine carbonate δ^{18}O, δ^{13}C, ^{87}Sr/^{86}Sr and δ^{34}S database through Earth history. *Earth-Science Reviews* **87**, 113-133.

Rae, J. W. B., Foster, G. L., Schmidt, D. N., and Elliott, T., 2011. Boron isotopes and B/Ca in benthic foraminifera: Proxies for the deep ocean carbonate system. *Earth Planet. Sci. Lett.* **302**, 403-413.

Ries, J. B., 2010. Review: geological and experimental evidence for secular variation in seawater Mg/Ca (calcite-aragonite seas) and its effects on marine biological calcification. *Biogeosciences* **7**, 2795-2849.

Rose-Koga, E. F. and Albarède, F., 2010. A data brief on magnesium isotope compositions of marine calcareous sediments and ferromanganese nodules. *Geochem. Geophys. Geosyst.* **11**, Q03006.

Rosenthal, Y., 2007. Elemental Proxies for Reconstructing Cenozoic Seawater Paleotemperatures from Calcareous Fossils. In: Hillaire-Marcel, C. and A., D. V. Eds.), *Proxies in Late Cenozoic Paleoceanography*. Elsevier.

Rothman, D. H., 2002. Atmospheric carbon dioxide levels for the last 500 million years. *Proceedings of the National Academy of Sciences* **99**, 4167-4171.

Rowley, D. B., 2002. Rate of plate creation and destruction: 180 Ma to present. *Geol. Soc. Am. Bull.* **114**, 927-933.

Royer, D. L., 2006. CO_2-forced climate thresholds during the Phanerozoic. *Geochim. Cosmochim. Acta* **70**, 5665-5675.

Royer, D. L., Berner, R. A., and Park, J., 2007. Climate sensitivity constrained by CO_2 concentrations over the past 420 million years. *Nature* **446**, 530-532.

Rüggeberg, A., Fietzke, J., Liebetrau, V., Eisenhauer, A., Dullo, W.-C., and Freiwald, A., 2008. Stable strontium isotopes ($\delta^{88/86}$Sr) in cold-water corals - A new proxy for reconstruction of intermediate ocean water temperatures. *Earth Planet. Sci. Lett.* **269**, 570-575.

Sandberg, P. A., 1983. An oscillating trend in Phanerozoic non-skeletal carbonate mineralogy. *Nature* **305**, 19-22.

Schneider, S., Fürsich, F., and Werner, W., 2009. Sr-isotope stratigraphy of the Upper Jurassic of central Portugal (Lusitanian Basin) based on oyster shells. *International Journal of Earth Sciences* **98**, 1949-1970.

Shields, G. and Veizer, J., 2002. Precambrian marine carbonate isotope database: Version 1.1. *Geochem. Geophys. Geosyst.* **3**, 1031.

Smalley, P. C., Higgins, A. C., Howarth, R. J., Nicholson, H., Jones, C. E., Swinburne, N. H. M., and Bessa, J., 1994. Seawater Sr Isotope Variations through Time - a Procedure for Constructing a Reference Curve to Date and Correlate Marine Sedimentary-Rocks. *Geology* **22**, 431-434.

Spooner, E. T. C., 1976. The strontium isotopic composition of seawater, and seawater-oceanic crust interaction. *Earth Planet. Sci. Lett.* **31**, 167-174.

Stanley, S. M., 2001. *Historische Geologie*. Spektrum Akademischer Verlag, Heidelberg, Berlin.

Stanley, S. M. and Hardie, L. A., 1998. Secular oscillations in the carbonate mineralogy of reef-building and sediment-producing organisms driven by tectonically forced shifts in seawater chemistry. *Palaeogeography, Palaeoclimatology, Palaeoecology* **144**, 3-19.

Steuber, T. and Veizer, J., 2002. Phanerozoic record of plate tectonic control of seawater chemistry and carbonate sedimentation. *Geology* **30**, 1123-1126.

Stoll, H. M., Schrag, D. P., and Clemens, S. C., 1999. Are seawater Sr/Ca variations preserved in quaternary foraminifera? *Geochim. Cosmochim. Acta* **63**, 3535-3547.

Turchyn, A. V., Schrag, D. P., Coccioni, R., and Montanari, A., 2009. Stable isotope analysis of the Cretaceous sulfur cycle. *Earth Planet. Sci. Lett.* **285**, 115-123.

Vance, D., Teagle, D. A. H., and Foster, G. L., 2009. Variable Quaternary chemical weathering fluxes and imbalances in marine geochemical budgets. *Nature* **458**, 493-496.

Veizer, J., 1989. Strontium Isotopes in Seawater through Time. *Annu. Rev. Earth Planet. Sci.* **17**, 141-167.

Veizer, J., Ala, D., Azmy, K., Bruckschen, P., Buhl, D., Bruhn, F., Carden, G. A. F., Diener, A., Ebneth, S., Godderis, Y., Jasper, T., Korte, C., Pawellek, F., Podlaha, O. G., and Strauss, H., 1999. $^{87}Sr/^{86}Sr$, $\delta^{13}C$ and $\delta^{18}O$ evolution of Phanerozoic seawater. *Chem. Geol.* **161**, 59-88.

Veizer, J., Buhl, D., Diener, A., Ebneth, S., Podlaha, O. G., Bruckschen, P., Jasper, T., Korte, C., Schaaf, M., Ala, D., and Azmy, K., 1997. Strontium isotope stratigraphy: potential resolution and event correlation. *Paleogeogr. Paleoclimatol. Paleoecol.* **132**, 65-77.

Veizer, J., Clayton, R. N., and Hinton, R. W., 1992. Geochemistry of precambrian carbonates: IV. Early paleoproterozoic (2.25 ± 0.25 ga) seawater. *Geochim. Cosmochim. Acta* **56**, 875-885.

Veizer, J., Clayton, R. N., Hlnton, R. W., Von Brunn, V., Mason, T. R., Buck, S. G., and Hoefs, J., 1990. Geochemistry of Precambrian carbonates: 3-shelf seas and non-marine environments of the Archean. *Geochim. Cosmochim. Acta* **54**, 2717-2729.

Veizer, J. and Compston, W., 1976. $^{87}Sr/^{86}Sr$ in Precambrian carbonates as an index of crustal evolution. *Geochim. Cosmochim. Acta* **40**, 905-914.

Veizer, J., Compston, W., Clauer, N., and Schidlowski, M., 1983. in Late Proterozoic carbonates: evidence for a "mantle" event at ~900 Ma ago. *Geochim. Cosmochim. Acta* **47**, 295-302.

Veizer, J., Godderis, Y., and Francois, L. M., 2000. Evidence for decoupling of atmospheric CO_2 and global climate during the Phanerozoic eon. *Nature* **408**, 698-701.

Veizer, J., Hoefs, J., Lowe, D. R., and Thurston, P. C., 1989a. Geochemistry of Precambrian carbonates: II. Archean greenstone belts and Archean sea water. *Geochim. Cosmochim. Acta* **53**, 859-871.

Veizer, J., Hoefs, J., Ridler, R. H., Jensen, L. S., and Lowe, D. R., 1989b. Geochemistry of Precambrian carbonates: I. Archean hydrothermal systems. *Geochim. Cosmochim. Acta* **53**, 845-857.

Veizer, J. and Mackenzie, F. T., 2010. Evolution of Sedimentary Rocks. In: Holland, H. D. and Turekian, K. K. Eds.), *Readings from the Treatise of Geochemistry*. Elsevier.

Voegelin, A. R., Nägler, T. F., Samankassou, E., and Villa, I. M., 2009. Molybdenum isotopic composition of modern and Carboniferous carbonates. *Chem. Geol.* **265**, 488-498.

Walker, J. C. G., 1986. Global geochemical cycles of carbon, sulfur and oxygen. *Marine Geology* **70**, 159-174.

Wallmann, K., 2001a. Controls on the cretaceous and cenozoic evolution of seawater composition, atmospheric CO_2 and climate. *Geochim. Cosmochim. Acta* **65**, 3005-3025.

Wallmann, K., 2001b. The geological water cycle and the evolution of marine $\delta^{18}O$ values. *Geochim. Cosmochim. Acta* **65**, 2469-2485.

Wallmann, K., 2004. Impact of atmospheric CO_2 and galactic cosmic radiation on Phanerozoic climate change and the marine $\delta^{18}O$ record. *Geochem. Geophys. Geosyst.* **5**.

Walther, B. D. and Thorrold, S. R., 2006. Water, not food, contributes the majority of strontium and barium deposited in the otoliths of a marine fish. *Marine Ecology Progress Series* **311**, 125-130.

Wenzel, B., Lécuyer, C., and Joachimski, M. M., 2000. Comparing oxygen isotope records of silurian calcite and phosphate $\delta^{18}O$ compositions of brachiopods and conodonts. *Geochim. Cosmochim. Acta* **64**, 1859-1872.

Young, S. A., Saltzman, M. R., Foland, K. A., Linder, J. S., and Kump, L. R., 2009. A major drop in seawater $^{87}Sr/^{86}Sr$ during the Middle Ordovician (Darriwilian): Links to volcanism and climate? *Geology* **37**, 951-954.

Zhou, L., Gao, S., Chris, H., Corey, A., and Xie, S., 2009. Preliminary Mo isotope data of Phanerozoic clastic sediments from the northern margin of the Yangtze block and its implication for paleoenvironmental conditions. *Chinese Science Bulletin* **54**, 822-829.

Zhu, P. and Macdougall, J. D., 1998. Calcium isotopes in the marine environment and the oceanic calcium cycle. *Geochim. Cosmochim. Acta* **62**, 1691-1698.

II. Chapter

Determination of radiogenic and stable strontium isotope ratios ($^{87}Sr/^{86}Sr$, $\delta^{88/86}Sr$) by thermal ionization mass spectrometry applying an $^{87}Sr/^{84}Sr$ double spike

Andre Krabbenhöft[ab], Jan Fietzke[a], Anton Eisenhauer[a], Volker Liebetrau[a], Florian Böhm[a] and Hauke Vollstaedt[a]

[a] *Wischhofstraße 1-3, D-24148 Kiel, Germany. Tel: +49-(0)431-600-2109;*

[b] *corresponding author (andre.krabbenhoeft@tesa.com)*

Published in *Journal of Analytical Atomic Spectrometry* 74 (2009), 1267-1271

Abstract

Recent findings of natural strontium isotope fractionation have opened a new field of research in non-traditional stable isotope geochemistry. While previous studies were based on data obtained by MC-ICP-MS we here present a novel approach combining thermal ionization mass spectrometry (TIMS) with the use of an $^{87}Sr/^{84}Sr$ double spike (DS). Our results for the IAPSO sea water and JCp-1 coral standards, respectively, are in accord with previously published data. Strontium isotope composition of IAPSO sea water standard was determined as $\delta^{88/86}Sr=0.386(5)‰$ (δ values relative to the SRM987), $^{87}Sr/^{86}Sr^*=0.709312(9)$ n=10 and a corresponding conventionally normalized $^{87}Sr/^{86}Sr=0.709168(7)$ (all uncertainties 2SEM). For JCp-1 coral standard we obtained $\delta^{88/86}Sr=0.197(8)‰$, $^{87}Sr/^{86}Sr^*=0.709237(2)$ and $^{87}Sr/^{86}Sr=0.709164(5)$ n=3. We show that applying this DS-TIMS method the precision is improved by at least a factor of 2 - 3 when compared to MC-ICP-MS.

II.1. Introduction

The Rubidium/Strontium (Rb/Sr) radiogenic isotope system is one of the oldest isotopic applications measured by mass-spectrometry (NIER, 1938; NIER, 1940; PAPANASTASSIOU and WASSERBURG, 1973) and probably the most frequently applied one for absolute and stratigraphic age dating as well as for provenance studies (GOLDSTEIN and JACOBSEN, 1988; TÜTKEN et al., 2002). Thermal ionization mass spectrometry (TIMS) or alternatively multi-collector-inductively-coupled-plasma-mass-spectrometry (MC-ICP-MS) are the common methods in order to determine the radiogenic in-growth and variations of $^{87}Sr/^{86}Sr$ from the radioactive beta minus decay of ^{87}Rb to ^{87}Sr via a half-live of about 48 billion years. TIMS and MC-ICP-MS based Sr isotope measurements usually provide an external reproducibility of ~10 to ~15 ppm because during the mass-spectrometer runs any fluctuation of the $^{87}Sr/^{86}Sr$-ratio due to mass and temperature dependent isotope fractionation is normalized and corrected relative to the commonly accepted $^{86}Sr/^{88}Sr$-ratio of 0.1194 (NIER, 1938). Following this procedure only the radiogenic in-growth of the $^{87}Sr/^{86}Sr$ can be determined whereas any other variation due to equilibrium or kinetic isotope fractionation is invisible and cannot be used to constrain additional geochemical information.

Recent studies applying the MC-ICP-MS combined with the bracketing standard method (FIETZKE and EISENHAUER, 2006; HALICZ et al., 2008; OHNO and HIRATA, 2007; RÜGGEBERG et al., 2008) showed that the $^{88}Sr/^{86}Sr$-ratio of seawater ($\delta^{88/86}Sr$~0.381‰) significantly deviates from the $^{88}Sr/^{86}Sr$-ratio of SRM987 (per definition $\delta^{88/86}Sr=0$). In the same study (FIETZKE and EISENHAUER, 2006) it was also found that $\delta^{88/86}Sr$ values of marine and artificially precipitated calcium carbonates show a temperature controlled isotopic difference of 0.17 to 0.36‰ between the carbonate precipitates and the bulk solution, with the carbonates isotopically lighter than the seawater. Either one or both major sources for Sr to the ocean (hydrothermal sources and continental weathering) must be fractionated relative to the SRM987.

Although bracketing standard is a suitable method to determine simultaneous natural fractionation of $^{87}Sr/^{86}Sr$ and $\delta^{88/86}Sr$, it can be assumed that TIMS in combination with a double-spike (DS-TIMS) may provide even higher precision and accuracy. So far MC-ICP-MS methods were burdened with the problem of potential fractionation during ion chromatographic Sr separation and the sensitivity for matrix effects during the ICP-MS measurements (FIETZKE and EISENHAUER, 2006; HALICZ et al., 2008; OHNO and HIRATA, 2007; RÜGGEBERG et al., 2008; YANG et al., 2008). Both problems can be overcome by the use of an appropriate double spike.

Sr double spikes have already successfully been used in order to determine Sr isotope values for the early solar system (PATCHETT, 1980a; PATCHETT, 1980b). The application of a Sr double spike follows earlier attempts in the Pb-isotope analytic where double spikes have been used in the sixties of the last century (COMPSTON and OVERSPY, 1969) with recent progress in application induced by the pioneering work of Galer (GALER, 1999). In order to use a DS for Sr isotope analysis at least two isotope measurements have to be performed. One unspiked run (ic-run, isotope composition) and one run with the double spike added to the sample solution (id-run, isotope dilution). Data reduction and the simultaneous calculation of $^{87}Sr/^{86}Sr^*$- ($^{87}Sr/^{86}Sr^*$=fractionated $^{87}Sr/^{86}Sr$ ratio from our spike correction algorithm) and $\delta^{88/86}Sr$ can be performed following certain numerical procedures previously designed for Pb (COMPSTON and OVERSPY, 1969) and Ca isotope analysis (HEUSER et al., 2002).

Here we present the application of a $^{87}Sr/^{84}Sr$ double spike for the simultaneous determination of $^{87}Sr/^{86}Sr^*$ and $\delta^{88/86}Sr$, respectively. The results of earlier studies could be reproduced with higher external precision (FIETZKE and EISENHAUER, 2006; HALICZ et al., 2008).

II.2. Experimental methods and TIMS measurement

$^{87}Sr/^{84}Sr$-double spike preparation

In order to prepare an $^{87}Sr/^{84}Sr$ spike solution we purchased two Sr-cabonates enriched in ^{84}Sr and in ^{87}Sr, respectively, from Oak Ridge National Laboratory, USA with a certified isotopic compositions given in Tab. II.1. The abundance of interfering ^{87}Rb was reported to be less than 1 ppm in the ^{84}Sr solution and less than 56 ppm in the ^{87}Sr solution. In order to reach the anticipated $^{87}Sr/^{84}Sr$-ratio of ~1 we mixed the two solutions in a way that the mixture consists of 48% of the ^{87}Sr-solution and 52% of the ^{84}Sr-solution, respectively.

With the given abundances of Sr isotopes in the two solutions we calculated theoretical values for $^{86}Sr/^{84}Sr$-, $^{87}Sr/^{84}Sr$- and $^{88}Sr/^{84}Sr$-ratios of the desired $^{87}Sr/^{84}Sr$ spike solution. These values were used as start values for the calibration of the spike relative to the SRM987 $SrCO_3$ standard from the National Institute of Standards and Technology (NIST) as described below.

TIMS multicollector measurement procedure

Sr was extracted from all samples by using standard ion chromatographic procedure (Tab. II.2). Prior to the TIMS measurements the solutions were evaporated to dryness and redissolved in 2 µL H_3PO_4. For TIMS measurements rhenium ribbon single filaments are used in combination with a Ta_2O_5-activator which stabilizes the signal and enhances the ionization rate. About 2 µL of the Ta_2O_5-activator solution is first added on the filament and heated to near dryness at a current of about 0.5 A. Then 2 µL of the sample solution containing 250 to 500 ng Strontium were added to the activator solution and heated to dryness at a current of 1 A. Finally we increased the current to a value of 1.6 A and kept it there for about one minute until the sample color turned into a light brown. The last step in this procedure was to heat up the filament until a light red glow was visible. The current was

kept at this setting for about 20 to 30 seconds. For the measurements of the SRM987 no column chemistry was necessary because of the negligible amounts of interfering ^{87}Rb in the standard material. Nevertheless aliquots of SRM987 standard material were also separated by the above mentioned ion exchange method showing no significant deviation from the untreated material.

Sr isotope measurements were carried out at the IFM-GEOMAR mass spectrometer facilities in Kiel, Germany, using a TRITON mass spectrometer (ThermoFisher, Bremen, Germany) which operates in positive ionization mode with a 10 kV acceleration voltage and 10^{11} Ω resistors for the Faraday cups. The instrument is equipped with nine moveable Faraday cups as detection system which account for the dispersion of the whole Sr isotope mass range from ~84 to 88 amu, respectively.

Mass 85 is measured in order to monitor the interfering ^{87}Rb. Prior to each measurement session a gain calibration of all amplifiers was carried out. Measurement started with a heatup-sequence (pyrometer controlled) heating up the filament by increasing the current to 2.6 A (ramping velocity of 0.5 A/min). The final current usually corresponds to a temperature of ~1380 °C. The ion beam was then automatically focused (including wheel focus) and peak centering was performed. Then the filament was slowly (0.05 A/min) heated up to ~3.2 A corresponding to a temperature of ~1430 to 1490 °C. When the signal intensity reached 6 V on mass 88, data acquisition was started. 14 scans with 17 seconds integration time and 3 seconds idle time eachare summarized to one block. For each sample 9 blocks corresponding to 126 scans were measured. Before each block the baseline (deflected beam) was recorded and the amplifier rotation was performed.

Applying the double spike technique at least two separate runs for one measurement are necessary: one ic-run and one id-run where the $^{86}Sr/^{84}Sr$-, $^{87}Sr/^{84}Sr$- and $^{88}Sr/^{84}Sr$-ratios are determined. To correct for isotope fractionation during TIMS measurement the $^{86}Sr/^{84}Sr$,

$^{87}Sr/^{84}Sr$ and the $^{88}Sr/^{84}Sr$-ratios are normalized to the mean of the first block of the $^{87}Sr/^{84}Sr$ isotope ratio.

Double spike algorithm

The mean of the measured and normalized $^{86}Sr/^{84}Sr$-, $^{87}Sr/^{84}Sr$- and $^{88}Sr/^{84}Sr$-ratio of the two ic-runs are taken as start values for the spike correction algorithm (Fig.II.1).

The results of the id-runs need to be denormalized and corrected for the added DS. In order to decompose the sample/spike mixture we used an iterative routine closely following the one presented earlier for Ca-isotopes (HEUSER et al., 2002) based on the classical isotope dilution equation and on an similar algorithm presented earlier for Pb isotopes (COMPSTON and OVERSPY, 1969). The algorithm starts with the calculation of the sample to spike ratio ($Q_{86}(84)=Q_{88}(84)=^{84}Sr_{sample}/^{84}Sr_{spike}$) from the measured $^{86}Sr/^{84}Sr$ ($Q_{86}(84)$) and $^{88}Sr/^{84}Sr$ ($Q_{88}(84)$) ratios and their corresponding values of the id- and ic-run (Eqs. 11 and 12 in Fig.II.1). Although the approximation of $^{84}Sr_{sample}/^{84}Sr_{spike}$ from $Q_{86}(84)$ and $Q_{88}(84)$ are supposed to be identical they differ to a certain extend prior to the denormalization procedure. The $^{87}Sr/^{84}Sr_{calc}$ (Eq. 1) can be calculated from the $^{87}Sr/^{84}Sr$-ratio of the ic-run and the $^{87}Sr/^{84}Sr$-ratio of the spike as well as from the mean of Q86(84) and Q88(84) in Eq. 13, respectively. Comparison of $^{87}Sr/^{84}Sr_{calc}$ and $^{87}Sr/^{84}Sr_{meas}$ in Eq. 2 then allows the calculation of a fractionation factor ß which is used to denormalize the $^{86}Sr/^{84}Sr$ and $^{88}Sr/^{84}Sr$-ratios in Eq.3 and 4, respectively. A first approximate $^{88}Sr/^{86}Sr$-ratio can then be determined by a comparison of $^{88}Sr/^{84}Sr_{calc}$ and $^{86}Sr/^{84}Sr_{calc}$ (Eq. 5), respectively. From Q_{86} (Eq. 6) and $^{88}Sr/^{86}Sr_{calc}$ a new $^{88}Sr/^{86}Sr$ is determined (Eq. 7) which is then used for iterative calculation of an improved Sr isotope fractionation factor ($ß_{new}$). This $ß_{new}$ allows us to calculate new start values for the algorithm (Eq. 9 and 10). They again are used to simultaneously calculate $Q_{86}(84)$ and $Q_{88}(84)$. The algorithm usually needs ~20 iterative steps in order to meet the stop

criteria being the difference of $Q_{86}(84)$ and $Q_{88}(84)$ smaller than $1 \cdot 10^{-17}$. Latter stop criteria guarantees that $ß_{new}$ becomes zero.

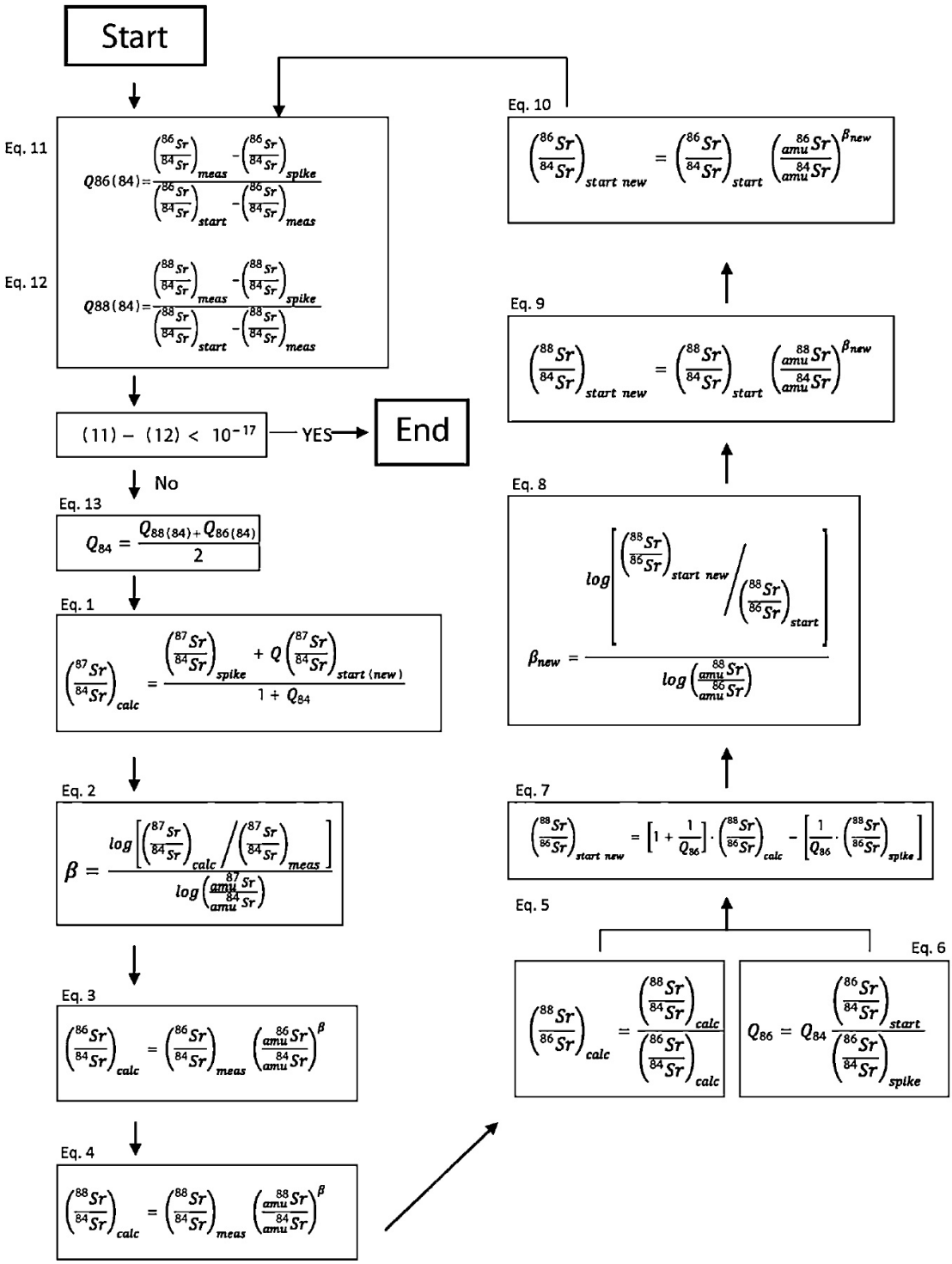

Figure II.1 - Flow Chart of the Sr-double spike algorithm applied in order to denormalize measured 88Sr/86Sr and 87Sr/86Sr data and to calculate paired 87Sr/86Sr*-δ88/86Sr values. Usually about 20 cycles are necessary in order to achieve the desired precision.

The $^{88}Sr/^{86}Sr$-ratios are reported in the common δ-notation. The session offset corrected $^{88}Sr/^{86}Sr$-ratios are normalized to the accepted value $^{88}Sr/^{86}Sr=8.375209$ and reported in the usual δ-notation (Eq. II.1) as defined earlier (FIETZKE and EISENHAUER, 2006).

$$\delta^{88/86}Sr_{sample} = \left(\frac{\left(\frac{^{88}Sr}{^{86}Sr} \right)_{sample}}{\left(\frac{^{88}Sr}{^{86}Sr} \right)_{SRM\,987}} - 1 \right) \times 1000 \qquad [II.1]$$

II.3. Results

Spike calibration

In order to perform double spike calibration measurements we used two different Sr standards: (1) NIST SRM987 and (2) the international seawater standard IAPSO. The first one was needed to calibrate the double spike and worked as a general reference standard for all of our measurements. The second standard has a known offset to the SRM987 in its $\delta^{88/86}Sr$-value of ~0.381(10)‰ and serves as an independent control point (FIETZKE and EISENHAUER, 2006). For calibration and spike optimization the SRM987 standard solutions were spiked with different amounts in order to produce solutions with $^{84}Sr_{spike}/^{84}Sr_{sample}$ ratios in a range from 5 to 30. The calculated spike isotope ratios using the certified isotope compositions of the enriched solutions (Tab. II.1) produced results showing that the $\delta^{88/86}Sr$ values vary with the $^{84}Sr_{spike}/^{84}Sr_{sample}$-ratio (Fig. II.2).

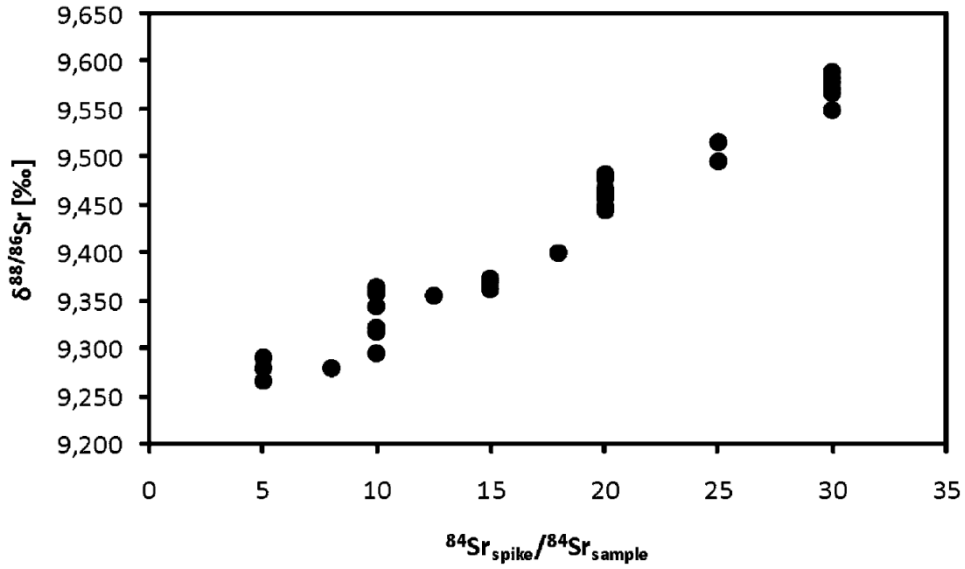

FIGURE II.2 - The SRM987 standard solutions were spiked with different amounts of spike in order to produce solutions with $^{84}Sr_{sample}/^{84}Sr_{spike}$ ratios in a range from 5 to 30. We observed that the measured $\delta^{88/86}Sr$ values are positively correlated with the $^{84}Sr_{spike}/^{84}Sr_{sample}$-ratio when using the spike isotope ratios for $^{86}Sr/^{84}Sr$, $^{87}Sr/^{84}Sr$ and $^{88}Sr/^{84}Sr$ as calculated from the reported certified values.

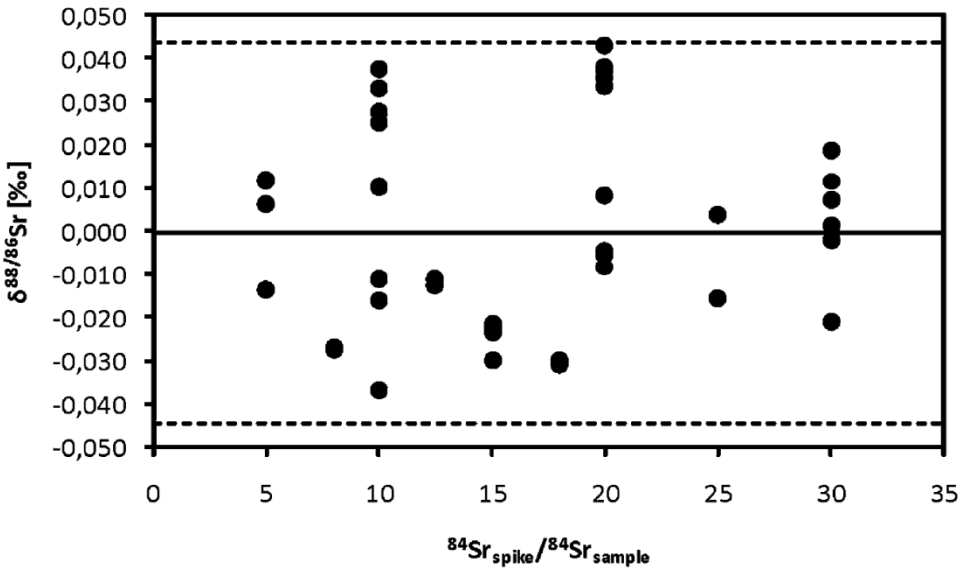

FIGURE II.3 - After optimization of the spike ratios there is no further dependency of the $\delta^{88/86}Sr$ from the $^{84}Sr_{spike}/^{84}Sr_{sample}$ -ratio. The black line marks the average value of ~0 and the broken line the ±2SD standard deviation from the defined value.

This is a consequence of the deviation of the calculated spike values from the real composition. In order to extract the real composition and for an optimization procedure we generated the least square sum of all measured $\delta^{88/86}Sr$ values of SRM987 and minimized it by slightly varying the spike isotope ratios using a least square fit which was performed with

the solver function of Microsoft Excel®. After this optimization procedure no further dependency of the $\delta^{88/86}Sr$ on the $^{84}Sr_{spike}/^{84}Sr_{sample}$ ratio could be found (Fig. II.3). Latter values are then assumed to be the best approximation of the "true" Sr double spike composition as presented in Tab. II.3. During the course of the double spike calibration ~40 measurements of SRM987 standard with varying $^{84}Sr_{spike}/^{84}Sr_{sample}$ ratios have been performed. The typical internal precision of the single measurements was ±7 ppm (RSD) for the $^{86}Sr/^{84}Sr$-ratio and 9 ppm for the $^{88}Sr/^{84}Sr$-ratio in the ic-runs. We measured ±11 ppm (RSD) for the $^{86}Sr/^{84}Sr$-ratio and 21 ppm for the $^{88}Sr/^{84}Sr$-ratio in the id-run. The internal precision correlates with the $^{84}Sr_{spike}/^{84}Sr_{sample}$-ratio.

Results of standard measurements

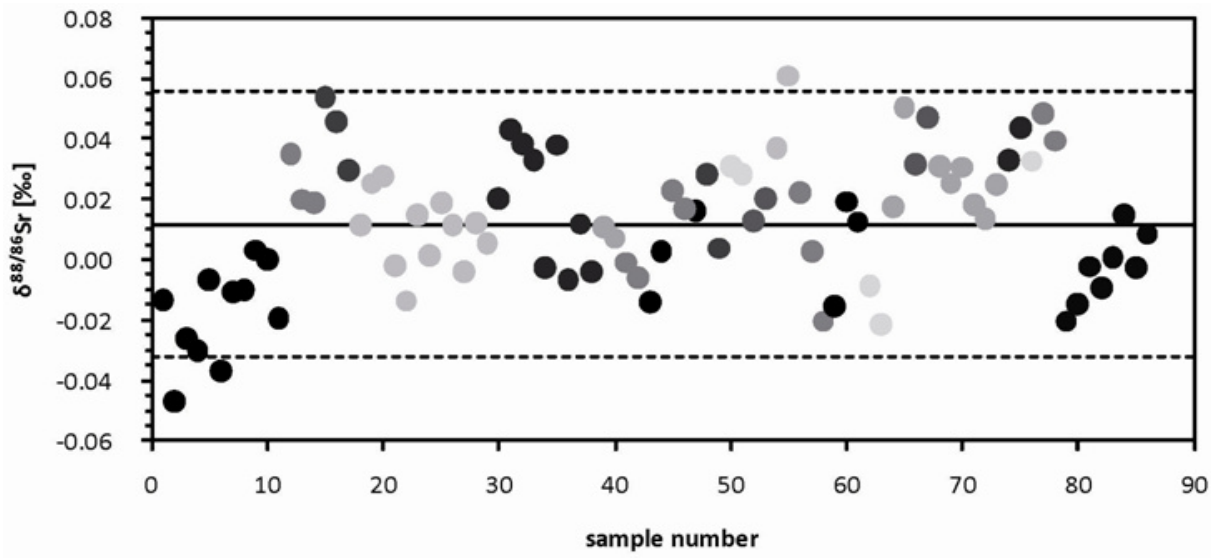

FIGURE II.4 - Long term session-to-session variations for the SRM987 standard result in a $\delta^{88/86}Sr_{mean}$ of ~0.012±0.044 (2SD). Different color marks different measurement sessions of SRM987. Black line marks the average value and the broken lines mark the 2sd-standard deviation.

Our measurements show that there are significant session-to-session variations in the isotopic ratios of the standard SRM987 measurements (Fig. II.4). This behavior is also known for other isotope measurements using TIMS. The reasons for this phenomena are not entirely known. Potential sources could be e.g. the Faraday Cup degradation or differing source vacuum conditions due to the use of two distinct cryo traps. In order to account for this

observation we calculated the mean of the fractionation corrected isotope $\delta^{88/86}Sr$- and $^{87}Sr/^{86}Sr^*$-ratios of SRM987 and determined its offset to the accepted value for $^{88}Sr/^{86}Sr=8.375209$ ($\delta^{88/86}Sr=0$) and $^{87}Sr/^{86}Sr=0.710240$, respectively (NIER, 1938). This offset was then used to correct the corresponding values of every single sample and resulted in the session corrected $\delta^{88/86}Sr$- and $^{87}Sr/^{86}Sr^*$-values.

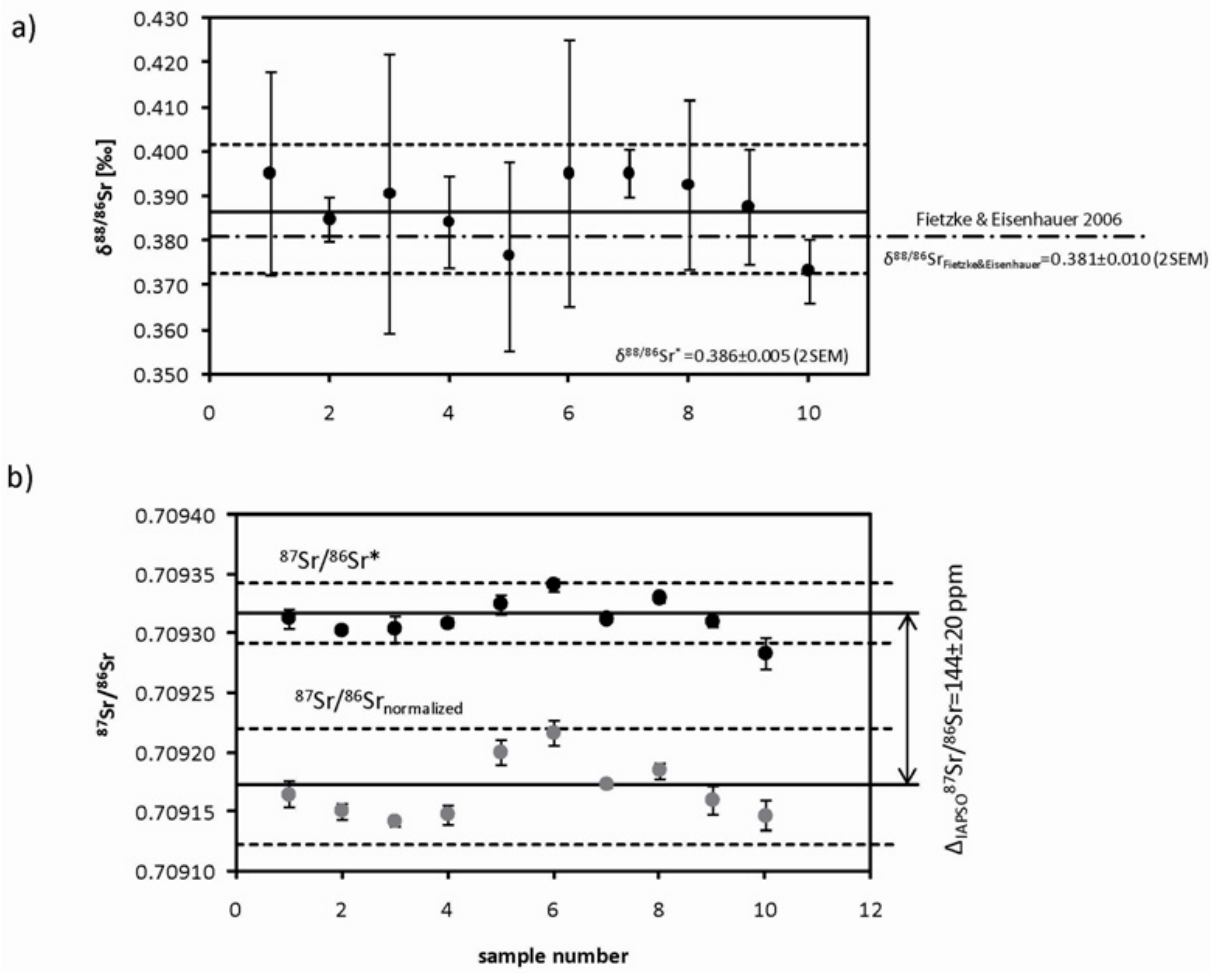

FIGURE II.5 - a: Long-term measurements of the IAPSO seawater standard. Every data point represents the mean of up to 5 single measurements of the same solution. The determined value of $\delta^{88/86}Sr_{mean}=0.386\pm0.005$ (2SEM) of the measurements (black line) is in agreement with previous data. The error bars are ±2SD (broken lines). b: $^{87}Sr/^{86}Sr^*$ (black points) and $^{87}Sr/^{86}Sr_{norm}$-values (grey points) of the IAPSO seawater standard are significantly different ($^{87}Sr/^{86}Sr^*=0.709312(9)$; $^{87}Sr/^{86}Sr_{norm}=0.709173(18)$) corresponding to a value of ~144±20 ppm.

During the course of this project the $\delta^{88/86}Sr$- and $^{87}Sr/^{86}Sr^*$-values of the IAPSO seawater standard (Fig. II.5 a/b) were found to be 0.386(5)‰ and 0.709312(9) (2SEM, n=10),

respectively. The $\delta^{88/86}Sr$ value for the IAPSO is in general accord with the value determined earlier (FIETZKE and EISENHAUER, 2006).

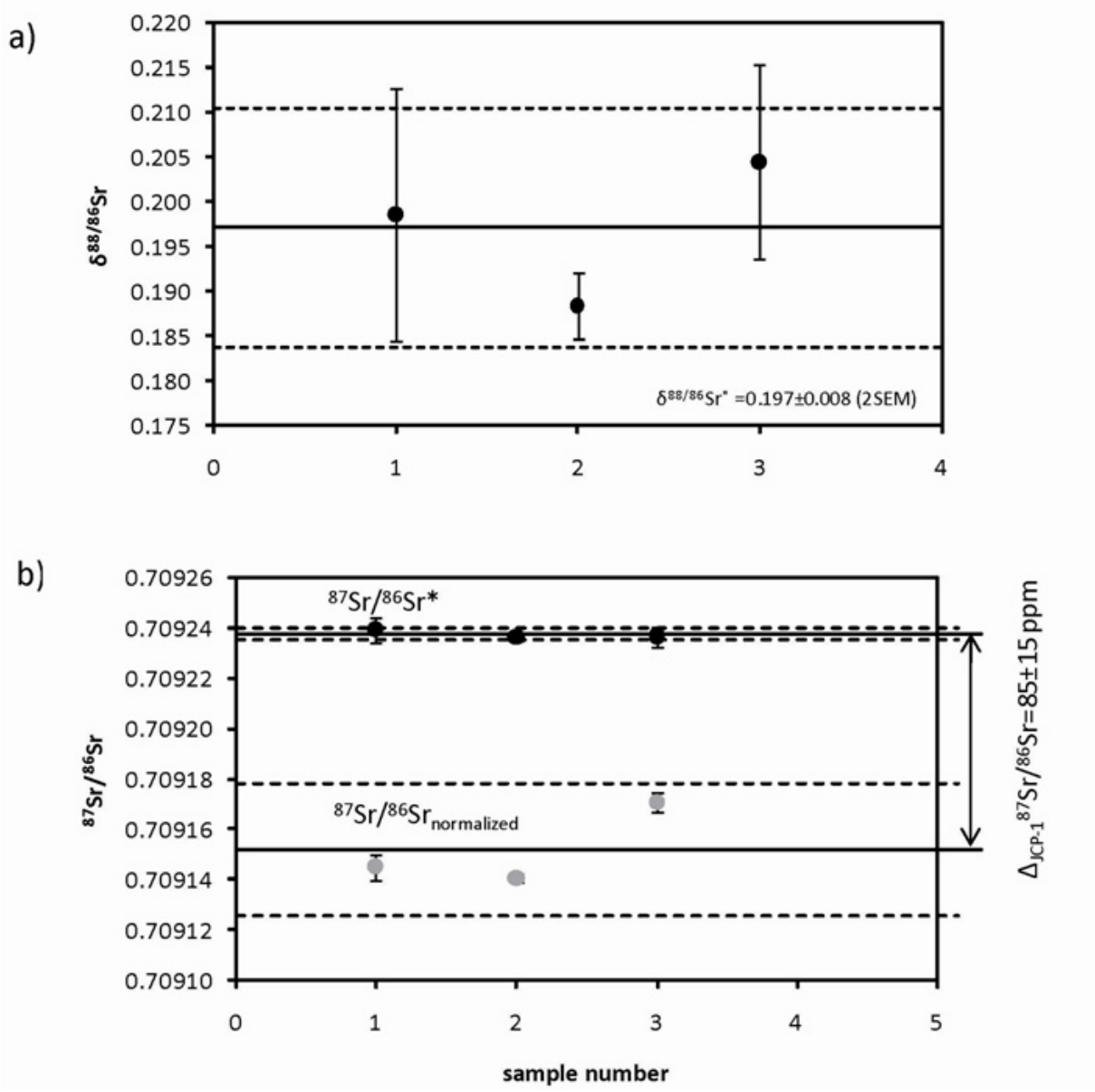

FIGURE II.6 - The $\delta^{88/86}Sr_{JCp\text{-}1\text{-}mean}$=0.197(8) (2SEM, black line) of the coral standard JCp-1 measurements. Every data point represents the mean of up to 3 single measurements of the same solution. Note, that the $\delta^{88/86}Sr_{JCp\text{-}1\text{-}mean}$ is isotopically about a factor of 2 lighter than $\delta^{88/86}Sr_{Seawater}$. This is due to mass dependent Sr isotope fractionation during $CaCO_3$ precipitation. The error bars are 2SD (broken lines). b: $^{87}Sr/^{86}Sr^*$- (black points; 0.709237(2)) and $^{87}Sr/^{86}Sr_{norm}$ -values (grey; 0.709164(15)) of coral standard JCp-1 are significantly different. Note that the $^{87}Sr/^{86}Sr^*$ of JCp-1 is isotopically lighter than $^{87}Sr/^{86}Sr^*$ of seawater by ~80 ppm.

The $^{87}Sr/^{86}Sr^*$ value is significantly different from the accepted $^{87}Sr/^{86}Sr_{norm}$ seawater ratio of 0.709168(7). Latter difference of 144 ppm (Fig. II.5 a/b) is due to the conventional

normalization procedure where the measured $^{87}Sr/^{86}Sr$ ratio is normalized to a constant $^{88}Sr/^{86}Sr$-ratio of 8.375209 ($\delta^{88/86}Sr=0$) neglecting any kind of natural Sr isotope fractionation. Renormalization of our measured $^{87}Sr/^{86}Sr^*$ value of 0.709312(9) to a $\delta^{88/86}Sr$ value of zero results in an average value of $^{87}Sr/^{86}Sr_{norm}$ 0.709166(9) which is in accord with the generally accepted radiogenic $^{87}Sr/^{86}Sr$-ratio for seawater (FANTLE and DEPAOLO, 2006). This is not a contradiction to the above stated value of $^{87}Sr/^{86}Sr=0.709168(7)$ of seawater but a consequence of two different ways of calculating the $^{87}Sr/^{86}Sr_{norm}$ and $^{87}Sr/^{86}Sr^*$, respectively. The first value is purely the result of the conventional Sr measurement (ic-run) while the latter uses both measurements (ic-/id-run) for the calculation.The values for the modern coral standard JCp-1 are plotted in the same way as for the IAPSO above (Fig. II.6 a/b).

The measurements show a value of 0.197(8)‰ (2SEM) for $\delta^{88/86}Sr$ and of 0.709237(2) for the $^{87}Sr/^{86}Sr^*$ ratio. There is a significant difference of the $\delta^{88/86}Sr$ values for JCp-1 and IAPSO in the order of 189±9 ppm. Similar to this observation there is also a significant 75±15 ppm difference between our measured $^{87}Sr/^{86}Sr^*$ ratio for JCp-1 and seawater (0.709312(9)). The ~80 ppm difference of the JCp-1 carbonate standard to the IAPSO seawater standard in the $^{87}Sr/^{86}Sr^*$ and the ~2 times larger difference in the $\delta^{88/86}Sr$-value indicate mass- and probably temperature dependent Sr isotope fractionation during the precipitation of $CaCO_3$ from seawater.

This results are in accord with earlier studys (FIETZKE and EISENHAUER, 2006; HALICZ et al., 2008; RÜGGEBERG et al., 2008). Comparison of our data with previous studies show that the here presented DS-TIMS method produces accurate results. The major advantage of our method is the 2 - 3 times better external precision. Additionally the use of a double spike solves the problems inherent in published MC-ICP-MS methods like fractionation during chemical sample pretreatment and matrix related mass bias fluctuations. The analytical blank was determined to 0.3 ng of Sr which was considered to be neglectable.

II.4. Conclusions

With our DS-TIMS method we are able to determine the stable $\delta^{88/86}Sr$ and the radiogenic $^{87}Sr/^{86}Sr^*$ simultanously. The use of a double spike overcomes the problem of any uncontrolled fractionation during sample pretreatment in particular ion chromatographic separation of Strontium from the sample matrix. The external precision could be improved by a factor of 2 - 3 compared to established MC-ICP-MS methods. Finally this DS-TIMS method is not burdened by mass bias fluctuations known from MC-ICP-MS bracketing standard approaches.

II.5. Tables

TABLE II.1 - Original isotope composition of the two Oak Ridge National Laboratory Sr carbonate standards.

	^{84}Sr (%)	^{86}Sr (%)	^{87}Sr (%)	^{88}Sr (%)	*Solution*
1.	~0.01	0.82(2)	91.26(10)	7.91(10)	^{87}Sr-Solution
2.	99.64(1)	0.14(1)	0.03(1)	0.19(1)	^{84}Sr-Solution

TABLE II.2 - Sample treatment prior mass spectrometric analysis

step	description
1	Addition of 2 ml 4.5 N HNO_3 to the weighed and grinded sample
2	Splitting the samples into two fractions
3	Addition of the spike solution to one fraction
4	Drying the samples at ~90°C
5	Column separation of the spiked and unspiked sample. BIO-RAD 650 µl columns with Eichrom Sr-SPS resin (mesh size 50-100 µm). To perform this separation we filled the columns to one third with the resin followed by a washing procedure
6	Drying the separated samples at ~90°C
7	Addition of 200 µl 4.5 N HNO_3 and 50 µl 30 % H_2O_2 and heating the solution in a closed beaker at least 5 hours at ~80°C
8	Drying the sample at ~80°C
9	Loading the sample with 2µL H_3PO_4 solution onto Re filaments
10	Measuring the samples

TABLE II.3 - Strontium isotopic composition of the double spike

$^{86}Sr/^{84}Sr$	$^{87}Sr/^{84}Sr$	$^{88}Sr/^{84}Sr$
0.009898	0.925937	0.083292

II.6. Acknowledgements

We wish to thank Ana Kolevica for supporting the lab work of this study. We also thank the two anonymous referees for providing a constructive and kind report. Finally, Torben Stichel is kindly acknowledged for providing the image of "his personal double spike" which was used for the graphical entrance of the article.

II.7. References

Nier, A. O., 1938. The isotopic constitution of strontium, barium, bismuth, thallium and mercury. Physical Review 5, 275-279.

Nier, A. O., 1940. A mass spectrometer routine for isotope abundance measurements. Rev. Sci. Instr. 18, 398-411.

Goldstein, S. J. and Jacobsen, S. B., 1987. The Nd and Sr isotopic systematics of river-water dissolved material: Implications for the sources of Nd and Sr in seawater. Chemical Geology: Isotope Geoscience section 66, 245-272.

Tütken, T., Eisenhauer, A., Wiegand, B., and Hansen, B. T., 2002. Glacial-interglacial cycles in Sr and Nd isotopic composition of Arctic marine sediments: changes in sediment provenance triggered by the Barents Sea ice sheet. Marine Geology 182, 351-372.

Fietzke, J. and Eisenhauer, A., 2006. Determination of temperature-dependent stable strontium isotope (88Sr/86Sr) fractionation via bracketing standard MC-ICP-MS. Geochemistry Geophysics Geosystems 7, Q08009, doi:10.1029/2006GC001243.

Halicz, L., Segal, I., Fruchter, N., Stein, M., and Lazar, B., 2008. Strontium stable isotopes fractionate in the soil environments? Earth and Planetary Science Letters 272, 406-411.

Rüggeberg, A., Fietzke, J., Liebetrau, V., Eisenhauer, A., Dullo, W. C., and Freiwald, A., 2008. Stable strontium isotopes (δ88/86Sr) in cold-water corals - A new proxy for reconstruction of intermediate ocean water temperatures. Earth and Planetary Science Letters 269, 569-574.

Ohno, T. and Hirata, T., 2007. Simultaneous determination of mass-dependent isotopic fractionation and radiogenic isotope variation of strontium in geochemical samples by multiple collector-ICP-mass spectrometry. Anal. Sci. 23, 1275-1280.

Yang, L., Peter, C., Panne, U., and Sturgeon, R. E., 2008. Use of Zr for mass bias correction in strontium isotope ratio determinations using MC-ICP-MS. Journal of Analytical Atomic Spectrometry 23, 1269-1274.

Patchett, P. J., 1980a. Sr isotopic fractionation in Allende chondrules: A reflection of solar nebular processes. Earth and Planetary Science Letters 50, 181-188.

Patchett, P. J., 1980b. Sr isotopic fractionation in Ca-Al inclusions from the Allende meteorite. Nature 283, 438-441.

Compston, W. and Overspy, V. M., 1969. Lead isotopic analysis using a double spike. Journal of Geophsical Research 74, 4338-4348.

Galer, J. G. S., 1999. Optimal double and triple spiking for high precision lead isotopic measurement. Chemical Geology 157, 255-274.

Heuser, A., Eisenhauer, A., Gussone, N., Bock, B., Hansen, B. T., and Nagler, T. F., 2002. Measurement of calcium isotopes (δ44/40Ca) using a multicollector TIMS technique. International Journal of Mass Spectrometry 220, 385-397.

Fantle, M. S. and DePaolo, D. J., 2006. Sr isotopes and pore fluid chemistry in carbonate sediment of the Ontong Java Plateau: Calcite recrystallization rates and evidence for a rapid rise in seawater Mg over the last 10 million years. Geochimica et Cosmochimica Acta 70, 3883-3904.

III. Chapter

Constraining the Marine Strontium Budget with Natural Strontium Isotope Fractionations ($^{87}Sr/^{86}Sr^*$, $\delta^{88/86}Sr$) of Carbonates, Hydrothermal Solutions and River Waters

A. Krabbenhöft*, A. Eisenhauer*, F. Böhm*, H. Vollstaedt*, J. Fietzke*, V. Liebetrau*, N. Augustin*, B. Peucker-Ehrenbrink#, M. N. Müller*, C. Horn*, B. T. Hansen°, N. Nolte° and K. Wallmann*

* *Leibniz-Institut für Meereswissenschaften, IFM-GEOMAR, Wischhofstr. 1-3, 24148 Kiel, Germany*

° *Geowissenschaftliches Zentrum der Universität Göttingen (GZG), Abteilung für Isotopengeologie, Goldschmidtstr. 1, 37077 Göttingen, Germany*

Woods Hole Oceanographic Institution, Department of Marine Chemistry and Geochemistry, Woods Hole, MA 02543, USA

Published in *Geochimica et Cosmochimica Acta* 74 (2010), 4097-4109

Abstract

We present strontium (Sr) isotope ratios that, unlike traditional $^{87}Sr/^{86}Sr$ data, are not normalized to a fixed $^{88}Sr/^{86}Sr$ ratio of 8.375209 (defined as $\delta^{88/86}Sr=0$ relative to NIST SRM 987). Instead, we correct for isotope fractionation during mass spectrometry with a ^{87}Sr-^{84}Sr double spike. This technique yields two independent ratios for $^{87}Sr/^{86}Sr$ and $^{88}Sr/^{86}Sr$ that are reported as ($^{87}Sr/^{86}Sr^*$) and ($\delta^{88/86}Sr$), respectively. The difference between the traditional radiogenic ($^{87}Sr/^{86}Sr$ normalized to $^{88}Sr/^{86}Sr=8.375209$) and the new $^{87}Sr/^{86}Sr^*$ values reflect natural mass-dependent isotope fractionation. In order to constrain glacial/interglacial changes in the marine Sr budget we compare the isotope composition of modern seawater ($(^{87}Sr/^{86}Sr^*, \delta^{88/86}Sr)_{Seawater}$) and modern marine biogenic carbonates ($(^{87}Sr/^{86}Sr^*, \delta^{88/86}Sr)_{Carbonates}$) with the corresponding values of river waters ($(^{87}Sr/^{86}Sr^*, \delta^{88/86}Sr)_{River}$) and hydrothermal solutions ($(^{87}Sr/^{86}Sr^*, \delta^{88/86}Sr)_{HydEnd}$) in a triple isotope plot. The measured $(^{87}Sr/^{86}Sr^*, \delta^{88/86}Sr)_{River}$ values of selected rivers that together account for ~18% of the global Sr discharge yield a Sr flux-weighted mean of (0.7114(8), 0.315(8)‰). The average $(^{87}Sr/^{86}Sr^*, \delta^{88/86}Sr)_{HydEnd}$ values for hydrothermal solutions from the Atlantic Ocean are (0.7045(5), 0.27(3)‰). In contrast, the $(^{87}Sr/^{86}Sr^*, \delta^{88/86}Sr)_{Carbonates}$ values representing the marine Sr output are (0.70926(2), 0.21(2)‰). We estimate the modern Sr isotope composition of the sources at (0.7106(8), 0.310(8) ‰). The difference between the estimated $(^{87}Sr/^{86}Sr^*, \delta^{88/86}Sr)_{input}$ and $(^{87}Sr/^{86}Sr^*, \delta^{88/86}Sr)_{output}$ values reflects isotope disequilibrium with respect to Sr inputs and outputs. In contrast to the modern ocean, isotope equilibrium between inputs and outputs during the last glacial maximum (10-30 ka before present) can be explained by invoking three times higher Sr inputs from a uniquely "glacial" source: weathering of shelf carbonates exposed at low sea levels. Our data are also consistent with the "weathering peak" hypothesis that invokes enhanced Sr inputs resulting from weathering of post-glacial exposure of abundant fine-grained material.

III.1. Introduction

The residence time of Sr in seawater of 2.4 Myr is long compared to the mixing time of the oceans of ~1.5 kyr. The radiogenic Sr isotope composition ($^{87}Sr/^{86}Sr$: ~0.709175; (VEIZER, 1989) is therefore homogeneous in seawater and in modern marine carbonates (FAURE and FELDER, 1981; MCARTHUR, 1994; MCARTHUR et al., 2001). The modern $^{87}Sr/^{86}Sr$ value of seawater is determined by mixing of two isotopically distinct sources: 1) Sr from the weathering of old, rubidium (Rb)-rich continental silicate rocks that have been enriched in ^{87}Sr by the decay of ^{87}Rb; 2) Sr with low $^{87}Sr/^{86}Sr$ values derived from the Earth´s mantle that enters the ocean at mid-ocean ridges and ridge flanks, and from weathering of mantle-derived rocks exposed on the continents (PALMER and EDMOND, 1992; GODDERIS and VEIZER, 2000). A minor Sr influx from diagenetic alteration and dissolution of sediments on the seafloor has a $^{87}Sr/^{86}Sr$ value only slightly lower than modern seawater (ELDERFIELD and GIESKES, 1982). While average riverine $^{87}Sr/^{86}Sr$ values are distinctly different from seawater, the large difference in Sr concentration ($[Sr]_{Rivers}$~1.0 µM, $[Sr]_{Seawater}$~90 µM) ensures that even in marginal seas with high riverine input seawater $^{87}Sr/^{86}Sr$ values are close to the global seawater value ($^{87}Sr/^{86}Sr$=0.709175). Exceptions are brackish seas such as the Baltic Sea with salinities below 15 psu (ANDERSSON et al., 1992). The average Sr concentration of river waters that are dominated by silicate weathering input is ~0.2 µM. The average $^{87}Sr/^{86}Sr$ value of young volcanic provinces is ~0.705, but is ~0.735 for old crustal terrains (PALMER and EDMOND, 1992). Rivers draining carbonate rocks, in contrast, have much higher Sr concentrations of ~4 µM with typical $^{87}Sr/^{86}Sr$ values ranging from 0.707 to 0.709 (GAILLARDET et al., 1999). On average, global river water is characterized by Sr concentration of ~1 µM and a $^{87}Sr/^{86}Sr$ value of ~0.7111 (PEUCKER-EHRENBRINK et al., 2010). About one third of this riverine Sr is derived from silicate weathering and about two thirds from weathering of carbonate rocks exposed on the continents (PALMER and EDMOND, 1989; GAILLARDET et al., 1999).

Although the principles of marine Sr geochemistry are well understood, there is an ongoing discussion about the effects of glacial/interglacial changes in continental weathering on the marine Sr budget. Recent findings indicate that ~70% of the silicate weathering flux is affected by non-steady-state processes, possibly creating a ~100 kyr periodicity and an imbalance between input and output fluxes during the Quaternary (VANCE et al., 2009). However, the Sr imbalance created by the non-steady state conditions cannot be quantified by radiogenic Sr ratios alone. Marine Sr budgets that are solely based on radiogenic Sr focus on the input fluxes, because marine calcium carbonate ($CaCO_3$) and seawater have identical radiogenic Sr isotope values. This approach is a direct consequence of the normalization of measured $^{87}Sr/^{86}Sr$ values to a fixed $^{88}Sr/^{86}Sr$ ratio of 8.375209 (NIER 1938) to correct for mass dependent isotope fractionation in nature and during mass-spectrometry, thereby loosing the ability to extract information about natural isotope fractionation.

In order to overcome this obstacle and investigate combined radiogenic and stable Sr isotope compositions, we determine natural Sr isotope fractionation with a TIMS double spike method (KRABBENHÖFT et al., 2009). First results showed that the $(^{87}Sr/^{86}Sr^*, \delta^{88/86}Sr)_{Seawater}$ is homogeneous (LIEBETRAU et al., 2009). We also demonstrated that the stable Sr isotope composition of marine carbonates and corals ($\delta^{88/86}Sr_{Carbonates}$) is ~0.2 ‰ lighter than seawater. This is caused by the preferential uptake of lighter isotopes during carbonate precipitation (FIETZKE and EISENHAUER, 2006; HALICZ et al., 2008; OHNO et al., 2008). The still limited data base of stable Sr isotope ratios indicates that marine basalts have $\delta^{88/86}Sr$ values of ~0.25 ‰ (HALICZ et al., 2008; OHNO et al., 2008), significantly different from continental igneous rocks and soils that show lighter values in the range of ~ -0.2 to 0.2 ‰.

When natural Sr isotope fractionation is taken into account the Sr isotope composition of marine carbonates and seawater differ. This allows for the simultaneous calculation of input and output fluxes using complete Sr budget equations. This new approach extends the well-established radiogenic Sr isotope systematic to an additional dimension and allows for

simultaneous determination of paired ($^{87}Sr/^{86}Sr^*$, $\delta^{88/86}Sr$) ratios. Here, we present the first results of paired ($^{87}Sr/^{86}Sr^*$, $\delta^{88/86}Sr$) values for rivers, hydrothermal fluids, marine carbonates and seawater to constrain the contemporary marine Sr budget.

III.2. Materials and Methods

River Waters

In order to reevaluate the Sr isotope supply via river discharge to the ocean and to constrain the riverine Sr budget for paired ($^{87}Sr/^{86}Sr^*$, $\delta^{88/86}Sr$) ratios, we analyzed a suite of rivers representing ~18 % of the global annual riverine Sr flux to the ocean. The Sr isotope values are presented together with complementary information about water discharges, sampling locations and the riverine Sr fluxes (Tab. III.1 and Fig. III.1). The analyzed rivers drain various proportions of 9 of the 16 large-scale exorheic drainage regions on Earth (GRAHAM et al., 1999; PEUCKER-EHRENBRINK and MILLER, 2004). We assume that river water samples investigated here are reasonably representative of the 9 large-scale draining regions, because both the average bedrock age (399 Ma) and the relative abundances of sedimentary (70%), volcanic (9%) and intrusive/metamorphic (21%) bedrock are similar to global exorheic bedrock weighted according to water discharge (405 Ma, 73%, 9%, 18%, respectively). The set of rivers investigated here thus does not appear to be significantly biased with respect to the lithological setting and bedrock ages (PEUCKER-EHRENBRINK and MILLER, 2004).

Hydrothermal solutions

Seven hydrothermal vent-fluid samples from the active area at 4°48´S on the Mid-Atlantic Ridge (MAR) have been analyzed for this study (Tab. III.2). The 4°48´S hydrothermal system is located on-axis at a water depth of ~3000 m. It is dominated by fresh to slightly altered lava flows and pillows (HAASE et al., 2007). On this plateau at least three high-temperature vent

fields (Turtle Pits [TP], Comfortless Cove [CC] and Red Lion [RL]) are located on a flat, 2 km wide, volcanically and tectonically active area (HAASE et al., 2007). The samples analyzed in this study were taken from these high-temperature vent fields using an ROV equipped with a "Multiport Valve-based all-Teflon Fluid Sampling System, (KIPS)" during the RV l´Atalante cruise MARSUED IV in 2007. Comfortless Cove as well as TP are characterized by high fluid temperatures >407 °C at 2990 m water depth, close to the critical point of seawater, and show indications of phase separation (HAASE et al., 2007). The RL vent field emits ~370 °C fluids that show no indications of phase separation.

The measured Mg and Sr concentrations of the fluids are positively correlated suggesting that $[Sr]_{HydEnd}$ of the phase-separated Sr sources is lower than seawater. Extrapolating Mg/Sr ratios of the TP and CC fluid samples to a Mg/Sr ratio of zero yields a $[Sr]_{HydEnd}$ of 34(5) μM. Likewise, the $[Sr]_{HydEnd}$ of RL was estimated at ~56(5) μM. Strontium isotope compositions measured in this study are presented in Tab. III.2 and in Fig. III.2a and b.

Marine carbonates

The major sink of Sr in the ocean is the formation of aragonitic and calcitic $CaCO_3$ (MILLIMAN and DROXLER, 1996b) where calcium (Ca) is substituted by Sr. In order to quantify the Sr burial flux and its isotope composition we performed Sr isotope measurements on important calcifying marine organisms (Tab. III.3). $CaCO_3$ deposition rates are primarily (~39 %) controlled by species living on the shelves and slopes (e.g. mussels, star fish, sea urchins, benthic foraminifera, bryozoans, calcareous algae). Most of the remainder is determined in almost equal proportions by reef corals (20 %), coccoliths (16 %) and planktic foraminifera (20 %). The higher Sr concentrations in aragonite cause larger Sr/Ca ratios than observed in calcite (see Tab. III.3). Sr/Ca ratios are well constrained for reef corals, Halimeda, planktic foraminifera and also for many shelf and slope species (e.g. mussels: 1.5 mM, star fish: 2.5 mM, aragonitic algae: 11 mM). However, the average value for shelf and slope species cannot

be constrained well because the relative proportions of calcite and aragonite are not well known. We therefore arbitrarily assume that shelf species are composed of two thirds aragonite (Sr/Ca: ~9 mM) and one third calcite (Sr/Ca: ~1.8 mM), yielding an average shelf carbonate Sr/Ca of ~6.6 mM.

Sample preparation

All solid carbonate samples were weighed in Teflon beakers together with 2 ml H_2O (18.2 MΩ Milli-Q water). Samples were dissolved in 500 µl 4.5 N HNO_3, heated for at least 5 hours and then dried at ~90 °C. In order to remove organic matter 50 µl H_2O_2 and 200 µl 2N HNO_3 were added and samples were heated to ~80 °C for at least 5 hours in closed beakers. Subsequently, samples were dried again at ~80 °C, dissolved in 2 ml 8 N HNO_3 and split into two fractions that each contained 1000–1500 ng Sr, corresponding to a carbonate sample weight of 1-2 mg. The Sr double spike was added to one fraction and both fractions were then dried at ~90 °C. Chromatographic column separation was performed using 650 µl BIO-RAD columns filled to one third with Eichrom Sr-SPS resin (grain size 50-100 µm). The resin was washed three times with 4.5 ml H_2O and 4.5 ml 8 N HNO_3. The resin was then conditioned three times with 1 ml 8 N HNO_3 before the sample - dissolved in 1 ml 8 N HNO_3 – was loaded onto the column. In order to remove the sample matrix the resin was washed six times with 1 ml 8 N HNO_3. The Sr-fraction was eluted into a Teflon beaker in three steps with 1 ml H_2O each. Any resin residue was removed by drying down and then heating samples to 80°C in 50 µl H_2O_2 and 200 µl 2N HNO_3 for at least 5 hours in closed beakers. Finally, samples were dried at ~80 °C. About 500 ng Sr was loaded together with 2 µl H_3PO_4 onto a single Re filament after addition of 1.5 µl of Ta_2O_5-activator to stabilize signal intensity. The sample was then heated on the filament at 0.6 A to near dryness before being dried at 1 A and slowly heated to 1.8 A within 2 minutes. Then, the sample was heated to a dark red glow. After keeping the filament glowing for about 30 seconds the current was

turned down and the filament was mounted onto the sample wheel. With the exception of the dissolution step, hydrothermal- and river water samples were treated as described above.

TIMS measurements

The use of a ^{87}Sr-^{84}Sr double spike enables us to determine natural Sr isotope fractionation after correction for mass-dependent fractionation during TIMS measurements. The details of the ^{87}Sr-^{84}Sr double spike production, measurement procedure and data reduction are discussed by (KRABBENHÖFT et al., 2009).

The Sr isotope measurements were carried out at the IFM-GEOMAR mass spectrometer facility in Kiel and at the "Geowissenschaftliches Zentrum der Universität Göttingen", Germany, using TRITON mass spectrometers (ThermoFisher, Bremen, Germany). The TRITONs were operated in positive ionization mode with a 10 kV acceleration voltage. The instruments are equipped with nine moveable Faraday cups with 10^{11} Ω resistors that allow for simultaneous detection of all Sr masses.

Mass 85 was measured in order to monitor and correct for interfering ^{87}Rb assuming an $^{85}Rb/^{87}Rb$ ratio of 2.59. Data were acquired at a typical signal intensity of 10 V for mass 88 at an average filament temperature of ~1450°C. For each sample 9 blocks with 14 cycles corresponding to 126 single scans were measured. Before each block the baseline was recorded and the amplifier rotation was performed.

The ^{87}Sr-^{84}Sr double spike technique required two separate analyses of each sample: one ic-analysis (ic = isotope composition; unspiked) and one id-analysis (id = isotope dilution; spiked) with well-known $^{86}Sr/^{84}Sr$-, $^{87}Sr/^{84}Sr$- and $^{88}Sr/^{84}Sr$-ratios of the double spike. The $^{86}Sr/^{84}Sr$- and the $^{88}Sr/^{84}Sr$-ratios are normalized to the mean of the first block of the $^{87}Sr/^{84}Sr$ isotope ratio using an exponential fractionation law in an off-line data processing routine. Following this procedure the average internal precision of single $^{86}Sr/^{84}Sr$-ratio measurements

is ~7 ppm (RSD), and ~9 ppm for single $^{88}Sr/^{84}Sr$-ratio determinations in the ic-analyses. We measured ~11 ppm (RSD) for the $^{86}Sr/^{84}Sr$-ratio and ~21 ppm for the $^{88}Sr/^{84}Sr$-ratio in the id-analyses. Variations in $^{88}Sr/^{86}Sr$ are reported in the usual δ-notation: $\delta^{88/86}Sr$ [‰]=($^{88}Sr/^{86}Sr_{sample}/^{88}Sr/^{86}Sr_{SRM987}$-1)*1000. We use the SRM987 standard with an internationally accepted $^{88}Sr/^{86}Sr$ value of 8.375209 (NIER 1938) for normalization. Notations (e.g. $^{87}Sr/^{86}Sr_{Norm}$ and $^{87}Sr/^{86}Sr^*$) and additional information about mass-dependent fractionation are summarized in Appendix 1.

III.3. Results

Sr isotope composition of the marine input

Sr composition of the riverine discharge to the ocean

The $^{87}Sr/^{86}Sr_{Norm}$ and $^{87}Sr/^{86}Sr^*$ values of rivers presented in Tab. III.1 and Fig. III.1 show variations from 0.707321(8) to 0.727705(9) and from 0.707417(9) to 0.727798(6), respectively. The Sr flux-weighted mean river values for $^{87}Sr/^{86}Sr_{Norm}$ and $^{87}Sr/^{86}Sr^*$ are 0.7113(4) and 0.7114(8), respectively. The $^{87}Sr/^{86}Sr_{Norm}$ value in particular is in good agreement with the $^{87}Sr/^{86}Sr$ value published by (GAILLARDET et al., 1999) and is similar to the values of 0.7101 (GOLDSTEIN and JACOBSEN, 1987) and 0.7119 (PALMER and EDMOND, 1989). The good agreement between our more restricted dataset (18% of the river water flux) and earlier comprehensive analyses (47% of the river water flux) of Exoreic Rivers (e.g. (PALMER and EDMOND, 1989)) clearly indicates that our sample set is representative of global river runoff.

The $\delta^{88/86}Sr$ values vary between 0.243(6)‰ for the Lena river and 0.42(2)‰ for the Maipo river. The Sr flux-weighted mean ($^{87}Sr/^{86}Sr^*$, $\delta^{88/86}Sr$) values are (0.7114(8), 0.315(8)‰). The good agreement of the $^{87}Sr/^{86}Sr_{Norm}$ values with the conventional $^{87}Sr/^{86}Sr$ values (Tab. III.1) clearly indicates that the double spike method can reproduce conventional radiogenic values

in addition to yielding new information on the non-radiogenic Sr isotope composition of the samples.

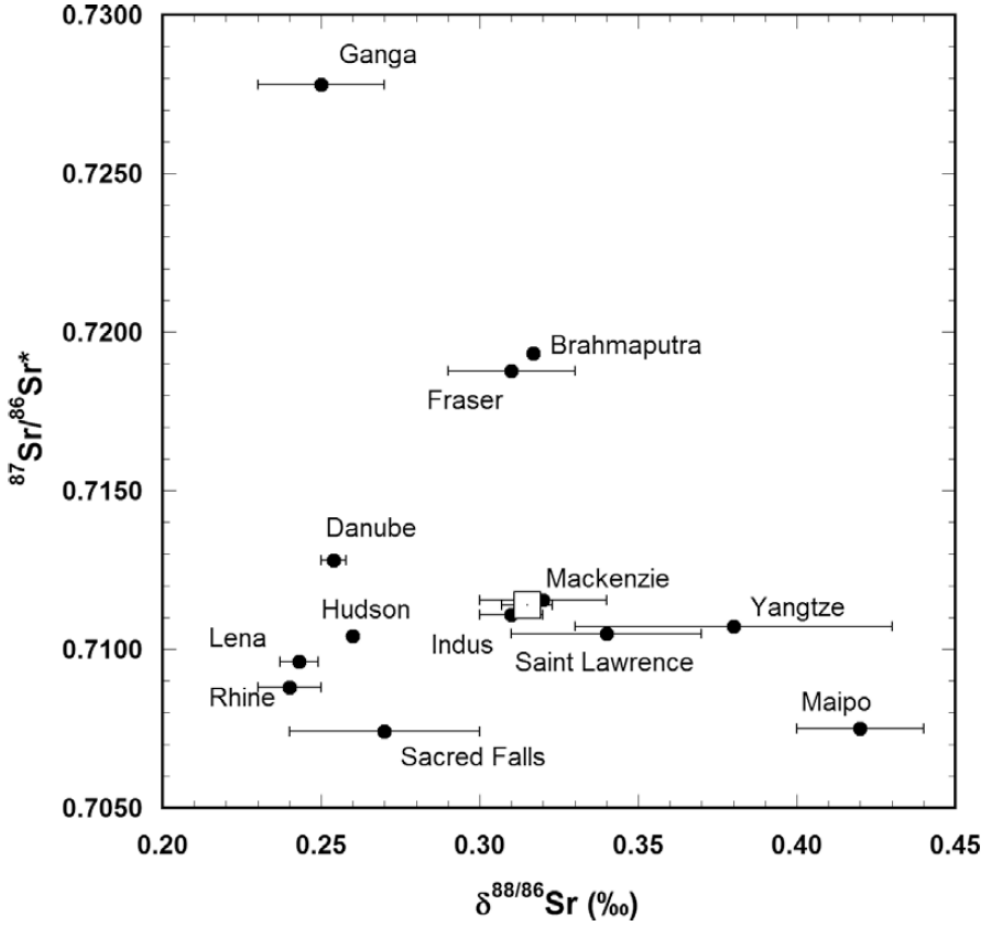

FIGURE III.1 - Individual ($^{87}Sr/^{86}Sr^*$, $\delta^{88/86}Sr)_{River}$-values corresponding to ~18 % of the global Sr discharge to the ocean are plotted in a triple isotope plot. There is a considerable scatter in both the $^{87}Sr/^{86}Sr^*$ and the $\delta^{88/86}Sr$ values. The Sr flux-weighted global mean of all rivers is marked by a square.

Sr isotope composition of the hydrothermal discharge to the ocean

Following the procedure of (AMINI et al., 2008) and assuming that pure hydrothermal solutions are free of Mg, we estimated the ($^{87}Sr/^{86}Sr^*$, $\delta^{88/86}Sr)_{HydEnd}$-values at (0.7045(5), 0.27(3)‰) by extrapolating the measured values to a Mg/Sr ratio of zero (Tab. III.2, Fig. III.2a, b). The $\delta^{88/86}Sr_{HydEnd}$ values are isotopically lighter than seawater.

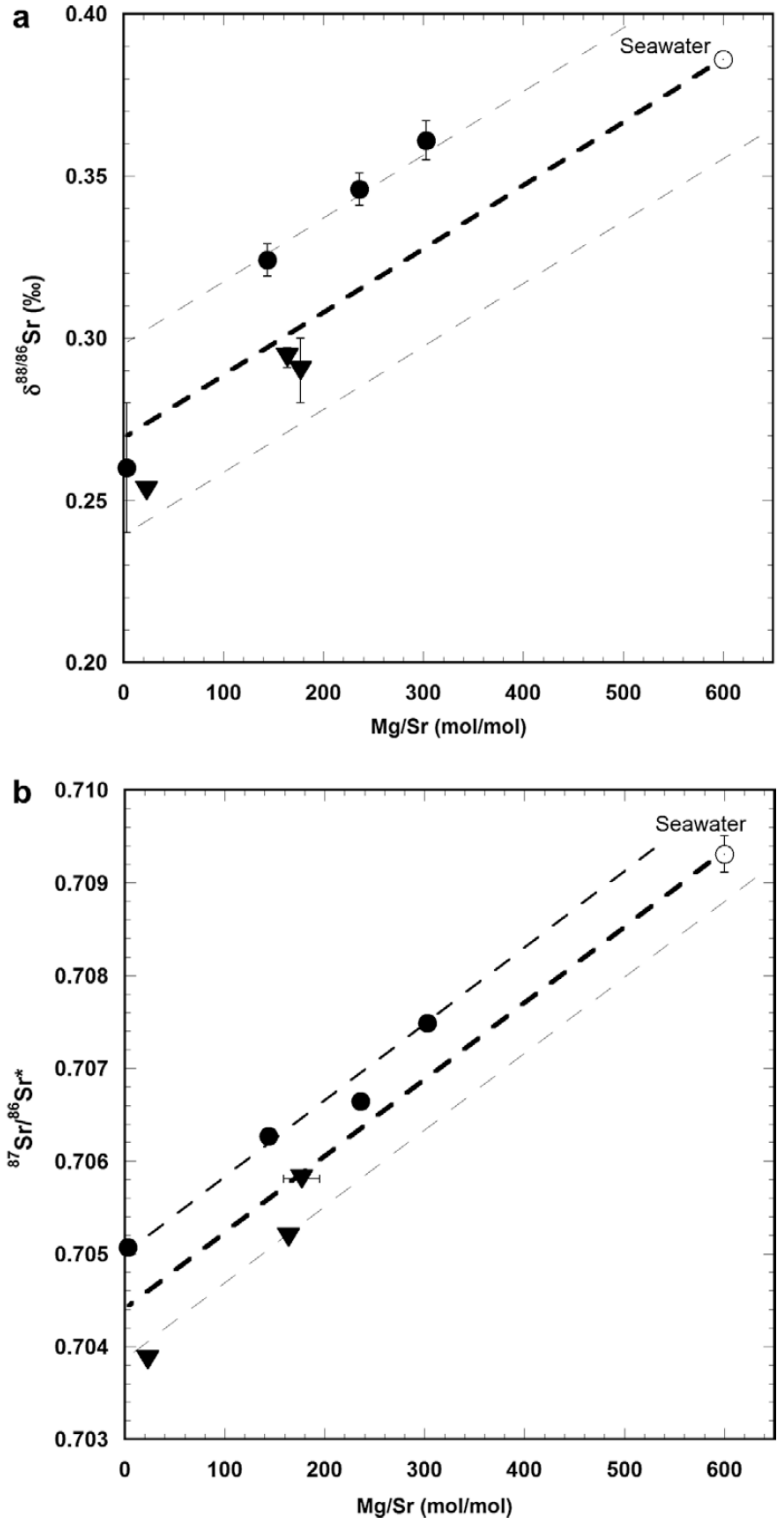

FIGURE III.2 - ($^{87}Sr/^{86}Sr^*$, $\delta^{88/86}Sr$)-values of hydrothermal fluid samples. Assuming that pure hydrothermal solutions are free of Mg (Mg/Sr=0), hydrothermal $\delta^{88/86}Sr$ (a) and $^{87}Sr/^{86}Sr^*$ (b) end members can be extrapolated (dotted line) from our data. Circles refer to Comfortless Cove (CC) and Turtle Pits (TP), whereas triangles refer to the Red Lion (RL) hydrothermal field at the mid-Atlantic Ridge. Broken lines mark the uncertainties associated with the extrapolated values in (a) and (b).

This is in good agreement with the reported radiogenic $^{87}Sr/^{86}Sr$- and $\delta^{88/86}Sr$-values of basalt of 0.70412(4) and 0.26(3)‰, respectively (OHNO et al., 2008). The latter observation indicates that the isotopic composition of hydrothermal fluids simply reflect the isotopic composition of ocean crust.

Sr isotope composition of the combined riverine and hydrothermal input to the ocean

The mean ocean input flux and its corresponding isotope compositions can be estimated from the measured and compiled values of the riverine discharge and of the hydrothermal input (Tab. III.4; $(^{87}Sr/^{86}Sr^*, \delta^{88/86}Sr)_{Input}$: (~0.7106(8), ~0.310(8)‰). These composite values are afflicted with larger uncertainties that reflect the assumptions that are described in detail in Tab. III.4. The compilation of flux data in Tab. III.4 show that the present day Sr supply of ~$56 \cdot 10^9$ mol/yr is mainly (~60%) controlled by Sr delivered by riverine discharge to the ocean and to a lesser extent by groundwater (~29%) and hydrothermal (~4%) inputs. Our total flux estimate is in good agreement with the global Sr flux of ~$50 \cdot 10^9$ mol/a that (BASU et al., 2001) estimated based on riverine and groundwater inputs alone. They did not include Sr from low temperature alteration of oceanic crust and diagenetic mobilization of Sr from marine sediments. Our estimate is higher than that of (STOLL and SCHRAG, 1998) and (STOLL et al., 1999) of ~$40 \cdot 10^9$ mol/yr, because these authors did not take groundwater inputs into account. Addition of our estimate of the groundwater Sr flux ($16.5 \cdot 10^9$ mol/yr) brings both estimates in close agreement.

Isotope composition of the marine Sr output

The primary sink for marine Sr is marine $CaCO_3$ precipitation. The most simplistic approach to estimate mean global ocean $(^{87}Sr/^{86}Sr^*, \delta^{88/86}Sr)_{Carbonate}$ values is to average $(^{87}Sr/^{86}Sr^*, \delta^{88/86}Sr)$ values of the major calcifying species such as tropical corals, green algae (Halimeda),

foraminifera and coccoliths (Tab. III.3). This approach yields mean global ($^{87}Sr/^{86}Sr^*$, $\delta^{88/86}Sr)_{Carbonate}$ values of (0.70924(3), 0.22(5)‰), (Tab. III.3).

A more refined approach for determining mean global ocean ($^{87}Sr/^{86}Sr^*$, $\delta^{88/86}Sr)_{Carbonate}$ values is to also consider the individual Sr burial fluxes. These burial fluxes can be estimated from the species-dependent $CaCO_3$-burial rates (Tab. III.3) and the respective species-dependent Sr/Ca ratios. The mean global ($^{87}Sr/^{86}Sr^*$, $\delta^{88/86}Sr)_{Carbonates}$ values are determined by the Sr burial flux-weighted means of the major calcifying species and their respective ($^{87}Sr/^{86}Sr^*$, $\delta^{88/86}Sr$) values. The main disadvantage of this approach is related to the fact that $CaCO_3$ burial rates are uncertain by at least 50% (MILLIMAN and DROXLER, 1996a).

For corals we adopt the ($^{87}Sr/^{86}Sr^*$, $\delta^{88/86}Sr$)-values of the JCp-1 coral standard (0.70923(1), 0.19(1)‰). Aragonitic azooxanthellate coldwater corals of the species *Lophelia pertusa* that grow between 6 °C and 10 °C show slightly lower $\delta^{88/86}Sr$ values of 0.06-0.18 ‰ (RÜGGEBERG et al., 2008). However, coldwater corals contribute only ~1 % to the global carbonate sediment budget (LINDBERG and MIENERT, 2005) and are therefore not included in the Sr isotope budget. In contrast, tropical coral reefs contribute ~31 % to the ocean´s Sr burial flux (Tab. III.3). For tropical corals we did not take into account any temperature sensitivity of the paired ($^{87}Sr/^{86}Sr^*$, $\delta^{88/86}Sr$)-values, as the new double spike technique did not confirm the previously predicted temperature sensitivity of Sr isotope fractionation (FIETZKE and EISENHAUER, 2006).

For this study paired ($^{87}Sr/^{86}Sr^*$, $\delta^{88/86}Sr$)-values of aragonitic Halimeda specimen from Tahiti and the Mediterranean Sea yielded average values of 0.70926(3), 0.27(3)‰ (Tab. III.3). Halimeda mounds contribute ~9 % to the ocean´s Sr burial flux.

Despite being calcitic, the ($^{87}Sr/^{86}Sr^*$, $\delta^{88/86}Sr$)-values of ~0.70926(3), 0.26(7)‰ from cultured coccoliths are similar to those of the aragonitic species (Tab. III.3). Coccoliths contribute ~6 % to the global Sr burial flux.

The two species *G. ruber* and *G. sacculifer* are taken to be representative of the Sr isotope composition of calcitic planktic foraminifera. They show identical ($^{87}Sr/^{86}Sr^*$, $\delta^{88/86}Sr$)-values of (0.70920(2), 0.14(1)‰). Note that the paired ($^{87}Sr/^{86}Sr^*$, $\delta^{88/86}Sr$)-values of these foraminifera are considerably lower than those of other species, pointing to a strong physiological control of the trace metal uptake by planktic foraminifera. Planktic foraminifera, like coccoliths, contribute ~5 % to the ocean´s Sr burial flux.

A significant part of the Sr flux is contributed by non-reef carbonate production on the continental shelf and slope (MILLIMAN and DROXLER, 1996b). However, shelf carbonate contributions are rather uncertain due to the unknown partitioning between calcitic and aragonitic species and the lack of knowledge on $CaCO_3$ production rates of different contributing taxa (Tab. III.3). Based on the data compiled in Tab. III.3 we approximate the mean ($^{87}Sr/^{86}Sr^*$, $\delta^{88/86}Sr$)-ratios of shelf carbonates at ~(0.70924(1), 0.22(3)‰). We assume that shelf and slope carbonates are two-thirds aragonitic with mean ($^{87}Sr/^{86}Sr^*$, $\delta^{88/86}Sr$) values of reef corals and Halimeda (0.70925, 0.23‰), and one-third calcitic with mean ($^{87}Sr/^{86}Sr^*$, $\delta^{88/86}Sr$) values of coccoliths and planktic foraminifera (0.70923, 0.20‰).

Based on data summarized in Tab. III.3 we estimate the Sr burial flux-weighted ($^{87}Sr/^{86}Sr^*$, $\delta^{88/86}Sr$)-ratios of the total marine carbonate production at (~0.70926(2), ~0.21(2)‰). The mean global ($^{87}Sr/^{86}Sr^*$, $\delta^{88/86}Sr)_{Carbonate}$ values are therefore similar to the values of continental shelf and slope taxa. Furthermore, the flux-weighted average values are within statistical uncertainty identical to those estimated by just averaging the ($^{87}Sr/^{86}Sr^*$, $\delta^{88/86}Sr$) values of the main calcifying species (0.70924(2), 0.22(2)‰; Tab. III.3). The close agreement between the two approaches may indicate that the relative contributions of the various burial fluxes are well constrained despite considerable uncertainties in the absolute burial fluxes. Hence, we consider both approaches to be reasonable approximations of the true mean global ($^{87}Sr/^{86}Sr^*$, $\delta^{88/86}Sr)_{Carbonate}$ values.

III.4. Discussion

Compilations of the modern input and output data (Tab. III.3 and III.4) indicate that the Sr outputs (~174·10^9 mol/yr) are larger than Sr inputs (~56·10^9 mol/yr), and that the Sr isotope compositions of input and output fluxes are considerably different. Although the estimated difference between input and output values seems to be large, we cannot assign statistical significance because all estimates are afflicted with considerable uncertainties. In order to further examine and better constrain the observed trends, we compare the Sr isotope balance of Sr inputs, outputs and of $[Sr]_{Seawater}$ in a triple-isotope-plot. This new approach in Sr isotope geochemistry critically depends on taking Sr isotope fractionation into account.

Sr budget of the global ocean

In Fig. III.3 the global means of the ($^{87}Sr/^{86}Sr^*$, $\delta^{88/86}Sr)_{River}$- and ($^{87}Sr/^{86}Sr^*$, $\delta^{88/86}Sr)_{HydroEnd}$-values define the two end-members of a binary mixing line between the two major sources of Sr in the modern ocean. The calculated combined ($^{87}Sr/^{86}Sr^*$, $\delta^{88/86}Sr)_{Input}$-values fall on this binary mixing line and plot relatively close to the Sr isotope composition of average river water, indicating that riverine input is the major Sr source to the present-day ocean (~60%). In contrast, the modern Sr isotope values of ($^{87}Sr/^{86}Sr^*$, $\delta^{88/86}Sr)_{Seawater}$ and ($^{87}Sr/^{86}Sr^*$, $\delta^{88/86}Sr)_{Carbonates}$ form a mass-dependent isotope fractionation line. Carbonates are isotopically lighter because they preferentially incorporate the lighter isotopes and leave seawater enriched in the heavy ones.

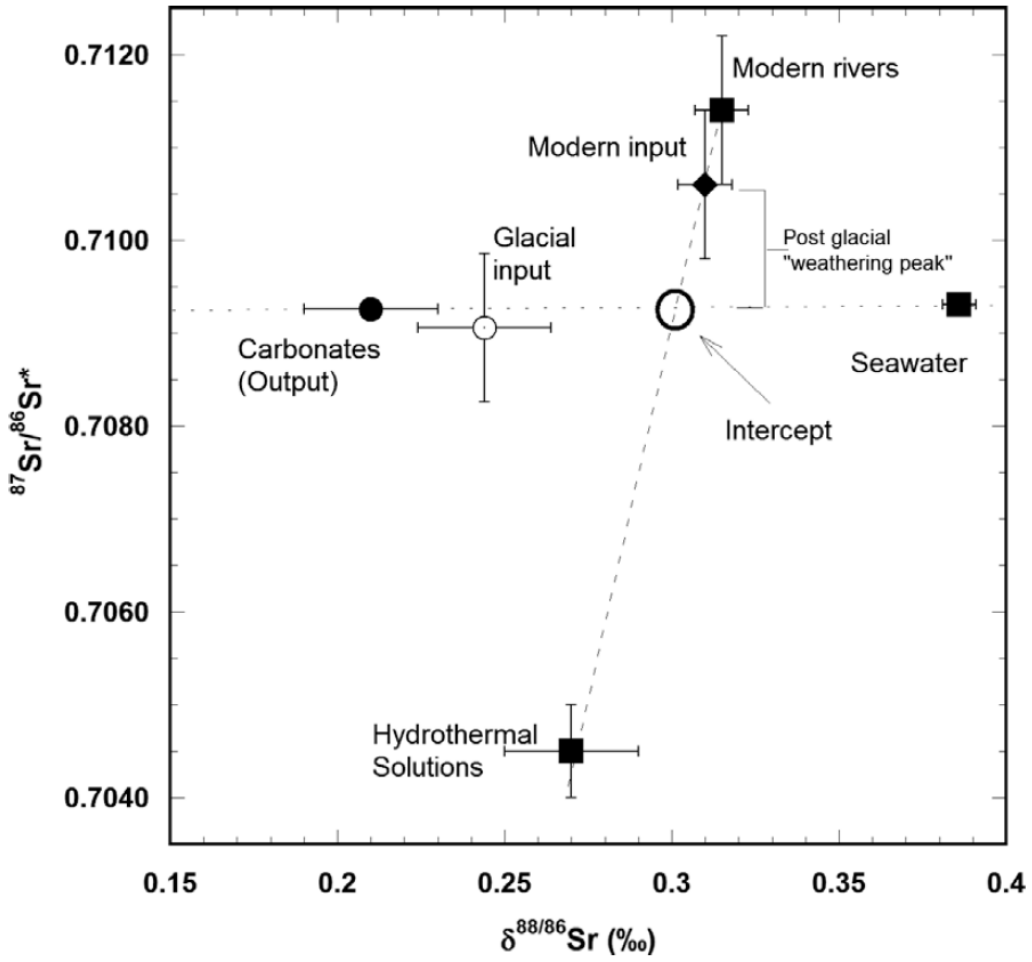

FIGURE III.3 - Triple isotope plot showing the flux-weighted average Sr isotope values of rivers, hydrothermal fluids, marine carbonates and seawater. The ($^{87}Sr/^{86}Sr^*$, $\delta^{88/86}Sr)_{Seawater}$ and the ($^{87}Sr/^{86}Sr^*$, $\delta^{88/86}Sr)_{Carbonates}$ values define a mass-dependent fractionation line, whereas ($^{87}Sr/^{86}Sr^*$, $\delta^{88/86}Sr)_{Rivers}$ and ($^{87}Sr/^{86}Sr^*$, $\delta^{88/86}Sr)_{HydEnd}$ values define a binary mixing line. The calculated ($^{87}Sr/^{86}Sr^*$, $\delta^{88/86}Sr)_{Input}$ values plots along the binary mixing line but are considerably offset from the isotope composition of marine carbonates. Note that the estimated glacial ($^{87}Sr/^{86}Sr^*$, $\delta^{88/86}Sr)_{Input}$ value is close to that of carbonates, indicating isotope equilibrium. The difference between modern ($^{87}Sr/^{86}Sr^*$, $\delta^{88/86}Sr)_{Input}$ and ($^{87}Sr/^{86}Sr^*$, $\delta^{88/86}Sr)_{Intercept}$ defines the "weathering peak".

The intercept of the binary mixing line and the fractionation line ($^{87}Sr/^{86}Sr^*$, $\delta^{88/86}Sr)_{Intercept}$ (~0.70927, ~0.30 ‰) defines the isotope composition of the combined Sr input into the ocean (Fig. III.3). These values are significantly different (~0.0011(8), ~0.01(2)‰) from the calculated ($^{87}Sr/^{86}Sr^*$, $\delta^{88/86}Sr)_{Input}$-values, and this difference reflects isotope disequilibrium. There is also a significant difference between the Sr isotopic composition of the ($^{87}Sr/^{86}Sr^*$, $\delta^{88/86}Sr)_{Input}$ and the Sr output values represented by ($^{87}Sr/^{86}Sr^*$, $\delta^{88/86}Sr)_{Carbonates}$ of (~0.0011(8), ~0.10(2)‰). This also indicates disequilibrium between inputs and outputs, because at

isotope equilibrium ($^{87}Sr/^{86}Sr^*$, $\delta^{88/86}Sr)_{Input}$ and ($^{87}Sr/^{86}Sr^*$, $\delta^{88/86}Sr)_{Carbonates}$ (output) should be identical (see Appendix).

In a first approach taking only $^{87}Sr/^{86}Sr^*$ values into account and leaving J_{HydEnd}, J_{OCC} and J_{Dia} (Tab. III.4) unchanged we can calculate from our isotope data that the combined J_{River} and J_{GW} input (~$49 \cdot 10^9$ mol/a) is about a factor of three too high to be in agreement with the $^{87}Sr/^{86}Sr^*$ output values. This observation is in general accord with earlier statements using traditional $^{87}Sr/^{86}Sr$ ratios that the estimated modern riverine flux is relatively accurate within ~30 % but is probably not representative of the past, particularly not for elements with residence times in excess of 10^5 years. In this regard, our observation that the modern ($^{87}Sr/^{86}Sr^*$, $\delta^{88/86}Sr)_{Input}$-value is higher than the ($^{87}Sr/^{86}Sr^*$, $\delta^{88/86}Sr)_{Intercept}$–value is compatible with earlier statements based on traditional $^{87}Sr/^{86}Sr$ values that modern continental weathering rates are 2-3 times higher than the long-term mean (VANCE et al., 2009). This post glacial "weathering peak" (Fig. III.3) is likely caused by weathering of fine-grained material left exposed by the retreating continental ice masses (c.f. (BLUM and EREL, 1997), see discussion in section 6).

At equilibrium the complete marine Sr budget requires agreement in the $^{87}Sr/^{86}Sr^*$ and $\delta^{88/86}Sr$ values of input and output fluxes. Interestingly, this cannot simply be achieved by reducing individual input fluxes because - within statistical uncertainties - there is no Sr source with a corresponding $\delta^{88/86}Sr$ value equal to or even lower than the modern $\delta^{88/86}Sr_{Carbonates}$ value (see Tab. III.4). This major discrepancy indicates that the marine Sr budget cannot be at equilibrium given the known Sr sources. At least one additional Sr source of sufficient size and with a $\delta^{88/86}Sr$ value lower than the mean $\delta^{88/86}Sr_{Carbonates}$ value is required to achieve equilibrium. The nature of this isotopically light, missing Sr source is discussed below.

Isotope equilibrium can be disturbed by sufficiently large addition or removal of Sr relative to the size of the marine Sr reservoir, provided the isotope composition is significantly different from that of seawater (STOLL and SCHRAG, 1998). The duration of such a perturbation is a function of the residence time, ~2.4 Myr in the case of Sr. On time scales

much longer than the Sr residence time slight imbalances between input and output fluxes can occur in quasi isotope equilibrium. It is thus very unlikely that the Sr fluxes and isotope compositions of hydrothermal sources are subject to a rapid change, as submarine hydrothermal circulation is controlled by processes in the Earth´s mantle characteristic time scales of 10^6-10^8 yrs, far in excess of the residence time of Sr in seawater.

A change of the preferred carbonate polymorphism may also lead to changes in Sr concentration of seawater, because Sr/Ca ratios of aragonite are about an order of magnitude higher than those of calcite. Strontium isotope measurements of calcitic foraminifera (Tab. III.3) confirm earlier conclusions based on Ca isotopes (FARKAŝ et al., 2007) that fractionation factors for aragonite and calcite differ. A change of the preferred carbonate polymorphism could therefore lead to changes in the isotopic composition of seawater. However, global changes of the preferred marine carbonate polymorphism occur on time scales much longer than the residence time of Sr in seawater (STANLEY and HARDIE, 1998), leaving the system in quasi steady state.

In contrast, continental weathering and related riverine inputs into the ocean may be subject of relatively rapid changes (10 to 100 kyr) when compared to the Sr residence time (~2.4 Myr). In addition, glacial/interglacial changes in sea level and the related dynamics of weathering of carbonates exposed on continental shelves may be responsible for substantial and short-term disequilibria between Sr inputs and outputs of the ocean, as proposed earlier by (STOLL and SCHRAG, 1998).

Sr isotope equilibrium in the ocean during the last glacial

A ~120 m drop in glacial sea level (STOLL and SCHRAG, 1998) exposed continental shelves and provided an additional supply of elements from the continents to the ocean. In particular, alkaline earth elements such as Mg, Ca and Sr are mobilized from weathering of carbonate-dominated continental shelves in larger amounts during glacial periods (c.f. STOLL et al.,

1999). Polymorphism exerts strong controls over Mg and Sr delivery, because calcite is Mg-rich compared to aragonite, whereas aragonite contains about 10 times more Sr than calcite (Tab. III.3). During meteoric diagenesis aragonite will eventually recrystallize to calcite and release Sr to the sea. (STOLL and SCHRAG, 1998) and (STOLL et al., 1999) hypothesize that this additional flux caused Sr/Ca of glacial seawater to increase. In contrast, sea level high-stand during interglacials flooded the shelves that then act as Sr sinks, causing seawater Sr/Ca values to decrease. These glacial/interglacial variations result in an oscillation of the marine Sr/Ca ratio of the order of ~±1% relative to the present day value (STOLL and SCHRAG, 1998). From the numerical integration of the (STOLL and SCHRAG, 1998) data we estimate, for the time interval from 10 to 20 ka, the average annual Sr flux of $\sim 150 \cdot 10^9$ mol/yr, approximately three times larger than the modern global mean Sr input ($\sim 56 \cdot 10^9$ mol/yr, Tab. III.4). The Sr input during the last glacial maximum ($\sim 206 \cdot 10^9$ mol/yr) was therefore dominated by carbonate weathering on the continental shelves rather than by weathering of the continental interiors. Taking shelf carbonate weathering and the above data into account, we estimate glacial ($^{87}Sr/^{86}Sr^*$, $\delta^{88/86}Sr)_{Input}$-values of (~0.7091(8), ~0.24(2)‰). These values differ significantly from the present-day ($^{87}Sr/^{86}Sr^*$, $\delta^{88/86}Sr)_{Input}$-values of (0.7106(8), 0.310(8)‰). Most importantly, the estimated glacial ($^{87}Sr/^{86}Sr^*$, $\delta^{88/86}Sr)_{Input}$-values are within uncertainty of the modern ($^{87}Sr/^{86}Sr^*$, $\delta^{88/86}Sr)_{Carbonates}$-values of (0.70926(2), 0.21(2)‰), indicating isotope equilibrium rather than disequilibrium conditions during the last glacial maximum (Fig. III.3).

Creating Sr budget disequilibrium during glacial/interglacial transitions

The predicted marine Sr equilibrium was probably terminated at the end of the glacial period by the rapid ~120 m sea level rise between the glacial low-stand at ~20 ka and the Holocene sea level maximum at ~6 ka. This rise eliminated shelf carbonate weathering as the major source of Sr, leaving riverine, groundwater and hydrothermal inputs as the major,

though drastically reduced, Sr fluxes to the modern ocean. Without shelf carbonate weathering, the new post-glacial mean Sr input value is expected to approach the intercept value defined by the binary mixing line and the mass-dependent fractionation line (Fig. III.3). However, the post-glacial (0.7106(8), 0.310(8) ‰)$_{Input}$-value is significantly more radiogenic in $^{87}Sr/^{86}Sr^*$ and tend to be heavier in the $\delta^{88/86}Sr$ value than the intercept values (~0.70927, ~0.30‰). This could indicate that riverine Sr inputs increased during glacial/interglacial transitions while continental shelf input decreased. Enhanced continental weathering may be caused by warmer post-glacial climate, higher atmospheric pCO_2 and enhanced precipitation. The retreating continental glaciers have also exposed finely ground material that provided an extra supply ("weathering peak", Fig. III.3) of isotopically more radiogenic Sr to the ocean (c.f. BLUM and EREL, 1995, VANCE et al., 2009). This "weathering peak" has not yet disappeared, and the Sr isotope compositions of modern input and output values have not yet reached a new post-glacial equilibrium.

III.5. Conclusion

During glacial periods weathering of continental shelf carbonates complemented inputs from rivers, groundwater and hydrothermal fluids as a fourth source of Sr to seawater. This fourth source dominated Sr fluxes to the ocean during glacial periods. The close agreement of the glacial Sr input values with modern carbonate output values is suggestive of isotope equilibrium during the last glacial maximum. A fundamental change in weathering regime during the glacial/interglacial transition perturbed the glacial Sr equilibrium towards the observed modern disequilibrium. The inferred change in weathering regime was facilitated by the rapid post-glacial sea level rise that flooded the continental shelves, terminated weathering fluxes from shelf carbonates and left riverine, groundwater and hydrothermal Sr fluxes as the major sources to the modern oceans. An additional shift towards heavier and more radiogenic Sr isotope composition may have occurred due to an additional flux of

isotopically heavy and radiogenic Sr ("weathering peak") from the fine-grained, highly reactive detritus that the retreating continental ice shields left behind.

III.6. Acknowledgements

Financial support was provided by the "Deutsche Forschungsgemeinschaft, DFG, Ei272/29-1 and Ei272/30-1 (TRION)". We thank A. Kolevica, T. Atwood and C. Miller for laboratory assistance and technical support. The comments and suggestions of two anonymous reviewers and the associate editor Prof. S. Krishnaswami helped to significantly improve this article.

III.7. Appendix

Notation and Terminology

$^{87}Sr/^{86}Sr$	This is the notation for the traditional radiogenic Sr isotope value. This ratio is measured by plasma or thermal ionization mass spectrometry and normalized to a $^{88}Sr/^{86}Sr$ ratio of 8.375209.
$^{87}Sr/^{86}Sr^*$	This ratio refers to the $^{87}Sr/^{86}Sr$ ratio as measured and normalized to a ^{87}Sr-^{84}Sr double spike (see Krabbenhöft et al., 2009). This ratio was <u>not</u> normalized to a $^{88}Sr/^{86}Sr$ ratio of 8.375209.
$\delta^{88/86}Sr$	This ratio refers to the $^{88}Sr/^{86}Sr$ ratio as measured and normalized to an ^{87}Sr-^{84}Sr double spike (see Krabbenhöft et al., 2009). The measured $^{88}Sr/^{86}Sr$ ratio is presented in the usual δ–notation in permil (‰) deviation from the SRM987 standard. Note that a $^{88}Sr/^{86}Sr$ ratio of 8.375209 corresponds to a $\delta^{88/86}Sr$-value of zero.
$^{87}Sr/^{86}Sr_{Norm}$	This ratio refers to the $^{87}Sr/^{86}Sr^*$ ratio which is renormalized to a $^{88}Sr/^{86}Sr$ ratio of 8.375209. The subscript "Norm" stands for normalization. The $^{87}Sr/^{86}Sr_{Norm}$ is equivalent to the traditional radiogenic $^{87}Sr/^{86}Sr$ ratio. However, in order to provide comparability and to emphasis the double-spike origin of the original value it is marked with the subscript "Norm".

Sr mass fractionation

$^{87}Sr/^{86}Sr^*$ and $^{88}Sr/^{86}Sr$ are determined from a double spike measurement following the procedures previously described by (KRABBENHÖFT et al., 2009). The relationship between the traditional radiogenic $^{87}Sr/^{86}Sr$ ratio, $^{87}Sr/^{86}Sr_{Norm}$ and $^{87}Sr/^{86}Sr^*$ is defined by equation III.A1:

$$III.A1: \quad \frac{\left(\frac{^{87}Sr}{^{86}Sr}\right)_{Norm}}{\left(\frac{^{87}Sr}{^{86}Sr}\right)^{*}} = \left[\frac{\left(\frac{^{88}Sr}{^{86}Sr}\right)_{Nier}}{\left(\frac{^{88}Sr}{^{86}Sr}\right)}\right]^{\frac{\ln(m_{87}/m_{86})}{\ln(m_{88}/m_{86})}}$$

The $(^{87}Sr/^{86}Sr)_{Nier}$ value has been defined as 8.375209 (NIER 1938), and corresponds to a $\delta^{88/86}Sr=0$ relative to NIST SRM 987. The masses of the various Sr isotopes are: m_{86} = 85.909273 m_{87} =86.908890, and m_{88} = 87.905625. For further details see (KRABBENHÖFT et al., 2009).

Error notation and propagation

All statistical uncertainties represent 2 standard errors of the mean ($2\sigma_{Mean}$). We present the statistical uncertainties for $^{87}Sr/^{86}Sr$ and $\delta^{88/86}Sr$ in brackets. The values in the brackets refer to the last digit of the measured values. For example $^{87}Sr/^{86}Sr$ = 0.711111(1) correspond to 0.711111±0.000001 and $\delta^{88/86}Sr$=0.386(1) correspond to 0.386±0.001‰.

Calculation of flux-weighted mean global river discharge to the ocean

$$\left(\frac{^{87}Sr}{^{86}Sr}\right)_{River} = \frac{\sum^{i} \left(\frac{^{87}Sr}{^{86}Sr}\right)^{i} \cdot Discharge\ river\ i}{\sum^{i} (Discharge\ river\ i)}$$

$$\delta^{88/86}Sr_{River} = \frac{\sum^{i} \left(\delta^{88/86}Sr\right)^{i} \cdot Discharge\ river\ i}{\sum^{i} (Discharge\ river\ i)}$$

Calculation of flux-weighted mean global input to the ocean

$$\left(\frac{^{87}Sr}{^{86}Sr}\right)_{Input} = \frac{\sum^{i} \left(\frac{^{87}Sr}{^{86}Sr}\right)^{i} \cdot Input\ i}{\sum^{i} (Input\ i)}$$

$$\delta^{88/86}Sr_{River} = \frac{\sum^{i} \left(\delta^{88/86}Sr\right)^{i} \cdot Input\ i}{\sum^{i} (Input\ i)}$$

Isotope equilibrium

Following the approach of (DE LA ROCHA and DEPAOLO, 2000) the condition of isotope equilibrium with respect to element input and output fluxes to the ocean can be mathematically described for the Sr isotope systems as follows. Note that the equations are given for $\delta^{88/86}Sr$, but are analogous for $^{87}Sr/^{86}Sr^{*}$:

$$III.A2: \quad N_{Sr} \cdot \frac{\partial \delta^{88/86}Sr_{Seawater}}{\partial t} = J_{Input} \cdot \left(\delta^{88/86}Sr_{Input} - \delta^{88/86}Sr_{Seawater}\right) - J_{Output} \cdot \Delta_{Output}$$

In a steady-state ocean where Sr input and output fluxes are equal ($J_{input}=J_{output}$) both the Sr isotope composition of seawater and the amount of Sr present in seawater are invariant ($d[Sr]_{Seawater}/dt=d(\delta^{88/86}Sr(t))/dt=0$). Equations III.A1 and III.A2 are reduced to III.A3:

$$III.A3: \Delta_{Output} = \delta^{88/86}Sr_{Carbonates} - \delta^{88/86}Sr_{Seawater}$$

III.8. Tables

TABLE III.1 - Sr flux and isotope composition of selected rivers

Nr.	River	Sample date and location	Water discharge [km³/yr]	Sr [μM]* ***	Sr Flux [mol/yr] ·10⁸	$^{87}Sr/^{86}Sr$	$^{87}Sr/^{86}Sr^*$	$^{87}Sr/Sr^{86}_{norm}$	$\delta^{88/86}Sr$ [‰]
1	Brahmaputra	06/21/06; 25.2833°N, 89.6333°E	510⁺	6,37	3.25	0.719218(26)	0.719320(3)	0.709205(3)	0.317(1)
2	Danube	05/04/07; 48.2261°N, 16.4086°E	207⁺	27,58	5.71	0.712723 (7)	0.712808(2)	0.712717(2)	0.254(4)
3	Fraser	08/08/06; 49.5633°N, 121.4028°W	112⁺	8,53	0.955	0.718662 (1)	0.718764(6)	0.718653(6)	0.31 (2)
4	Ganga	08/17/07; 24.0553°N, 89.0314°E	493⁺	6,59	3.25	0.727702 (9)	0.727798(6)	0.727705(6)	0.25 (2)
5	Hudson	07/02/08; 42.75°N,73.68°W	12⁺⁺	14,50	0.174	0.710328 (1)	0.710425(1)	0.710332(1)	0.260(1)
6	Indus	02/28/07; 25.4422°N, 68.3164°E	90⁺	33,33	3.00	0.711003(24)	0.711100(4)	0.710990(4)	0.31 (1)
7	Lena	n.a.	525⁺	11,01	5.78	0.709536(20)	0.709617(9)	0.709530(8)	0.243(6)
8	Mackenzie	04/07/07; 68.4659°N,134.1283°W	308⁺	23,70	7.30	0.711442 (8)	0.711547(7)	0.711434(7)	0.32 (2)
9	Maipo	01/29/07; 33.6288°N, 70.3548°W	3.6⁺⁺⁺	318,47	1.00	n.a.	0.707506(9)	0.707355(9)	0.42 (2)
10	Sacred Falls Punaluu, Hawaii	n.a.	n.a.	n.a.	1.00	0.707323 (8)	0.707417(9)	0.707321(2)	0.27 (3)
11	Rhine	8/25/07; 50.9481°N,6.9714°E	69.4⁺	62,25	4.32	0.709377 (9)	0.708799(6)	0.708713(9)	0.24 (1)
12	Saint Lawrence	05/18/08; 45.8586°N, 73.2397°W	337⁺	14,81	4.99	0.710362 (7)	0.71048 (1)	0.710354(7)	0.34 (3)
13	Yangtze	2007; 30.2872°N, 111.5264°E	900⁺⁺	22,31	20.7	0.710587 (7)	0.71072 (2)	0.710587(7)	0.38 (5)

Note: "n.a." = data not available. Data marked with (⁺) are from (GAILLARDET et al., 1999), (⁺⁺) (PALMER and EDMOND, 1989) and (⁺⁺⁺) from the United States Geological Survey (http://www.sage.wisc.edu/riverdata/). The errors are 2 standard error of the mean ($2\sigma_{mean}$). The $^{87}Sr/^{86}Sr_{norm}$ value is determined from the $\delta^{88/86}Sr$ and the $^{87}Sr/^{86}Sr^*$ value renormalized to $\delta^{88/86}Sr=0$ (see Appendix 2). (****): The Sr concentrations have typical uncertainties of ~2%. The Sr flux-weighted global mean ($^{87}Sr/^{86}Sr^*$, $\delta^{88/86}Sr)_{River}$ value of (0.7114(8), 0.315(8)‰) was calculated with equation A4 (Appendix).

TABLE III.2 - Mg/Sr and Sr isotope composition of hydrothermal fluids from MAR, 4°48′S

Label	Location	Depth [m]	Fluid [%]	T [°C]	Mg/Sr [mol/mol]	$^{87}Sr/^{86}Sr$*	$\delta^{88/86}Sr$ [‰]
42ROV-3	4°48′S, CC	2990	72	>400	303	0.707488(4)	0.361(6)
42ROV-4	4°48′S, CC	2990	80	>400	236	0.706643(3)	0.346(5)
42ROV-7	4°48′S, CC	2995	88	>400	144	0.706276(2)	0.324(5)
35ROV-8	4°48′S, TP	2990	100	450	3	0.705066(3)	0.26(2)
67ROV-4	4°48′S, RL	3045	80	366	177	0.705808(3)	0.29(1)
67ROV-5	4°48′S, RL	3045	98	366	23	0.703857(1)	0.253(1)
67ROV-6	4°48′S, RL	3045	81	366	164	0.705179(1)	0.294(3)

Note: TP = Turtle Pits, CC = Comfortless Cove; RL = Red Lion. The errors are 2 standard error of the mean ($2\sigma_{mean}$).

TABLE III.3 - Sr burial fluxes and isotopic composition

Carbonate Sediment Type	$CaCO_3$ Deposition [10^{12} mol/yr]	$CaCO_3$ polymorph	Mean Sr/Ca [mmol/mol]	Sr Burial Flux (10^9 mol/yr)	$^{87}Sr/^{86}Sr^*$	$\delta^{88/86}Sr$ [‰] (SRM987)
	1.	2.	3.	4.	5.	6.
Reef Corals (JCp-1 coral standard)	~6.0 (0%)	Aragonite	~9.0	~54 (31%)	0.70923(1)	0.19(1)‰
Halimeda	~1.5 (5%)	Aragonite	~11	~16 (9%)	0.70926(3)	0.27(3)‰
Coccoliths	~5.0 (6%)	Calcite	2.2	~11 (6%)	0.70926(3)	0.26(7)‰
Planktic Foraminifera	~6.0 (0%)	Calcite	1.4	~8 (5%)	0.70920(2)	0.14(1)‰
Continental shelf and slope taxa (mussels, starfish, etc.)	~13.0 (39%)	Aragonite and calcite	~6.6	~85 (49%)	0.70924(1)	0.22(3)‰
Total Carbonates	~32.0 (100%)	---	n.a.	~174(100%)		
Average					0.70924(2)	0.22(2)‰
Sr burial flux weighted average					0.70926(2)	0.21(2)‰

Column 1: Reef Corals: The deposition rate of reefs has been estimated at $7.0 \cdot 10^{12}$ mol/yr (MILLIMAN and DROXLER, 1996). Note that the deposition rates in column 1 are afflicted with large statistical uncertainties: reef corals, coccoliths, and planktic foraminfera have uncertainties on the order of ±50%, and continental shelf and slope taxa have uncertainties of 50% and >100%, respectively. The $CaCO_3$ burial rate related to reef coral formation is estimated at $\sim 6.0 \cdot 10^{12}$ mol/yr based on estimates that ~85% of reef $CaCO_3$ is derived solely from corals (HUBBARD et al., 1990). Mean Sr/Ca values are compiled from published data on *Acropora, Diploria, Montastrea, Montipora, Pavona* and *Porites* (COHEN and THORROLD, 2007; GALLUP et al., 2006; SUN et al., 2005). The average ($^{87}Sr/^{86}Sr^*$, $\varepsilon^{88/86}Sr$)-values are adopted from the long-term average value of the JCp-1 coral standard.

Halimeda: Halimeda Sr/Ca ratio is from (DELANEY et al., 1996). ($^{87}Sr/^{86}Sr^*$, $\varepsilon^{88/86}Sr$) values are measured on Halimeda specimens from Tahiti and the Mediterranean Sea.

Coccoliths: $CaCO_3$ burial rate is from (SCHIEBEL, 2002) and (BROECKER and CLARK, 2009). Mean Sr/Ca ratios are from (STOLL and SCHRAG, 2000). The $\varepsilon^{88/86}Sr$ value is the average of various measurements on laboratory-cultured *Emiliania huxleyi* and *Coccolithus pelagicus*.

Planktic Foraminifera: The $CaCO_3$ burial rate is from (SCHIEBEL, 2002). Mean Sr/Ca ratios are from (KISAKÜREK et al., 2008). The ($^{87}Sr/^{86}Sr^*$, $\varepsilon^{88/86}Sr$)-values were determined on *G. ruber* and *G. sacculifer*, separated from core SO 164-03-4 from the central Caribbean Sea (16°32'37''N, 72°12'31''W, 2744 m).

Continental shelf and slope taxa: $CaCO_3$ sediments on the continental shelves and slopes are produced by a variety of taxa, including species mentioned above. For further discussion we assume shelf species to be two-thirds aragonitic (Sr/Ca ~9 mmol/mol) and one-third calcitic (Sr/Ca ~1.8 mmol/mol), yielding a Sr/Ca ratio of ~6.6 mmol/mol. Note, that despite their importance to the total Sr burial flux, the contribution of the shelf taxa is afflicted a with large uncertainty (50 - > 100%).

Column 4 is calculated from the values in columns 1 and 3. The values in brackets in columns 5 and 6 correspond to $2\sigma_{mean}$ that reflect only Sr isotope error propagation. Burial rate uncertainties are not included in the uncertainties in columns 5 and 6.

TABLE III.4 - Sources of Sr to the ocean:

Sr Sources		$^{87}Sr/^{86}Sr$	$^{87}Sr/^{86}Sr_{norm}$	$^{87}Sr/^{86}Sr^*$	$\delta^{88/86}Sr$ [‰]	Flux [10^9 mol/yr]
River discharge	J_{River}	0.7119(9)[1#]	0.7113(4)	0.7114(8)	0.315(8)	~33.3±10[1]
Groundwater discharge	J_{GW}	0.7110[2]	n.a.	n.a.	n.a.	~16.5± 8[2]
Oceanic crust-seawater interaction at mid-ocean ridges	J_{HydEnd}	0.7025[3]	0.70438(3)	0.7045(5)	0.27(3)	~2.3[3]±1.2°
Low-temperature interaction on ridge flanks and within the cold oceanic crust	J_{OCC}	0.7025[3]	n.a.	n.a.	n.a.	~0.8±0.4[3]
Diagenetic flux from marine sediments	J_{DIA}	0.7084[1]	n.a.	n.a.	n.a.	~3.4±1.7[1]
Sr Flux-weighted average	J_{Input}	~0.7109	n.a.	~0.7106(8)	~0.310(8)	~56.3±13

Note: All ($^{87}Sr/^{86}Sr^*$, $\delta^{88/86}Sr$)-values are from this study. (1) (PALMER and EDMOND, 1989), (2) (BASU et al., 2001), 50% uncertainty is arbitrarily assigned to this value, (3) (DAVIS et al., 2003), 50% uncertainty is arbitrarily assigned to this value. The major Sr inputs to the ocean are river discharge (J_{RW}), groundwater discharge (J_{GW}) and oceanic crust-seawater interaction (J_{OCH}) at mid ocean ridges. All other Sr fluxes generated by low temperatures interactions on ridge flanks, (J_{OCC}), Sr inputs from sedimentary pore waters and from recrystallizing sediments (J_{DIA}) are arbitrarily assigned uncertainties of 50%. **"n.a."**: **n**ot **a**vailable. The Sr isotope composition of the input is calculated from the values above. For simplification and due to the lack of data we assume that the ($^{87}Sr/^{86}Sr^*$, $\delta^{88/86}Sr$) -values of J_{GW} are equal to J_{Rivers} and that the ($^{87}Sr/^{86}Sr^*$, $\delta^{88/86}Sr$)-values of J_{OCC} and of J_{DIA} are equal to J_{HydEnd}**. #:** the statistical uncertainty was estimated from the half difference between the minimum estimate of the global mean value of 0.7101 (GOLDSTEIN and JACOBSEN (1987) and the maximum estimate by PALMER and EDMOND (1989). **°:** Estimates of the hydrothermal input range from minimum values of ~$1.9 \cdot 10^9$ mol/yr (GOLDSTEIN and JACOBSEN (1987) to $15 \cdot 10^9$ mol/yr (PALMER and EDMOND, 1989). However, the maximum value is estimated based on the assumption of Sr equilibrium, whereas the lower values are based on different independent approaches. Hence, for our discussion we adopted the most recent estimate of (DAVIS et al., 2003) as the best approximation of the global hydrothermal Sr flux. The Sr flux-weighted global mean ($^{87}Sr/^{86}Sr^*$, $\delta^{88/86}Sr)_{Input}$ values of (0.7106(8), 0.310(8)‰) were calculated with equation A6 (Appendix).

III.9. References

Amini, M., Eisenhauer, A., Böhm, F., Fietzke, J., Bach, W., Garbe-Schönberg, D., Rosner, M., Bock, B., Lackschewitz, K. S., and Hauff, F., 2008. Calcium Isotope (◎44/40Ca) Fractionation Along Hydrothermal Pathways, Logatchev Field (Mid-Atlantic Ridge, 14° 45'N). Geochim. Cosmochim. Acta 72, 4107-4122.

Andersson, P. S., Wasserburg, G. J., and Ingri, J., 1992. The Sources and Trasport of Sr and Nd Isotopes in the Baltic Sea. Earth Planet. Sci. Lett. 113, 459-472.

Basu, A. R., Jacobsen, S. B., Poreda, R. J., Dowling, C. B., and Aggarwal, P. K., 2001. Large Groundwater Strontium flux to the Oceans from the Bengal Basin and the Marine Strontium Isotope Record. Science 293, 1470-1473.

Bard E., B. Hamelin, M. Arnold, L. Montaggioni, G. Cabioch, G. Faure and F. Rougerie, 1996. Deglacial sea-level record from Tahiti corals and the timing of global meltwater discharge. Nature 382, 241-244.

Blum and Erel, 1995. A silicate weathering mechanism linking increases in marine 87Sr/86Sr with global glaciation. Nature, 373, 415-418.

Broecker, W. and Clark, E., 2009. Ratio of coccolith CaCO3 to foraminifera CaCO3 in late Holocene deep sea sediments. Paleoceanography 24, doi:10.1029/2009PA001731.

Butterfield, D. A., Nelson, B. K., Wheat, C. G., Mottl, M. J., and Roe, K. K., 2001. Evidence for Basaltic Sr in Mid Ocean Ridge-Flank Hydrothermal Systems and Implications for the Global Oceanic Sr Isotope Balance. Geochim. Cosmochim. Acta 65, 4141-4153.

Cohen, A. L. and Thorrold, S. R., 2007. Recovery of Temperature Records from slow-growing Corals by fine Scale Sampling of Skeletons. Geophys. Res. Lett. 34, 6, L17706, doi:10.1029/2007GI030967.

Davis, A. C., Bickle, M. J., and Teagle, D. A. H., 2003. Imbalance in the Oceanic Strontium Budget. Earth Planet. Sci. Lett. 211, 173-187.

De La Rocha, C. L. and DePaolo, D. J., 2000. Isotopic Evidence for Variations in the Marine Calcium Cycle over the Cenozoic. Science 289, 1176-1178.

Delaney, M. L., Linn, L. J., and Davies, P. J., 1996. Trace and minor element ratios in Halimeda aragonite from the Great Barrier Reef. Coral Reefs 15, 181-189.

Elderfield, H. and Gieskes, J. M., 1982. Sr Isotopes in Interstitial Waters of Marine Sediments from deep-sea Drilling Project Cores. Nature 300, 493-497.

Fairbanks, R.F., 1989. A 17,000-year glacio-eustatic sea level record: influence of glacial melting rates on the Younger Dryas event and deep-ocean circulation. Nature, 342, 637-642.

Farkaŝ, J., Buhl, D., Blenkinsop, J., and Veizer, J., 2007. Evolution of the Oceanic Calcium Cycle During the late Mesozoic: Evidence from Delta ◎44/40Ca of Marine Skeletal Carbonates. Earth Planet. Sci. Lett. 253, 96-111.

Faure, G. and Felder, R. P., 1981. Isotopic Composition of Strontium and Sulfur in Secondary Gypsum Crystals, Brown Hills, Transantarctic Mountains. Journal of Geochemical Exploration 14, 265-270.

Fietzke, J. and Eisenhauer, A., 2006. Determination of Temperature-Dependent Stable Strontium Isotope (88Sr/86Sr) Fractionation via Bracketing Standard MC-ICP-MS. Geochem. Geophys. Geosyst. 7(8) doi: 10.1029/2006GC001244.

Gaillardet, J., Dupre, B., and Allègre, C. J., 1999. Geochemistry of Large River Suspended Sediments: Silicate Weathering or Recycling Tracer? Geochim. Cosmochim. Acta 63, 4037-4051.

Gallup, C. D., Olson, D. M., Edwards, R. L., Gruhn, L. M., Winter, A., and Taylor, F. W., 2006. Sr/Ca-Sea Surface Temperature Calibration in the Branching Caribbean Coral Acropora Palmata. Geophys. Res. Lett. 33, 4, L03606, doi:10.1029/2005GL024935.

Godderis, Y. and Veizer, J., 2000. Tectonic Control of Chemical and Isotopic Composition of Ancient Oceans: The Impact of Continental Growth. Am. J. Sci. 300, 434-461.

Goldstein S. J. and Jacobsen S. B. 1987. The Nd and Sr isotopic systematics of river-water dissolved material: implications for the sources of Nd and Sr in seawater. Chem. Geol. 66, 245-272.

Graham, S. T., Famiglietti, J. S., and Maidment, D. R., 1999. Five-Minute, 1/2 Degrees, and 1 Degrees data sets of Continental Watersheds and River Networks for use in Regional and Global Hydrologic and Climate System Modeling Studies. Water Resources Research 35, 583-587.

Haase, K. M., Petersen, S., Koschinsky, A., Seifert, R., Devey, C. W., Keir, R., Lackschewitz, K. S., Melchert, B., Perner, M., Schmale, O., Suling, J., Dubilier, N., Zielinski, F., Fretzdorff, S., Garbe-Schönberg, D., Westernstroer, U., German, C. R., Shank, T. M., Yoerger, D., Giere, O., Kuever, J., Marbler, H., Mawick, J., Mertens, C., Stober, U., Ostertag-Henning, C., Paulick, H., Peters, M., Strauss, H., Sander, S., Stecher, J., Warmuth, M., and Weber, S., 2007. Young Volcanism and Related Hydrothermal Activity at 5° S on the Slow-Spreading Southern Mid-Atlantic Ridge. Geochem. Geophys. Geosyst. 8, 17, doi: 10.1029/2006GC001509.

Halicz, L., Segal, I., Fruchter, N., Stein, M., and Lazar, B., 2008. Strontium Stable Isotopes Fractionate in the soil Environments? Earth Planet. Sci. Lett. 272, 406-411.

Hubbard, D. K., Miller, A. I., and Scaturo, D., 1990. Production and Cycling of Calcium-Carbonate in a Shelf-edge reef System (St.Croix, United-States Virgin-Islands) - Applications to the Nature of reef Systems in the Fossil Record. Journal of Sedimentary Petrology 60, 335-360.

Kisakürek, B., Eisenhauer, A., Böhm, F., Garbe-Schönberg, D., and Erez, J., 2008. Controls on Shell Mg/Ca and Sr/Ca in Cultured Planktonic Foraminifera. Earth Planet. Sci. Lett 273, 260-269.

Krabbenhöft, A., Fietzke, J., Eisenhauer, A., Liebetrau, V., Böhm, F., and Vollstaedt, H., 2009. Determination of radiogenic and stable strontium isotope ratios (87Sr/86Sr/⍟88/86Sr) by thermal ionization mass spectrometry applying an 87Sr/84Sr double spike. Journal of Analytical Atomic Spectrometry 24, 1267-1271.

Liebetrau, V., Eisenhauer, A., Krabbenhöft, A., Fietzke, J., Böhm, F., Rüggeberg, A., and Guers, K., 2009. New Perspectives on the Marine Sr-isotope record: ⍟88/86Sr, 87Sr/86Sr* and ⍟44/40Ca Signatures of Aragonitic Molluscs Throughout the last 27 Ma. Geochim. Cosmochim. Acta 73, A762.

Lindberg, B. and Mienert, J., 2005. Postglacial Carbonate Production by cold-water Corals on the Norwegian Shelf and their role in the Global Carbonate Budget. Geology 33, 537-540.

McArthur, J. M., 1994. Recent Trends in Srontium Isotope Stratigraphy. Terr. Nova 6, 331-358.

McArthur, J. M., Howarth, R. J., and Bailey, T. R., 2001. Strontium Isotope Stratigraphy: LOWESS Version 3: Best fit to the Marine Sr-Isotope Curve for 0-509 Ma and Accompanying look-up Table for Deriving Numerical age. Journal of Geology 109, 155-170.

Milliman, J. D. and Droxler, A. W., 1996. Neritic and Pelagic Carbonate Sedimentation in the Marine Environment: Ignorance is not Bliss. Geol. Rundsch. 85, 496-504.

Mottl, M. J., Wheat, G., Baker, E., Becker, N., Davis, E., Feely, R., Grehan, A., Kadko, D., Lilley, M., Massoth, G., Moyer, C., and Sansone, F., 1998. Warm Springs Discovered on 3.5 Ma Oceanic Crust, Eastern Flank of the Juan de Fuca Ridge. Geology 26, 51-54.

Nier , A. O., 1938. The Isotopic Constitution of Strontium, Barium, Bismuth, Thallium and Mercury. Physical Review 5, 275-279.

Ohno, T., Komiya, T., Ueno, Y., Hirata, T., and Maruyama, S., 2008. Determination of 88Sr/86Sr Mass-Dependent Isotopic and Radiogenic Isotope Variation of 87Sr/86Sr in the Neoproterozoic Doushantuo Formation. Gondwana Res. 14, 126-133.

Palmer, M. R. and Edmond, J. M., 1989. The Strontium Isotope Budget of the Modern Ocean. Earth Planet. Sci. Lett. 92, 11-26.

Palmer, M. R. and Edmond, J. M., 1992. Controls Over the Strontium Isotope Composition of River Water. Geochim. Cosmochim. Acta 56, 2099-2111.

Peucker-Ehrenbrink, B. and Miller, M. W., 2007. Quantitative bedrock geology of the continents and large-scale drainage regions. Geochem. Geophys. Geosyst. 8 (6), doi: 10.1029/2006GC001544

Peucker-Ehrenbrink, B., 2009. Land2Sea database of river drainage basin sizes, annual water discharges, and suspended sediment fluxes. Geochem. Geophys, Geosyst. 10 (6), doi: 10.1029/2008GC002356.

Peucker-Ehrenbrink B., Miller M. W., Arsouze T., and Jeandel C. (in press) Continental bedrock and riverine fluxes of strontium and neodymium isotopes to the oceans. Geochemistry Geophysics Geosystems.

Ravizza, G., Blusztajn, J., Von Damm, K. L., Bray, A. M., Bach, W., and Hart, S. R., 2001. Sr Isotope Variations in vent Fluids from 9° 46 '- 9° 54 ' N East Pacific Rise: Evidence of a non-zero-Mg Fluid Component. Geochim. Cosmochim. Acta 65, 729-739.

Rüggeberg, A., Fietzke, J., Liebetrau, V., Eisenhauer, A., Dullo, W. C., and Freiwald, A., 2008. Stable Strontium Isotopes (◎88/86Sr) in Cold-Water Corals - A new Proxy for Reconstruction of Intermediate Ocean Water Temperatures. Earth Planet. Sci. Lett. 269, 569-574.

Schiebel, R., 2002. Planktic Foraminiferal Sedimentation and the Marine Calcite Budget. Glob. Biogeochem. Cycle 16, 21.

Stanley, S. M. and Hardie, L. A., 1998. Secular Oscillations in the Carbonate Mineralogy of Reef-Building and Sediment-Producing Organisms Driven by Tectonically Forced Shifts in Seawater Chemistry. Paleogeogr. Paleoclimatol. Paleoecol. 144, 3-19.

Stoll, H. M. and Schrag, D. P., 1998. Effects of Quaternary sea Level Cycles on Strontium in Seawater. Geochim. Cosmochim. Acta 62, 1107-1118.

Stoll, H. M., Schrag, D. P., and Clemens, S. C., 1999. Are Seawater Sr/Ca Variations Preserved in Quaternary Foraminifera? Geochim. Cosmochim. Acta 63, 3535-3547.

Stoll, H. M. and Schrag, D. P., 2000. Coccolith Sr/Ca as a new Indicator of Coccolithophorid Calcification and Growth rate. Geochem. Geophys. Geosys. 1, 1999GC000015.

Sun, Y., Sun, M., Lee, T., and Nie, B., 2005. Influence of Seawater Sr Content on Coral Sr/Ca and Sr Thermometry. Coral Reefs 24, 23-29.

Vance, D., Teagle, D. A. H., and Foster, G. L., 2009. Variable Quaternary Chemical Weathering Fluxes and Imbalances in Marine Geochemical Budgets. Nature 458, 493-496.

Veizer, J., 1989. Strontium Isotopes in seawater through time. Annu. Rev. Earth Planet. Sci. 17, 141-167.

IV. Chapter

Linking marine carbonate burial and long-term anoxia to the end-Permian mass extinctions

Hauke Vollstaedt[1], Anton Eisenhauer[1], Florian Böhm[1], Jan Fietzke[1], Klaus Wallmann[1], Volker Liebetrau[1], André Krabbenhöft[1,+], Juraj Farkaš[2,3], Adam Tomašových[4], and Ján Veizer[5]

[1] *GEOMAR, Helmholtz-Zentrum für Ozeanforschung Kiel, Wischhofstr. 1-3, 24148 Kiel, Germany*
[2] *Department of Geochemistry, Czech Geological Survey, Geologická 6, 152 00 Prague 5, Czech Republic*
[3] *Department of Environmental Geosciences, Czech University of Life Sciences, Kamýcká 129, 165 21 Prague 6, Czech Republic*
[4] *Department of Geophysical Sciences, The University of Chicago, 5734 S Ellis Ave., IL 30367, Chicago, USA*
[5] *Ottawa-Carleton Geoscience Center, University of Ottawa, Ottawa ON K1N 6N5, Canada*
[+] *Present address: Leyegasse 4, 69117 Heidelberg, Germany*

In review in *Geology*

Abstract

The largest mass extinctions within the Phanerozoic Eon occurred at the Permian/Triassic (P/T) boundary with the extinction of ~96 % of all marine species. The extinction scenarios suggested include ocean acidification, ocean anoxia, a methane release to the ocean-atmosphere system, and an extraterrestrial impact. Although these scenarios are relevant for the P/T marine carbonate system the seawater carbonate chemistry has yet to be constrained. Here we produce the first Phanerozoic seawater $\delta^{88/86}$Sr-record to constrain carbonate burial rates. The largest change of $\delta^{88/86}$Sr occurred across the P/T boundary that lasted for ~21 Myrs. We use a numerical model to ascribe this $\delta^{88/86}$Sr-excursion to an enhanced marine carbonate burial and related alkalinity production which was most likely driven by bacterial sulfate reduction (BSR) in deeper anoxic waters. In contrast to earlier inferences, we consider the long-term seawater anoxia to be generally responsible for both end-Permian mass extinctions recorded at ~260 Ma and ~251 Ma. However, the combination of long-term seawater anoxia and short-term ocean acidification which has been observed in earlier studies explains why the Siberian Traps were much more deadly for biota than other large igneous provinces (LIPs) of comparable size.

IV.1. Introduction

The largest mass extinctions within the Phanerozoic Eon occurred at the end of the Permian period, killing ~96 % of all marine species (Raup, 1979; Wignall, 2007). Several killing mechanisms have been suggested to explain this severe biotic crisis: i) CO_2-driven ocean acidification linked to Siberian Trap volcanism; ii) a global oceanic anoxic event associated with the overturning of ocean water; iii) a sudden methane (CH_4) release to the ocean-atmosphere system; and iv) an extraterrestrial impact (WIGNALL, 2007; CHEN and BENTON, 2012; PAYNE and CLAPHAM, 2012).

Information about the environmental conditions and triggers for the end-Permian extinctions can be inferred from the geological record and in particular from the analysis of suitable isotope systems as well as from the extinction selectivity (WIGNALL, 2007; PAYNE and CLAPHAM, 2012). Patterns of taxonomic and ecologic selectivity at the end-Guadalupian (~260 Ma) and the P/T transition (~251 Ma) reveal a selection against genera with poorly buffered respiratory physiology, suggesting a combination of warming, hypercapnia, ocean acidification and hypoxia as a cause for both mass extinctions (Payne and Clapham, 2012). Isotope records of carbon (C), calcium (Ca), and sulfur (S) suggest i) the injection of ^{13}C-depleted carbon to the oceans and atmosphere, ii) a short-term marine carbonate dissolution event caused by ocean acidification resulting from massive CO_2 related to Siberian Trap volcanism, and iii) long-term high BSR rates associated with increased pyrite burial in the deep ocean superimposed by the upwelling of deep anoxic waters at the P/T boundary, respectively (Payne and Clapham, 2012). The large rate of increase (~0.0001 $Myrs^{-1}$) in the radiogenic strontium (Sr) isotope ratio ($^{87}Sr/^{86}Sr$) across the P/T boundary has been best attributed to enhanced continental weathering rates due to increased pCO_2 levels in the atmosphere and the fragmentation of the Pangaea supercontinent (Kramm and Wedepohl, 1991; Martin and Macdougall, 1995).

Arguments for a long-term crisis prior to the P/T event may be tested by verifying the carbonate budget of the P/T ocean based on the novel $\delta^{88/86}Sr$-record of Phanerozoic seawater ($\delta^{88/86}Sr_{sw}$). We measured both radiogenic and natural Sr fractionation ($\delta^{88/86}Sr$) on globally distributed brachiopod samples to constrain changes in paleo-seawater chemistry. The novel $\delta^{88/86}Sr_{sw}$-record adds quantitative information about the marine Sr output flux, primarily controlled by the burial of marine carbonates (Krabbenhöft et al., 2010). This is because the precipitation of calcite and aragonite preferentially incorporates the light Sr isotope, leaving seawater isotopically heavier (Fietzke and Eisenhauer, 2006; Krabbenhöft et al., 2010). Consequently, increasing $\delta^{88/86}Sr_{sw}$ values are indicative of a ratio below unity between Sr input and output fluxes in the oceans and vice versa.

IV.2. Results and discussion

We found that the $\delta^{88/86}Sr$ values of modern brachiopods are independent of habitat location and water temperature with a mean of 0.176±0.016 ‰ (Fig. IV.1B). This corresponds to a fractionation factor of $\Delta^{88/86}Sr$ = -0.21 ‰ with respect to modern seawater ($\delta^{88/86}Sr_{sw}$ = 0.386±0.016 ‰ (2 s.d. of the mean, n=10 (Krabbenhöft et al., 2009))). We therefore propose that brachiopod samples are a reliable archive for the reconstruction of $\delta^{88/86}Sr$ values of seawater in geological history. In contrast, studies on warm and cold water corals found a temperature-dependent isotope fractionation in carbonates (Fietzke and Eisenhauer, 2006; Rüggeberg et al., 2008). This species dependent behavior is analogous to Ca isotopes and a result of diverse biomineralization processes (Farkaš et al., 2007).

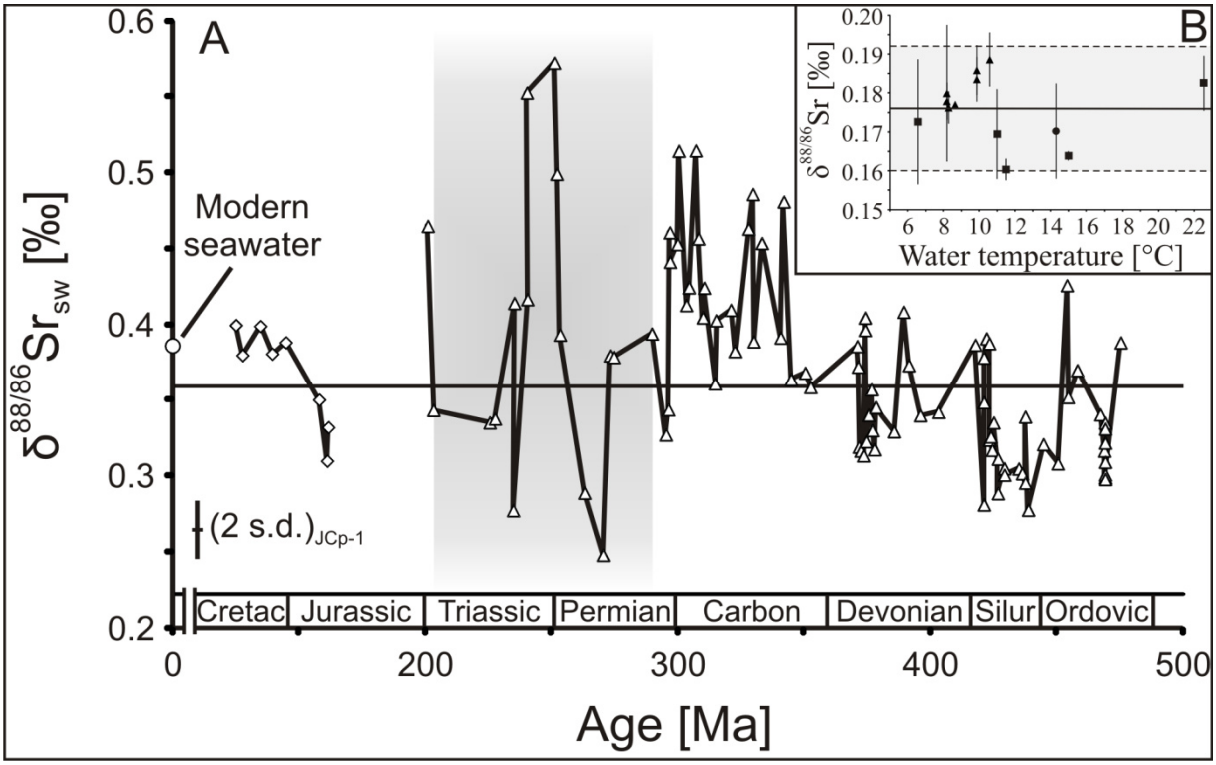

FIGURE IV.1 - A. Phanerozoic $\delta^{88/86}Sr_{sw}$ record from brachiopod (triangles) and belemnite (diamonds) samples (See the methods description, Table IV.DR1, IV.DR5, and IV.DR6). Prominent excursions in $\delta^{88/86}Sr_{sw}$ are observed across the P/T transition. The time scale and stratigraphic periods are taken from (Ogg et al., 2008). Modern $\delta^{88/86}Sr_{sw}$ (open circle) is taken from (Krabbenhöft et al., 2010). The horizontal line represents the mean Phanerozoic $\delta^{88/86}Sr_{sw}$ of 0.36‰. Grey shaded area marks the time interval between ~290Ma and ~203Ma which is the focus of the numerical model. Abbreviations for geological periods: Ordovic = Ordovician, Silur = Silurian, Carbon = Carboniferous, Cretac = Cretaceous. B. $\delta^{88/86}Sr$ measured in modern brachiopods. We found that $\delta^{88/86}Sr$ is independent of habitat location (Triangles = North Atlantic, squares = Pacific, circle = Mediterranean Sea), species, and water temperature with a mean of 0.176±0.016 ‰ (black line with 2 s.d. of the mean (dashed line), n=13, table IV.DR1 in the supplementary material (section IV.5)).

Our Phanerozoic $\delta^{88/86}Sr_{sw}$ record shows significant variations between 0.24 ‰ and 0.57 ‰ with a mean of 0.36 ‰ (Fig. IV.1A). The largest variability with both the lowest and the highest $\delta^{88/86}Sr_{sw}$ values is observed right across the P/T boundary. $\delta^{88/86}Sr_{sw}$ and chemically similar $\delta^{44/40}Ca_{sw}$ (Farkaš et al., 2007) reveal different patterns that are a result of different controlling factors of these two marine isotope systems. In particular, carbonate mineralogy, temperature, carbonate ion concentration, dolomitization, and changes in organic/inorganic precipitation are supposed to have a different impact on the Sr and Ca isotope systems (Farkaš et al., 2007). The observed fluctuations in $\delta^{88/86}Sr_{sw}$ suggest major

perturbations of the marine carbonate burial fluxes. In order to quantify P/T carbonate burial fluxes and to extend earlier published P/T scenarios we developed a numerical box model to investigate in changes in the inventory and fluxes of Sr, Ca, and total alkalinity (TA) (See Fig. IV.DR3-DR11, Table IV.DR2-DR4, and the model description in the supplementary material (section IV.5)). The marine Sr budget can be described by the fluxes of continental weathering ($\delta^{88/86}Sr_{weath}$ = 0.21 ‰), hydrothermal input ($\delta^{88/86}Sr_{hyd(in)}$ = 0.27 ‰), alteration of the oceanic crust ($\Delta^{88/86}Sr_{hyd(out)}$ = 0.0 ‰), and carbonate-related net flux of burial and dissolution ($\Delta^{88/86}Sr_{carb}$ = -0.24 ‰) (Fig. IV.DR3, table IV.DR4). Sr and Ca input fluxes from continental weathering and at mid-ocean ridges are constrained from continental weathering rates and published $^{87}Sr/^{86}Sr$ ratios (Veizer et al., 1999; Wallmann, 2001) (Fig. IV.2A). The carbonate-related net fluxes of Sr ($F(Sr)_{carb}$) and Ca ($F(Ca)_{carb}$) are calculated both from the new $\delta^{88/86}Sr_{sw}$-values and the published seawater Sr/Ca record (Steuber and Veizer, 2002) ($(Sr/Ca)_{sw}$, Fig. IV.2A).

Our model results suggest that the decline in $\delta^{88/86}Sr_{sw}$, recorded at ~272 Ma and ~236 Ma (Fig. IV.2A) reflects a net-input of $F(Sr)_{carb}$ and a corresponding increase in the seawater Sr concentration (Sr_{sw}) (Fig. IV.2B). This is possibly due to a weathering pulse of exposed isotopically light shelf carbonates related to the end of the Permo-Carboniferous continental glaciations (Haq and Schutter, 2008) (Fig. IV.2B). The trend towards high $\delta^{88/86}Sr_{sw}$-values in the time interval from the Late Permian and Early Triassic period (~262 Ma to ~241 Ma) reflect a prolonged period of enhanced carbonate burial (on average ~17 Tmol Ca/yr) with a maximum right at the P/T boundary. This has not been recognized before and the increasing carbonate burial rates correspond to decreasing Sr_{sw} (Fig. IV.2B),

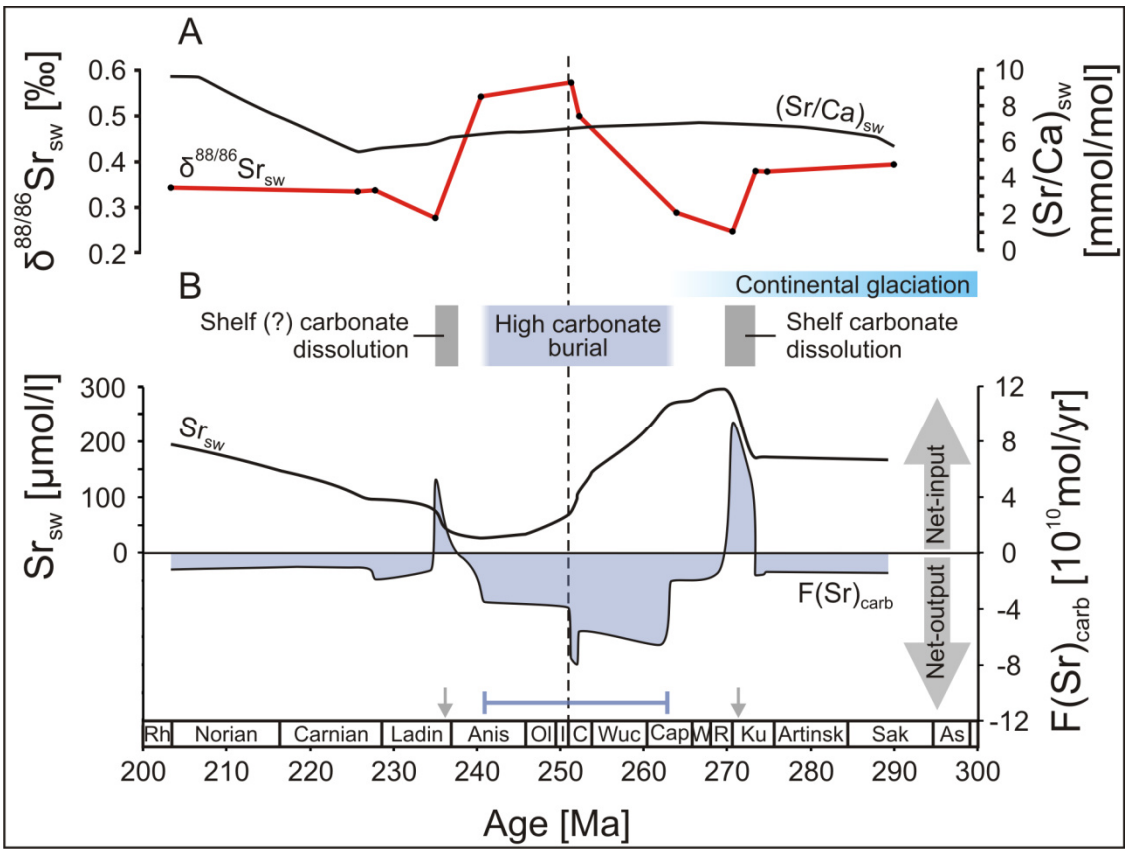

FIGURE IV.2 - A: Model input parameters. Measured $\delta^{88/86}Sr_{sw}$ (red curve), seawater Sr/Ca ratios after (Steuber and Veizer, 2002) ($(Sr/Ca)_{sw}$, black curve), and averaged seawater $^{87}Sr/^{86}Sr$ ratios from(Wallmann, 2001). B: Modelled marine Sr budget in the Permian and Triassic period. The modelled carbonate-related Sr net flux ($F(Sr)_{carb}$) is represented by the blue shaded area and modelled Sr_{sw} concentration by the solid black curve. Note that negative $F(Sr)_{carb}$ indicate Sr carbonate burial fluxes exceeding Sr carbonate dissolution fluxes and vice versa. Modelled periods of shelf carbonate dissolution at ~236 Ma and ~272 Ma are also indicated by the grey arrows on the x-axis. Modelled period of high carbonate burial from ~262 Ma to ~241 Ma is additionally indicated by the blue bar on the x-axis. Carboniferous-Permian glaciation from (Haq and Schutter, 2008). The P/T boundary is marked by a vertical dashed line at 251 Ma. Timescale and stratigraphic stages are from (Ogg et al., 2008). Abbreviations for stages: As = Asselian, Sak = Sakmarian, Artinsk = Artinskian, Ku = Kungurian, R = Roadian, W = Wordian, Cap = Capitanian, Wuc = Wuchiapingian, C = Changhsingian, I = Induan, Ol = Olenekian, Anis = Anisian, Ladin = Ladinian, Rh = Rhaetian.

TA_{sw} (Fig. IV.3A), and Ca_{sw} (Fig. IV.3B) concentrations. Deposition of evaporites account only for a minor fraction of the calcium flux (~0.05 to ~0.4 Tmol Ca/yr) within the last 20 Myrs of the Late Permian (HOLSER, 1984; HAY et al., 2006). The diminished Sr and Ca inventories and ocean residence times, as well as the lack of the deep-sea $CaCO_3$ compensation in the Neritan ocean increased the sensitivity of the Sr and Ca isotope systems to track short-term changes in their input/output fluxes. This may account for the

relatively large and rapid variations observed in the $\delta^{88/86}Sr_{sw}$, $^{87}Sr/^{86}Sr$, and $\delta^{44/40}Ca_{sw}$ records across the P/T boundary (KRAMM and WEDEPOHL, 1991; MARTIN and MACDOUGALL, 1995; FARKAŠ et al., 2007; PAYNE and CLAPHAM, 2012). The model results suggest that Sr_{sw}, Ca_{sw}, and TA_{sw} concentrations remained low until ~236 Ma when a carbonate dissolution event occurred and the system returned back to more average Phanerozoic conditions (Fig. IV.2B).

Our model calculations yielded considerable fluctuations in $F(Ca)_{carb}$ values (ranging from ~-20 Tmol Ca/yr to ~5 Tmol Ca/yr; average: ~-10 Tmol Ca/yr) which corresponds to a decrease in Ca_{sw} concentrations from 40 mmol/l to 4 mmol/l within the Late Permian to Early Triassic period (Fig. IV.3B). Similarly, TA_{sw} concentrations also decreased over the same time interval eventually becoming even negative in the model from ~262 Ma to ~241 Ma. This drop of the TA_{sw} concentration below zero in the model requires an additional alkalinity flux on average in the order of 9.0 Tmol/yr for the ~21 Myrs time period (Fig. IV.3A) in order to balance the negative TA_{sw} values and to sustain calcite saturation in shallow seawater which is achieved by a minimum TA_{sw} concentration of 3 mmol/l (See model description in the supplementary material (section IV.5)).

A potential source of additional carbonate alkalinity in the P/T ocean is extensive BSR, a process that produces large amounts of bicarbonate (HCO_3^-) while not contributing extra Ca to the ocean (See model description in the supplementary material (section IV.5) for other potential TA input fluxes). This additional TA flux ($F(TA)_{BSR}$) now quantifies the BSR-controlled HCO_3^--buildup in deeper waters as qualitatively proposed earlier by the ocean overturn theory (Knoll et al., 1996). This hypothesis implies widespread and long-lasting anoxic bottom water conditions during the Late Permian and Early Triassic times (KNOLL et al., 1996; ISOZAKI, 1997).

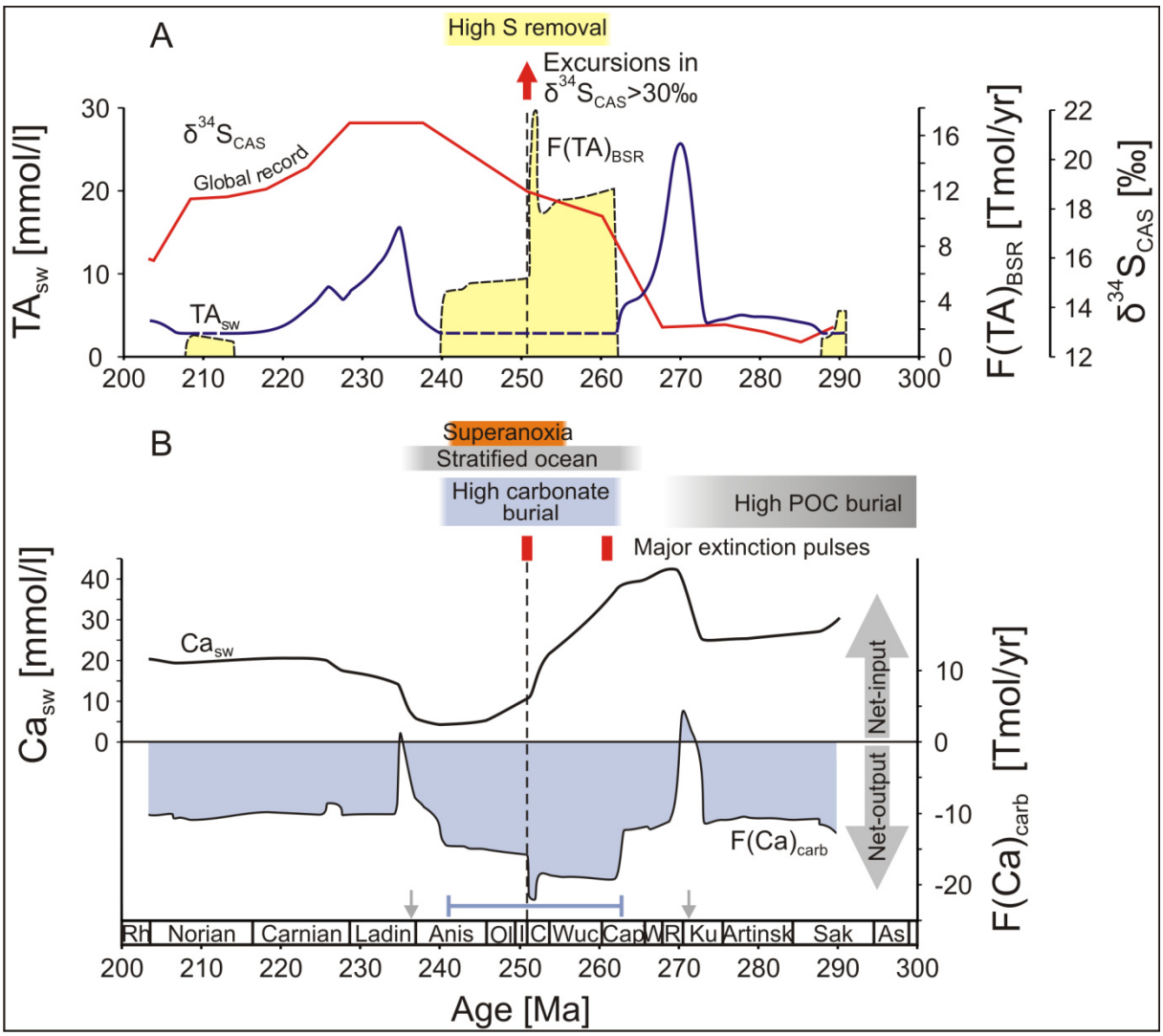

FIGURE IV.3 - Modelled marine TA and Ca budget. A: Model results for TA_{sw} concentrations (blue curve). Note, the TA_{sw} concentrations lower than 3 mmol/l (dashed blue line) are balanced by the supply of additional TA inferred to be a result of enhanced BSR ($F(TA)_{BSR}$) and sulphur removal rates (yellow shaded areas) coinciding with the period of increasing $\delta^{34}S_{CAS}$ values in the P/T ocean after (Kampschulte and Strauss, 2004) (red curve). B: Model results for the Ca_{sw} concentration (black curve) are presented together with the carbonate-related Ca net flux ($F(Ca)_{carb}$) from the ocean (blue shaded area). Note that negative $F(Ca)_{carb}$ indicate $CaCO_3$ burial fluxes exceeding $CaCO_3$ dissolution fluxes and vice versa. Periods of modelled carbonate dissolution at ~236 Ma and ~272 Ma are marked by the grey arrows on the x-axis. The period of modelled high carbonate burial (marked by the blue shaded area and the blue bar on the x-axis) between ~262 Ma and ~241 Ma coincides with major extinction pulses (marked with red rectangles), increasing $\delta^{34}Sr_{CAS}$ (Fig. IV.3A), and periods of stratified and superanoxic ocean conditions as defined by (Isozaki, 1997). The grey box represents the time of high particulate organic carbon burial (POC) after (Berner and Canfield, 1989). Timescale and geological stages are from (Ogg et al., 2008). Abbreviations for stratigraphic stages are the same as for figure caption IV.2.

Our model results are also in general accord with the geological record that shows a contemporaneous increase in $\delta^{34}S$ of carbonate associated sulfates (CAS) values with

distinct maxima at the P/T boundary (Kampschulte and Strauss, 2004; Payne and Clapham, 2012) and the suppression of deep-sea chert deposition, suggesting that lethal superanoxic conditions decreased radiolarian productivity in pelagic water (Isozaki, 1997) (Fig. IV.3A and IV.3B). Anoxic ocean conditions were also demonstrated by studies applying redox-sensitive U ($\delta^{238}U$) and Mo isotopes on P/T sediments (ZHOU et al., 2009; BRENNECKA et al., 2011).

Accordingly, we suggest that the massive carbonate formation was triggered by the upwelling of BSR-produced deep alkaline waters. This intermittent deep water overturning caused CO_2- and H_2S-degassing to the atmosphere and supersaturation with respect to calcium carbonate ($CaCO_3$) leading to inorganic precipitation of sea-floor $CaCO_3$ cements in Late Permian reef complexes and Early Triassic carbonate platforms and pelagic plateaus (GROTZINGER and KNOLL, 1995; KNOLL et al., 1996; WOODS et al., 1999; RIDING and LIANG, 2005; BAUD et al., 2007; KERSHAW et al., 2011). With this study, we give evidence for carbonate-supersaturated deep waters supporting the upwelling model as an explanation for carbonate growth (RIDING and LIANG, 2005; KERSHAW et al., 2011). The long-lasting anoxic conditions were probably supported and amplified by a combination of additional factors including extreme global warming (Wignall and Twitchett, 2002), a stagnant and stratified ocean (Knoll et al., 1996), and long-term high nutrient fluxes to the oceans from the weathering of coal-swamp deposits during the Late Permian and Early Triassic period (Berner and Canfield, 1989) (Fig. IV.3B). In particular, an enhanced influx of nutrients increased marine primary production causing a significant transfer of atmospheric CO_2 to the deep ocean, and burial of organic carbon in oceanic sediments as it is documented in the geological record (Wignall and Twitchett, 2002).

According to our scenario, the proposed $F(TA)_{BSR}$ increase of ~9.0 Tmol/yr in the time interval from ~262 Ma to ~241 Ma, needed to balance the excess carbonate burial, requires

an increase in BSR of ~4.5 Tmol/yr within the same period of time. Such an increase in BSR rates at the P/T transition has to be accompanied by a permanent storage of sulfide in sedimentary pyrite, as H_2S in deep waters, and/or by H_2S degassing to the atmosphere. As a result of intense BSR, seawater sulfate concentrations ($(SO_4)_{sw}$) decrease and $\delta^{34}S_{CAS}$ increase (Fig. IV.3A). These implications are in general agreement with earlier studies that suggest $(SO_4)_{sw}$ as low as ~1 to ~4 mmol/l, relatively high $\delta^{34}S_{CAS}$ signatures of more than 30 ‰ (Payne and Clapham, 2012) and the occurrence of pyrite in P/T sediments (Wignall and Twitchett, 2002).

We argue that the intermittent overturning of anoxic deep seawater bringing CO_2- and H_2S-rich toxic waters to the surface ocean considerably affected marine biodiversity during both major end-Permian extinction pulses at ~260 Ma and ~251 Ma (Payne and Clapham, 2012) (Fig. IV.3B). This overturning is documented in the geological record of the P/T boundary extinction horizon at Meishan, China, where short-term decreases in $\delta^{34}S_{CAS}$ and $\delta^{238}U$ are interpreted by a release of isotopically light H_2S from intermediate waters to the surface (KAIHO et al., 2006; GORJAN and KAIHO, 2007; BRENNECKA et al., 2011). Furthermore, high $F(TA)_{BSR}$ and increasingly heavy $\delta^{34}S_{CAS}$ values recorded into the Anisian stage (Fig. IV.3A), suggest that deep-sea anoxic conditions were still present ~10 Myrs after the P/T event (Isozaki, 1997; Kampschulte and Strauss, 2004; Newton et al., 2004). This may explain the prolonged biotic recovery and diversification of marine life after the end-Permian mass extinctions (KNOLL et al., 1996; WIGNALL and TWITCHETT, 2002; KAIHO et al., 2006; CHEN and BENTON, 2012).

The predicted long-term deep-sea anoxic conditions as seen from the $\delta^{88/86}Sr_{sw}$-record and deep water ocean overturning could explain both mass extinctions (~260 Ma and ~251 Ma) and the impeded biotic recovery in the Triassic. However, these long-term harsh conditions for marine life appear to be punctuated by short-term ocean acidification as seen from petrological studies and the $\delta^{44/40}Ca_{sw}$-record amplifying and accelerating mass

extinctions as seen at the P/T boundary (SOBOLEV et al., 2011; PAYNE and CLAPHAM, 2012). This short-term acidification event is not visible in our long-term $\delta^{88/86}Sr_{sw}$ record, but we predict that a decrease in $\delta^{88/86}Sr_{sw}$, similar to observations in Ca isotopes, will be observed in future high resolution studies across the P/T boundary. Therefore, the predicted long-term seawater anoxia is not necessarily in contradiction to the occurrence of a short-term ocean acidification event in the order of a few hundred thousand years (SOBOLEV et al., 2011; PAYNE and CLAPHAM, 2012). Probably, the combination of both short-term and long-term processes is necessary to explain the magnitude of the P/T mass extinction. In particular, the combination of long-term seawater anoxia and short-term ocean acidification as observed by previous studies may then explain why the Siberian Traps were much more damaging to biota than other large igneous provinces (LIPs) of comparable size (Sobolev et al., 2011).

In summary, the novel $\delta^{88/86}Sr_{sw}$ record and related model results suggest enhanced carbonate burial in the P/T Ocean due to increased carbonate alkalinity resulting from BSR in the deep anoxic waters of the stratified P/T Ocean. We suggest that the long-term ocean stratification lasting ~21 Myrs was interrupted by the occasional overturning of anoxic and H_2S-rich deep waters to the surface ocean (KAIHO et al., 2006; GORJAN and KAIHO, 2007; BRENNECKA et al., 2011). These conditions caused a biogeochemical crisis and physiological stress to marine life. Most likely, the combination of short-term surface ocean acidification induced by the Siberian Trap volcanism with long-term seawater anoxia accelerated and amplified the P/T boundary mass extinction, making it the most extreme catastrophe for life on Earth.

IV.3. Acknowledgements

Financial support: DFG, Ei272/29-1 (QUASAR); CIFAR-ESEP; GACR grant (P210/12/P631). We thank A. Kolevica, F. Hauff, J. Raddatz, A. Rüggeberg and K. Hissmann, B. Hansen, N. Nolte, P. Wickham, and E. Hathorne.

IV.4. Supplementary material

Methods

Delta Notation

The ratio of stable Sr is given as $\delta^{88/86}$Sr in relation to the $SrCO_3$ standard SRM987 distributed by the National Institute of Standards and Technology (NIST) (FIETZKE and EISENHAUER, 2006).

$$\delta^{88/86}Sr\ [‰] = \left(\frac{\frac{^{88}Sr}{^{86}Sr}_{sample}}{\frac{^{88}Sr}{^{86}Sr}_{SRM987}} - 1 \right) * 1000$$

Sample preparation

Modern brachiopods were sampled by mechanically separating a piece of the shell with a teflon tweezers. To remove organic coatings the sample was reacted in a 10 % sodium hypochlorite solution (~ 1 % active chlorine) for at least 12 hours in a teflon PFA vial. The sample was washed afterwards in ultrapure water (>18 MΩ).

Our fossil samples were provided by Ján Veizer (Veizer et al., 1999) (Table IV.DR6). In order to minimize the influence of diagenetic alteration only samples with low Mn, Fe and Mg concentrations as well as low $^{87}Sr/^{86}Sr$ and high $\delta^{18}O$ ratios when compared to coeval samples were analyzed. The carbonate powders of the samples used for our Phanerozoic record were drilled using a conventional dentist drill. Carbonate powders were weighed into a teflon PFA vial and ultrasonically cleaned in ultrapure water for about 30 minutes. This cleaning procedure was repeated at least twice. Usually 1200ng of Sr corresponds to a carbonate net weight of ~1 mg.

All samples were dissolved in 0.5 N HNO_3. Undissolved residual parts were removed by centrifuging. In order to remove organic components, the samples were heated in a mixture of 100 µl of 30 % H_2O_2 and 200 µl of 8 N HNO_3 at 80°C for at least 6 hours and evaporated to dryness afterwards.

In order to check for diagenetic alteration some samples (Table IV.DR6) were measured for their $\delta^{13}C$- and $\delta^{18}O$-composition on a Finnigan MAT 252 stable isotope ratio mass spectrometer with a Kiel CARBO device at GEOMAR. Reproducibility of the method is 0.05 ‰ (2 s.d.) for both $\delta^{13}C$ and $\delta^{18}O$, respectively. Isotope ratios were normalized to Vienna Pee Dee Belemnite (VPDB) standard. For trace element analysis, the samples were dissolved in 2 % HNO_3. The Ca, Mg, Mn, Fe and Sr concentrations were determined by ICP-MS (Agilent 7500 series) at GEOMAR. Assuming that our sample material is pure calcite, the element concentrations were normalized to the sum of the main divalent cations (Ca, Mg, Sr) equal to 40wt.-%. Further sample treatment including the addition of the $^{87}Sr/^{84}Sr$ double spike (DS) solution and column chemistry followed the published method of (Krabbenhöft et al., 2009). Here, the sample was loaded onto BIO-RAD 650 µl columns filled to one third with Triskem Sr-SPS resin (particle size 50–100 µm).

TIMS measurements

Measurement procedures generally follow the strontium double spike (DS) method (Krabbenhöft et al., 2009). We used rhenium ribbon single filaments in combination with a Ta_2O_5-activator which was found to stabilize the signal and enhance the ionization rate. For each sample two spiked and two unspiked runs were performed to get $^{86}Sr/^{84}Sr$, $^{87}Sr/^{84}Sr$ and $^{88}Sr/^{84}Sr$ ratios for the DS algorithm (Krabbenhöft et al., 2009). The measurements were carried out on a TRITON thermal ionization multicollector mass spectrometer (Thermo Fisher) at the GEOMAR mass spectrometer facilities as well as on an identical mass-spectrometer at the GZG, University of Göttingen, Germany. The

measurement was started when signal intensity of 10 V on mass 88 was achieved. This corresponds to a filament temperature of ~1500 °C and a filament current of ~3500mA.

The application of the DS-technique in combination with an iterative spike correction algorithm using an exponential law for the mass fractionation correction (Krabbenhöft et al., 2009) allows us to calculate natural $^{88}Sr/^{86}Sr$-ratios in addition to the conventional radiogenic $^{87}Sr/^{86}Sr$-ratios. All conventional radiogenic $^{87}Sr/^{86}Sr$-ratios of the samples were normalized as usual to a $^{86}Sr/^{88}Sr$ ratio of 0.1194. Samples were also corrected for the offset between the measured value of SRM987 of the individual session and the international agreed value for the $^{87}Sr/^{86}Sr$-ratio of 0.710240 (Veizer et al., 1999). The external reproducibility (two standards of the mean, 2 s.d.) for all $\delta^{88/86}Sr$ measurements is determined by the repeated $\delta^{88/86}Sr$ analysis of the coral standard JCp-1 (distributed by the Geological Survey of Japan) over a period of 15 months. The resulting $\delta^{88/86}Sr$ value is 0.195±0.019 ‰ (n=19; 2 s.d. of the mean) and is in agreement with published data (OHNO and HIRATA, 2007; KRABBENHÖFT et al., 2009; KRABBENHÖFT et al., 2010). The conventional radiogenic $^{87}Sr/^{86}Sr$-ratio on JCp-1 is determined to be 0.709171 ± 0.000022 (n=19; 2 s.d. of the mean). Whole procedure analytical blank was determined to be less than 0.3 ng Sr, which is ~0.1 % of the Sr amount in our samples.

Reconstruction of the Phanerozoic isotope and elemental records

Fractionation factor between carbonate recording phases

We found that the $\delta^{88/86}Sr$ values of modern brachiopods are independent of habitat location and water temperature with a mean of 0.176±0.016 ‰ (2 s.d. of the mean, n=13; table IV.DR1). corresponding to a fractionation factor of $\Delta^{88/86}Sr$ = -0.21 ‰ with respect to modern seawater ($\delta^{88/86}Sr_{sw}$ = 0.386±0.016 ‰ (2 s.d. of the mean, n=10 (Krabbenhöft et al., 2009))).

In order to examine the Sr isotope fractionation factor of belemnites we analyzed eleven samples of coeval Jurassic belemnites and brachiopods from the Swabian Alb and Swiss Jura, originating from four stratigraphic units (table IV.DR5). The samples originate from a time interval from the Middle Oxfordian to the Upper Kimmeridgian and were deposited in a sponge-microbial marly limestone facies. The age of the samples is determined on the basis of biozones (ammonite taxon-range zone; table IV.DR5). However, two brachiopod samples showed increased Fe and Mn concentrations, low $\delta^{18}O$ values, and elevated $^{87}Sr/^{86}Sr$-ratios indicating diagenetic alteration of these samples (Ur2-9-70 bra shell and Hol23 bra shell; table IV.DR5). We excluded these two data points from further discussion. The remaining samples from three different stratigraphic units indicate that the $\delta^{88/86}Sr$ values of brachiopods and belemnites were identical within statistical uncertainty in two of the three stratigraphic units (Supplementary figure IV.1 (Fig. IV.DR1)). Only in one of three stratigraphic units $\delta^{88/86}Sr$ values of brachiopods were slightly higher when compared to belemnites. Therefore, as a first order approach, the isotope fractionation factor $\Delta^{88/86}Sr$ for both species can be considered to be identical within statistical uncertainty.

Reconstructing the Phanerozoic seawater record for $\delta^{88/86}Sr$, $^{87}Sr/^{86}Sr$, and Sr/Ca

The Phanerozoic $\delta^{88/86}Sr_{sw}$ record was reconstructed by applying the fractionation factor of $\Delta^{88/86}Sr$ = -0.21 ‰ to the fossil samples (Fig. IV.1). To increase the robustness of our record we applied the following selection criteria for samples included into the $\delta^{88/86}Sr_{sw}$ record: i) as carbonate matrix samples represent mixtures of inorganic and biogenic precipitates as well as composites of skeletons of different organisms with deviating fractionation factors we excluded these samples from further discussion, ii) samples were rejected if $^{87}Sr/^{86}Sr$ ratios were more than 100ppm higher than values measured on the same samples (Veizer

et al., 1999) (Fig. IV.DR2), and iii) further rejection reasons were Mn concentrations higher than 250ppm and Sr concentrations lower than 300ppm.

$(Sr/Ca)_{sw}$ data were taken from (Steuber and Veizer, 2002) applying a 1 Myr running mean to smooth the large scatter of the data points.

All numerical sample ages from (Veizer et al., 1999) where transferred to the Geological Time Scale 2008 by the International Commission on Stratigraphy (Ogg et al., 2008).

Numerical box model

The marine Sr budget can be described by the fluxes of continental weathering ($F(Sr)_{weath}$), hydrothermal input ($F(Sr)_{hyd(in)}$), alteration of the oceanic crust ($F(Sr)_{hyd(out)}$), and carbonate-related net flux of burial and dissolution ($F(Sr)_{carb}$) (Krabbenhöft et al., 2010) (Fig. IV.DR3). We developed a one box model to calculate changes in the inventories of Sr, Ca and TA. All Sr, Ca and TA fluxes considered in the model and related parameters can be found in tables IV.DR2 and IV.DR3, respectively. Changes in the inventories of Sr, Ca and TA (here represented by "X") in the ocean with time are given by:

$$\frac{d[X]_{sw}}{dt} = F(X)_{hyd(in)} + F(X)_{weath} - F(X)_{carb} - F(X)_{hyd(out)} \quad \textbf{[IV.1]}$$

The hydrothermal input fluxes ($F_{hyd(in)}$) and continental weathering fluxes (F_{weath}) for Sr, Ca and TA were taken from (Farkaš et al., 2007) and calculated from seawater $^{87}Sr/^{86}Sr$ ratios and an estimate for continental weathering rates, including atmospheric pCO_2, land area, exposed rocks, and runoff (Wallmann, 2001). The Sr, Ca and TA removal due to the alteration of the oceanic crust ($F_{hyd(out)}$) is taken to be proportional to the product of mid ocean ridge spreading rates and the respective concentration in seawater (Table IV.DR2).

The Sr mass balance is now better constrained with a new isotope mass balance equation taking our novel $\delta^{88/86}Sr$ proxy into account, including the carbonate-related Sr net flux

($F(Sr)_{carb}$), using the approach presented earlier in (Lemarchand et al., 2000) (Eq. IV.2 and IV.3). Isotope compositions and related parameters can be found in Table IV.DR3 and IV.DR4. Assuming negligible isotope fractionation in the alteration of the oceanic crust, changes in the stable Sr isotope composition of the ocean are given by:

$$\frac{d\left({}^{88}Sr/{}^{86}Sr_{sw}\right)}{dt} = \frac{F(Sr)_{weath}}{[Sr]_{sw}} \times \frac{1+{}^{88}Sr/{}^{86}Sr_{sw}}{1+{}^{88}Sr/{}^{86}Sr_{weath}} \times ({}^{88}Sr/{}^{86}Sr_{weath} - {}^{88}Sr/{}^{86}Sr_{sw})$$

$$+ \frac{F(Sr)_{hyd(in)}}{[Sr]_{sw}} \times \frac{1+{}^{88}Sr/{}^{86}Sr_{sw}}{1+{}^{88}Sr/{}^{86}Sr_{hyd(in)}} \times ({}^{88}Sr/{}^{86}Sr_{hyd(in)} - {}^{88}Sr/{}^{86}Sr_{sw}) \quad \textbf{[IV.2]}$$

$$- \frac{F(Sr)_{carb}}{[Sr]_{sw}} \times \frac{1+{}^{88}Sr/{}^{86}Sr_{sw}}{1+{}^{88}Sr/{}^{86}Sr_{carb}} \times ({}^{88}Sr/{}^{86}Sr_{carb} - {}^{88}Sr/{}^{86}Sr_{sw})$$

By rearranging equation [2] the carbonate-related Sr flux can be calculated:

$$F(Sr)_{carb} = \left(-[Sr]_{sw} \times \frac{d\left({}^{88}Sr/{}^{86}Sr_{sw}\right)}{dt} - F(Sr)_{weath} \times \left(\frac{1+{}^{88}Sr/{}^{86}Sr_{sw}}{1+{}^{88}Sr/{}^{86}Sr_{weath}} \right) \right.$$

$$\left. \times ({}^{88}Sr/{}^{86}Sr_{weath} - {}^{88}Sr/{}^{86}Sr_{sw}) - F(Sr)_{hyd(in)} \times \left(\frac{1+{}^{88}Sr/{}^{86}Sr_{sw}}{1+{}^{88}Sr/{}^{86}Sr_{hyd(in)}} \right) \times ({}^{88}Sr/{}^{86}Sr_{hyd(in)} - {}^{88}Sr/{}^{86}Sr_{sw}) \right) \quad \textbf{[IV.3]}$$

$$/ \left(\frac{1+{}^{88}Sr/{}^{86}Sr_{sw}}{1+{}^{88}Sr/{}^{86}Sr_{carb}} \times \left({}^{88}Sr/{}^{86}Sr_{carb} - {}^{88}Sr/{}^{86}Sr_{sw} \right) \right)$$

The carbonate-related Ca net flux ($F(Ca)_{carb}$) is calculated by taking the $(Sr/Ca)_{sw}$ ratio derived from marine carbonate data (Steuber and Veizer, 2002) (Fig. IV.2A) as border conditions into account, thereby reducing the number of unknowns from four (Sr_{sw}, Ca_{sw}, $F(Sr)_{carb}$, $F(Ca)_{carb}$) to three (Sr_{sw}, $F(Sr)_{carb}$, $F(Ca)_{carb}$) (Eq. IV.4).

$$F(Ca)_{carb} = F(Ca)_{hyd(in)} + F(Ca)_{weath} - F(Ca)_{hyd(out)} - \frac{d\left(\frac{\left(Sr/Ca\right)_{sw}}{[Sr]_{sw}}\right)}{dt} \quad \textbf{[IV.4]}$$

Note, that the carbonate-related alkalinity flux ($F(TA)_{carb}$) is two times higher than $F(Ca)_{carb}$, because two moles of alkalinity are consumed/released by the formation/dissolution of $CaCO_3$ (see eq. IV.5 and IV.7).

$$\frac{d[TA]_{sw}}{dt} = F(TA)_{hyd(in)} + F(TA)_{weath} - 2 * F(Ca)_{carb} - F(TA)_{hyd(out)} \quad \textbf{[IV.5]}$$

The standard case

Taking the high $\delta^{88/86}Sr_{sw}$ of 0.57 ‰ prior to the P/T boundary (Fig. IV.2A) into account a minimum value of the fractionation factor $\Delta^{88/86}Sr_{carb}$ of -0.23 ‰ for bulk marine carbonates ($\Delta^{88/86}Sr_{carb} = \delta^{88/86}Sr_{carb} - \delta^{88/86}Sr_{sw}$) is required. Model runs with $\Delta^{88/86}Sr_{carb}$ values more positive than -0.23 ‰ would result in very low Sr_{sw} and Ca_{sw} concentrations and incomprehensible model conditions. Therefore, we chose a $\Delta^{88/86}Sr_{carb}$ value of -0.24 ‰ which is within the range of modern carbonates ($\Delta^{88/86}Sr$ = -0.12 ‰ to -0.37 ‰ (Eisenhauer et al., 2011), Fig. IV.DR9) and close to the average value of -0.18‰ (Krabbenhöft et al., 2010). A bulk carbonate fractionation factor for the Permian and Triassic period slightly different from the modern one is not unlikely, taking into account that most of the modern marine calcifiers did not exist in the P/T oceans.

The precipitation of $CaCO_3$ requires seawater saturation with respect to calcite. Assuming that carbonate precipitation takes place in shallow water (<100 m water depth, a water temperature of 20°C, a salinity of 35psu, calcite saturation of $\Omega_{calcite} \geq 1$, a maximum atmospheric CO_2 concentration of 1500ppm within P/T times (Royer, 2006), and a

minimum Ca_{sw} concentration of 4 mmol/l (Fig. IV.3B)) would require a TA_{sw} concentration of 2.8 mmol/l taking the equations and kinetic constants of (Zeebe and Wolf-Gladrow, 2001) into account. Hence, we infer an additional TA flux to sustain a minimum seawater TA concentration of 3 mmol/l.

Sensitivity analysis

In order to determine the model output sensitivity related to the uncertainty in our input parameters we performed sensitivity analysis. In a first approach we altered both the weathering and hydrothermal input fluxes of Sr, Ca, and TA. Here, we varied both input fluxes ($F_{hyd(in)}$ and F_{weath}) of (Farkaš et al., 2007) in two scenarios simultaneously in between 80 % and 120 % (Fig. IV.DR4). The results of this sensitivity analysis reveal that varying $F_{hyd(in)}$ and F_{weath} result in changes of the model output parameters (Sr_{sw}, Ca_{sw}, and TA_{sw} concentrations, and $F(Sr)_{carb}$) of up to max. 25 % (Fig. IV.DR5 and IV.DR6). The variations in the model output parameters are therefore within the same magnitude as the changes in the model input parameters.

In a second approach, we changed the fractionation factor of bulk marine carbonates ($\Delta^{88/86}Sr_{carb}$) in two scenarios to -0.23 ‰ and -0.26 ‰ (Fig. IV.DR7 and IV.DR8), respectively. Taking $\Delta^{88/86}Sr_{carb}$ values more positive than -0.23 ‰ into account result in incomprehensible model conditions. The results of this sensitivity analysis reveal that varying $\Delta^{88/86}Sr_{carb}$ result in changes of the model output parameters (Sr_{sw}, Ca_{sw}, and TA_{sw} concentrations, and $F(Sr)_{carb}$) of up to max. 60 % (Fig. IV.DR7 and IV.DR8). This reveals that the model output is more sensitive to changes in $\Delta^{88/86}Sr_{carb}$ than to variations of the input fluxes. However, in all scenarios similar additional alkalinity fluxes in between 8.2 Tmol/yr and 9.3 Tmol/yr from BSR are requested to sustain TA_{sw} concentrations of 3 mmol/l across the P/T transition.

In the standard case, our model results reveal distinct variations in paleo-seawater concentrations of Sr, Ca, and TA in the P/T oceans which are in general agreement with long-term changes in Ca_{sw} concentrations from fluid inclusions (Horita et al., 2002) (Fig. IV.DR9). In a third approach of the sensitivity analysis we tested if the measured $\delta^{88/86}Sr_{sw}$, $(Sr/Ca)_{sw}$ (Steuber and Veizer, 2002), and long-term Ca_{sw} concentrations from fluid inclusions (Horita et al., 2002) might be explained by variations in $\Delta^{88/86}Sr_{carb}$. Our modelling results indicate that $\Delta^{88/86}Sr_{carb}$ values as high as +0.5 ‰ and as low as -0.8 ‰ are requested to account for the observed variations in $\delta^{88/86}Sr_{sw}$, $(Sr/Ca)_{sw}$, and Ca_{sw} concentrations (Fig. IV.DR10) exceeding the modern $\Delta^{88/86}Sr$ range, which is in between -0.12 ‰ and -0.37 ‰ (KRABBENHÖFT et al., 2010; EISENHAUER et al., 2011). The observed variations in $\delta^{88/86}Sr_{sw}$, $(Sr/Ca)_{sw}$ (Steuber and Veizer, 2002), and Ca seawater concentrations (Horita et al., 2002) in the P/T oceans are therefore probably not due to changes in $\Delta^{88/86}Sr$. In general, $\Delta^{88/86}Sr$ is controlled by changes in biomineralization processes and possible shifts in faunal assemblages (Krabbenhöft et al., 2010).

From the carbonate-related net fluxes of Sr and Ca a molar distribution coefficient $D_{Sr} = (Sr/Ca)_{carb}/(Sr/Ca)_{sw}$ could be calculated (Fig. IV.DR11). We calculated changes in between 0.04 and 70 with a mean of 0.45. In general, our results are in agreement with theoretical considerations that D_{Sr} should be in between the endmember values for calcite (D_{Sr} ~0.1) and aragonite (D_{Sr} ~1). However, during times of modelled times of shelf recrystallization (and therefore positive $F(Sr)_{carb}$ and $F(Ca)_{carb}$) we modelled D_{Sr} above 1. This is most probably a result of preferred Sr release during shelf recrystallization. Please note that the modelled D_{Sr} are calculated from carbonate-related net fluxes of Sr and Ca (including carbonate dissolution and carbonate burial) and does not implicitly represent a D_{Sr} of precipitated carbonates.

Alkalinity increase by bacterial sulphate reduction

In an anoxic water column, organic material ($C(H_2O)$) is preferentially oxidized by bacteria while reducing sulfate to hydrogen sulfide. During bacterial sulfate reduction, 2 mole of HCO_3^- are produced for 1 mol of SO_4^{2-}:

$$2\ C(H_2O) + SO_4^{2-} \rightarrow 2\ HCO_3^- + H_2S \qquad \textbf{[IV.6]}$$

This process leads to an increase in TA and therefore an increase in $CaCO_3$ saturation. During the precipitation of $CaCO_3$, 2 moles of HCO_3^- are consumed for the production of 1 mol $CaCO_3$:

$$2\ HCO_3^- + Ca^{2+} \rightarrow CaCO_3 + 2H^+ \qquad \textbf{[IV.7]}$$

Thus, the reduction of 1 mol SO_4^{2-} in an anoxic water column leads to the precipitation of 1 mol $CaCO_3$. We propose that the additional alkalinity flux of 9.0 Tmol/yr needed for sustaining an alkalinity concentration of 3 mmol/l in the Late Permian and Early Triassic come from the reduction of sulfate with a flux of 4.5 Tmol/yr.

Besides bacterial sulfate reduction, the processes of denitrification and Fe and Mn oxide reduction may account for a TA supply to ocean without contributing an additional Sr or Ca flux (e.g. summarized in (Bohlen et al., 2011)). However, the reservoirs of N, Fe, and Mn are too small to account for an additional TA flux of 9 Tmol/yr during a 21Myrs time interval.

Supplementary figures

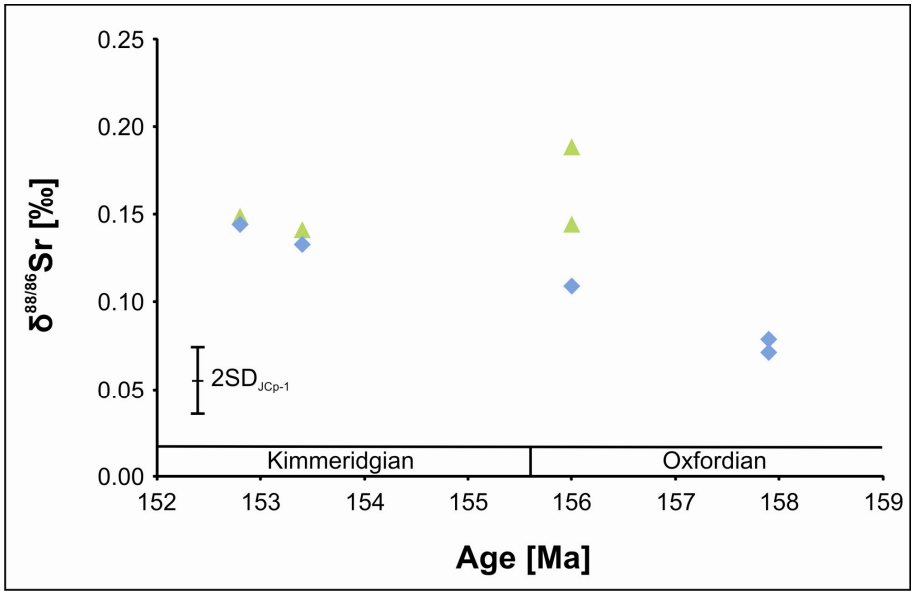

FIGURE IV.DR1 - This figure shows the $\delta^{88/86}Sr$ composition of Jurassic brachiopods and belemnites. Brachiopods are represented by green triangles. Belemnites are represented by blue diamonds. The external reproducibility of our method is represented by 2 s.d. of the mean of the coral standard JCp-1 (0.019 ‰, n=19). The time scale and stratigraphic stages are taken from (Ogg et al., 2008).

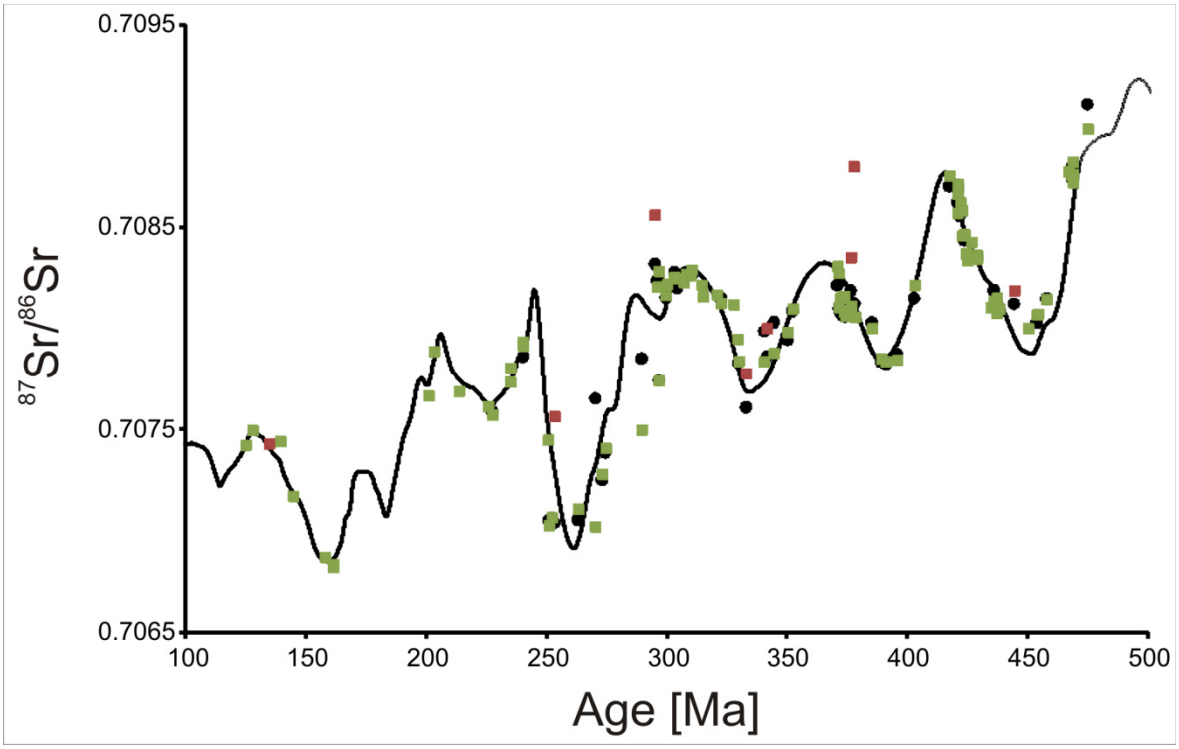

FIGURE IV.DR2 - This figure shows the $^{87}Sr/^{86}Sr$ composition of our fossil carbonate samples (red and green squares) together with literature data (VEIZER et al., 1999; MCARTHUR et al., 2001). For the samples indicated by green squares we have no evidence for diagenetic alteration. Samples were rejected (red squares) if $^{87}Sr/^{86}Sr$ ratios were more than 100 ppm higher than values measured on the same samples (black dots, Veizer et al., 1999). Compiled seawater $^{87}Sr/^{86}Sr$ curve indicated by the black line is from (McArthur et al., 2001).

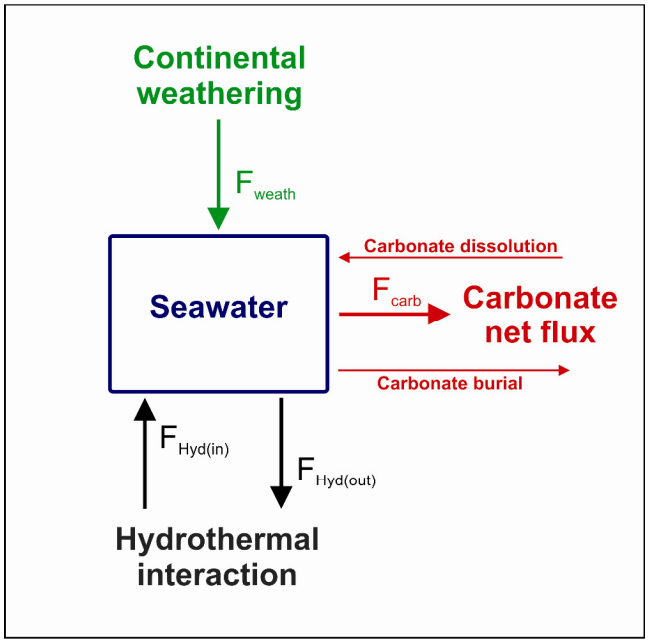

FIGURE IV.DR3 - Set-up of the numerical one box model.

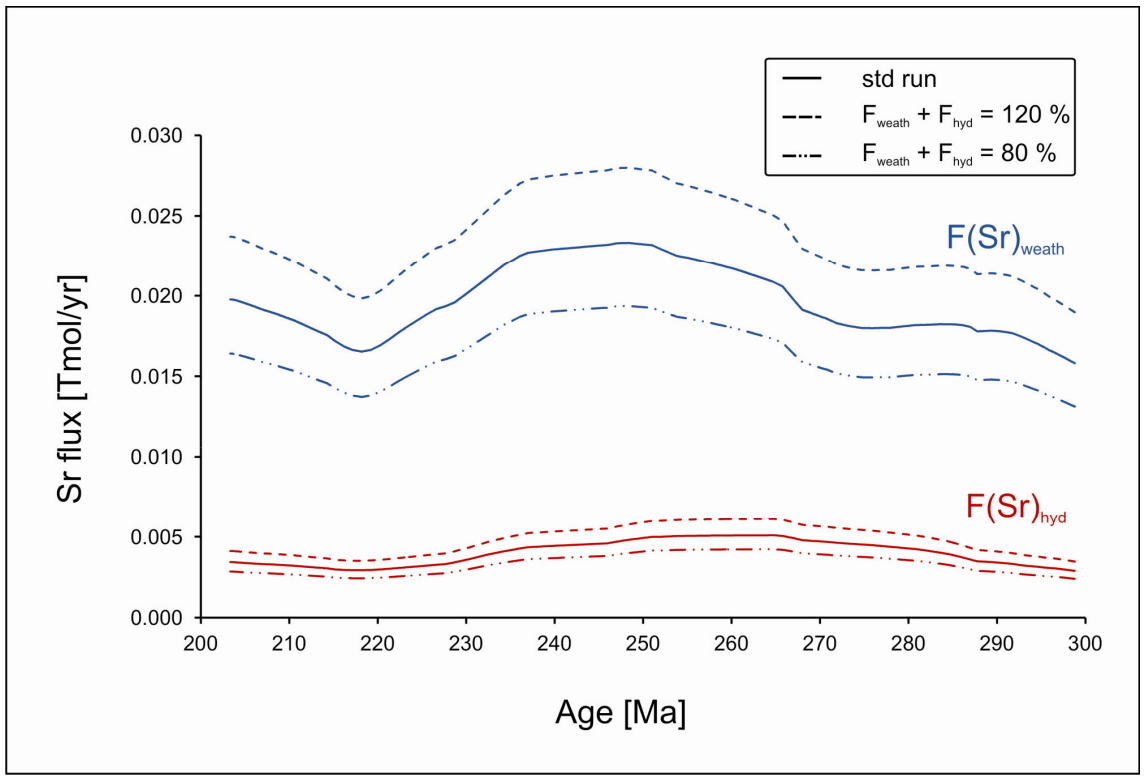

FIGURE IV.DR4 - This figure shows the model input parameters $F(Sr)_{weath}$ and $F(Sr)_{hyd(in)}$ for different sensitivity analysis scenarios. In two scenarios we altered $F(Sr)_{weath}$ and $F(Sr)_{hyd(in)}$ to 80 % (dashed-dotted line) and 120 % (dashed line), respectively. The standard run (std) is represented by the solid line.

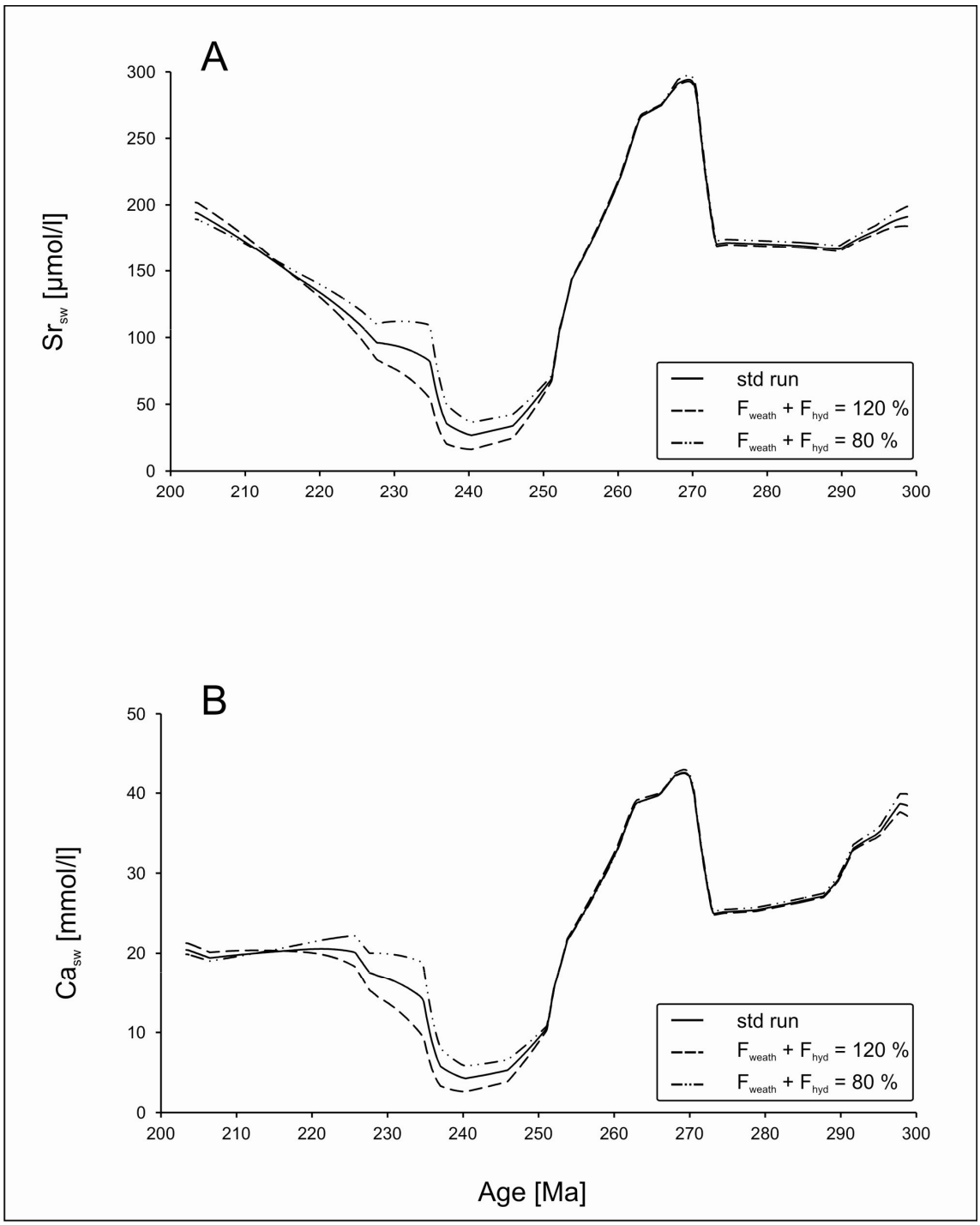

FIGURE IV.DR5 - This figure shows the model output parameters of Sr_{sw} (A) and Ca_{sw} (B) concentrations in different sensitivity analysis scenarios. The standard (std) run is represented by the solid line. The model runs with F_{weath} and $F_{hyd(in)}$ = 120 % and F_{weath} and $F_{hyd(in)}$ = 80 % (Fig. IV.DR4) are represented by the dashed and the dashed-dotted line, respectively.

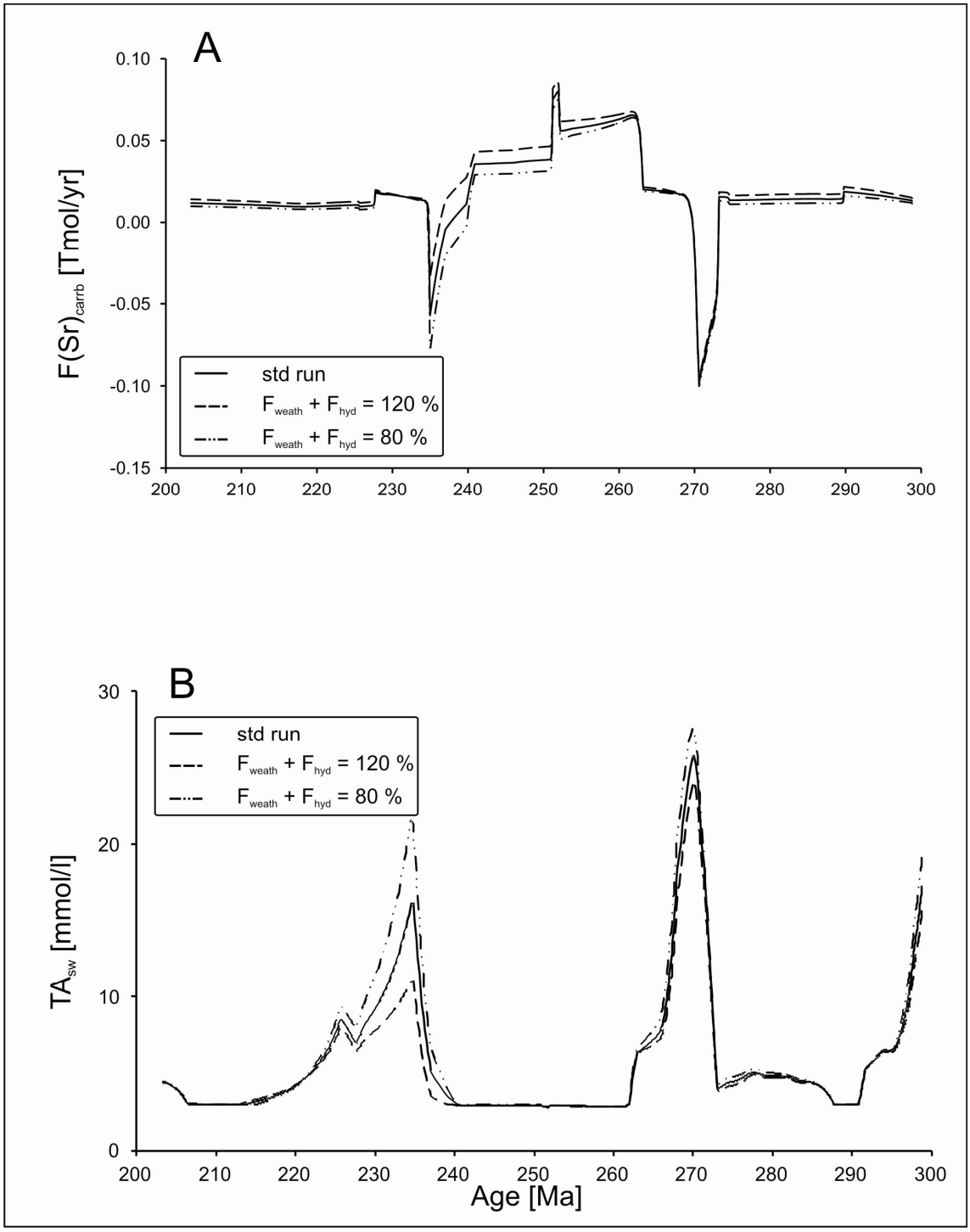

FIGURE IV.DR6 - This figure shows the model output parameters of the carbonate-related Sr flux ($F(Sr)_{carb}$) (A) and seawater TA concentration (B) in different sensitivity analysis scenarios. Note that positive $F(Sr)_{carb}$ values indicate Sr carbonate burial fluxes exceeding Sr carbonate dissolution fluxes and vice versa. The standard (std) run is represented by the solid line. The model runs with F_{weath} and $F_{hyd(in)}$ = 120 % and F_{weath} and $F_{hyd(in)}$ = 80 % (Fig. IV.DR4) are represented by the dashed and the dashed-dotted line, respectively.

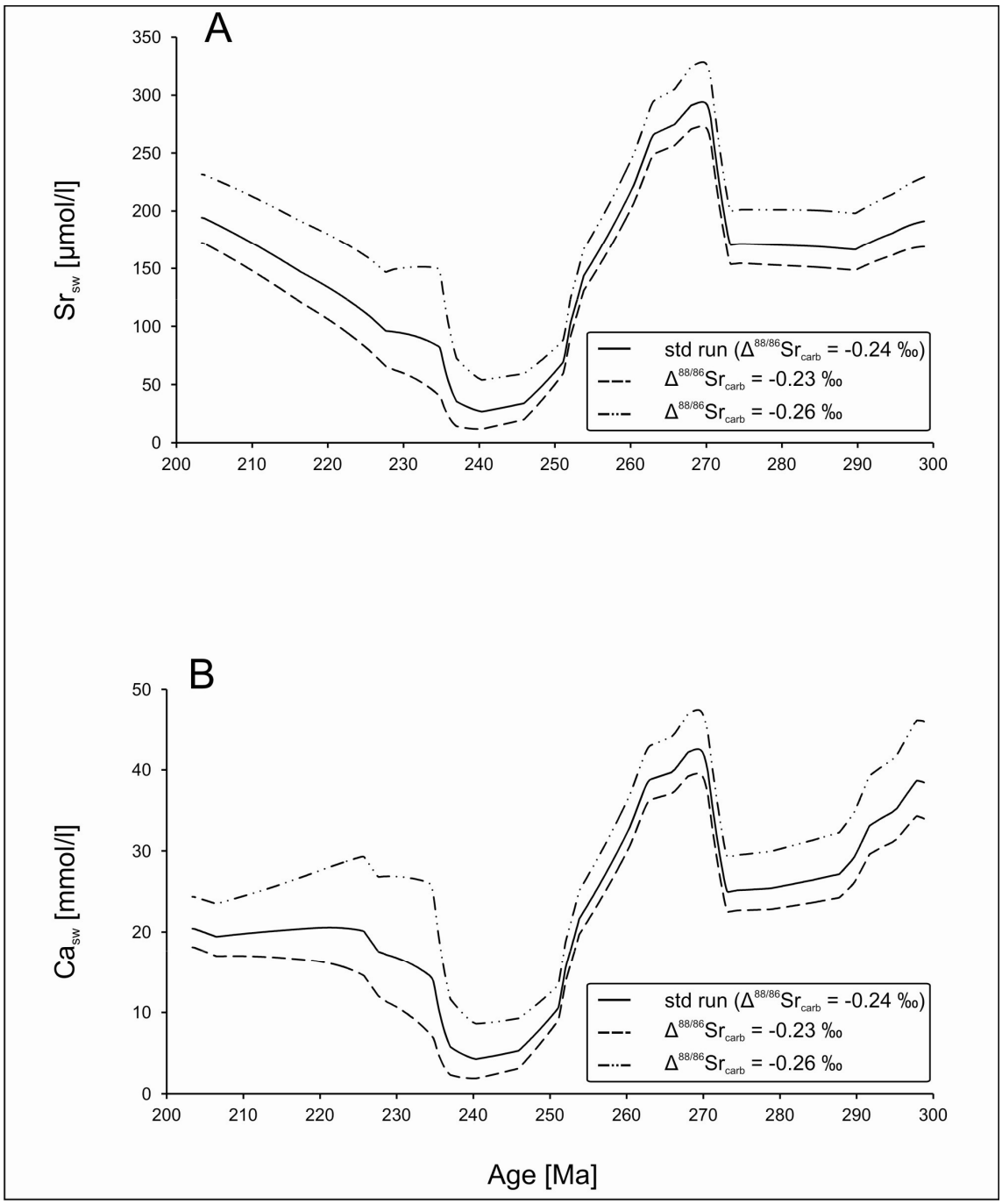

FIGURE IV.DR7 - This figure shows the model output parameters of Sr_{sw} (A) and Ca_{sw} (B) concentrations in different sensitivity analysis scenarios. The standard (std) run ($\Delta^{88/86}Sr_{sw}$ = -0.24 ‰) is represented by the solid line. The model runs with $\Delta^{88/86}Sr_{sw}$ = -0.23 ‰ and -0.26 ‰ are represented by the dashed and the dashed-dotted line, respectively.

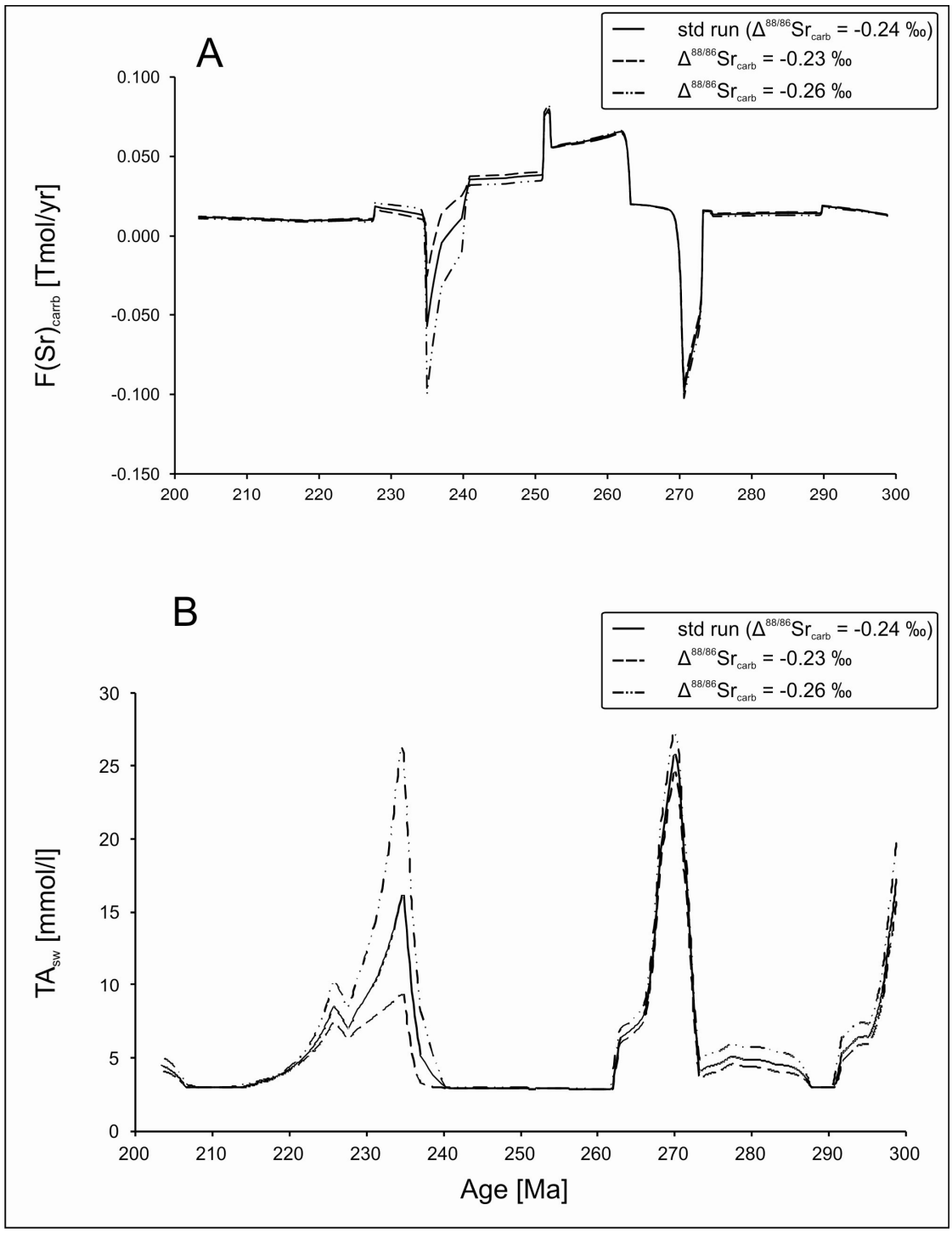

FIGURE IV.DR8 - This figure shows the model output parameters of the carbonate-related Sr flux ($F(Sr)_{carb}$) (A) and seawater TA concentration (B) in different sensitivity analysis scenarios. Note that positive $F(Sr)_{carb}$ values indicate Sr carbonate burial fluxes exceeding Sr carbonate dissolution fluxes and vice versa. The standard (std) run ($\Delta^{88/86}Sr_{carb}$ = -0.24 ‰) is represented by the solid line. The model runs with $\Delta^{88/86}Sr_{carb}$ = -0.23 ‰ and -0.26 ‰ are represented by the dashed and the dashed-dotted line, respectively.

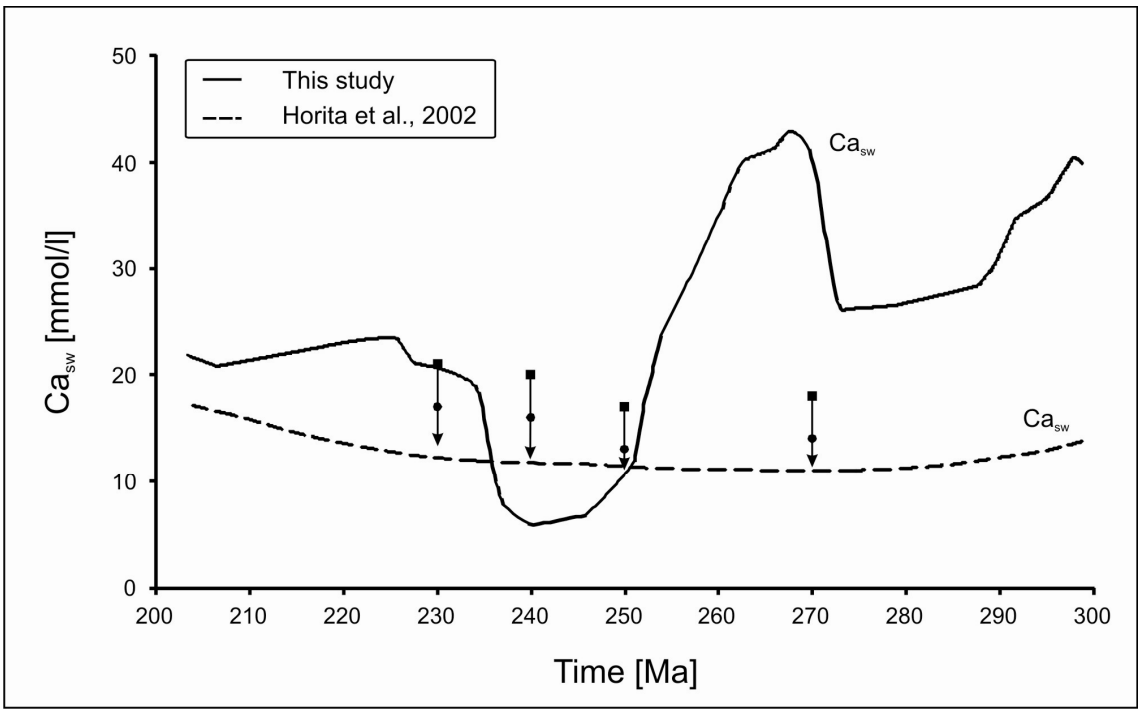

FIGURE IV.DR9 - This figure shows the modelled Ca_{sw} concentrations from this study in the standard run (solid line) and the long-term Ca_{sw} concentrations (Horita et al., 2002) (dashed line) reconstructed from fluid inclusions in marine halite (solid symbols; circles and squares are based on different assumptions (Horita et al., 2002).

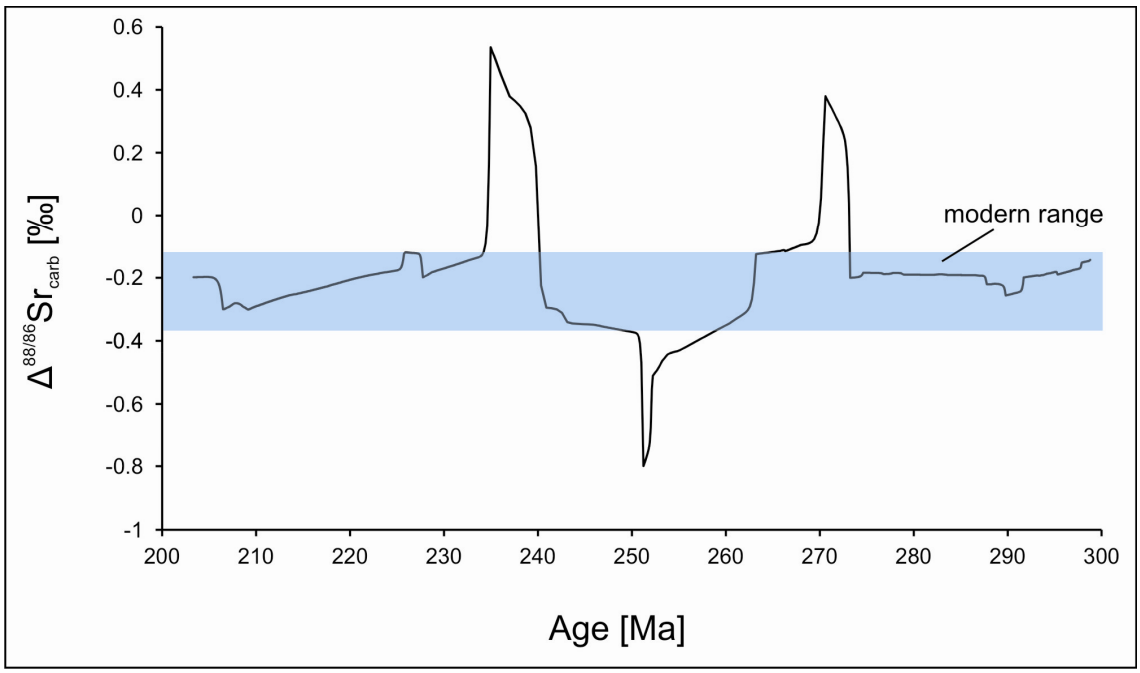

FIGURE IV.DR10 - This figure shows the calculated fractionation factor $\Delta^{88/86}Sr_{carb}$ in a sensitivity analysis scenario. In contrast to the standard run, where $\Delta^{88/86}Sr_{carb}$ is assumed to be constant at -0.24‰, it is here calculated $\Delta^{88/86}Sr_{carb}$ from reconstructed $\delta^{88/86}Sr_{sw}$, $(Sr/Ca)_{sw}$ (Steuber and Veizer, 2002), and long-term Ca_{sw} concentrations from fluid inclusions (Horita et al., 2002) (Fig. IV.DR9). Modelled variations in $\Delta^{88/86}Sr_{carb}$ exceed the modern range of $\Delta^{88/86}Sr_{carb}$ (Krabbenhöft et al., 2010; Eisenhauer et al., 2011), which is represented by the blue shaded area. Therefore, changes in $\delta^{88/86}Sr_{sw}$ cannot be exclusively explained by changes in $\Delta^{88/86}Sr_{carb}$.

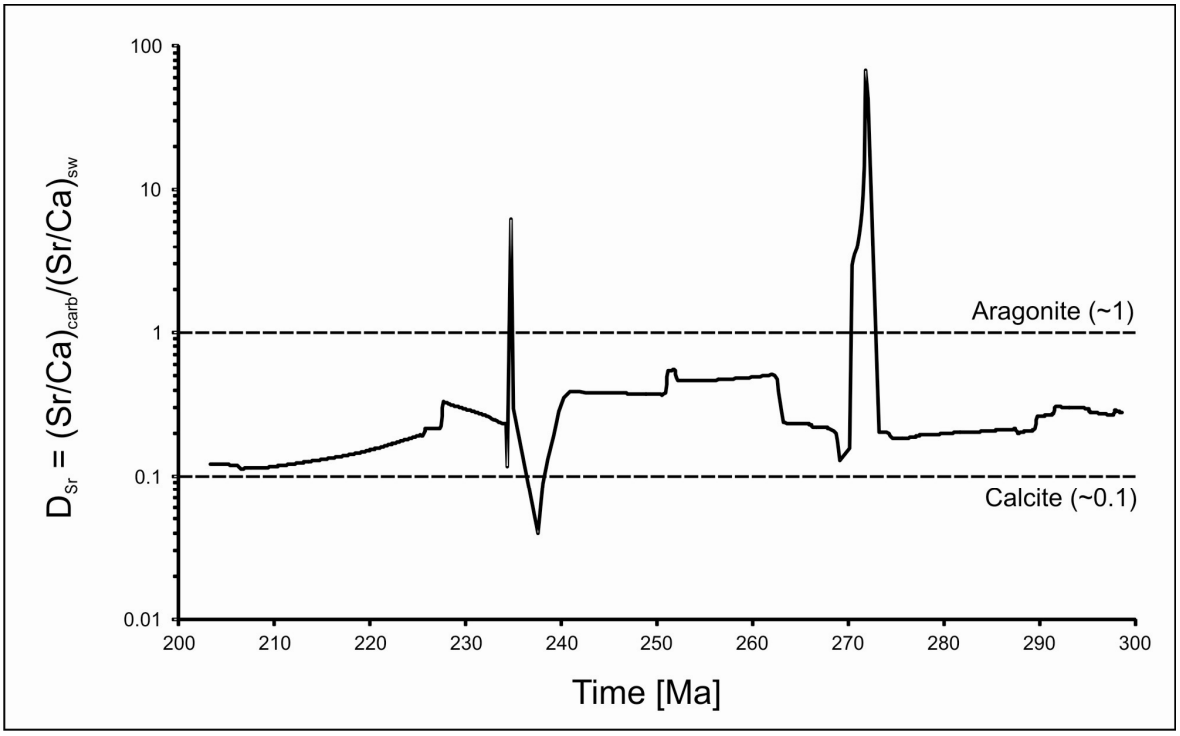

FIGURE IV.DR11 - This figure shows the calculated D_{Sr} in the standard run ranging in between 0.04 and 70, most of the time in the range between calcite (D_{Sr} ~0.1) and aragonite (D_{Sr} ~1). Higher values than 1 are observed during times of proposed shelf weathering/recrystallization (Fig. IV.2) and are a result of a preferred release of Sr to the ocean.

Supplementary tables

TABLE IV.DR1 - Sample list of modern brachiopods (n = 13).

Cruise and station No.	*Location*	*Species*	*T [°C]*	*Water depth [m]*	*Salinity [psu]*	*Sr [ppm]*	*$^{87}Sr/^{86}Sr$*	*[2 s.e.m.]*	*$\delta^{88/86}Sr$ [‰]*	*[2 s.e.m.]*	*n*
So 168 St.84	Pacific, 44°30'24.00"S ; 175°56'27.63"W	*Liothyrella sp.*	5.57*	700*		1028	0.709170	0.000001	0.173	0.016	6
M61-3 St. 607	Atlantic, 56°29.98 N, 17°18.63 W	*Macandrenia cranium*	8.87*	683*		1123	0.709163	0.000001	0.184	0.006	6
M61-3 St. 617	Atlantic, 56°29.84 N, 17°18.30 W	*Terebratulina retusa*	8.87*	668*		1096	0.709168	0.000005	0.186	0.006	4
M61-1 St. 276	Atlantic, 51°27.16 N, 11°43.61 W	*Dallina septigera*	9.59*	905*		997	0.709162	0.000004	0.189	0.007	6
ARK XXII1a St. 70/3/2	Atlantic, 67°31.9 N 9°30.3 E	*Terebratulina retusa*	7.28*	318*	35.19[1]	1130	0.709168	0.000003	0.176	0.004	4
Pos391-563-1	Atlantic, 64°05.916 N, 08°05.494 E	*Terebratulina retusa*	7.65*	287*	35.20[1]	1239	0.709168	0.000000	0.177	0.001	4
Pos391-542-1	Atlantic, 70°56.022 N, 22°12.326 E	*Macandrenia cranium*	7.18*	193*	34.97[1]	1221	0.709171	0.000002	0.178	0.005	4
Pos391-535-1	Atlantic, 70°55.138 N, 22°11.259 E	*Macandrenia cranium*	7.18*	201*	34.97[1]	1236	0.709161	0.000000	0.180	0.018	2
CNY	Mediterranean sea; 42°N, 6°E	*Grypheus vitreus*	13.3†	400*		723	0.709166	0.000003	0.170	0.012	4
SJ/1	Pacific, San Juan Island, Juan de Fuca Strait, 48.5°N, 123°W	*Terebratalia transversa*	10.0†			1167	0.709160	0.000001	0.169	0.011	4
Yoko	Pacific, Yokohama, 35.5°N, 139.5°E	Pictothyris	21.6†	20*		1138	0.709164	0.000004	0.183	0.007	4
Hit1	Pacific, Pudget Sound, Seattle, 47°N, 122°W	*Terebratalia transversa*	10.5†			1286	0.709160	0.000002	0.160	0.003	4
CrRck	Pacific, New Zealand 43°S, 180°	*Calloria inconspicua*	14.0†	0*		1237	0.709164	0.000001	0.164	0.001	2
	Mean [2 s.d.]					**1125**	**0.709165**	0.000007	**0.176**	0.016	13

*CTD measurements in course of the cruise (Hoernle and participants, 2003; Pfannkuche and participants, 2004; Ratmeyer and participants, 2006), †Mean water temperatures from World Ocean Atlas (2005), n = number of measurements.

TABLE IV.DR2 - Sr, Ca, and TA fluxes and related variables considered in the model.

Flux	Equation/Abbreviation
Hydrothermal Sr, Ca and TA flux into the ocean*	$F(Sr)_{hyd(in)}$, $F(Ca)_{hyd(in)}$, $F(TA)_{hyd(in)}$
Continental weathering Sr, Ca and TA flux into the ocean*	$F(Sr)_{weath}$, $F(Ca)_{weath}$, $F(TA)_{weath}$
Carbonate-related Sr, Ca, and TA net flux from the ocean*	$F(Sr)_{carb}$, $F(Ca)_{carb}$, $F(TA)_{carb}$
Hydrothermal Sr flux from the ocean	$F(Sr)_{hyd(out)} = f_{hyd}(t) * ([Sr]_{sw}(t) / [Sr(Q)]_{sw}(t)) * F(Q)(Sr)_{hyd(out)}$
Hydrothermal Ca flux from the ocean	$F(Ca)_{hyd(out)} = f_{hyd}(t) * ([Ca]_{sw}(t) / [Ca(Q)]_{sw}(t)) * F(Q)(Ca)_{hyd(out)}$
Hydrothermal TA flux from of the ocean	$F(TA)_{hyd(out)} = f_{hyd}(t) * ([TA]_{sw}(t) / [TA(Q)]_{sw}(t)) * F(Q)(TA)_{hyd(out)}$

[Sr(Q)], [Ca(Q)], and [TA(Q)] as well as F(Q)(Sr), F(Q)(Ca), F(Q)(TA) represent Quaternary values for inventory and fluxes of Sr, Ca, and TA, respectively.*Data from (Farkaš et al., 2007).

TABLE IV.DR3 - Parameters used in the definition of Sr, Ca and TA fluxes.

Parameter	Definition
Phanerozoic volcanic/tectonic activity (Farkaš et al., 2007)	$f_{hyd}(t)$
Molar ratio of Sr and Ca in seawater	$(Sr/Ca)_{sw}$
Quaternary Sr concentration in seawater (De Villiers et al., 1994)	$[Sr(Q)]_{sw}$ = 90 μmol/l
Quaternary Ca concentration in seawater (De Villiers et al., 1994)	$[Ca(Q)]_{sw}$ = 10 mmol/l
Quaternary TA concentration in seawater (Zeebe and Wolf-Gladrow, 2001)	$[Ta(Q)]_{sw}$ = 2.3 mmol/l
Quaternary Sr uptake in oceanic crust (Farkaš et al., 2007)	$F(Q)(Sr)_{hyd(out)} = 3.5x10^9$ mol/yr
Quaternary Ca uptake in oceanic crust (Farkaš et al., 2007)	$F(Q)(Ca)_{hyd(out)} = 0.5 * F(Q)(TA)_{hyd(out)}$
Quaternary TA uptake in oceanic crust (Farkaš et al., 2007)	$F(Q)(TA)_{hyd(out)}$ = 1.5 Tmol/yr
Molar partition coefficient of Sr in calcium carbonate	$k_D = (Sr/Ca)_{Carb}/(Sr/Ca)_{sw}$

TABLE IV.DR4 - Isotope signatures and related parameters for Sr input and output fluxes.

Continental weathering flux	$\delta^{88/86}Sr_{weath}$ = 0.21 ‰ †*
Hydrothermal input flux	$\delta^{88/86}Sr_{hyd(in)}$ = 0.27 ‰†
Carbonate-related flux	$\delta^{88/86}Sr_{carb} = \delta^{88/86}Sr_{sw} - \Delta^{88/86}Sr_{carb}$
Mean fractionation factor between marine carbonates and coeval seawater	$\Delta^{88/86}Sr_{carb}$ = -0.24 ‰

†Data from (Krabbenhöft et al., 2010) *Quaternary value for $\delta^{88/86}Sr_{weath}$ assuming long-term equilibrium between Sr input and Sr output fluxes (Krabbenhöft et al., 2010).

TABLE IV.DR5 - Sample list of Jurassic brachiopods and belemnites.

Running No.	*Species*	*Region*	*Zone*	*Time*	*Age [Ma]*	*Section & Bed*	*Ca [wt%]*	*Mg [wt-%]*	*Fe [ppm]*	*Mn [ppm]*	*Sr [ppm]*	*$\delta^{18}O$ [‰]*	*$\delta^{13}C$ [‰]*	*$^{87}Sr/^{86}Sr$*	*$\delta^{88/86}Sr$ [‰]*
Ur2-9-68 bra	Lacunosella multiplicata	Swabian Alb	Aulacostephanus mutabilis	Upper Kimmeridgian	152.8	Ursental 2-9	39.85	0.11	149	13	455	-1.29	2.79	0.707035	0.149
Ur2-9-70 bra	Lacunosella multiplicata	Swabian Alb	Aulacostephanus mutabilis	Upper Kimmeridgian	152.8	Ursental 2-9	39.57	0.39	2845	72	439	-3.25	1.35	0.707439	0.129
Ur2-9bel	belemnite indet.	Swabian Alb	Aulacostephanus mutabilis	Upper Kimmeridgian	152.8	Ursental 2-9	39.68	0.27	371	26	506			0.706994	0.144
Gei13 bel	Belemnite indet.	Swabian Alb	Crussoliceras divisum	Lower Kimmeridgian	153.3	Geisingen 13	39.60	0.28	55	3	1200			0.707007	0.133
Gei13 bra	Nucleata nucleata	Swabian Alb	Crussoliceras divisum	Lower Kimmeridgian	153.3	Geisingen 13	39.67	0.28	469	33	530	-2.22	2.28	0.707017	0.141
Gos7-54 bra	Lacunosella subsimilis	Swabian Alb	Epipeltoceras bimammatum	Upper Oxfordian	156.1	Gosheim 7	39.86	0.10	167	23	365			0.706998	0.189
Gos7-007-87 bra	Placothyris rollieri	Swabian Alb	Epipeltoceras bimammatum	Upper Oxfordian	156.1	Gosheim 7	39.68	0.27	670	21	506	-0.86	2.80	0.707091	0.144
Gos7 bel	belemnite indet.	Swabian Alb	Epipeltoceras bimammatum	Upper Oxfordian	156.1	Gosheim 7	39.52	0.35	94	9	1237			0.706983	0.109
Hol23 bra	Argovithyris birmensdorfensis	Swiss Jura	Gregoryceras transversarium	Middle Oxfordian	157.9	Holderbank 23	39.53	0.42	4808	340	522	-5.40	0.64	0.708413	0.204
Hol23 bel	belemnite indet.	Swiss Jura	Gregoryceras transversarium	Middle Oxfordian	157.9	Holderbank 23								0.706832	0.071
Hol23 bel	belemnite indet.	Swiss Jura	Gregoryceras transversarium	Middle Oxfordian	157.9	Holderbank 23								0.706885	0.079

IV.5. References

Baud, A., Richoz, S., and Pruss, S., 2007. The lower Triassic anachronistic carbonate facies in space and time. *Global and Planetary Change* **55**, 81-89.

Berner, R. A. and Canfield, D. E., 1989. A new model for atmospheric oxygen over Phanerozoic time. *Am J Sci* **289**, 333-361.

Bohlen, L., Dale, A. W., Sommer, S., Mosch, T., Hensen, C., Noffke, A., Scholz, F., and Wallmann, K., 2011. Benthic nitrogen cycling traversing the Peruvian oxygen minimum zone. *Geochim. Cosmochim. Acta* **75**, 6094-6111.

Brennecka, G. A., Herrmann, A. D., Algeo, T. J., and Anbar, A. D., 2011. Rapid expansion of oceanic anoxia immediately before the end-Permian mass extinction. *Proceedings of the National Academy of Sciences* **108**, 17631-17634.

Chen, Z.-Q. and Benton, M. J., 2012. The timing and pattern of biotic recovery following the end-Permian mass extinction. *Nature Geosci* **5**, 375-383.

De Villiers, S., Shen, G. T., and Nelson, B. K., 1994. The Sr /Ca-temperature relationship in coralline aragonite: Influence of variability in $(Sr/Ca)_{seawater}$ and skeletal growth parameters. *Geochim. Cosmochim. Acta* **58**, 197-208.

Eisenhauer, A., Böhm, F., Vollstaedt, H., Krabbenhöft, A., Liebetrau, V., Fietzke, J., Kisakürek, B., and Erez, J., 2011. Strontium isotope fractionation and its application in earth system sciences*Goldschmidt 2011*, Prague, Czech Republic, 19 August 2011.

Farkaš, J., Böhm, F., Wallmann, K., Blenkinsop, J., Eisenhauer, A., van Geldern, R., Munnecke, A., Voigt, S., and Veizer, J., 2007. Calcium isotope record of Phanerozoic oceans: Implications for chemical evolution of seawater and its causative mechanisms. *Geochim. Cosmochim. Acta* **71**, 5117-5134.

Fietzke, J. and Eisenhauer, A., 2006. Determination of temperature-dependent stable strontium isotope ($^{88}Sr/^{86}Sr$) fractionation via bracketing standard MC-ICP-MS. *Geochem. Geophys. Geosyst.* **7**.

Gorjan, P. and Kaiho, K., 2007. Correlation and comparison of seawater $\delta^{34}S_{CAS}$ records at the Permian-Triassic transition. *Chem. Geol.* **243**, 275-285.

Grotzinger, J. P. and Knoll, A. H., 1995. Anomalous carbonate precipitates; is the Precambrian the key to the Permian? *Palaios* **10**, 578-596.

Haq, B. U. and Schutter, S. R., 2008. A chronology of Paleozoic sea-level changes. *Science* **322**, 64-68.

Hay, W. W., Migdisov, A., Balukhovsky, A. N., Wold, C. N., Flögel, S., and Söding, E., 2006. Evaporites and the salinity of the ocean during the Phanerozoic: Implications for climate, ocean circulation and life. *Palaeogeography, Palaeoclimatology, Palaeoecology* **240**, 3-46.

Hoernle, K. and participants, C., 2003. FS/RV SONNE, Fahrtbericht SO168 = Cruise report SO168 : causes and effects of plume and rift-related cretaceous and cenozoic volcanism on Zealandia ; Wellington, Sydney, Lyttelton/Christchurch ; December 03, 2002 - January 16, 2003*GEOMAR Report*. GEOMAR, Kiel.

Holser, W. T., 1984. Gradual and Abrupt Shifts in Ocean Chemistry During Phanerozoic Time. In: Holland, H. D. and Trendall, A. F. Eds.), *Patterns of Change in Earth Evolution*. Springer, Berlin, Heidelberg, New York, Tokyo.

Horita, J., Zimmermann, H., and Holland, H. D., 2002. Chemical evolution of seawater during the Phanerozoic: Implications from the record of marine evaporites. *Geochim. Cosmochim. Acta* **66**, 3733-3756.

Isozaki, Y., 1997. Permo-Triassic boundary superanoxia and stratified superocean: Records from lost deep sea. *Science* **276**, 235-238.

Kaiho, K., Kajiwara, Y., Chen, Z.-Q., and Gorjan, P., 2006. A sulfur isotope event at the end of the Permian. *Chem. Geol.* **235**, 33-47.

Kampschulte, A. and Strauss, H., 2004. The sulfur isotopic evolution of Phanerozoic seawater based on the analysis of structurally substituted sulfate in carbonates. *Chem. Geol.* **204**, 255-286.

Kershaw, S., Crasquin, S., Li, Y., Collin, P. Y., Forel, M. B., Mu, X., Baud, A., Wang, Y., Xie, S., Maurer, F., and Guo, L., 2011. Microbialites and global environmental change across the Permian–Triassic boundary: a synthesis. *Geobiology* **10**, 25-47.

Knoll, A. H., Bambach, R. K., Canfield, D. E., and Grotzinger, J. P., 1996. Comparative earth history and Late Permian mass extinction. *Science* **273**, 452-457.

Krabbenhöft, A., Eisenhauer, A., Böhm, F., Vollstaedt, H., Fietzke, J., Liebetrau, V., Augustin, N., Peucker-Ehrenbrink, B., Hansen, B. T., Nolte, N., and Wallmann, K., 2010. Constraining the marine strontium budget with natural strontium isotope fractionations ($^{87}Sr/^{86}Sr^{*}$-$\delta^{88/86}Sr$) of carbonates, hydrothermal solutions and river waters. *Geochim. Cosmochim. Acta* **74**, 4097-4109.

Krabbenhöft, A., Fietzke, J., Eisenhauer, A., Liebetrau, V., Böhm, F., and Vollstaedt, H., 2009. Determination of radiogenic and stable strontium isotope ratios ($^{87}Sr/^{86}Sr$; $\delta^{88/86}Sr$) by thermal ionization mass spectrometry applying an $^{87}Sr/^{84}Sr$ double spike. *J. Anal. At. Spectrom.* **24**, 1267-1271.

Kramm, U. and Wedepohl, K. H., 1991. The isotopic composition of strontium and sulfur in seawater of Late Permian (Zechstein) age. *Chem. Geol.* **90**, 253-262.

Lemarchand, D., Gaillardet, J., Lewin, E., and Allègre, C. J., 2000. The influence of rivers on marine boron isotopes and implications for reconstructing past ocean pH. *Nature* **408**, 951-954.

Martin, E. E. and Macdougall, J. D., 1995. Sr and Nd isotopes at the Permian/Triassic boundary: A record of climate change. *Chem. Geol.* **125**, 73-99.

McArthur, J. M., Howarth, R. J., and Bailey, T. R., 2001. Strontium Isotope Stratigraphy: LOWESS version 3: Best fit to the marine Sr-isotope curve for 0-509 Ma and accompanying look-up table for deriving numerical age. *The Journal of Geology* **109**, 155-170.

Newton, R. J., Pevitt, E. L., Wignall, P. B., and Bottrell, S. H., 2004. Large shifts in the isotopic composition of seawater sulphate across the Permo-Triassic boundary in northern Italy. *Earth Planet. Sci. Lett.* **218**, 331-345.

Ogg, J. G., Ogg, G., and Gradstein, F. M., 2008. *The concise geologic time scale*. Cambridge University Press.

Ohno, T. and Hirata, T., 2007. Simultaneous determination of mass-dependent isotopic fractionation and radiogenic isotope variation of strontium in geochemical samples by Multiple Collector-ICP-Mass Spectrometry. *Anal. Sci.* **23**, 1275-1280.

Payne, J. L. and Clapham, M. E., 2012. End-Permian Mass Extinction in the Oceans: An Ancient Analog for the Twenty-First Century? *Annu. Rev. Earth Planet. Sci.* **40**, 89-111.

Pfannkuche, O. and participants, C., 2004. Meteor-Berichte 06-2. Cruise No. 61, Leg 1. Geo-biological investigations on azooxanthellate cold-water coral reefs on the carbonate mounds along the

Celtic contintental slope, Northeast Atlantic, April 19 to May 4, 2004, Lisbon - Cork*Meteor-Berichte 06-2*.

Ratmeyer, V. and participants, c., 2006. Report and preliminary results of RV Meteor Cruise M61/3. Development of carbonate mounds on the Celtic continental margin, Northeast Atlantic, Cork (Ireland) - Ponta Delgada (Portugal), 04. - 21.06.2004. In: Fachbereich 5, U. B. (Ed.),*Berichte*. Fachbereich Geowissenschaften, Universität Bremen, Bremen.

Raup, D. M., 1979. Size of the Permo-Triassic Bottleneck and Its Evolutionary Implications. *Science* **206**, 217-218.

Riding, R. and Liang, L., 2005. Geobiology of microbial carbonates: metazoan and seawater saturation state influences on secular trends during the Phanerozoic. *Palaeogeography, Palaeoclimatology, Palaeoecology* **219**, 101-115.

Royer, D. L., 2006. CO_2-forced climate thresholds during the Phanerozoic. *Geochim. Cosmochim. Acta* **70**, 5665-5675.

Rüggeberg, A., Fietzke, J., Liebetrau, V., Eisenhauer, A., Dullo, W.-C., and Freiwald, A., 2008. Stable strontium isotopes ($\delta^{88/86}$Sr) in cold-water corals - A new proxy for reconstruction of intermediate ocean water temperatures. *Earth Planet. Sci. Lett.* **269**, 570-575.

Sobolev, S. V., Sobolev, A. V., Kuzmin, D. V., Krivolutskaya, N. A., Petrunin, A. G., Arndt, N. T., Radko, V. A., and Vasiliev, Y. R., 2011. Linking mantle plumes, large igneous provinces and environmental catastrophes. *Nature* **477**, 312-316.

Steuber, T. and Veizer, J., 2002. Phanerozoic record of plate tectonic control of seawater chemistry and carbonate sedimentation. *Geology* **30**, 1123-1126.

Veizer, J., Ala, D., Azmy, K., Bruckschen, P., Buhl, D., Bruhn, F., Carden, G. A. F., Diener, A., Ebneth, S., Godderis, Y., Jasper, T., Korte, C., Pawellek, F., Podlaha, O. G., and Strauss, H., 1999. $^{87}Sr/^{86}Sr$, $\delta^{13}C$ and $\delta^{18}O$ evolution of Phanerozoic seawater. *Chem. Geol.* **161**, 59-88.

Wallmann, K., 2001. Controls on the cretaceous and cenozoic evolution of seawater composition, atmospheric CO_2 and climate. *Geochim. Cosmochim. Acta* **65**, 3005-3025.

Wignall, P. B., 2007. The End-Permian mass extinction – how bad did it get? *Geobiology* **5**, 303-309.

Wignall, P. B. and Twitchett, R. J., 2002. Extent, duration, and nature of the Permian-Triassic superanoxic event. *Geological Society of America Special Papers* **356**, 395-413.

Woods, A. D., Bottjer, D. J., Mutti, M., and Morrison, J., 1999. Lower Triassic large sea-floor carbonate cements: Their origin and a mechanism for the prolonged biotic recovery from the end-Permian mass extinction. *Geology* **27**, 645-648.

Zeebe, R. E. and Wolf-Gladrow, D., 2001. *CO_2 in seawater: equilibrium, kinetics, isotopes*. Elsevier.

Zhou, L., Gao, S., Chris, H., Corey, A., and Xie, S., 2009. Preliminary Mo isotope data of Phanerozoic clastic sediments from the northern margin of the Yangtze block and its implication for paleoenvironmental conditions. *Chinese Science Bulletin* **54**, 822-829.

V. Chapter

The Phanerozoic $\delta^{88/86}$Sr Record of Seawater: New Implications for Strontium Isotope Stratigraphy and the Ocean Chemistry of the past

Hauke Vollstaedt[1], Anton Eisenhauer[1], Klaus Wallmann[1], Florian Böhm[1], Volker Liebetrau[1], Jan Fietzke[1], André Krabbenhöft[1,+], Jacek Raddatz[1], and Ján Veizer[2]

[1] *GEOMAR, Helmholtz-Zentrum für Ozeanforschung Kiel, Wischhofstr. 1-3, 24148 Kiel, Germany*

[2] *Ottawa-Carleton Geoscience Center, University of Ottawa, Ottawa ON K1N 6N5, Canada*

[+] *Present address: Leyegasse 4, 69117 Heidelberg, Germany*

In preparation to be submitted to *Geochimica et Cosmochimica Acta*

Abstract

The isotopic composition of Phanerozoic marine sediments provides important information about changes in seawater chemistry. In particular, the well-established radiogenic $^{87}Sr/^{86}Sr$ isotope system is a powerful tool to constrain plate tectonic processes and their influence on atmospheric CO_2 concentrations. However, it is insensitive to stable isotope fractionation processes and therefore not able to trace changes in the Sr output flux, mainly represented by marine carbonates. Hence, the Sr budget of the Phanerozoic ocean, including changes in carbonate sedimentation, has yet not been constrained. Here, we extend the existing stable Sr isotope record of seawater ($\delta^{88/86}Sr_{sw}$) to a total number of 154 data points, showing considerable variations in $\delta^{88/86}Sr_{sw}$ from 0.25‰ to 0.60‰ with a mean of 0.37‰. The Phanerozoic $\delta^{88/86}Sr_{sw}$ record is similar to the Ca isotope record ($\delta^{44/40}Ca_{sw}$), but considerably different to the radiogenic Sr record ($(^{87}Sr/^{86}Sr)_{sw}$), implying different controlling mechanisms for the two Sr isotope systems. With a consequent numerical modeling approach we calculate for the first time changes in Phanerozoic seawater Sr fluxes and concentrations. Our results reveal that the carbonate-related flux of Sr ($F(Sr)_{carb}$; negative sign represents a net output flux and vice versa) varied between -4.7×10^{10}mol/Myr and $+2.3 \times 10^{10}$mol/Myr and a mean of -1.6×10^{10}mol/Myr. On short-term timescales $F(Sr)_{carb}$ is controlled by carbonate sedimentation, shelf weathering/recrystallization, ocean acidification and ocean anoxia, whereas on long-term timescales it is controlled by changes between "aragonite seas" and "calcite seas". We also show for first time changes in the Sr residence time (τ_{Sr}) of the ocean, being in the range of ~1Myrs to ~20Myrs, implying significant changes in the sensitivity of the two Sr isotope systems. We demonstrate that the higher sensitivity of $\delta^{88/86}Sr_{sw}$ and the different controlling mechanisms of $\delta^{88/86}Sr_{sw}$ and $(^{87}Sr/^{86}Sr)_{sw}$ significantly improve the Strontium Isotope Stratigraphy (SIS) extending the time range of SIS application.

V.1. Introduction

The weathering of continental rocks is probably the most important sink for atmospheric CO_2 and therefore one of the major processes that control climate on earth on geological timescales. In order to reconstruct the atmospheric CO_2 history from Quaternary to Phanerozoic timescales the radiogenic isotope systems like Re/Os and Rb/Sr are powerful tools in order to gain information about the past dynamic of continental weathering and its interaction with atmospheric pCO_2.

With a concentration of 7.74ppm (FAURE and MENSING, 2005) and a residence time of $2.5x10^6$years (HODELL et al., 1990) in the ocean, Sr is considered to be a conservative trace element being homogeneously distributed within the modern ocean and marginal seas with salinities as low as 14 psu (VEIZER et al., 1983; VEIZER, 1989). The higher mean $^{87}Sr/^{86}Sr$-ratio in the continental runoff in contrast to seawater is buffered by seawater interaction between hydrothermal fluids and oceanic crust (SPOONER, 1976; RICHTER et al., 1992) to a certain value which in the modern ocean is 0.709175 (MCARTHUR, 1994). Therefore it is concluded that the radiogenic Sr isotope composition of seawater is controlled by an exogenic system with plate tectonics as the main force (VEIZER, 1988; VEIZER et al., 1999). According to that, changes in $(^{87}Sr/^{86}Sr)_{sw}$ are a function of seafloor spreading, orogenesis and uplift of continents. Beside the use of $(^{87}Sr/^{86}Sr)_{sw}$ ratios for the reconstruction of plate tectonic processes in the past the $^{87}Sr/^{86}Sr$ ratio of Phanerozoic seawater is used for SIS. This well established method for stratigraphic dating of marine carbonate sediments is suitable especially when fossils are lacking or their amount is too small. The precision of this method is limited to the slope of the $(^{87}Sr/^{86}Sr)_{sw}$ cruve and by the age model reconstructed from biostratigraphy and is less than 0.15Myr up to 2Myr in most cases (MCARTHUR, 1994; MCARTHUR et al., 2001). Furthermore $^{87}Sr/^{86}Sr$-ratios differ between distinct biozones leading to a global geological reproducibility not better than $5x10^{-5}$ (DIENER et al., 1996). Therefore

the seawater Sr isotope curve can only be resolved as a band, reflecting the uncertainties in biostratigraphy, geochronology, and further uncertainties due to early diagenesis of the sample material (VEIZER et al., 1997).

Although the $^{87}Sr/^{86}Sr$ system is well understood there are still discrepancies between modeled and observed $(^{87}Sr/^{86}Sr)_{sw}$ ratios, especially in the Cenozoic (VEIZER, 1989; VANCE et al., 2009). In this context weathering rates after deglaciations and tectonic uplifts (HODELL et al., 1989; TAYLOR and BLUM, 1995; STOLL and SCHRAG, 1998; PORDER et al., 2007; VANCE et al., 2009; KRABBENHÖFT et al., 2010) incongruent weathering of silicates after deglaciation (BLUM and EREL, 1997) the role of island arc weathering (ALLÈGRE et al., 2010), and low-temperature alteration of the oceanic crust (BUTTERFIELD et al., 2001; DERRY, 2009) are still subjects of debate. Furthermore, the radiogenic Sr isotope system can only provide information about the mixing of the Sr input fluxes to the ocean. No information can be gained about the Sr output fluxes due to the neglection of isotope fractionation processes inherent to the radiogenic isotope systematic. Therefore, modeled changes in seawater Sr concentration ($[Sr]_{sw}$) depend on less constraint $(Sr/Ca)_{sw}$ ratios and seawater calcium concentrations ($[Ca]_{sw}$) based on fluid inclusion data (HORITA et al., 2002; STEUBER and VEIZER, 2002; WALLMANN, 2004; LOWENSTEIN et al., 2005).

Latter problem can be overcome by extending the Sr systematic by the stable Sr isotope ratio $^{88}Sr/^{86}Sr$. The ratio of stable Sr is given as $\delta^{88/86}Sr$ in relation to the $SrCO_3$ standard SRM987 distributed by the National Institute of Standards and Technology (NIST) (FIETZKE and EISENHAUER, 2006).

$$\delta^{88/86}Sr\ [‰] = \left(\frac{\frac{^{88}Sr}{^{86}Sr}_{sample}}{\frac{^{88}Sr}{^{86}Sr}_{SRM987}} - 1 \right) * 1000$$

$^{88}Sr/^{86}Sr$-ratios in modern marine carbonates have been found to be distinctly lower than present seawater (KRABBENHÖFT et al., 2009; KRABBENHÖFT et al., 2010; BÖHM et al., 2012).

Thus, changes in isotope signatures of seawater and marine carbonates through Earth's history are not solely influenced by variations in the Sr sources of the ocean but also by variations in the carbonate output flux out of the ocean. With a simultaneous determination of $^{88}Sr/^{86}Sr$- and $^{87}Sr/^{86}Sr$-ratios it is possible to constrain the complete Phanerozoic Sr budget of the ocean, including Sr carbonate fluxes, thereby improving our understanding of the interaction between continental weathering, ocean chemistry and climate change. As to the modern ocean, Krabbenhöft et al. (2010) pointed out that sea-level change with associated changes in weathering regimes leads to changes in $\delta^{88/86}Sr$ of the Sr input flux to the ocean on glacial/interglacial timescales. A first study on changes in the stable Sr isotope composition at the Permian/Triassic (P/T) boundary indicates that $\delta^{88/86}Sr_{sw}$ is strongly controlled by variations in the Sr carbonate output flux. In particular, changes in sea-levels or changes in seawater alkalinity due to ocean anoxia can have a strong influence on marine carbonate fluxes and hence $\delta^{88/86}Sr_{sw}$ (VOLLSTAEDT et al., in review).

The goal of this study is to determine the causative mechanisms for variations of the $\delta^{88/86}Sr_{sw}$ values on Phanerozoic timescales. Beside this, our method contributes an additional isotope curve to the SIS which may improve the precision of this stratigraphic dating method. In particular, when the slope of the $^{87}Sr/^{86}Sr$ curve does not provide adequate time resolution, a combined $\delta^{88/86}Sr_{sw}$-$(^{87}Sr/^{86}sr)_{sw}$ SIS could improve the precision significantly.

V.2. Materials and Methods

In order to investigate in changes in $\delta^{88/86}Sr_{sw}$ through Earth's history, we extended the existing $\delta^{88/86}Sr_{sw}$ record (VOLLSTAEDT et al., in review) to a total number of 177 Phanerozoic carbonate samples from brachiopods, belemnites and carbonate matrixes. The samples were checked for diagenesis (low element concentrations of Mn, Fe and Mg as well as low coeval $^{87}Sr/^{86}Sr$ and ordinary coeval $\delta^{18}O$ ratios (VEIZER et al., 1999)) prior to analysis. The

measurement was done with a $^{87}Sr/^{84}Sr$ double spike (DS) technique combined with thermal ionization mass spectrometry (TIMS) as introduced by (KRABBENHÖFT et al., 2009).

Brachiopod as well as belemnite samples represent the most stable fossil carbonate archives in the Phanerozoic (SMALLEY et al., 1994). The samples used for the Phanerozoic record are from a previously published dataset (VEIZER et al., 1999) and extend a previous investigation (VOLLSTAEDT et al., in review). The fossils are dated on the basis on biostratigraphic zones which have a resolution in the order of 1-2Myr (VEIZER et al., 1999). Prior to chemical preparation the carbonate samples were checked for diagenesis. Selected samples are low-Mg calcites from brachiopods, belemnites and carbonate matrixes samples largely originating from 30°S to 30°N paleolatitudes. Modern brachiopods contain <460ppm Mn and 200ppm to 2150ppm Sr (LEPZELTER et al., 1983; MORRISON and BRAND, 1988) while well-preserved Phanerozoic brachiopods contain <250ppm Mn and 300ppm to 3400ppm Sr (POPP et al., 1986). 95% of our fossil brachiopod samples have Sr concentrations in the range of modern species. 74% of our brachiopod samples have Mn concentrations below the cut-off limit of 200ppm (AZMY et al., 1998; BRUCKSCHEN et al., 1999). Furthermore we observe no correlation between Sr and Mn concentrations in our samples, indicating the absence of any obvious diagenesis.

Because brachiopod sample availability is very limited in the Mesozoic, low-Mg belemnites are used as best available sample archives regarding post-depositional stability and utility (JONES et al., 1994a; JONES et al., 1994b; VEIZER et al., 1999). Well preserved Phanerozoic fossil belemnite samples have Fe concentrations <150 ppm and Mn concentrations <20ppm (JONES et al., 1994a; JONES et al., 1994b). 74% of our samples have Fe and Mn concentrations of <150 ppm and <9ppm, respectively. Further, we observe no correlation between Mn and Fe concentrations in our belemnite samples and therefore propose that our samples retained their original Sr isotope signature. For the $\delta^{88/86}Sr_{sw}$ record only skeletal carbonates with i) $^{87}Sr/^{86}Sr$ that were not higher than 0.0001 when compared to previous measurements on the

same samples (Veizer et al., 1999) and ii) not >0.00035 lower as the coeval $(^{87}Sr/^{86}Sr)_{sw}$ curve were considered (McArthur et al., 2001) (See also fig. V.1).

The carbonates originate from Australia, Austria, Belgium, Canada, China, Germany, Hungary, Italy, Latvia, Lithuania, New Zealand, USA, Russia, Slovakia, Sweden, Switzerland, and Ukraine (further details on stratigraphy, location and age in supplementary material and references in (Veizer et al., 1999)).

Sampling procedure and measurement method follow (VOLLSTAEDT et al., in review). In summary, the sample carbonate powders were gained by drilling with a conventional dental drill or alternatively a New Wave© micro mill, depending on the size of the shell. Carbonate powders were ultrasonically cleaned twice in ultrapure water for about 30 minutes. All samples were dissolved in 0.5N HNO_3, undissolved residual parts were removed, and samples were heated in a mixture of 100µl of 30% H_2O_2 and 200µl of 8N HNO_3 at 80°C to dissolve organic components. The samples were split afterwards and an $^{87}Sr/^{84}Sr$ double spike (DS) was added to one split of the dissolved sample. Ionchromatography was performed with BIO-RAD 650µl columns which were filled to one third with Triskem Sr-SPS resin (particle size 50µm to 100µm).

In order to verify for diagenetic alteration some samples (Table V.S3) were measured for their $\delta^{13}C$- and $\delta^{18}O$-composition on a Finnigan MAT 252 stable isotope ratio mass spectrometer with a Kiel CARBO device at GEOMAR. Reproducibility of the method is 0.05‰ (2 s.d.) for both $\delta^{13}C$ and $\delta^{18}O$, respectively. The Ca, Mg, Mn, Fe and Sr concentrations were determined by ICP-MS (Agilent 7500 series) at GEOMAR.

TIMS measurement procedures generally follow the strontium double spike (DS) method (Krabbenhöft et al., 2009). Briefly, the samples were loaded on rhenium ribbon single filaments in combination with a Ta_2O_5-activator. The measurements were carried out on a TRITON thermal ionization multi-collector mass spectrometer (Thermo Fisher) at the

GEOMAR mass spectrometer facilities. The measurement was started when signal intensity of 10V on mass 88 was achieved.

The application of the DS-technique in combination with an iterative spike correction algorithm using an exponential law for the mass fractionation correction (Krabbenhöft et al., 2009) allows us to calculate natural $^{88}Sr/^{86}Sr$-ratios in addition to the conventional radiogenic $^{87}Sr/^{86}Sr$-ratios. All conventional radiogenic $^{87}Sr/^{86}Sr$-ratios of the samples were normalized as usual to an $^{86}Sr/^{88}Sr$ ratio of 0.1194. Samples were also corrected for the offset between the measured value of SRM987 of the individual session and the international agreed $^{87}Sr/^{86}Sr$-ratio of 0.710240 (Veizer et al., 1999). The external reproducibility (2 s.d.) for all $\delta^{88/86}Sr$ measurements is determined by the repeated $\delta^{88/86}Sr$ analysis of the coral standard JCp-1 (distributed by the Geological Survey of Japan) over a period of 28 months. The resulting $\delta^{88/86}Sr$ value is 0.193±0.022‰ (n=32; 2 s.d.) and is in agreement with published data (OHNO and HIRATA, 2007; KRABBENHÖFT et al., 2009; KRABBENHÖFT et al., 2010). The conventional radiogenic $^{87}Sr/^{86}Sr$-ratio on JCp-1 is determined to be 0.709172 ± 0.000022 (n=32; 2 s.d.). Whole procedure analytical blank was determined to be less than 0.3ng Sr, which is ~0.1% of the Sr amount in our samples.

V.3. Results

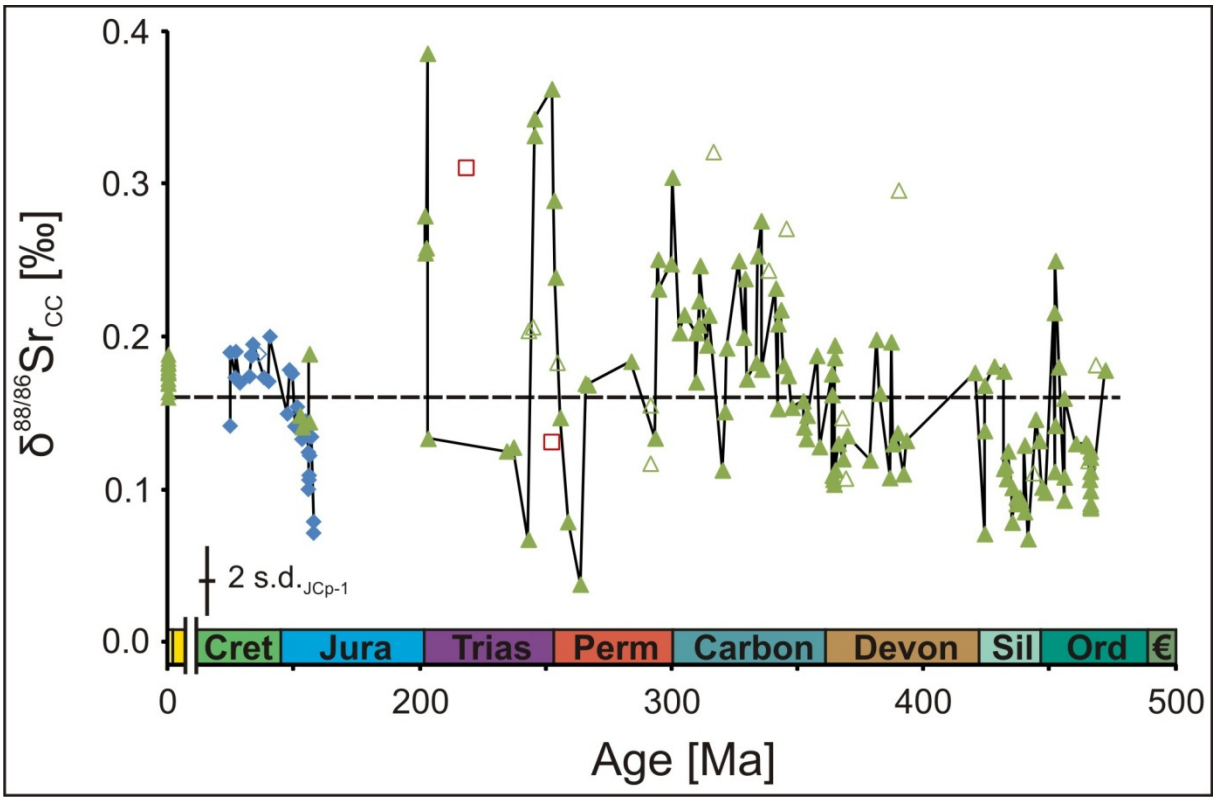

FIGURE V.1 - $\delta^{88/86}Sr$ of marine carbonates ($\delta^{88/86}Sr_{cc}$) through geological time (Triangles = brachiopods, diamonds = belemnites, squares = carbonate matrixes). Open symbols represent samples with unreliable samples according to our selection criteria. Closed symbols represent samples with reliable $^{87}Sr/^{86}Sr$, Mn, Fe, and $\delta^{18}O$ values that are used to reconstruct seawater $\delta^{88/86}Sr$ (Fig. V.2). External reproducibility (2 s.d.) of coral standard JCp-1 corresponds to ±0.023‰ (n=32). The horizontal black dashed line represents Phanerozoic mean $\delta^{88/86}Sr_{sw}$ of 0.16‰. Timescale and geological periods are from GTS 2012 (Gradstein et al., 2012). Abbreviations for geological periods: N = Neogene, P = Paleogene, Cret = Cretaceous, Jura = Jurassic, Trias = Triassic, Perm = Permian, Carbon = Carboniferous, Devon = Devonian, Sil = Silurian, Ord = Ordovician, € = Cambrian. Coloring of periods follows the Commission for the Geological Map of the World (http://www.ccgm.org).

We observe significant variations in $\delta^{88/86}Sr$ of Phanerozoic calcium carbonate samples ($\delta^{88/86}Sr_{CC}$, Fig. V.1). Mean value of all fossil carbonate samples is 0.16‰. Highest values are observed in the late Permian and late Triassic period ($\delta^{88/86}Sr_{cc}$ = 0.36‰ and 0.39‰, respectively), whereas the lowest values are in late Silurian and early Permian period ($\delta^{88/86}Sr_{cc}$ = 0.07‰ and 0.04‰, respectively). In the Paleozoic Eon, a decrease from the late Ordovician period ($\delta^{88/86}Sr_{cc}$ ≈ 0.15‰) to the late Silurian period ($\delta^{88/86}Sr$ ≈ 0.10‰) with a subsequent long-term increase in $\delta^{88/86}Sr_{cc}$ to Early Permian period ($\delta^{88/86}Sr_{cc}$ ≈ 0.25‰) is

observed. In the Permian period $\delta^{88/86}Sr_{cc}$ decreases to Phanerozoic minimum of 0.04‰ and increases afterwards up to one of the highest values of the Phanerozoic right at the P/T transition. In the Early Triassic $\delta^{88/86}Sr_{CC}$ decrease back to very low ratios of 0.07‰ and increase in the Late Triassic to more average Phanerozoic values. The rate of change in the Permian and Triassic period is the highest for the whole Phanerozoic Eon (0.024‰/Myr). Data for Jurassic to Early Cretaceous period represented by belemnites and brachiopods indicates an increase from ~0.1‰ to ~0.2‰ during the Jurassic to early Cretaceous period.

V.4. Discussion

Sr fractionation factor between seawater and carbonate recording phase

In order to reconstruct the Phanerozoic $\delta^{88/86}Sr_{sw}$ record, the fractionation factor between seawater and the recording carbonate phase needs to be known. For modern calcitic brachiopods it was shown that neither habitat location, water temperature, or species have a significant influence on $\delta^{88/86}Sr_{cc}$ (VOLLSTAEDT et al., in review). Modern brachiopods have similar values with a mean of 0.176‰ ± 0.016‰ (2 s.d., n=13) (VOLLSTAEDT et al., in review). Therefore it has been proposed that brachiopod samples are an applicable archive to reconstruct seawater $\delta^{88/86}Sr$ values in geological history (VOLLSTAEDT et al., in review).

The fractionation factor of our species is assumed to be constant through time. The fractionation factor $\alpha_{CC\text{-}SW}$ between seawater and the carbonate phase is expressed as:

$$\alpha_{CC-SW} = \left(\delta^{88/86}Sr_{CC} + 1000\right)/\left(\delta^{88/86}Sr_{SW} + 1000\right)$$

where $\delta^{88/86}Sr_{cc}$ and $\delta^{88/86}Sr_{sw}$ represent the stable Sr isotope composition of the carbonate phase and seawater, respectively. Taken the IAPSO seawater standard as representative for $\delta^{88/86}Sr_{SW}$ ($\delta^{88/86}Sr_{IAPSO}$ = 0.386‰ (KRABBENHÖFT et al., 2009)) we observe a fractionation factor of 0.99979 ($\Delta^{88/86}Sr_{cc\text{-}sw}$ = -0.21‰) for modern brachiopods. Concerning extinct belemnites, it was shown that their fractionation factor is constant and comparable to brachiopods

(VOLLSTAEDT et al., in review). Carbonate matrix samples are significantly higher in $\delta^{88/86}Sr$ compared to coeval brachiopod and belemnite samples in three of four cases and always higher in $^{87}Sr/^{86}Sr$ (Table V.1). Additionally, the offset between $\delta^{88/86}Sr$ of macrofossil and carbonate matrix samples varies considerably, implying that carbonate matrix samples are much less reliable for the reconstruction of $\delta^{88/86}Sr_{sw}$.

TABLE V.1 – The radiogenic and stable Sr isotope composition of Jurassic brachiopods, belemnites, and their host limestones (matrixes). Samples are from three different sections in the Swabian Alb and Swiss Jura. Matrixes always show and elevated $^{87}Sr/^{86}Sr$ ratios and $\delta^{88/86}Sr$ ratios compared to their included macrofossils. Macrofossil data from (VOLLSTAEDT et al., in review).

Archive	*Species*	$^{87}Sr/^{86}Sr$	$\delta^{88/86}Sr_{cc}$ [‰]
Swabian Alb, Ursental section (Bed 2-9), Upper Kimmeridgian, Aulacostephanus mutabilis zone			
Brachiopod (Ur2-9-68)	Lacunosella multiplicata	0.707035	0.149
Matrix (Ur2-9-68)		0.707911	0.250
Swabian Alb, Geisingen section (Bed 13), Lower Kimmeridgian, Crussoliceras divisum zone			
Belemnite (Gei13)	Belemnite indet.	0.707007	0.133
Matrix 1/2 (Gei13)		0.707876	0.355
Matrix 2/2 (Gei13)		0.707400	0.152
Swiss Jura, Holderbank section (Bed 23), Middle Oxfordian, Gregoryceras transversarium zone			
Belemnite 1/2 (Hol23)	Belemnite indet.	0.706832	0.071
Belemnite 2/2 (Hol 23)	Belemnite indet.	0.706885	0.079
Matrix (Hol 23)		0.707602	0.297

$\delta^{88/86}Sr$ of Phanerozoic seawater

Applying the fractionation factor of $\Delta^{88/86}Sr_{cc\text{-}sw}$ = -0.21‰ of our carbonate recording phases (brachiopods and belemnites), the Phanerozoic $\delta^{88/86}Sr_{sw}$ could be reconstructed (Fig. V.2). With this study we extend the published record of (VOLLSTAEDT et al., in review) to a total number of 154 $\delta^{88/86}Sr_{sw}$ values. The $\delta^{88/86}Sr_{sw}$ varies in between 0.25‰ and 0.60‰ with a mean of 0.37 ± 0.12‰ (2 s.d.).

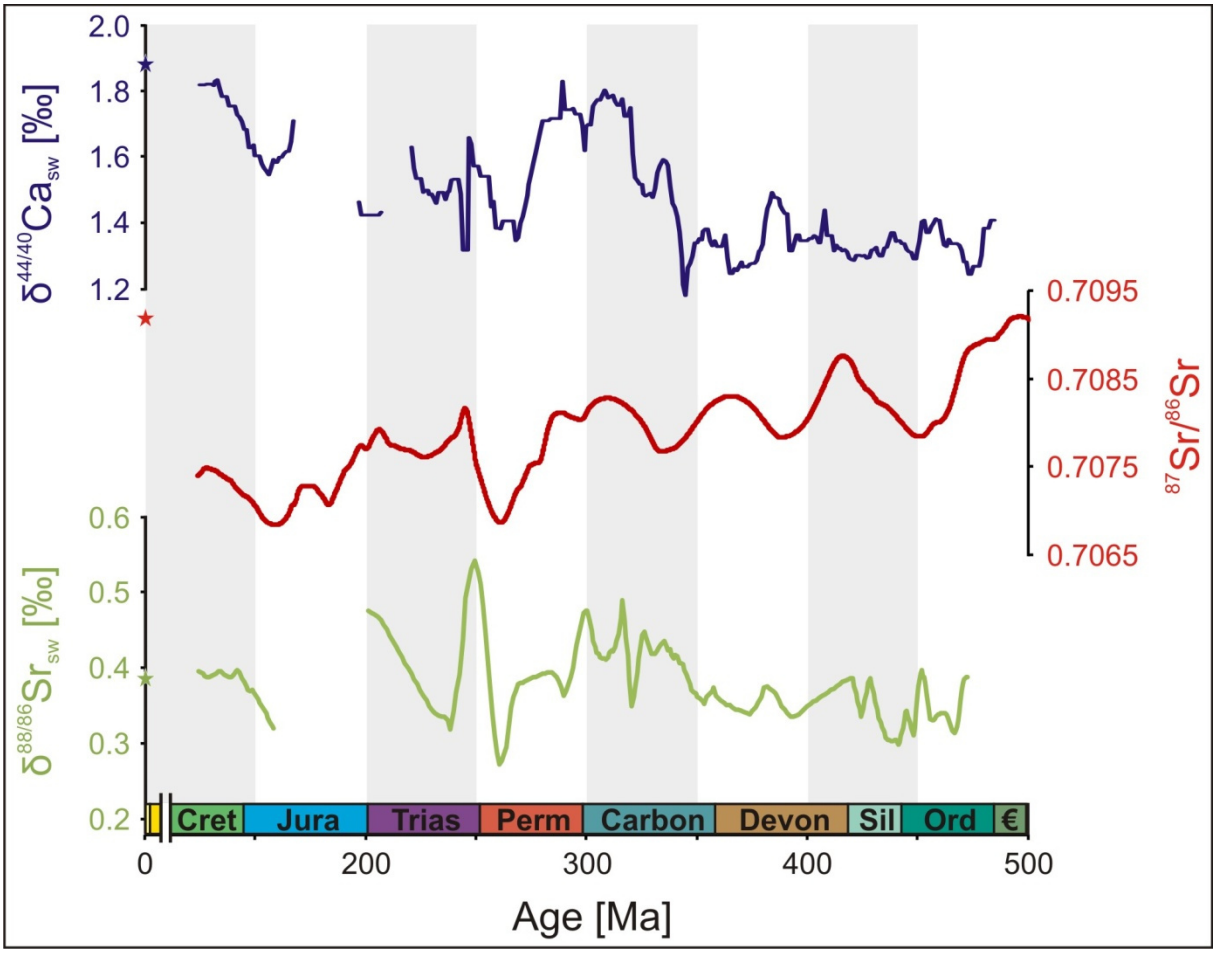

FIGURE V.2 – The stable and radiogenic strontium and calcium isotope composition of Phanerozoic seawater. Green curve represents a 5Myr running mean $\delta^{88/86}Sr_{sw}$ record reconstructed from brachiopods and belemnites (Fig. V.1). Red curve represents $^{87}Sr/^{86}Sr$ data compiled by (McArthur et al., 2001). Blue curve represents a 10Myr running mean through the data of (Farkaš et al., 2007). Green, red, and blue stars represent modern seawater isotope ratios for $\delta^{88/86}Sr$, $^{87}Sr/^{86}Sr$, and $\delta^{44/40}Ca$, respectively (MCARTHUR, 1994; HIPPLER et al., 2003; KRABBENHÖFT et al., 2009). Grey vertical bars represent 50Myrs time intervals and are for easing comparison between isotope curves. Timescale and geological periods from GTS 2012 (Gradstein et al., 2012). Abbreviations for geological periods are the same as in figure caption V.1.

When comparing Phanerozoic $^{87}Sr/^{86}Sr$ and $\delta^{88/86}Sr$ records we observe different patterns of the two Sr isotope systems (Fig. V.2). In particular, the seawater $^{87}Sr/^{86}Sr$ has characteristic ~50Myrs sinusoidal cycles with a general decreasing trend in the Paleozoic. In contrast, $\delta^{88/86}Sr_{sw}$ is decreasing from Ordovician (~0.35‰) to Silurian period (~0.30‰) and increasing afterwards to ~0.50‰ in the Early Permian. Further, $\delta^{88/86}Sr_{sw}$ does not have the characteristic sinusoidal cycles. However, this remains to be tested in future $\delta^{88/86}Sr_{sw}$ studies with a higher temporal resolution. During the P/T transition, both isotope systems show similar patterns with their Phanerozoic minimum values ($\delta^{88/86}Sr_{sw} \approx 0.25$‰, $(^{87}Sr/^{86}Sr)_{sw} \approx 0.7070$) in the Late Permian at ~260Ma and a steep increase until the early Triassic ($\delta^{88/86}Sr_{sw} \approx 0.57$‰, $(^{87}Sr/^{86}Sr)_{sw} \approx 0.7082$). However, the rate of change is significantly larger for $^{88}Sr/^{86}Sr$ (~0.000189/Myr) compared to $^{87}Sr/^{86}Sr$ (0.000081‰/Myr) (see also Fig. V.7). From the Triassic to Late Jurassic period ($(^{87}Sr/^{86}Sr)_{sw}$ is decreasing again to ~0.7069 and increases afterwards to ~0.7075 during Early Cretaceous period. In contrast, $\delta^{88/86}Sr_{sw}$ decreases directly after the P/T boundary to ~0.28‰ and increases afterwards to ~0.50‰ in the Late Triassic. Data distribution during Late Jurassic and Early Cretaceous periods indicate a slight increase from ~0.29‰ to ~0.40‰ in $\delta^{88/86}Sr_{sw}$. In summary, $\delta^{88/86}Sr_{sw}$ and $(^{87}Sr/^{86}Sr)_{sw}$ differ both on short- and long-term timescales as well as in rate of changes, although some parts during the Phanerozoic Eon (Permian period and Jurassic/Cretaceous boundary) reveal similarities in isotope trends.

Consequently, $\delta^{88/86}Sr_{sw}$ and $^{87}Sr/^{86}Sr$ must be controlled by different mechanisms on Phanerozoic timescales. The $\delta^{88/86}Sr_{sw}$ variations reflect changes in the carbonate-related flux of Sr (net flux which includes carbonate dissolution and precipitation; $F(Sr)_{carb}$), hydrothermal introduced fluids and precipitates into the oceanic crust ($F(Sr)_{hyd\text{-}in}$, $F(Sr)_{alt}$), silicate and carbonate continental weathering ($F(Sr)_{ws}$, $F(Sr)_{wc}$), and their isotope signatures ($\Delta^{88/86}Sr_{carb\text{-}sw}$, $\delta^{88/86}Sr_{hyd(in)}$, $\Delta^{88/86}Sr_{alt\text{-}sw}$, $\delta^{88/86}Sr_{ws}$, $\delta^{88/86}Sr_{wc}$) (KRABBENHÖFT et al., 2010; VOLLSTAEDT et al., in review). Due to similar $\delta^{88/86}Sr$ values in the silicate weathering and hydrothermal input fluxes (~0.27‰; table V.2), variations in the ratio of these Sr input fluxes

to the oceans are supposed to have a negligible effect on $\delta^{88/86}Sr_{sw}$. Furthermore, hydrothermal $\delta^{88/86}Sr_{hyd(in)}$ signatures are supposed to be constant through time as the mantle is supposed to represent a homogenized reservoir with respect to Sr isotopes. The fractionation factor of inorganic calcite precipitates into the oceanic crust ($\Delta^{88/86}Sr_{alt\text{-}sw}$ = -0.01‰ (BÖHM et al., 2012)) is also supposed to be constant through time. However, changes in $F(Sr)_{wc}$, $F(Sr)_{carb}$ and its isotope fractionation factor $\Delta^{88/86}Sr_{carb\text{-}sw}$, as well as imbalances between Sr input and output fluxes are supposed to have large effects on $\delta^{88/86}Sr_{sw}$ (KRABBENHÖFT et al., 2010; VOLLSTAEDT et al., in review). The strong influence of the carbonate output flux on $\delta^{88/86}Sr_{sw}$ is in contrast to radiogenic Sr isotopes which are only controlled by the ratio of Sr input fluxes ($F(Sr)_{ws}$, $F(Sr)_{wc}$, and $F(Sr)_{hyd(in)}$).

In accordance with $\delta^{88/86}Sr_{sw}$, the Ca isotope composition of seawater ($\delta^{44/40}Ca_{sw}$, Fig. V.2) is likewise controlled by carbonates as the main output flux (FARKAŠ et al., 2007; BLÄTTLER et al., 2012). Accordingly, we expect similar trends in $\delta^{88/86}Sr_{sw}$ and $\delta^{44/40}Ca_{sw}$. In general, both isotope system show similar long-term trends which follow times of suggested "aragonite seas" and "calcite seas" (Stanley and Hardie, 1998) (see also Fig. V.5). However, for $\delta^{88/86}Sr_{sw}$, this trend is caused by higher Sr concentrations in the aragonite, whereas the observed $\delta^{44/40}Ca_{sw}$ trend is due to the higher fractionation factor of aragonite compared to calcite (FARKAŠ et al., 2007; BLÄTTLER et al., 2012). Both $\delta^{88/86}Sr_{sw}$ and $\delta^{44/40}Ca_{sw}$ have low isotope ratios in the Silurian buthigh isotope ratios in Early Permian period. However, this general trend of increasing isotope ratios is different on shorter timescales. In particular, $\delta^{44/40}Ca_{sw}$ is constant from Silurian period to early Carboniferous period at ~1.35‰ and increases afterwards to ~1.8‰ in the early Permian period. In similarity to $^{87}Sr/^{86}Sr$ and $\delta^{88/86}Sr_{sw}$, $\delta^{44/40}Ca_{sw}$ is decreasing in the mid-Permian period to ~1.35‰ and increasing in the late Permian and earliest Triassic period to ~1.65‰. In further accordance to $\delta^{88/86}Sr_{sw}$, $\delta^{44/40}Ca_{sw}$ decreases in the early Triassic to ~1.31‰ and increases afterwards to ~1.60‰ in the mid-

Triassic. Also in accordance with $\delta^{88/86}Sr_{sw}$, $\delta^{44/40}Ca_{sw}$ trends for the Jurassic and Cretaceous period reveal a general increasing trend from ~1.55‰ to ~1.82‰.

The influence of low temperature alteration of the oceanic crust as well as the process of dolomitization has not been studied at present. From theoretical consideration perspective (ARTEMOV et al., 1967) elements released during the process of dolomitization should be isotopically light. For Ca, this is supported by one study (HEUSER et al., 2005) and declined by one other (HOLMDEN, 2009). The alteration of Island Arcs and Oceanic Islands has not been studied for Ca and stable Sr isotopes at present but we assume that this process is a source of relatively light Sr compared to seawater due to low $\delta^{88/86}Sr$ of mid ocean ridge (MOR) fluids (KRABBENHÖFT et al., 2010) and basalts (OHNO and HIRATA, 2007; MOYNIER et al., 2010; SOUZA et al., 2010).

In summary, long-term trends $\delta^{88/86}Sr_{sw}$ and $\delta^{44/40}Ca_{sw}$ are quite similar in contrast to $\delta^{88/86}Sr_{sw}$ and $^{87}Sr/^{86}Sr$. However, this general coincidence is superimposed by short-term deviations in isotope trends which may be explained by a different impact of processes like carbonate mineralogy, dolomite formation, changes in biogenic and inorganic carbonate precipitation, and/or post-depositional transformation of aragonite to calcite on $\delta^{88/86}Sr_{sw}$ and $\delta^{44/40}Ca_{sw}$ (FARKAŠ et al., 2007; BLÄTTLER et al., 2012).

Numerical box model of the marine Sr budget

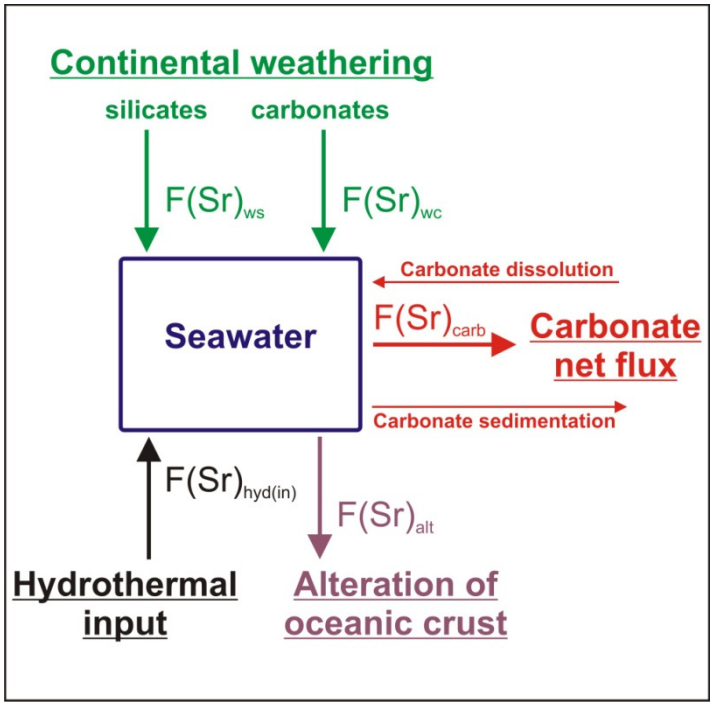

FIGURE V.3 – Model scheme for the marine Sr budget. Changes in seawater Sr concentrations and isotope compositions depend on changes in the fluxes of silicate and carbonate continental weathering ($F(Sr)_{ws}$ and $F(Sr)_{wc}$), hydrothermal input ($F(Sr)_{hyd(in)}$), alteration of the oceanic crust ($F(Sr)_{alt}$), and the carbonate-related net flux, consisting of carbonate dissolution and carbonate sedimentation fluxes ($F(Sr)_{carb}$).

To quantify our qualitative observation we extended the numerical box model from (Farkaš et al., 2007) and (Wallmann, 2004) considering coupled carbon/magnesium/calcium/strontium global budgets. In particular, we improved the strontium budget with added fluxes of hydrothermal alteration ($F(Sr)_{alt}$) and an additional isotope mass balance equation for the seawater $\delta^{88/86}Sr$ composition (see Fig. V.3 for model scheme and supplemental information for mass balance equations). Therefore, the Phanerozoic Sr budget can now completely be solved, without being dependent on $(Sr/Ca)_{sw}$ ratios. This provides a certain advantage because $(Sr/Ca)_{sw}$ ratios are associated with relatively large uncertainties (Steuber and Veizer, 2002; Wallmann, 2004) (Fig. V.5). However, as we don't have $\delta^{88/86}Sr_{sw}$ data for the last 125Myr, the model is still forced by $(Sr/Ca)_{sw}$ ratios as it is in the original model run (cf. figure V.5). The respective isotope

compositions of the Sr fluxes are presented in table V.2. With the three (isotope) mass balance equations for $[Sr]_{sw}$, $(^{87}Sr/^{86}Sr)_{sw}$, and $\delta^{88/86}Sr_{sw}$ and an independent determination for continental weathering rates ($F(Sr)_{ws}$, $F(Sr)_{wc}$; see basic model from (Wallmann, 2004) for details) it is possible to calculate changes in all Sr fluxes in and out of the ocean, including the carbonate-related net flux $F(Sr)_{carb}$.

TABLE V.2 – Definition and isotope composition of Sr fluxes considered in the numerical model

Strontium flux	*Abbrev.*	$\delta^{88/86}Sr$	$^{87}Sr/^{86}Sr$
Silicate continental weathering input flux	$F(Sr)_{ws}$	$\delta^{88/86}Sr_{ws}$ = 0.27‰$^{+}$	$^{87}Sr/^{86}Sr_{ws}$ = variable$^{\$}$
Carbonate continental weathering input flux	$F(Sr)_{wc}$	$\delta^{88/86}Sr_{carb}$ of last 200Ma	$^{87}Sr/^{86}Sr_{sw}$ of last 200Ma
Hydrothermal input flux	$F(Sr)_{hyd(in)}$	$\delta^{88/86}Sr_{hyd(in)}$ = 0.27‰*	$^{87}Sr/^{86}Sr_{hyd(in)}$ = 0.7025°
Alteration flux into the oceanic crust	$F(Sr)_{alt}$	$\Delta^{88/86}Sr_{alt}$ = -0.01‰$^{\#}$	$^{87}Sr/^{86}Sr_{alt} = {}^{87}Sr/^{86}Sr_{sw}$
Carbonate-related net flux	$F(Sr)_{carb}$	$\Delta^{88/86}Sr_{carb}$ = -0.24‰$^{\sim}$	$^{87}Sr/^{86}Sr_{carb} = {}^{87}Sr/^{86}Sr_{sw}$

$^{+}$Calculated from a 1:1 mixture of basalts (0.25‰ (MOYNIER et al., 2010)) and granites (0.295‰ (OHNO and HIRATA, 2007)) assuming no isotope fraction during weathering processes. $^{\$}$The isotopic composition of the silicate continental weathering flux through geological time depends on spreading rates at MOR and continental erosion rates which have a different effects on weathering of basaltic ($^{87}Sr/^{86}Sr$ = 0.705) and non-basaltic ($^{87}Sr/^{86}Sr$ = 0.712) rocks (see basic model from (Wallmann, 2004) for details). Data from *(KRABBENHÖFT et al., 2010), $^{\#}$(BÖHM et al., 2012), $^{\sim}$(VOLLSTAEDT et al., in review), and °(DAVIS et al., 2003).

In our model simulation we keep $\Delta^{88/86}Sr_{carb\text{-}sw}$ constant at -0.24‰, being in the range of modern carbonates (-0.12‰ to -0.37‰ (KRABBENHÖFT et al., 2010; EISENHAUER et al., 2011)). Therefore, $\delta^{88/86}Sr_{sw}$ is only dependent on changes of $F(Sr)_{carb}$. In a similar approach for the chemically similar Ca isotopes, Blättler et al. (2012) and Farkaš et al. (2007) suggested that $\delta^{44/40}Ca_{sw}$ is mainly dependent on $\Delta^{44/40}Ca_{carb\text{-}sw}$ in the Phanerozoic ocean. Therefore, we also applied a sensitivity study where we changed $\Delta^{88/86}Sr_{carb\text{-}sw}$ to explain changes in $\delta^{88/86}Sr_{sw}$. However, we observed that changes in $\delta^{88/86}Sr_{sw}$ may not solely be explained by changing fractionation factors between carbonates and seawater, as it considerably exceeds the modern $\Delta^{88/86}Sr_{carb\text{-}sw}$ range (See supplemental information).

Results for Sr fluxes and seawater Sr concentration

This study shows the first time-dependent Phanerozoic changes in $[Sr]_{sw}$ and Sr fluxes (Fig. V.4). $[Sr]_{sw}$ varies in between 24 and 300µmol/l with a mean of 151µmol/l. The highest concentrations are observed in Ordovician to Devonian and in the Cretaceous period. Lowest concentrations are modeled in the Permian and Triassic period.

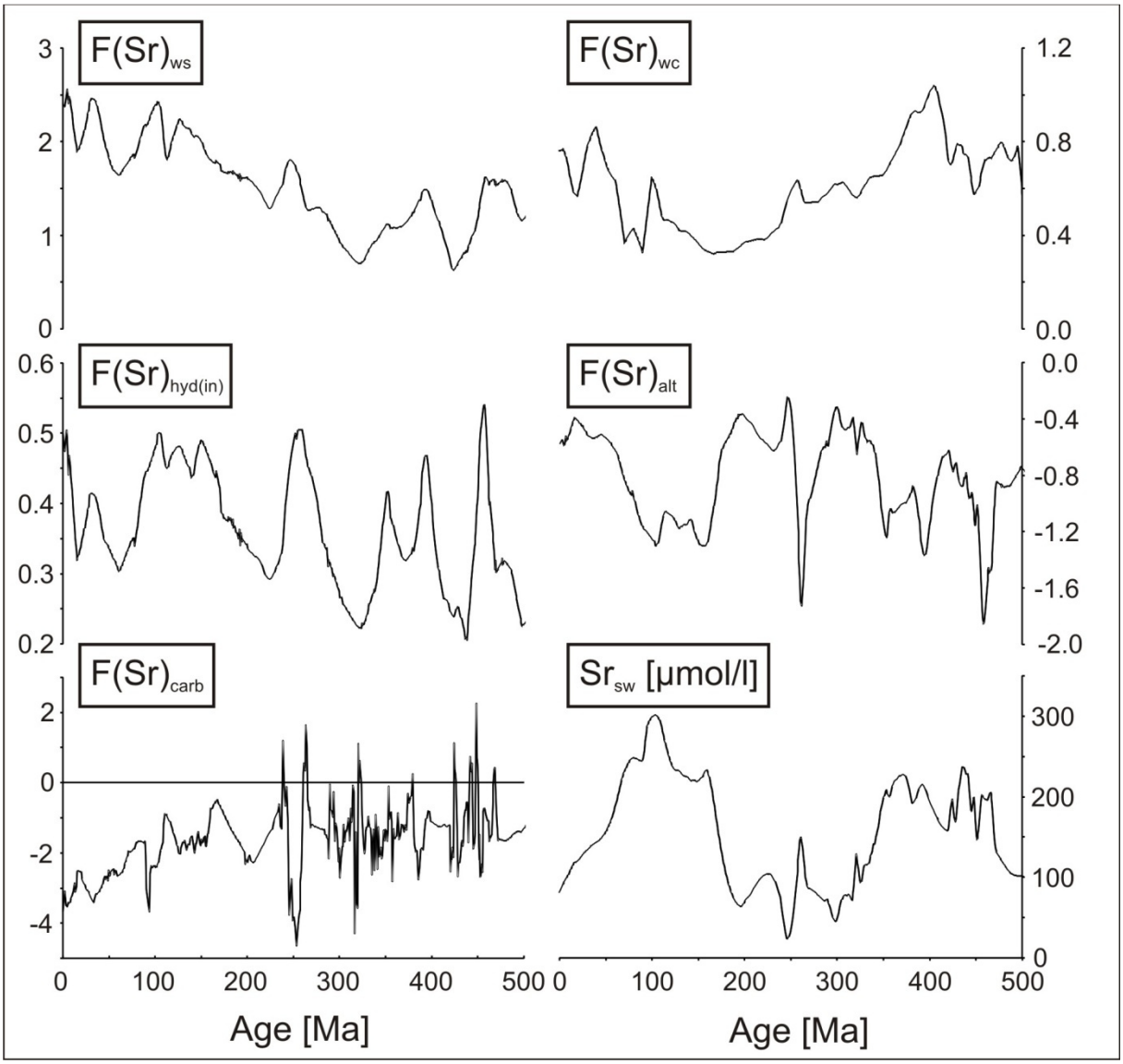

FIGURE V.4 – Modelled Sr fluxes (all in 10^{10}mol/yr) and seawater Sr concentration. Negative $F(Sr)_{carb}$ and $F(Sr)_{alt}$ correspond to a net output of Sr out of the ocean while positive $F(Sr)_{carb}$ and $F(Sr)_{alt}$ values correspond to a net input of Sr into the ocean.

Changes in the carbonate-related net Sr flux are highly frequent and of high amplitude, being in the range of -4.7x10^{10}mol/yr and 2.3x10^{10}mol/yr with a mean of -1.6x10^{10}mol/yr. The

largest variations in $F(Sr)_{carb}$ are observed at the Permian/Triassic boundary and are extensively discussed in (VOLLSTAEDT et al., in review). Besides $F(Sr)_{ws}$, $F(Sr)_{carb}$ is the most important flux in the Phanerozoic oceanic Sr budget. In general, we observe slightly lower $F(Sr)_{carb}$ in the Paleozoic ($1.3x10^{10}$mol/Myr) when compared to the Mesozoic Eon ($2.0x10^{10}$mol/Myr) presumably being a consequence of enhanced pelagic carbonate burial, starting in the early Mesozoic Eon. The modeled modern $F(Sr)_{carb}$, $F(Sr)_{ws}$, and $F(Sr)_{wc}$ are significantly lower when compared to other estimates for modern Sr fluxes ($17.4x10^{10}$mol/yr and ~$5x10^{10}$mol/yr for carbonate burial and combined silicate and carbonate continental weathering fluxes, respectively (PALMER and EDMOND, 1989; BASU et al., 2001; KRABBENHÖFT et al., 2010)). These Sr fluxes are in accordance to (VANCE et al., 2009) who predicted that modern observations for element fluxes to the ocean are broadly accurate but not representative for elements that have a longer residence time in the ocean than Quaternary glacial/interglacial cycles (see also (STOLL and SCHRAG, 1998)). In particular, Post-glacial weathering is supposed to occur ~ 10 times faster due to the demise of continental ice sheets leaving behind a fertile, finely grounded substrate (TAYLOR and BLUM, 1995; WHITE and BRANTLEY, 2003; PORDER et al., 2007; VANCE et al., 2009). Therefore, the modeled low rates of Sr weathering and burial rates (Fig. V.4) confirm that the modern Sr fluxes are exceptional high when compared to long-term estimates. In particular, we observe that not only Sr weathering fluxes, but also Sr carbonate burial fluxes are significantly increased in the modern ocean, when compared to average quaternary values. This implies that the modern marine carbonate system reacts nearly instantaneously to the increased input fluxes from the continents. These high frequent changes in Sr fluxes are not visible in the buffered Sr isotope record of seawater, which explains lower modeled Sr fluxes when compared to independent observations in the modern ocean.

Calcite and aragonite seas

With an independent estimate for $[Sr]_{sw}$, both the $(Sr/Ca)_{sw}$ ratio and also its ratio to the Sr and Ca carbonate-related output fluxes, here defined as $D(F)_{Sr}$, could be reconstructed.

$$D(F)_{Sr} = \frac{\left(F(Sr)_{carb} / F(Ca)_{carb}\right)}{(Sr/Ca)_{sw}} = \frac{(Sr/Ca)_{carb}}{(Sr/Ca)_{sw}}$$

This coefficient $D(F)_{Sr}$ is representative for to the Sr/Ca partion coefficient in marine carbonates D_{Sr}, which is ~0.1 for calcite and ~1.0 for aragonite. The $F(Ca)_{carb}$ fluxes are forced by carbonate saturation in the ocean within the model and discussed in the original paper of (Wallmann, 2004). Our results are in very good agreement with the $(Sr/Ca)_{sw}$ curve reconstructed from Phanerozoic carbonates (STEUBER and VEIZER, 2002) (Fig. V.5).

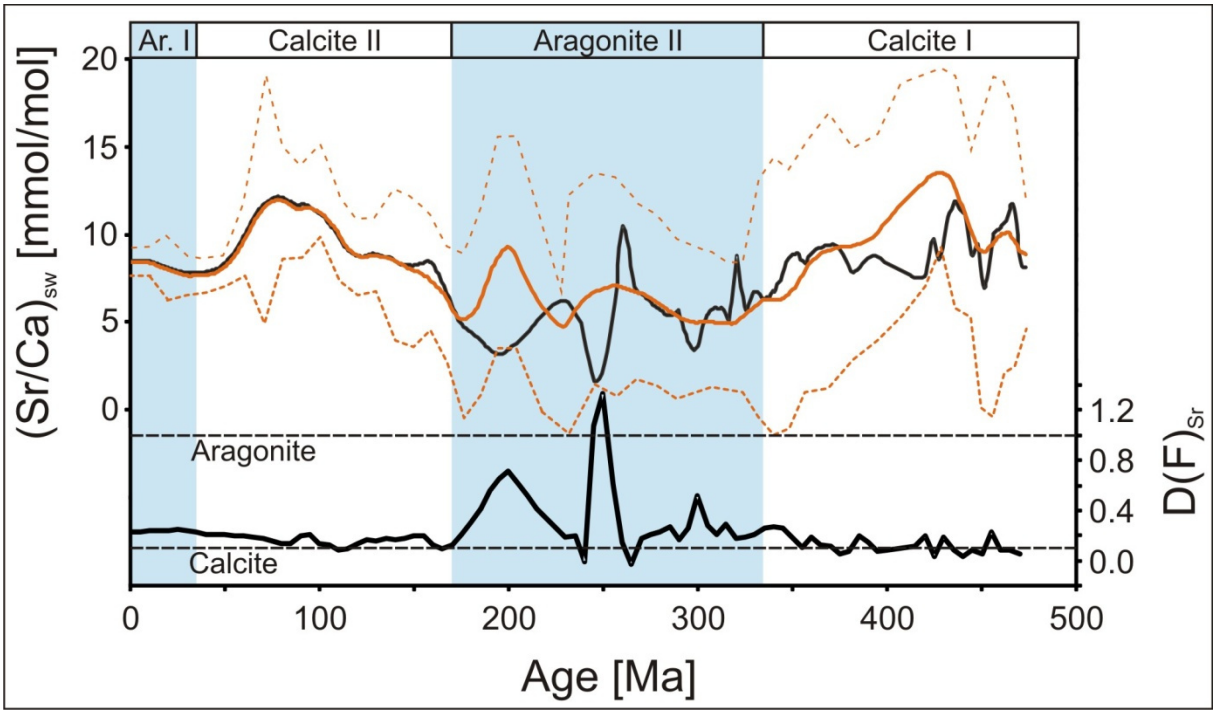

FIGURE 5 – Modelled $(Sr/Ca)_{sw}$ ratios and $D(F)_{Sr}$ during the Phanerozoic Eon are shown together with literature data. Upper part: Modeled $(Sr/Ca)_{sw}$ ratios (black line) show a general agreement with published $(Sr/Ca)_{sw}$ ratios (orange line with 2 s.d. (dashed orange line) (Steuber and Veizer, 2002)). Lower part: Modeled Sr partition coefficient D_{Sr} and endmember partition coefficients for aragonite ($D_{Sr} \approx 1$) and calcite ($D_{Sr} \approx 0.1$) (dashed horizontal lines).

Long-term modeled $[Sr]_{sw}$, $(Sr/Ca)_{sw}$, and $D(F)_{Sr}$ follow times of proposed "calcite seas" and "aragonite seas" (STANLEY and HARDIE, 1998) (Fig. V.4 and Fig. V.5). In particular, high

$(Sr/Ca)_{sw}$ low $D(F)_{Sr}$ are associated with "calcite seas" and low $(Sr/Ca)_{sw}$ and high $D(F)_{Sr}$ are associated with "aragonite seas" due to 3-5 times higher Sr concentrations in aragonite when compared to calcite (MILLIMAN et al., 1974). Our $D(F)_{Sr}$ is in between -0.08 and 1.23 with a mean of 0.21 and therefore roughly in the range between the calcium carbonate end members calcite ($D_{Sr} \approx 0.1$) and aragonite ($D_{Sr} \approx 1.0$). We observe a higher mean $D(F)_{Sr}$ of 0.52 during "Aragonite II" and a lower mean $D(F)_{Sr}$ of 0.13 during "Calcite I and II" (Fig. V.5). However, we observe that long-term changes in $D(F)_{Sr}$ underlie considerable short-term changes, especially during "Aragonite II". As our $F(Sr)_{carb}$ is a net carbonate flux it is smaller than a pure Sr carbonate burial flux. Therefore, the modeled $D(F)_{Sr}$ should be lower compared to the coeval precipitated carbonates. This might explain values below the calcite end member value of D_{Sr} ~0.1. Negative $D(F)_{Sr}$ are a consequence of negative $F(Sr)_{carb}$ values (Fig. V.4).

With this study and the first reconstruction of $F(Sr)_{carb}$ and $[Sr]_{sw}$, we observe that secular changes in the dominant non-skeletal carbonate mineralogy of precipitates (SANDBERG, 1983; STANLEY and HARDIE, 1998) have a large influence on $F(Sr)_{carb}$, $D(F)_{Sr}$, and $(Sr/Ca)_{sw}$. The dominant carbonate mineralogy is supposed to be controlled by $(Mg/Ca)_{sw}$. The causative mechanism for changing $(Mg/Ca)_{sw}$ ratios is, however, unclear. In particular, the role of seafloor spreading and dolomitization rates and associated changes in sea-level are still being debated (VEIZER and MACKENZIE, 2010). According to one scenario, low spreading rates during "aragonite seas" lead to high $(Mg/Ca)_{sw}$ ratios and low sea levels (HARDIE, 1996) (Fig. V.6). High seawater $[Mg]_{sw}$ inhibit the precipitation of inorganic calcite when compared to "calcite seas" (WILKINSON, 1979). This leads to low $(Sr/Ca)_{sw}$, and high D_{Sr} and $\delta^{88/86}Sr_{sw}$ during "aragonite seas" generated by a large Sr output flux of isotopically relatively light Sr. These causes and implications of $D(F)_{Sr}$ and $\delta^{88/86}Sr_{sw}$ trends are similar to the observations from the Ca isotopes (Farkaš et al., 2007). However, $\delta^{44/40}Ca$ amplitudes are smaller and

rather reflecting differences in Ca fractionation factors between calcite and aragonite (FARKAŠ et al., 2007; BLÄTTLER et al., 2012).

The effect of changing sea-levels and ocean anoxia on the marine carbonate budget

Carbonate burial and dissolution are closely linked to changes in seawater chemistry, e.g. by ocean anoxia and ocean acidification (KNOLL et al., 1996; WOODS et al., 1999; PAYNE et al., 2010; VOLLSTAEDT et al., in review). Further, massive weathering and recrystallization of continental carbonate shelves due to sea-level low stands contribute an additional flux of Sr to the ocean, thereby increasing $F(Sr)_{carb}$ (STOLL and SCHRAG, 1998; KRABBENHÖFT et al., 2010). Here, we test if changes in Phanerozoic $F(Sr)_{carb}$ are related to the occurrence of ocean anoxia and glacial intervals and associated sea-level changes (Fig. V.6).

The Phanerozoic $F(Sr)_{carb}$ values are generally negative, implying a net output flux of Sr by carbonate burial. However, this flux gets positive in six to eight time intervals during the Phanerozoic, implying that Sr carbonate dissolution fluxes exceeding Sr carbonate burial fluxes (Fig. V.6). This carbonate dissolution may be caused by either ocean acidification or weathering of carbonate shelves during sea-level low stands. In four of six cases these events occur during glacial intervals and therefore sea-level low stands. Therefore, it is likely that these positive $F(Sr)_{carb}$ excursions are mainly related to the weathering of carbonate shelves which considerably affects $F(Sr)_{carb}$, $[Sr]_{sw}$ and $\delta^{88/86}Sr_{sw}$. Further, atmospheric pCO_2 concentrations are considered to be lower during glacial periods which decrease the probability of an acidification-induced dissolution of carbonates. In two cases in the Early Triassic ~238Ma and the Late Silurian ~424Ma no glaciations are observed in the geological record. Hence, positive $F(Sr)_{carb}$ might be a result of ocean acidification leading to dissolution of marine carbonates.

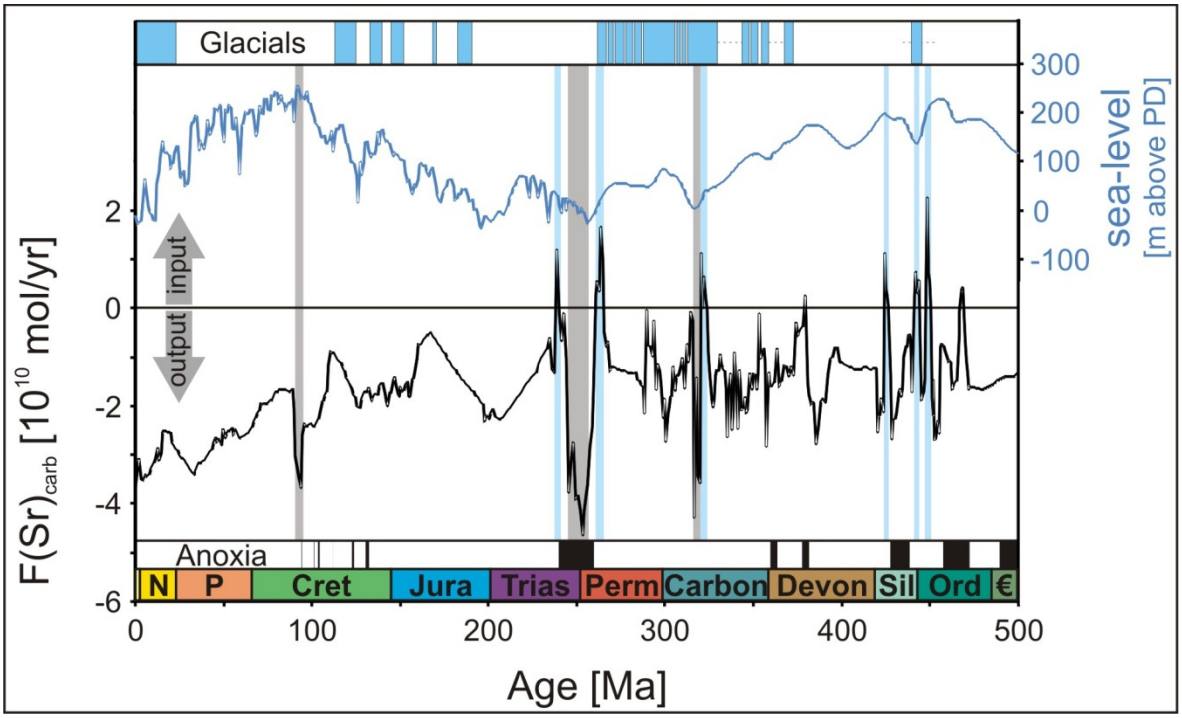

FIGURE V.6 – Modelled carbonate related Sr net flux ($F(Sr)_{carb}$, black line) is shown together with sea-level changes (blue line) and intervals of glaciations (blue boxes at the top with proposed intervals indicated by dashed lines) and ocean anoxia (black bars at the bottom). Times of a positive $F(Sr)_{carb}$ (marked in light blue) correlate in 4 of 6 cases with glacial intervals. Times of highly negative $F(Sr)_{carb}$ and therefore high carbonate burial (marked in grey) correlate in 2 of 3 cases with times of ocean anoxia. Sea-level and Paleozoic intervals of anoxia and glacials from (Haq et al., 1987; Haq and Schutter, 2008). Mesozoic glacial intervals from (Price, 1999). Mesozoic anoxic intervals from (Erba, 2004). Timing of the P/T anoxia from (Isozaki, 1997). Timescale and geological periods from GTS 2012 (Gradstein et al., 2012). Abbreviations for geological periods are the same as in figure caption V.1.

Further, we modeled three intervals of highly negative $F(Sr)_{carb}$ representing a massive burial of carbonates. The most prominent excursion in $F(Sr)_{carb}$ at the Permian/Triassic (P/T) boundary has been discussed in (VOLLSTAEDT et al., in review) and is related to long-term seawater anoxia and the build-up of alkalinity by bacterial sulfate reduction in deep waters of the stratified ocean. Temporal upwelling of these toxic and high alkaline water masses possibly caused massive carbonate burial on the seafloor and a biogeochemical crisis at the P/T boundary (VOLLSTAEDT et al., in review). In the present study, two additional time intervals of highly negative $F(Sr)_{carb}$ in the Carboniferous and Cretaceous period are observed. Concerning the Carboniferous period, there is no evidence for seawater anoxia at ~320Ma in the geological record. Therefore, highly negative $F(Sr)_{carb}$ are interpreted to be a

result of i) intense carbonate burial by biogenic and inorganic $CaCO_3$ precipitation or ii) ocean anoxia-related build up of alkalinity during the Carboniferous period which has yet not been detected in the geological record. Concerning the Cretaceous period, several ocean anoxic events (OAE) are recorded in marine sediments (Jenkyns, 2010). Therefore, we propose that modeled massive carbonate burial rates at the Cenomanian/Turonian boundary (~94Ma) are possibly linked to changes in seawater carbonate chemistry during OAE2 in analogue to the P/T period (KNOLL et al., 1996; VOLLSTAEDT et al., in review). In summary, we modeled several emerging maxima and minima in Phanerozoic $F(Sr)_{carb}$ values by which the majority could be related to time intervals of glaciations or ocean anoxia. Therefore, we propose that the marine carbonate budget is closely related to the occurrence of these phenomenons.

Changes in Sr residence time

We calculated for the first time Sr residence times (τ_{Sr}) that vary in between 1.2Myrs for the P/T ocean and 19.6Myrs for the Silurian Period with a mean of 9.2Myrs (modern value ~2.5Myrs (HODELL et al., 1990)) implying a nearly twenty-fold change in the sensitivity of the Sr isotope systems (Fig. V.7). Here, sensitivity is defined as the susceptibility to large rates of changes in seawater isotope ratios. Consequently, a high sensitivity of an isotope system is reached during low residence times. Not surprisingly, the largest rate of changes in both $(^{87}Sr/^{86}Sr)_{sw}$ and $\delta^{88/86}Sr_{sw}$ occur in times of a low Sr residence times at the P/T boundary. Further, high $d(^{88}Sr/^{86}Sr)_{sw}/dt$ are observed during Carboniferous and Late Ordovician period, while high $d(^{87}Sr/^{87}Sr)_{sw}/dt$ are observed during mid-Permian and mid-Ordovician. In general, high rate of changes are observed during low τ_{Sr}. Interestingly, high $d(^{88}Sr/^{86}Sr)_{sw}/dt$ do not always correlate with high $d(^{87}Sr/^{87}Sr)_{sw}/dt$ which underlines that the isotope systems are controlled by different parameters. Concerning absolute rate of changes, we observe that mean time-dependent changes in seawater $^{88}Sr/^{86}Sr$ ($0.000061Myr^{-1}$) are two times higher

contrast to $^{87}Sr/^{86}Sr$ (0.000027Myr^{-1}), implying a higher sensitivity of the stable isotope system. This is supposed to be mainly a consequence of $F(Sr)_{carb}$ which is the most important Sr flux (Fig. V.4) and only has an influence $\delta^{88/86}Sr_{sw}$. In contrast, $(^{87}Sr/^{86}Sr)_{sw}$ is controlled by the balance between continental weathering and hydrothermal activity.

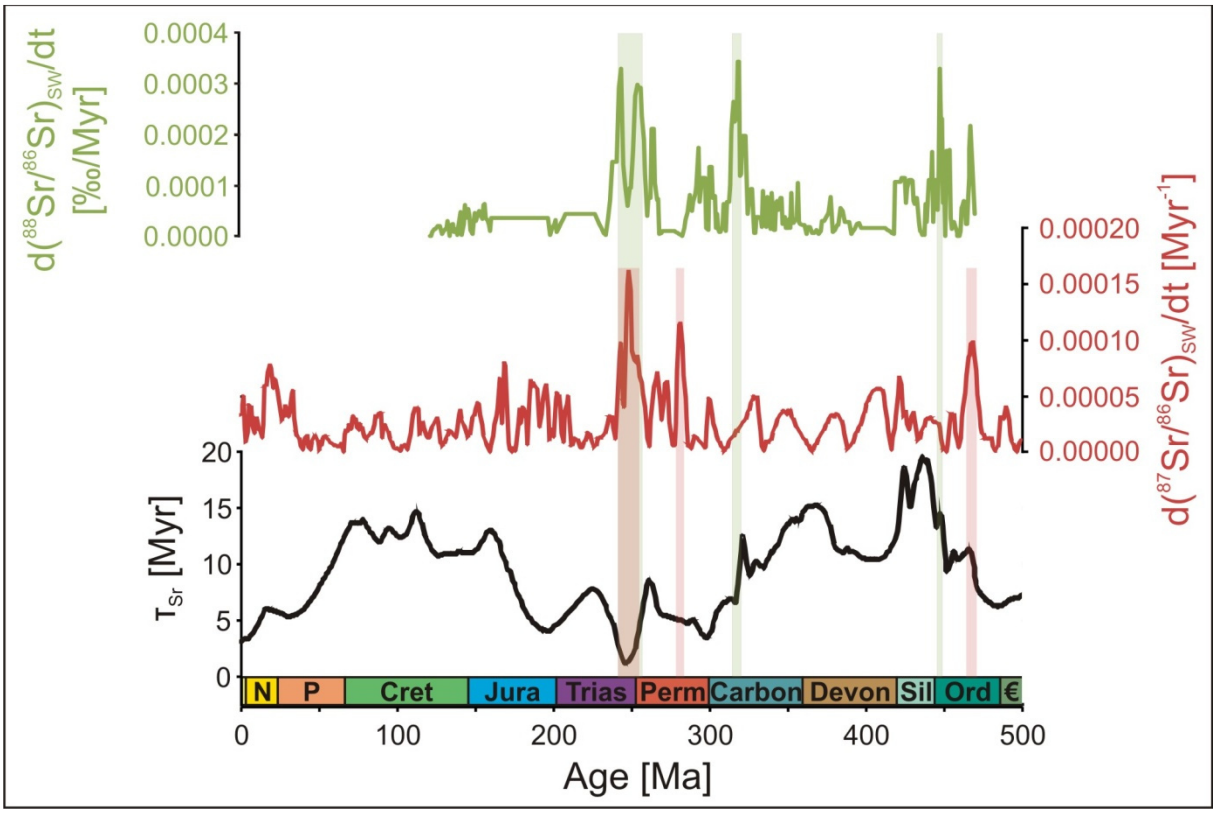

FIGURE V.7 – Modelled Sr residence time in the ocean (τ_{Sr}, black line) and rate of change in seawater $^{88}Sr/^{86}Sr$ (blue line) and $^{87}Sr/^{86}Sr$ (blue line, calculated from (McArthur et al., 2001). The highest rate of changes are indicated by light blue and red bars for $\delta^{88/86}Sr_{sw}$ and $(^{87}Sr/^{86}Sr)_{sw}$, respectively. The highest rate of changes in both isotope systems is observed during periods of relatively short marine Sr residence times. $\tau_{Sr} = M(Sr)_{sw} / F(Sr)_{input}$, where $M(Sr)_{sw}$ is moles of Sr in seawater and $F(Sr)_{input}$ is the sum of input fluxes in mol/Myr (this assumes steady state between Sr input and output fluxes). Timescale and geological periods from (Gradstein et al., 2012). Abbreviations for geological periods are the same as in figure caption V.1.

Further, the $\delta^{88/86}Sr_{sw}$ data distribution is considerably lower when compared to the high resolution $(^{87}Sr/^{86}Sr)_{sw}$ curve, which leads to lower calculated rates of change. Ultimately, our results reveal that ocean residence times have to be considered as variable through time which has consequences for the sensitivity of the element and isotope systems through time.

Implications for Strontium Isotope Stratigraphy

The $\delta^{88/86}Sr_{sw}$ values show distinct variations on Phanerozoic timescales (Fig. V.2) in the order of 0.4‰ and are therefore generally applicable for SIS. This requires a complete $\delta^{88/86}Sr_{sw}$ reference curve for the Phanerozoic as it is for the $^{87}Sr/^{86}Sr$ system. For this, the fractionation factors between the recording phase and seawater as well as possible environmental controlling factors on $\delta^{88/86}Sr_{CC}$ need to be known. This is a disadvantage compared to $^{87}Sr/^{86}Sr$ ratios because latter values are unaffected by isotope fraction processes and are therefore the same in every carbonate recording phase.

Assuming a known fractionation factor, independency of $\delta^{88/86}Sr_{CC}$ on temperature and species of the selected recording phase, it is possible to improve the precision of SIS. Especially during periods in geological history i) where the rate of change in $(^{87}Sr/^{86}Sr)_{sw}$ is low (e.g. Late Ordovician, Cretaceous, and Paleogene period; Fig. V.7) and an accurate age determination by SIS is impossible or ii) where $^{87}Sr/^{86}Sr$ values present several numerical ages due to the sinuosity of the $^{87}Sr/^{86}Sr$ calibration curve (McArthur, 1994) the precision of this stratigraphic dating method could be increased by combined $\delta^{88/86}Sr$-$^{87}Sr/^{86}Sr$ SIS. This additionally benefits from the overall higher sensitivity of $(^{88}Sr/^{86}Sr)_{sw}$ compared to $(^{87}Sr/^{86}Sr)_{sw}$ (Fig. V.7). Besides improving the precision of SIS, the combined application of stable and radiogenic Sr isotopes can help to detect samples that have undergone considerable alteration.

This combined use of $\delta^{88/86}Sr_{sw}$ and $(^{87}Sr/^{86}Sr)_{sw}$ is exemplified for the Late Permian period and illustrated in figure V.8. During this time interval both $\delta^{88/86}Sr_{sw}$ and $(^{87}Sr/^{86}Sr)_{sw}$ are increasing. Considering a theoretical marine carbonate sample with an age of ~254Ma yielding $\delta^{88/86}Sr_{sw}$ = 0.460‰ ± 0.023‰ and $^{87}Sr/^{86}Sr$ = 0.707208 ± 0.000025 (Fig. V.8). This would result in an age in between 253.17Ma and 254.61Ma for $\delta^{88/86}Sr_{sw}$ and in between 253.70Ma and 255.45Ma for $^{87}Sr/^{86}Sr$, respectively. Therefore the methods have an age uncertainty in

between 1.4Myrs and 1.8Myrs. The combined use of both result in an age between 253.70Ma and 254.61Ma, therefore decreasing the uncertainty in this example by nearly a factor of two to 0.9Myrs. However, we are aware that for the combined SIS a detailed $\delta^{88/86}Sr_{sw}$ reference curve needs to be constructed.

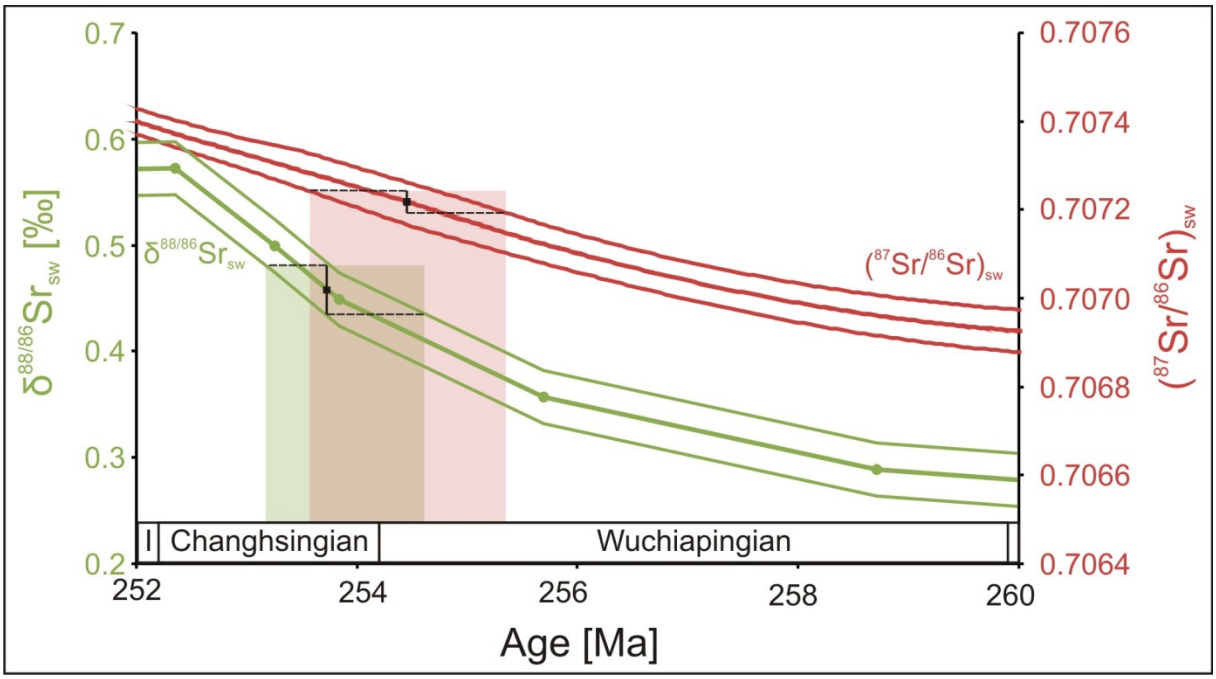

FIGURE V.8 – Example of SIS with combined $\delta^{88/86}Sr_{sw}$ and $(^{87}Sr/^{86}Sr)_{sw}$ values for the Late Permian period. Red curve represents published seawater $^{87}Sr/^{86}Sr$ curve from (McArthur et al., 2001) with upper and lower limits. Blue curve represents $\delta^{88/86}Sr_{sw}$ curve from this study with an assumed uncertainty of ±0.025‰ (blue points represent our $\delta^{88/86}Sr_{sw}$ data points). We take a marine carbonate sample with arbitrary $\delta^{88/86}Sr$ and $^{87}Sr/^{86}Sr$ values and typical uncertainties of 0.460±0.023‰ and 0.707208±0.000025 for $\delta^{88/86}Sr_{sw}$ and $^{87}Sr/^{86}Sr$, respectively (black squares with 2 s.d. error indicated by black vertical lines). These values refer to an age in between 253.17 Ma and 254.61Ma for $\delta^{88/86}Sr$ (light blue rectangle) and in between 253.70Ma and 255.45Ma for $^{87}Sr/^{86}Sr$ (light red rectangle). Combining both age determination (overlap of both rectangles) ends up in an age in between 253.70Ma and 254.61Ma, thereby decreasing the age uncertainty from ~1.5Myrs to ~0.9Myrs. Timescale and geological stages from (Gradstein et al., 2012).

V.5. Conclusions

This study investigates in changes of $\delta^{88/86}Sr$ of Phanerozoic seawater reconstructed from marine carbonates. With an expanded dataset we complement the published $\delta^{88/86}Sr_{sw}$ record (VOLLSTAEDT et al., in review). While brachiopods and belemnites are a reliable archive to

reconstruct changes in $\delta^{88/86}Sr_{sw}$, carbonate matrix samples are found to be considerably affected by diagenetic processes und restricting the use as a carbonate recording phase for $\delta^{88/86}Sr_{sw}$. Major fluctuations in seawater $\delta^{88/86}Sr$ suggest severe changes in the carbonate-related net Sr flux, mainly represented by marine carbonates. The combined modeling of seawater $^{87}Sr/^{86}Sr$, $\delta^{88/86}Sr$, and $[Sr]_{sw}$ allows for the first time to completely constrain the Sr budget of the ocean, including the carbonate-related Sr flux and alteration rates of the oceanic crust. $[Sr]_{sw}$ and $F(Sr)_{carb}$ vary in the range between 25mmol/l and 300mmol/l and -5x10^{10}mol/yr and +1x10^{10}mol/yr, respectively, indicating major changes in the carbonate-related flux of Sr. On short-term timescales, these changes are related to carbonate sedimentation, carbonate shelf recrystallization/weathering, carbonate dissolution and ocean anoxia within the Phanerozoic ocean. On long-term timescales, modeled $\delta^{88/86}Sr_{sw}$, $(Sr/Ca)_{sw}$ and $D(F)_{Sr}$ are in good agreement with literature data and are correlated with times of proposed "aragonite seas" and "calcite seas" hence coupled to $(Mg/Ca)_{sw}$ (Stanley and Hardie, 1998; Steuber and Veizer, 2002). This underlines the importance of the carbonate-related Sr flux of the ocean as the main controlling factor on $\delta^{88/86}Sr_{sw}$ which is in contrast to the $^{87}Sr/^{86}Sr$ system that is controlled by the balance between continental weathering and hydrothermal activity (Spooner, 1976). Further, we modelled considerable changes in Sr residence time being in between 1.2Myrs and 19.6Myrs, which significantly affects the sensitivity of the two Sr isotope systems. In accordance with modeled τSr we observe highest rate of change in $\delta^{88/86}Sr_{sw}$ and $(^{87}Sr/^{86}Sr)_{sw}$ during times of low τSr.

With the new Phanerozoic $\delta^{88/86}Sr_{sw}$ record we produce a second isotope reference curve for the Sr isotope system which has the potential to significantly improve the precision of the SIS by applying combined $\delta^{88/86}Sr$-$^{87}Sr/^{86}Sr$ isotope stratigraphy. In particular, the higher mean $d((^{88/86}Sr)_{sw})/dt$ and the different controlling mechanisms of $\delta^{88/86}Sr_{sw}$ and $(^{87}Sr/^{86}Sr)_{sw}$ have the potential to significantly improve SIS precision and to enhance the time range of the SIS application.

V.6. Acknowledgements

Financial support: DFG, Ei272/29-1 (QUASAR). We thank A. Kolevica, F. Hauff for technical support.

V.7. Supplementary information

Numerical model

Mass balance equations

For numerical equations we followed the approaches from (Lemarchand et al., 2000) and (VOLLSTAEDT et al., in review).

Sr mass balance equation for the ocean:

$$\frac{d[Sr]_{sw}}{dt} = F(Sr)_{ws} + F(Sr)_{wc} + F(Sr)_{hyd} - F(Sr)_{alt} - F(Sr)_{carb} \quad [V.1]$$

Radiogenic Sr isotope mass balance equation for the ocean:

$$\frac{d\left({}^{87}Sr/{}^{86}Sr\right)_{sw}}{dt} = \frac{F(Sr)_{ws}}{[Sr]_{sw}} * \left(\frac{1+\left({}^{87}Sr/{}^{86}Sr\right)_{sw}}{1+\left({}^{87}Sr/{}^{86}Sr\right)_{ws}}\right) * \left(\left({}^{87}Sr/{}^{86}Sr\right)_{ws} - \left({}^{87}Sr/{}^{86}Sr\right)_{sw}\right)$$

$$+ \frac{F(Sr)_{wc}}{[Sr]_{sw}} * \left(\frac{1+\left({}^{87}Sr/{}^{86}Sr\right)_{sw}}{1+\left({}^{87}Sr/{}^{86}Sr\right)_{wc}}\right) * \left(\left({}^{87}Sr/{}^{86}Sr\right)_{wc} - \left({}^{87}Sr/{}^{86}Sr\right)_{sw}\right) \quad [V.2]$$

$$+ \frac{F(Sr)_{hyd}}{[Sr]_{sw}} * \left(\frac{1+\left({}^{87}Sr/{}^{86}Sr\right)_{sw}}{1+\left({}^{87}Sr/{}^{86}Sr\right)_{hyd}}\right) * \left(\left({}^{87}Sr/{}^{86}Sr\right)_{hyd} - \left({}^{87}Sr/{}^{86}Sr\right)_{sw}\right)$$

Stable Sr isotope mass balance equation for the ocean:

$$\frac{d\left({}^{88}Sr/{}^{86}Sr\right)_{sw}}{dt} = \frac{F(Sr)_{ws}}{[Sr]_{sw}} * \left(\frac{1+\left({}^{88}Sr/{}^{86}Sr\right)_{sw}}{1+\left({}^{88}Sr/{}^{86}Sr\right)_{ws}}\right) * \left(\left({}^{88}Sr/{}^{86}Sr\right)_{ws} - \left({}^{88}Sr/{}^{86}Sr\right)_{sw}\right)$$

[V.3]

$$+ \frac{F(Sr)_{wc}}{[Sr]_{sw}} * \left(\frac{1+\left({}^{88}Sr/{}^{86}Sr\right)_{sw}}{1+\left({}^{88}Sr/{}^{86}Sr\right)_{wc}}\right) * \left(\left({}^{88}Sr/{}^{86}Sr\right)_{wc} - \left({}^{88}Sr/{}^{86}Sr\right)_{sw}\right)$$

$$+\frac{F(Sr)_{hyd}}{[Sr]_{sw}} * \left(\frac{1+\left({}^{88}Sr/{}^{86}Sr\right)_{sw}}{1+\left({}^{88}Sr/{}^{86}Sr\right)_{hyd}} \right) * \left(\left({}^{88}Sr/{}^{86}Sr\right)_{hyd} - \left({}^{88}Sr/{}^{86}Sr\right)_{sw} \right)$$

$$-\frac{F(Sr)_{alt}}{[Sr]_{sw}} * \left(\frac{1+\left({}^{88}Sr/{}^{86}Sr\right)_{sw}}{1+\left({}^{88}Sr/{}^{86}Sr\right)_{alt}} \right) * \left(\left({}^{88}Sr/{}^{86}Sr\right)_{alt} - \left({}^{88}Sr/{}^{86}Sr\right)_{sw} \right)$$

$$-\frac{F(Sr)_{carb}}{[Sr]_{sw}} * \left(\frac{1+\left({}^{88}Sr/{}^{86}Sr\right)_{sw}}{1+\left({}^{88}Sr/{}^{86}Sr\right)_{carb}} \right) * \left(\left({}^{88}Sr/{}^{86}Sr\right)_{carb} - \left({}^{88}Sr/{}^{86}Sr\right)_{sw} \right)$$

Sr carbonate and silicate continental weathering rates ($F(Sr)_{wc}$ and $F(Sr)_{ws}$) are reconstructed from a set of parameters including pCO_2, runoff, land area, and exposed rocks (Wallmann, 2004) (Table V.S1 and V.S2). Sr incorporation during the alteration of the oceanic crust ($F(Sr)_{alt}$) is taken to be proportional to the product of spreading rates and seawater Sr concentration (Table V.S1). Isotopic signatures for all Sr fluxes could be found in Table V.3. Therefore, the remaining unknowns $[Sr]_{sw}$, $F(Sr)_{carb}$, and $F(Sr)_{hyd(in)}$ could be calculated from the mass balance equations V.1 – V.3.

Sensitivity study

In order to determine the model output sensitivity related to the uncertainty in our input parameters we performed sensitivity analysis. In the standard model run, changes in $\delta^{88/86}Sr_{sw}$ are a function of varying Sr fluxes. Especially changes in the carbonate-related net flux of Sr ($F(Sr)_{carb}$) have a large influence on $\delta^{88/86}Sr_{sw}$ due to a large fractionation factor between carbonates and seawater ($\Delta^{88/86}Sr_{carb\text{-}sw}$ = -0.24‰). In a third approach of the sensitivity analysis we tested if the measured $\delta^{88/86}Sr_{sw}$ might be explained by variations in $\Delta^{88/86}Sr_{carb\text{-}sw}$. Therefore, we set $F(Sr)_{carb}$ to 1.33×10^{10} mol/yr which is the mean value for the time interval where we have $\delta^{88/86}Sr_{sw}$ data. Then, $\Delta^{88/86}Sr_{carb\text{-}sw}$ is modelled to account for variations in $\delta^{88/86}Sr_{sw}$.

Our modelling results indicate that $\Delta^{88/86}Sr_{carb\text{-}sw}$ values as high as +0.6‰ and as low as -1.3‰ are requested to account for the observed variations in $\delta^{88/86}Sr_{sw}$, $(Sr/Ca)_{sw}$, and Ca_{sw} concentrations (Fig. V.S1) exceeding the modern $\Delta^{88/86}Sr_{cc\text{-}sw}$ range, which is in between -0.12‰ and -0.37‰ (KRABBENHÖFT et al., 2010; EISENHAUER et al., 2011). The observed variations in $\delta^{88/86}Sr_{sw}$ can therefore not solely explained by shifts in the fractionation factor of carbonates. Especially positive fractionation factors are neither explained by theoretical considerations of kinetic isotope fractionation nor observed in modern carbonates.

Supplementary figures and tables

Supplementary figures

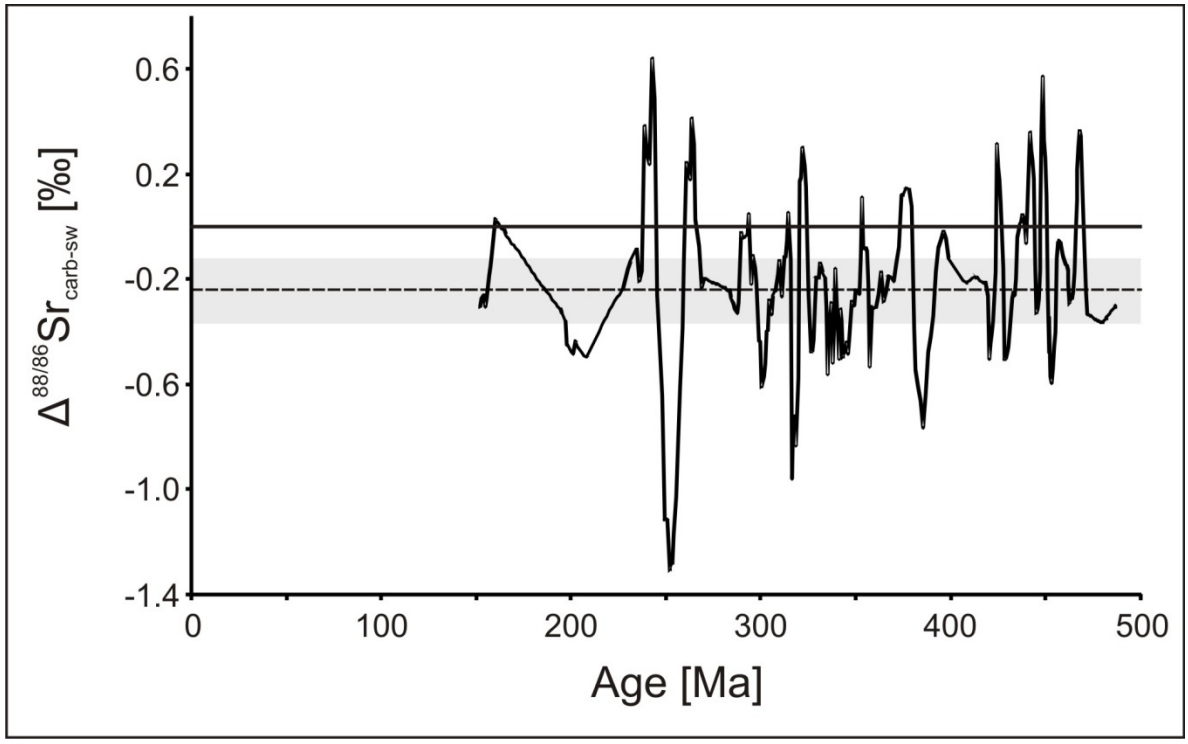

FIGURE V.S1 - This figure shows the calculated fractionation factor $\Delta^{88/86}Sr_{carb-sw}$ in a sensitivity analysis scenario. In contrast to the standard run, where $\Delta^{88/86}Sr_{carb-sw}$ is assumed to be constant at -0.24‰, it is here calculated $\Delta^{88/86}Sr_{carb-sw}$ to account for changes in $\delta^{88/86}Sr_{sw}$ while $F(Sr)_{carb}$ is set to $1.33x10^{10}$mol/yr . Modelled variations in $\Delta^{88/86}Sr_{carb-sw}$ exceed the modern range of $\Delta^{88/86}Sr_{carb-sw}$ (KRABBENHÖFT et al., 2010; EISENHAUER et al., 2011), which is represented by the grey shaded area. Therefore, changes in $\delta^{88/86}Sr_{sw}$ cannot be exclusively explained by changes in $\Delta^{88/86}Sr_{carb-sw}$.

Supplementary tables

TABLE V.S1 – Definition of Sr fluxes which are considered in the numerical box model

Hydrothermal Sr release from basalts (Wallmann, 2004)	$F(Sr)_{hyd(in)} = FQ(Sr)_{hyd(in)} * f_{SP}$
Sr release via carbonate continental weathering (Wallmann, 2004)	$F(Sr)_{wc} = f_E * f_{ER}^{eWC} * f_{LA} * f_D * f_{BCO2} * f_{BBT} * kWC * CC * (Sr/Ca)_{wc}$
Sr release via silicate continental weathering (Wallmann, 2004)	$F(Sr)_{ws} = f_E * (f_A * f_D)^{0.65} * f_{BCO2} * f_{BT} * \left(f_{ER}^{eWS} * FQsiSr + f_{ER}^{eWB} * f_{SP} * FQbaSr\right)$
Sr uptake during $CaCO_3$ formation into the altered oceanic crust	$F(Sr)_{alt} = FQ(Sr)_{alt} * f_{SP} * (1000/CO) * (Sr/Ca)_{sw} * D_{Sr(alt)}$

TABLE V.S2 – Definition of parameters and fluxes which are considered in table V.S1. Detailed information about parameters can be found in the basic model of Wallmann et al. (2004).

f_{SP}	Change in volcanic activity through time
f_{ER}	Change in physical erosion through time
f_{E}	Change in weathering intensity due to the spreading of land plants and angiosperms
f_{LA}	Change in land area covered by carbonates through time
f_{D}	Change in runoff due to changes in paleogeography
f_{BCO2}	CO_2 dependence of silicate and carbonate weathering
f_{BBT}	Temperature dependence of carbonate weathering
f_{BT}	Temperature dependence of silicate weathering
f_{A}	Change in total ice-free land area through time
$kWC = 13x0.5^{eWC/4000}$	Kinetic constant for carbonate weathering (Myr^{-1})
eWC = 0.3	Effect of erosion on carbonate weathering
eWS = 0.5	Effect of erosion on silicate weathering
eWB = 0.0	Effect of erosion on basalt weathering
$FQ(Sr)_{hyd(in)}$	Quaternary Sr release via hydrothermal circulation (10^{15} mol Myr^{-1})
$FQ(Sr)_{ws}^{VO}$ = 2.5 x	Quaternary Sr release via weathering of basaltic rocks (10^{15} mol Myr^{-1})
$FQ(Sr)_{ws}^{S}$	Quaternary Sr release via weathering of other silicate rocks (10^{15} mol Myr^{-1})
CC	Carbonates on the continental crust
CO	Carbonates on the oceanic crust
$(Sr/Ca)_{sw}$	Sr/Ca ratio of seawater

V.8. References

Allègre, C. J., Louvat, P., Gaillardet, J., Meynadier, L., Rad, S., and Capmas, F., 2010. The fundamental role of island arc weathering in the oceanic Sr isotope budget. *Earth Planet. Sci. Lett.* **292**, 51-56.

Artemov, Y. M., Strizhov, V. P., Ustinov, V. I., and Yaroshevskiy, A. A., 1967. Possible isotope fractionation during dolomitization (in russian). *Geokhimiya* **5**, 519-529.

Azmy, K., Veizer, J., Bassett, M. G., and Copper, P., 1998. Oxygen and carbon isotopic composition of Silurian brachiopods: Implications for coeval seawater and glaciations. *Geol. Soc. Am. Bull.* **110**, 1499-1512.

Basu, A. R., Jacobsen, S. B., Poreda, R. J., Dowling, C. B., and Aggarwal, P. K., 2001. Large Groundwater Strontium Flux to the Oceans from the Bengal Basin and the Marine Strontium Isotope Record. *Science* **293**, 1470-1473.

Blättler, C. L., Henderson, G. M., and Jenkyns, H. C., 2012. Explaining the Phanerozoic Ca isotope history of seawater. *Geology* **40**, 843-846.

Blum, J. D. and Erel, Y., 1997. Rb-Sr isotope systematics of a granitic soil chronosequence: The importance of biotite weathering. *Geochim. Cosmochim. Acta* **61**, 3193-3204.

Böhm, F., Eisenhauer, A., Tang, J., Dietzel, M., Krabbenhöft, A., Kisakürek, B., and Horn, C., 2012. Strontium isotope fractionation of planktic foraminifera and inorganic calcite. *Geochim. Cosmochim. Acta*.

Bruckschen, P., Oesmann, S., and Veizer, J., 1999. Isotope stratigraphy of the European Carboniferous: proxy signals for ocean chemistry, climate and tectonics. *Chem. Geol.* **161**, 127-163.

Butterfield, D. A., Nelson, B. K., Wheat, C. G., Mottl, M. J., and Roe, K. K., 2001. Evidence for basaltic Sr in midocean ridge-flank hydrothermal systems and implications for the global oceanic Sr isotope balance. *Geochim. Cosmochim. Acta* **65**, 4141-4153.

Davis, A. C., Bickle, M. J., and Teagle, D. A. H., 2003. Imbalance in the oceanic strontium budget. *Earth Planet. Sci. Lett.* **211**, 173-187.

Derry, L. A., 2009. Geochemistry: A glacial hangover. *Nature* **458**, 417-418.

Diener, A., Ebneth, S., Veizer, J., and Buhl, D., 1996. Strontium isotope stratigraphy of the Middle Devonian: Brachiopods and conodonts. *Geochim. Cosmochim. Acta* **60**, 639-652.

Eisenhauer, A., Böhm, F., Vollstaedt, H., Krabbenhöft, A., Liebetrau, V., Fietzke, J., Kisakürek, B., and Erez, J., 2011. Strontium isotope fractionation and its application in earth system sciences*Goldschmidt 2011*, Prague, Czech Republic, 19 August 2011.

Erba, E., 2004. Calcareous nannofossils and Mesozoic oceanic anoxic events. *Marine Micropaleontology* **52**, 85-106.

Farkaš, J., Böhm, F., Wallmann, K., Blenkinsop, J., Eisenhauer, A., van Geldern, R., Munnecke, A., Voigt, S., and Veizer, J., 2007. Calcium isotope record of Phanerozoic oceans: Implications for chemical evolution of seawater and its causative mechanisms. *Geochim. Cosmochim. Acta* **71**, 5117-5134.

Faure, G. and Mensing, T. M., 2005. *Isotopes - Principles and applications*. John Wiley & Sons Inc., Hoboken, New Jersey.

Fietzke, J. and Eisenhauer, A., 2006. Determination of temperature-dependent stable strontium isotope ($^{88}Sr/^{86}Sr$) fractionation via bracketing standard MC-ICP-MS. *Geochem. Geophys. Geosyst.* **7**.

Gradstein, F. M., Ogg, J. G., Schmitz, M., and Ogg, G., 2012. *The Geologic Time Scale 2012*. Elsevier.

Haq, B. U., Hardenbol, J., and Vail, P. R., 1987. Chronology of Fluctuating Sea Levels Since the Triassic. *Science* **235**, 1156-1167.

Haq, B. U. and Schutter, S. R., 2008. A chronology of Paleozoic sea-level changes. *Science* **322**, 64-68.

Hardie, L. A., 1996. Secular variation in seawater chemistry: An explanation for the coupled secular variation in the mineralogies of marine limestones and potash evaporites over the past 600 m.y. *Geology* **24**, 279-283.

Heuser, A., Eisenhauer, A., Bohm, F., Wallmann, K., Gussone, N., Pearson, P. N., Nagler, T. F., and Dullo, W. C., 2005. Calcium isotope ($\delta^{44/40}$Ca) variations of Neogene planktonic foraminifera. *Paleoceanography* **20**, 13.

Hippler, D., Schmitt, A.-D., Gussone, N., Heuser, A., Stille, P., Eisenhauer, A., and Nägler, T. F., 2003. Calcium Isotopic Composition of Various Reference Materials and Seawater. *Geostandards Newsletter* **27**, 13-19.

Hodell, D. A., Mead, G. A., and Mueller, P. A., 1990. Variation in the strontium isotopic composition of seawater (8 Ma to present) : Implications for chemical weathering rates and dissolved fluxes to the oceans. *Chemical Geology: Isotope Geoscience section* **80**, 291-307.

Hodell, D. A., Mueller, P. A., McKenzie, J. A., and Mead, G. A., 1989. Strontium isotope stratigraphy and geochemistry of the late Neogene ocean. *Earth Planet. Sci. Lett.* **92**, 165-178.

Holmden, C., 2009. Ca isotope study of Ordovician dolomite, limestone, and anhydrite in the Williston Basin: Implications for subsurface dolomitization and local Ca cycling. *Chem. Geol.* **268**, 180-188.

Horita, J., Zimmermann, H., and Holland, H. D., 2002. Chemical evolution of seawater during the Phanerozoic: Implications from the record of marine evaporites. *Geochim. Cosmochim. Acta* **66**, 3733-3756.

Isozaki, Y., 1997. Permo-Triassic boundary superanoxia and stratified superocean: Records from lost deep sea. *Science* **276**, 235-238.

Jenkyns, H. C., 2010. Geochemistry of oceanic anoxic events. *Geochem. Geophys. Geosyst.* **11**, Q03004.

Jones, C. E., Jenkyns, H. C., Coe, A. L., and Stephen, H. P., 1994a. Strontium isotopic variations in Jurassic and Cretaceous seawater. *Geochim. Cosmochim. Acta* **58**, 3061-3074.

Jones, C. E., Jenkyns, H. C., and Hesselbo, S. P., 1994b. Strontium isotopes in Early Jurassic seawater. *Geochim. Cosmochim. Acta* **58**, 1285-1301.

Knoll, A. H., Bambach, R. K., Canfield, D. E., and Grotzinger, J. P., 1996. Comparative earth history and Late Permian mass extinction. *Science* **273**, 452-457.

Krabbenhöft, A., Eisenhauer, A., Böhm, F., Vollstaedt, H., Fietzke, J., Liebetrau, V., Augustin, N., Peucker-Ehrenbrink, B., Hansen, B. T., Nolte, N., and Wallmann, K., 2010. Constraining the marine strontium budget with natural strontium isotope fractionations (^{87}Sr/^{86}Sr*-$\delta^{88/86}$Sr) of carbonates, hydrothermal solutions and river waters. *Geochim. Cosmochim. Acta* **74**, 4097-4109.

Krabbenhöft, A., Fietzke, J., Eisenhauer, A., Liebetrau, V., Böhm, F., and Vollstaedt, H., 2009. Determination of radiogenic and stable strontium isotope ratios (^{87}Sr/^{86}Sr; $\delta^{88/86}$Sr) by thermal ionization mass spectrometry applying an ^{87}Sr/^{84}Sr double spike. *J. Anal. At. Spectrom.* **24**, 1267-1271.

Lemarchand, D., Gaillardet, J., Lewin, E., and Allègre, C. J., 2000. The influence of rivers on marine boron isotopes and implications for reconstructing past ocean pH. *Nature* **408**, 951-954.

Lepzelter, C. G., Anderson, T. F., and Sandberg, P. A., 1983. Stable isotope variations in modern articulate brachiopods. *AAPG Bull.-Am. Assoc. Petr. Geol.* **67**, 500-501.

Lowenstein, T. K., Timofeeff, M. N., Kovalevych, V. M., and Horita, J., 2005. The major-ion composition of Permian seawater. *Geochim. Cosmochim. Acta* **69**, 1701-1719.

McArthur, J. M., 1994. Recent Trends in Strontium Isotope Stratigraphy. *Terr. Nova* **6**, 331-358.

McArthur, J. M., Howarth, R. J., and Bailey, T. R., 2001. Strontium Isotope Stratigraphy: LOWESS version 3: Best fit to the marine Sr-isotope curve for 0-509 Ma and accompanying look-up table for deriving numerical age. *The Journal of Geology* **109**, 155-170.

Milliman, J. D., Müller, G., and Förstner, U., 1974. *Recent sedimentary carbonates* Springer Verlag, New York, Heidelberg, Berlin.

Morrison, J. O. and Brand, U., 1988. An evaluation of diagenesis and chemostratigraphy of upper cretaceous molluscs from the Canadian Interior Seaway. *Chemical Geology: Isotope Geoscience section* **72**, 235-248.

Moynier, F., Agranier, A., Hezel, D. C., and Bouvier, A., 2010. Sr stable isotope composition of Earth, the Moon, Mars, Vesta and meteorites. *Earth Planet. Sci. Lett.* **300**, 359-366.

Ohno, T. and Hirata, T., 2007. Simultaneous determination of mass-dependent isotopic fractionation and radiogenic isotope variation of strontium in geochemical samples by Multiple Collector-ICP-Mass Spectrometry. *Anal. Sci.* **23**, 1275-1280.

Palmer, M. R. and Edmond, J. M., 1989. The strontium isotope budget of the modern ocean. *Earth Planet. Sci. Lett.* **92**, 11-26.

Payne, J. L., Turchyn, A. V., Paytan, A., DePaolo, D. J., Lehrmann, D. J., Yu, M., and Wei, J., 2010. Calcium isotope constraints on the end-Permian mass extinction. *Proceedings of the National Academy of Sciences* **107**, 8543-8548.

Popp, B. N., Anderson, T. F., and Sandberg, P. A., 1986. Brachiopods as indicators of original isotopic compositions in some Paleozoic limestones. *Geol. Soc. Am. Bull.* **97**, 1262-1269.

Porder, S., Hilley, G. E., and Chadwick, O. A., 2007. Chemical weathering, mass loss, and dust inputs across a climate by time matrix in the Hawaiian Islands. *Earth Planet. Sci. Lett.* **258**, 414-427.

Price, G. D., 1999. The evidence and implications of polar ice during the Mesozoic. *Earth-Science Reviews* **48**, 183-210.

Richter, F. M., Rowley, D. B., and DePaolo, D. J., 1992. Sr isotope evolution of seawater: the role of tectonics. *Earth Planet. Sci. Lett.* **109**, 11-23.

Sandberg, P. A., 1983. An oscillating trend in Phanerozoic non-skeletal carbonate mineralogy. *Nature* **305**, 19-22.

Smalley, P. C., Higgins, A. C., Howarth, R. J., Nicholson, H., Jones, C. E., Swinburne, N. H. M., and Bessa, J., 1994. Seawater Sr Isotope Variations through Time - a Procedure for Constructing a Reference Curve to Date and Correlate Marine Sedimentary-Rocks. *Geology* **22**, 431-434.

Souza, G. F. d., Reynolds, B. C., Kiczka, M., and Bourdon, B., 2010. Evidence for mass-dependent isotopic fractionation of strontium in a glaciated granitic watershed. *Geochim. Cosmochim. Acta* **74**, 2596-2614.

Spooner, E. T. C., 1976. The strontium isotopic composition of seawater, and seawater-oceanic crust interaction. *Earth Planet. Sci. Lett.* **31**, 167-174.

Stanley, S. M. and Hardie, L. A., 1998. Secular oscillations in the carbonate mineralogy of reef-building and sediment-producing organisms driven by tectonically forced shifts in seawater chemistry. *Palaeogeography, Palaeoclimatology, Palaeoecology* **144**, 3-19.

Steuber, T. and Veizer, J., 2002. Phanerozoic record of plate tectonic control of seawater chemistry and carbonate sedimentation. *Geology* **30**, 1123-1126.

Stoll, H. M. and Schrag, D. P., 1998. Effects of Quaternary sea level cycles on strontium in seawater. *Geochim. Cosmochim. Acta* **62**, 1107-1118.

Taylor, A. and Blum, J. D., 1995. Relation between soil age and silicate weathering rates determined from the chemical evolution of a glacial chronosequence. *Geology* **23**, 979-982.

Vance, D., Teagle, D. A. H., and Foster, G. L., 2009. Variable Quaternary chemical weathering fluxes and imbalances in marine geochemical budgets. *Nature* **458**, 493-496.

Veizer, J., 1988. The earth and its life: Systems perspective. *Origins of Life and Evolution of Biospheres* **18**, 13-39.

Veizer, J., 1989. Strontium Isotopes in Seawater through Time. *Annu. Rev. Earth Planet. Sci.* **17**, 141-167.

Veizer, J., Ala, D., Azmy, K., Bruckschen, P., Buhl, D., Bruhn, F., Carden, G. A. F., Diener, A., Ebneth, S., Godderis, Y., Jasper, T., Korte, C., Pawellek, F., Podlaha, O. G., and Strauss, H., 1999. $^{87}Sr/^{86}Sr$, $\delta^{13}C$ and $\delta^{18}O$ evolution of Phanerozoic seawater. *Chem. Geol.* **161**, 59-88.

Veizer, J., Buhl, D., Diener, A., Ebneth, S., Podlaha, O. G., Bruckschen, P., Jasper, T., Korte, C., Schaaf, M., Ala, D., and Azmy, K., 1997. Strontium isotope stratigraphy: potential resolution and event correlation. *Paleogeogr. Paleoclimatol. Paleoecol.* **132**, 65-77.

Veizer, J., Compston, W., Clauer, N., and Schidlowski, M., 1983. in Late Proterozoic carbonates: evidence for a "mantle" event at ~900 Ma ago. *Geochim. Cosmochim. Acta* **47**, 295-302.

Veizer, J. and Mackenzie, F. T., 2010. Evolution of Sedimentary Rocks. In: Holland, H. D. and Turekian, K. K. Eds.), *Readings from the Treatise of Geochemistry*. Elsevier.

Vollstaedt, H., Eisenhauer, A., Böhm, F., Fietzke, J., Wallmann, K., Liebetrau, V., Krabbenhöft, A., Farkaš, J., Tomašových, A., and Veizer, J., in review. Linking marine carbonate burial and long-term anoxia to the end-Permian mass extinctions.

Wallmann, K., 2004. Impact of atmospheric CO_2 and galactic cosmic radiation on Phanerozoic climate change and the marine $\delta^{18}O$ record. *Geochem. Geophys. Geosyst.* **5**.

White, A. F. and Brantley, S. L., 2003. The effect of time on the weathering of silicate minerals: why do weathering rates differ in the laboratory and field? *Chem. Geol.* **202**, 479-506.

Wilkinson, B. H., 1979. Biomineralization, paleoceanography, and the evolution of calcareous marine organisms. *Geology* **7**, 524-527.

Woods, A. D., Bottjer, D. J., Mutti, M., and Morrison, J., 1999. Lower Triassic large sea-floor carbonate cements: Their origin and a mechanism for the prolonged biotic recovery from the end-Permian mass extinction. *Geology* **27**, 645-648.

VI. Chapter

Environmental influences on the stable Sr-isotope, Sr/Ca, Mg/Ca, Li/Ca and Mg/Li ratios in the scleractinian cold-water coral *Lophelia pertusa*

J. Raddatz[1]*, V. Liebetrau[1], A. Rüggeberg[2], E. Hathorne[1], A, Krabbenhöft[1], A. Eisenhauer[1], F. Böhm[1], H. Vollstaedt[1], J. Fietzke[1], M. López Correa[3], A. Freiwald[4] and W.-Chr. Dullo[1]

[1] *GEOMAR | Helmholtz Zentrum für Ozeanforschung Kiel, Wischhofstr. 1-3, D-24148 Kiel, Germany.*
[2] *Renard Centre of Marine Geology, Ghent University, Krijgslaan 281 S8, B-9000 Ghent, Belgium.*
[3] *GeoZentrum Nordbayern (GZN), Universität Erlangen-Nürnberg, Loewenichstr. 28, D-91054 Erlangen, Germany.*
[4] *Senckenberg am Meer, Abteilung Meeresforschung, Südstrand 40, D-26382 Wilhelmshaven, Germany, and MARUM, Center for Marine Environmental Sciences, Loebener Str., D-28359 Bremen, Germany.*

In review in *Earth and Planetary Science Letters*

Abstract

The aragonitic skeletons of scleractinian cold-water corals serve as valuable archives in paleoceanographic studies. The potential of $\delta^{88/86}Sr$, Sr/Ca, Mg/Ca, Li/Ca and Mg/Li ratios of the cold-water coral *Lophelia pertusa* to record intermediate water mass properties has been investigated. Here we used samples from the European continental margin spanning a large temperature range from 6 to 14°C. Stable strontium isotope measurements were carried out with the recently developed double spike TIMS technique and our results differ from those obtained with less precise methods. In contrast to the strong positive relationship with temperature of previous studies, our results suggest that $\delta^{88/86}Sr$ measured in scleractinian cold-water corals is not controlled by seawater temperature, but reflects the Sr isotopic composition of seawater with an offset of $\Delta^{88/86}Sr = -0.196‰$.

As found in previous studies, the elemental ratios Sr/Ca, Li/Ca and Mg/Li measured in corals are significantly related to water temperature and do not correlate with salinity, Sr/Ca ratios in *L. pertusa* display the expected inverse correlation with temperature. However, the variance in the Sr/Ca data severely limits the accuracy of paleotemperature estimates. The Li/Ca and Mg/Li ratios in *L. pertusa* are more tightly related to temperature. In particular, the Mg/Li ratio in *L. Pertusa* seems to be less affected by vital effects than Li/Ca ratios and may serve as a new promising paleotemperature proxy for intermediate water masses. However, using the temperature dependence of 0.015 ± 0.004 (mol/mmol)/°C and the precision of 5.3% (2SD) only temperature variations larger than ~2 °C can be resolved with 95% confidence.

VI.1. Introduction

Since we are in a period of rapid climate change it is important to reconstruct the past seawater conditions and circulation to improve our ability to predict the impact of temperature increase in der modern ocean. Compared to traditional sedimentary archives, scleractinian corals have some advantages like the incorporation of high concentrations of Uranium in their aragonite skeleton, which facilitates accurate dating with the U/Th method (e.g. Cheng et al. 2000). Several geochemical tracers like Sr/Ca, Mg/Li, $\delta^{13}C$, $\delta^{18}O$, stable strontium isotopes ($\delta^{88/86}Sr$), etc. can potentially provide vital information about the intermediate and deep oceans of the past (e.g. Adkins et al. 2003, Case et al. 2011, Cohen et al. 2002, Rüggeberg et al. 2008). Significant efforts have been made to identify robust proxies for temperature reconstructions. Elemental ratios suggested to be related to water temperature are Ba/Ca (Sinclair et al. 2006), Mg/Ca (Mitsuguchi et al. 1996), U/Ca (e.g. Shen et al. 1995, Min et al. 1995) and Sr/Ca (e.g. Beck et al. 1992, Smith et al. 1979). The Sr/Ca ratio of tropical corals is a widely used and robust temperature proxy (e.g. Beck et al. 1992; Gagan et al. 1998). The combination of Li/Ca and Mg/Ca ratios to obtain Mg/Li ratios has been introduced as a potential paleotemperature proxy in benthic foraminifers (Bryan and Marchitto 2008), tropical (Hathorne et al. submitted) and cold-water corals (Case et al. 2010). The latter study showed that Mg/Li ratios in various scleractinian cold-water corals are primarily controlled by temperature. Combining Li/Ca and Mg/Ca ratios removes much of the heterogeneity related to the sampling of the coral micro-structures (Case et al. 2010). Additionally, non-traditional stable isotope systems have been introduced as potential paleotemperature proxies in both cold- and warm-water corals. While the applicability of sea-surface temperature reconstructions in tropical corals with $\delta^{44/40}Ca$ is very limited (Böhm et al. 2006), the use of $\delta^{88/86}Sr$ appears instead to be very promising (Fietzke and Eisenhauer 2006, Rüggeberg et al. 2008). The stable strontium isotope system was introduced by Fietzke

& Eisenhauer (2006) as a potential paleothermometer measured in the scleractinian warm-water coral *Pavona clavus*. Subsequently, Rüggeberg et al. (2008) analysed $\delta^{88/86}$Srin the cold-water coral *Lophelia pertusa* to develop a potential new proxy for the reconstruction of intermediate ocean water temperatures. They found a strong positive linear relationship of 0.026‰/°C across the temperature range of 5.9 to 9.5°C (Fig. VI.5) in Atlantic corals originating from 51°N to 70°N. Both studies have shown a similar slope of $\delta^{88/86}$Srwith temperature in tropical and cold-water corals, highlighting the potential of $\delta^{88/86}$Sr for seawater-temperature reconstructions.

However, besides environmental factors, the element incorporation and stable isotope fractionation (δ^{18}O and δ^{13}C) is also affected by biological factors known collectively as "vital effects" (e.g. Adkins et al. 2003, Blamart et al. 2005, Cohen et al. 2006, Gagnon et al. 2007, Gaetani et al. 2011, López Correa et al. 2010, Smith et al. 2000, 2002). These vital effects have an impact on the compositional variability of geochemical tracers, which can be further distinctly different between species. In general, the coral microstructure is characterized by the Centres Of Calcification (COC) and the surrounding theca wall, which is composed of aragonitic needles (Gladfelter 1982). Several studies have tried to explain the mechanisms controlling the distribution of elemental ratios and isotopes in and between these different coral skeleton features (e.g., Adkins et al. 2003, Cohen et al. 2006, Gaetani et al. 2011, Rollion-Bard et al. 2010). Most of these studies presume that coral calcification occurs within an Extracytoplasmic Calcifying Fluid (ECF, e.g. Adkins et al. 2003). Biomineralization models have invoked various mechanisms, which comprise e.g. (1) a pH-driven control of the solution chemistry on the skeletal composition (e.g. Adkins et al. 2003), (2) carbonate precipitation from a semi-enclosed system (Rayleigh fractionation, e.g Cohen et al. 2006, Gaetani et al. 2011), and (3) the formation of amorphous aragonite precursor phases of calcium carbonate (ACC, Rollion-Bard et al. 2010). Recent studies highlight that skeletal cations (calcium, strontium and barium) arrive at the site of calcification by direct seawater

transport (Erez and Braun et al. 2011, Gagnon et al. 2012, Tambutté et al. 2011). The observed variability of elemental ratios can be explained by the balance between seawater transport and precipitation (Gagnon et al. 2012).

This study is based on skeleton of the scleractinian cold-water coral *Lophelia pertusa* which is widely distributed in the world's oceans. Along the European continental margin they occur in Norwegian fjords, on the Irish Margin, the Bay of Biscay, the Gulf of Cadiz and a few occurrences are reported from the Mediterranean Sea (Fig. VI.1, Freiwald et al. 2004, Taviani et al. 2005). *L. pertusa* occurs at water depths from 40 m (Trondheimsfjord, Norway) to >3000 m on the New England seamount chain (Freiwald et al. 2004) and lives in water temperatures of 4-14°C and at salinities from 32.0 in Scandinavian fjords to 38.8 in the Mediterranean Sea (Strømgren 1971, Taviani et al. 2005). Several studies have shown that *L. pertusa* can extend up to 26 mm/yr (Mortensen and Rapp 1998, Gass and Roberts 2010, Orejas et al. 2008) and that each polyp can live several years. The distribution, origin, growth and demise of *L. pertusa* and its reefs and mounds on the European continental margin is controlled by oceanographic conditions such as temperature, current strength, nutrient availability and the density of seawater (e.g. Dullo et al. 2008, Freiwald et al. 2004, Roberts et al. 2006, Rüggeberg et al. 2007, Raddatz et al. 2011).

The development of new proxies for reconstructing past intermediate water mass temperature is important for the study of past climates and ocean circulation. To this end we focus on the temperature, salinity and depth sensitivity of $\delta^{88/86}$Sr, Sr/Ca, Mg/Ca, Li/Ca and Mg/Li ratios in the scleractinian coral-water coral *L. pertusa* to build a new framework to understand proxies extracted from cold-water coral skeletons. To estimate the dependency of proxies to environmental parameters in *L. Pertusa,* geochemical signals measured in the coral skeleton in the theca wall apart from the COC will be calibrated to the instrumental data. Moreover, we also investigate the compositional variability of each geochemical signal

within the coral skeleton to estimate the biological control on element incorporation and stable isotope fractionation.

VI.2. Materials and Methods

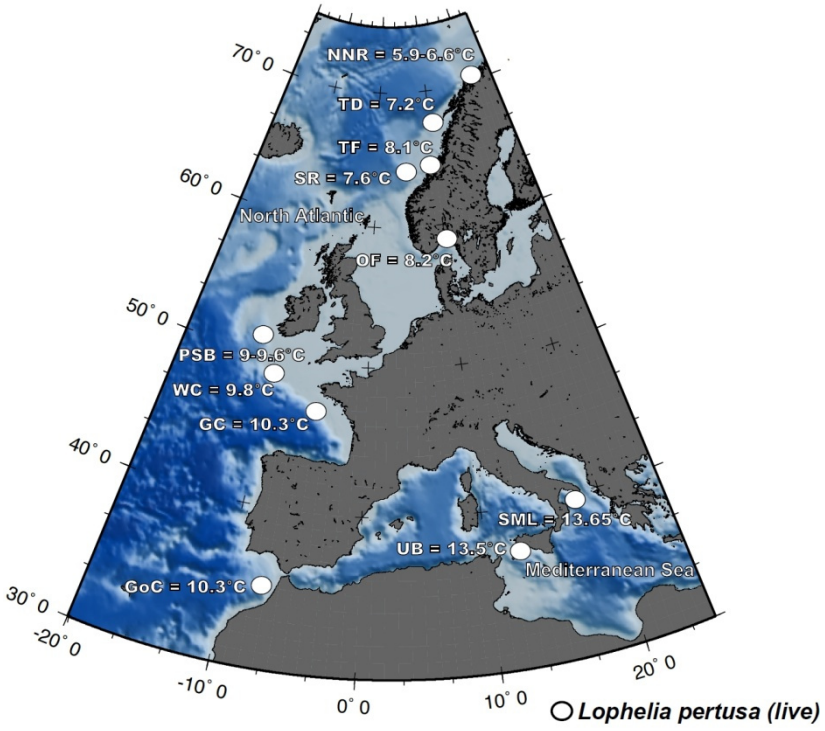

FIGURE VI.1 - Locations of live *in situ* sampled scleractinian cold-water coral *Lophelia pertusa* along the European continental margin and average water temperatures. NNR = Northern Norwegian Reefs (Stjernsund, Lopphavet, Sotbakken), TD = Trændadjupet, TF = Trondheimsfjord, SR = Sula Reef, OF = Oslo Fjord, PSB = Porcupine Seabight (Galway Mound, Little Galway Mound, Propeller Mound), WC = Whittard Canyon, GC = Guilvinec Canyon, GoC = Gulf of Cadiz, UB = Urania Bank, SML = Santa Maria di Leuca.

Living cold-water coral samples of *L. pertusa* were collected from different locations along the European continental margin (Fig. VI.1, Tab. VI.1). Initial $\delta^{88/86}Sr$ data for these samples (Galway Mound, Little Galway Mound, Stjernsund, Trondheimsfjord, Trændadjupet, Oslo Fjord; Tab. VI.1) were previously published (Rüggeberg et al. 2008). In order to extend this study, additional samples were taken from the Norwegian margin (Lopphavet, Sotbakken, Sula Reef, Oslo Fjord), from two different sites in the Mediterranean Sea (Urania Bank and Santa Maria di Leuca), from the Bay of Biscay (Whittard Canyon, Guilvinec Canyon), as well

as from the Gulf of Cadiz (Tab. VI.1, Fig. VI.1). Samples were obtained with the manned submersible "JAGO" of GEOMAR (Kiel), the ROV "QUEST" of MARUM (University of Bremen), the ROV "Genesis" of RCMG (University of Ghent), a video-guided grab (TV-G) and a Van Veen-Grab. All samples were immediately dried at 50°C and then stored away. Water temperatures and salinity were measured via CTD (Conductivity-Temperature-Depth) at the time of sample collection. CTD measurements are only snapshots and do not represent the entire annual variability. However, for carbonate mounds in the NE Atlantic Mienis et al. (2007) showed, that the bathyal temperature variation does not exceed 1.5°.

Sample preparation and $\delta^{88/86}$Sr measurements

For geochemical analyses the final polyp corresponding to the most recent accretion was taken. About 1 mg of carbonate was sampled with a micromill from each coral according to Rüggeberg et al. (2008), focusing on the theca and avoiding the centers of calcification (COC). To quantify the range of intra skeleton variations of $\delta^{88/86}$Sr and elemental ratios (Sr/Ca, Mg/Ca, Li/Ca, Mg/Li) of *L. pertusa* one longitudinal mid-plan section (Little Galway Mound**,** M61/1-218, Table VI.2, Fig. VI.4) was chosen. Using a micromill we were able to drill seven sub-samples across the skeleton. Coral powder was weighed in Teflon beakers together with 2 ml H_2O (18.2 MΩ Milli-Q water). Then samples were dissolved in 2% HNO_3 and heated for at least 5 h in closed beaker and then dried at 90°C. Organic matter was removed by adding 200 µl H_2O_2 (30%) and 200 µl 2N HNO_3 and heated for at least 6 hours in closed beaker.and evaporated to dryness afterwards. The sample was dissolved again in 2 ml 8N HNO_3 and separated into two fractions (isotope composition (ic) and isotope dilution (id)) for Sr isotope analysis, where each fraction contained 1000–1500ng Sr. To the id sample we added the $^{87}Sr/^{84}Sr$ double spike (DS) solution (Krabbenhöft et al., 2009). Chromatographic column separation was performed with 650µm BIO-RAD columns filled to one-third with Triskem Sr-SPS resin (grain size 50–100 µm). The Sr isotope measurements were carried out at

GEOMAR using a Thermo-Ionization-Mass-Spectrometer (TIMS, TRITON ThermoFisher). Here we measured two ic-analyses and two id-analyzes for each sample. The ratio of stable Sr is given as $\delta^{88/86}Sr$ in relation to the $SrCO_3$ standard SRM987 distributed by the National Institute of Standards and Technology (NIST) (FIETZKE and EISENHAUER, 2006). $\delta^{88/86}Sr = [^{88}Sr/^{86}Sr_{sample}/^{88}Sr/^{86}Sr_{SRM987} - 1] \times 1000$. For the SRM987 standard we used the generally accepted $^{88}Sr/^{86}Sr$ value of 8.375209 ($^{86}Sr/^{88}Sr$ = 0.1194, Nier, 1938) for normalization. The results of Sr isotope measurements are shown in Table VI.1. The long-term external reproducibility of the $\delta^{88/86}Sr$ ratios as measured on the JCp-1 *Porites* coral reference material (Okai et al. 2002) measured during the course of this study (n = 10) is 0.197 ± 0.020‰ (2SD) and corresponds to the error given in this study.

Elemental/Ca measurements

The solutions used for stable strontium isotope measurements were also analyzed for elemental ratios using an Agilent 7500cs Quadrupole-ICP-MS at GEOMAR. In a first step the Ca concentration was measured and samples were diluted to have ~10 ppm Ca and calibrated using standards made from single element solutions. Elemental/Ca ratios were calculated from the raw counts using the method of Rosenthal et al. (1999). Six aliquots of Porites sp. coral powder reference material JCp-1 (Okai et al. 2002) were treated like the Lophelia samples and the average values obtained during the course of this study (n = 10) were Li/Ca 6.17 ± 0.33 μmol/mol, Mg/Ca 4.15 ± 0.15 mmol/mol, Sr/Ca 8.76 ± 0.13 mmol/mol and Mg/Li ratio 0.673 ± 0.048 mol/mmol (all errors are 2 standard deviations (SD)). The corresponding 2 relative standard deviations (RSD) of the analyses are ~ 5.4% for Li/Ca, ~1.3 for Mg/Ca, ~1.5 % for Sr/Ca and ~5.3 % for the Mg/Li ratio. The corresponding absolute concentrations measured are within the uncertainties of the recommended JCp-1 values (Okai et al. 2002).

VI.3. Results

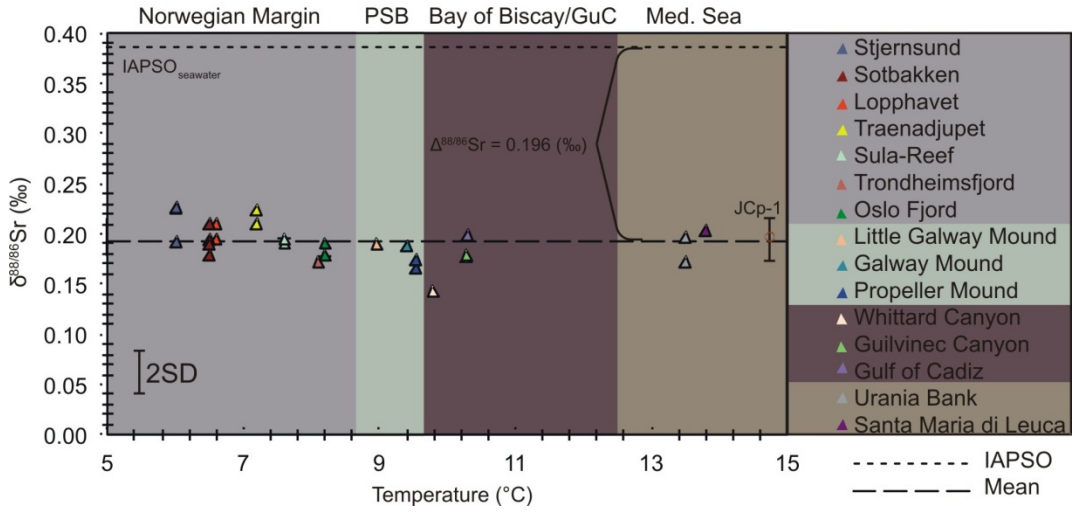

FIGURE VI.2 - Stable strontium isotopes in *Lophelia pertusa* between 6 and 14°C from various locations along the European continental margin show no correlation to temperature. Results (mean = big dotted line are the same within the uncertainty of the coral reference material JCp-1 (0.197 ±0.02‰, red circle). The *L. pertusa* $\delta^{88/86}$Sr values display an offset of -0.196 (‰) to the IAPSO $\delta^{88/86}$Sr seawater (small dotted line) value of 0.386 (‰) (Liebetrau et al. 2009; Krabbenhöft et al. 2010).

The habitats of *L. pertusa* analysed in this study cover a large temperature range for cold-water corals from 5.9°C to 13.8°C (Fig. VI.1). In total 25 bulk coral theca samples were analysed for stable strontium isotopes. The $\delta^{88/86}$Sr composition of the entire sample set ranges from 0.143 ± 0.02 ‰ to 0.226 ± 0.02 ‰ (Table VI.1) and does not show a significant correlation with temperature (Fig. VI.2). The mean of all samples is 0.19 ± 0.02 ‰. Note that this value is within the uncertainty the same as for the JCp-1 coral standard with 0.197 ± 0.02 ‰. Samples from the Stjernsund grew under the lowest temperatures (5.9°C) and have an average $\delta^{88/86}$Sr value of 0.217 ± 0.02 ‰. Samples from the Mediterranean Sea grew at 13.65 to 13.8°C, the highest water temperatures in our sample set, and the $\delta^{88/86}$Sr of these samples is 0.183 ± 0.02 ‰ and 0.203 ± 0.02 ‰. The three samples from the Porcupine Seabight originate from carbonate mounds (Propeller Mound, Galway Mound and Little Galway Mound) and grew at ~9.5°C showing a mean $\delta^{88/86}$Sr value of 0.190 ± 0.02 ‰. The *L. pertusa* sample from Whittard Canyon at 9.79°C has the lowest $\delta^{88/86}$Sr value of 0.143 ± 0.02‰.

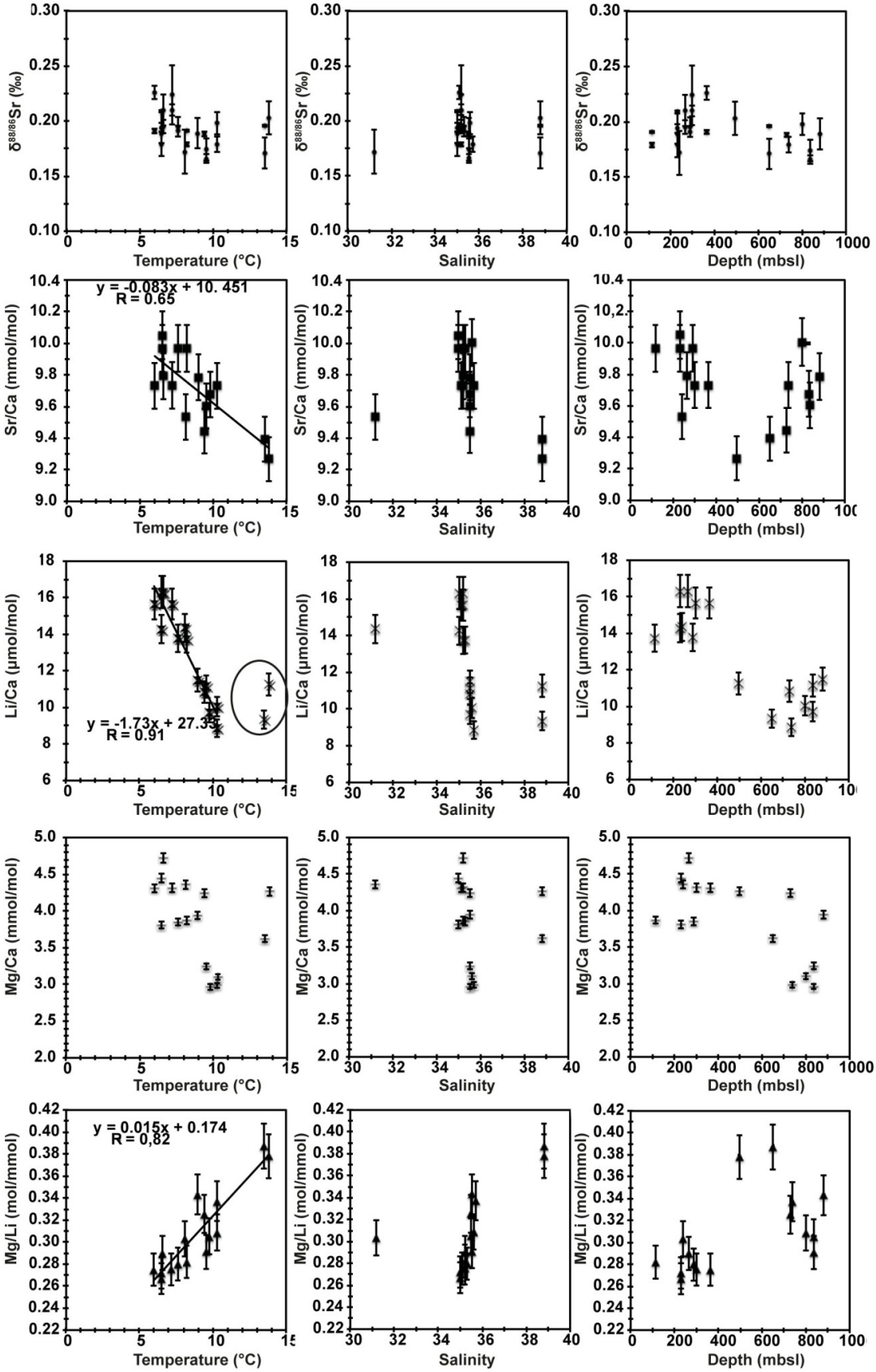

FIGURE VI.3 - Temperature, salinity and depth dependence of $\delta^{88/86}$Sr, Sr/Ca, Mg/Ca, Li/Ca and Mg/Li in L. pertusa. Results show that only Sr/Ca, Li/Ca and Mg/Li exhibit significant correlations to temperature (r2 = 0.65 for Sr/Ca, r2 = 0.91 for Li/Ca and r2 = 0.85 for Mg/Li).

Sr/Ca ratios vary from 9.27 mmol/mol at 13.8°C in the Mediterranean Sea to 10.05 mmol/mol at 6.5°C in the northern reefs (Lopphavet). The Sr/Ca ratios show a significant inverse correlation with temperature by excluding one possible outlier from the Guilvinec Canyon ($r^2 = 0.65$, $p = <0.001$; Fig. VI.3.)

$$Sr/Ca\ (mmol/mol) = -0.083 \pm 0.017\ T\ (°C) + 10.451 \pm 0.16 \quad \text{Eq. (VI.1)}$$

The Mg/Ca ratios vary from 2.99 to 4.72 (mmol/mol) and do not show a significant relationship with temperature (Fig. VI.3).

The Li/Ca ratios vary from 8.86 to 16.32 (µmol/mol) and exhibit a significant correlation ($r^2 = 0.61$, $p = 0.005$) with temperature. Excluding the samples from the Mediterranean Sea this relationship is enhanced to an $r^2 = 0.91$ ($p = <0.001$) and can be described by the following equation:

$$Li/Ca\ (\mu mol/mol) = -1.73 \pm 0.16\ T\ (°C) + 27.33 \pm 1.39 \quad \text{Eq. (VI.2)}$$

The Mg/Li ratios vary from 0.27 mol/mmol at low temperatures (5.9°C) to 0.39 mol/mmol at the highest temperature at Santa Maria di Leuca (13.65°C). The Mg/Li results display a positive linear correlation with temperature ($r^2 = 0.82$, $p = <0.001$; Fig. VI.3) that can be described by the following equation:

$$Mg/Li\ (mol/mmol) = 0.015 \pm 0.002\ T\ (°C) + 0.174 \pm 0.018 \quad \text{Eq. (VI.3)}$$

The $\delta^{88/86}Sr$, Sr/Ca, Mg/Ca, Li/Ca and Mg/Li ratios do not show any significant correlation with salinity (Fig. VI.3), across the large range from 31.2 in the Trondheimsfjord up to 38.8 in

the Mediterranean Sea. Moreover, also all investigated ratios do not show a significant relationship to water depth.

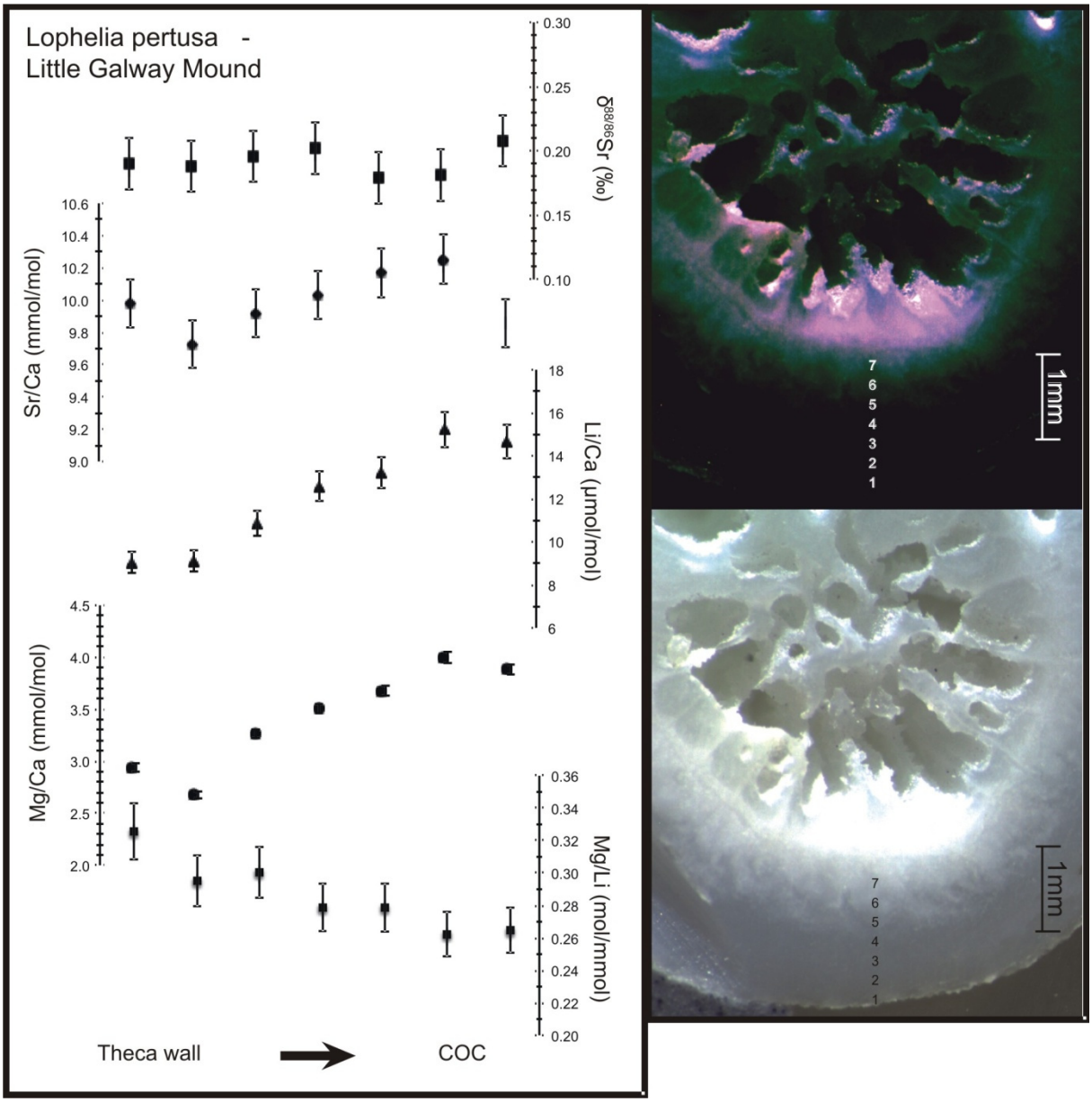

FIGURE VI.4 - Intra-individual heterogeneity test of $\delta^{88/86}$Sr, Sr/Ca, Mg/Ca, Li/Ca and Mg/Li compositions in a *L. pertusa* specimen from Little Galway Mound (M61/1-218). The displayed coral is a longitudinal section of the Little Galway Mound specimen shows the internal architecture of the skeleton. The $\delta^{88/86}$Sr, Sr/Ca, Mg/Li ratios are equal within measurement uncertainty, whereas Mg/Ca and Li/Ca show almost a twofold increase within the coral skeleton. All error bars correspond to 2SD. Coral pictures show the sampling profile drilled with the micromill (1-7) from the theca wall into the COC. For the Mg/Ca ratios the error bars are smaller than the dots.

The intra skeleton $\delta^{88/86}Sr$ values vary from 0.179 ± 0.030 ‰ to 0.208 ± 0.008 ‰ (Fig. VI.4). All values in this *L. pertusa* sample have a mean of $\delta^{88/86}Sr$ = 0.191 ± 0.020 ‰, which coincides with the JCp-1 *Porites* coral reference material (0.197 ± 0.019 ‰).

Similarly, the Sr/Ca values of this coral show no systematic behaviour within the microstructure, but show a variability of 0.53 mmol/mol, which is significant when compared to the external reproducibility (± 0.07) from 9.73 ± 0.07 to 10.25 ± 0.07 mmol/mol.

Li/Ca and Mg/Ca ratios vary strongly across the skeleton between the theca and the COC. Li/Ca ratios range from ~9 to ~15 µmol/mol and Mg/Ca ratios range from ~2.7 to ~4.0 mmol/mol with the highest ratios in the inner part of the corals close to the COC. The corresponding Mg/Li ratios show related variability of 0.063 mol/mmol change, from 0.325 mol/mmol to 0.263 mol/mmol, decreasing from the outer to the inner part (Fig. VI.4). These changes in the Mg/Ca and Li/Ca ratios are associated with the COC maxima. However, across the skeletal section of *L. pertusa* the Mg/Ca and Li/Ca ratios exhibit a strong positive relationship of r^2 = 0.96 (p = <0.001, Fig. VI.5).

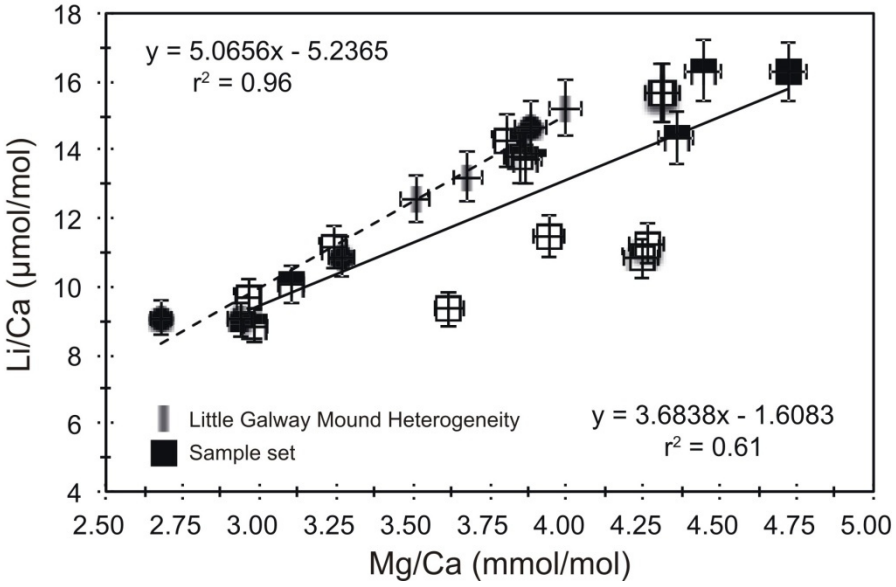

FIGURE VI.5 - Intra-individual (Little Galway Mound M61/1-218) and sample set correlation of Mg/Ca and Li/Ca ratios of *L. pertusa*. The intra-individual correlation of Mg/Ca and Li/Ca reveals a better correlation compared to the entire sample set.

VI.4. Discussion

Stable strontium isotopes in *L. Pertusa*

In contrast to earlier findings our $\delta^{88/86}Sr$ results exhibit no significant relationship with seawater temperature (Fig. VI.2 and VI.3). The measurements were carried out on corals from a large range of temperature from 6-14°C and even though we used some of the same *L. pertusa* samples from the European continental margin as from the study of Rüggeberg et al. (2008, Table VI.1), we could not reproduce the previously published temperature relationship (Fig. VI.6).

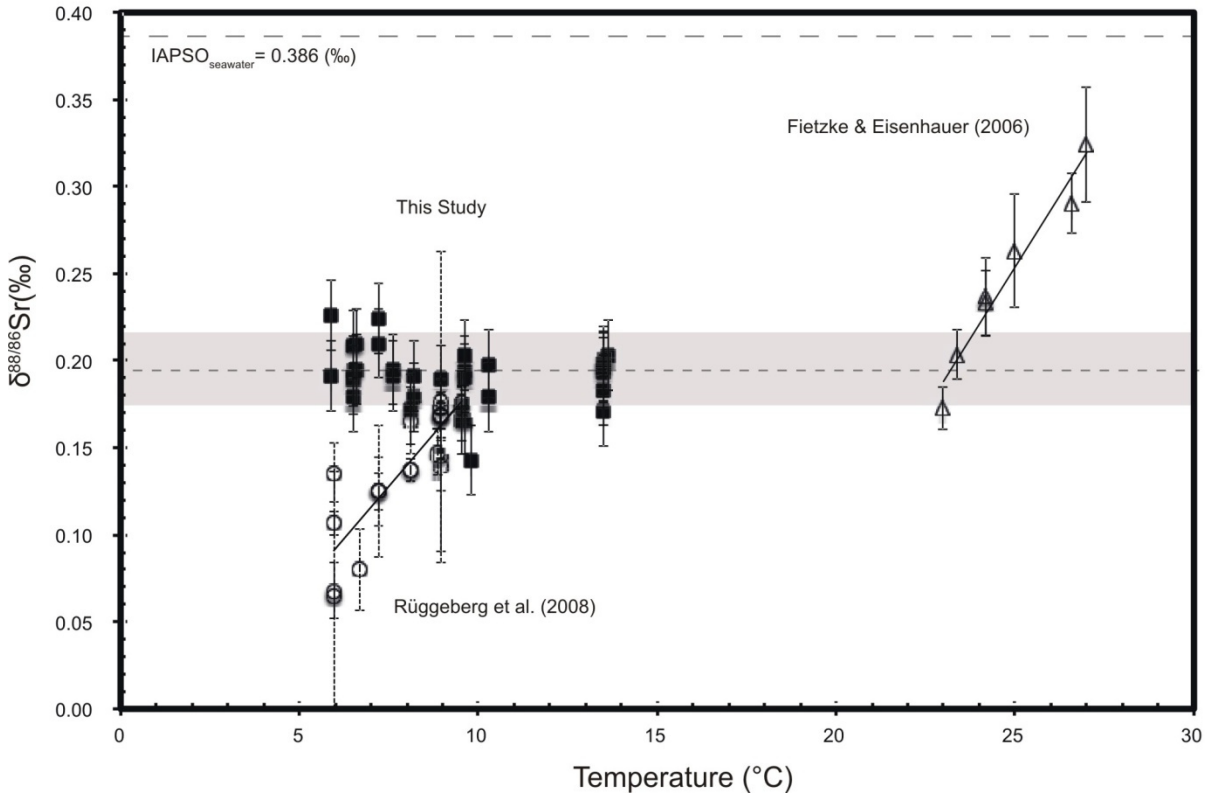

FIGURE VI.6 - All $\delta^{88/86}Sr$ values determined with the DS-TIMS technique compared to $\delta^{88/86}Sr$ measured with the bracketing standard method in the scleractinian cold-water coral *L. pertusa* (Rüggeberg et al., 2008) and the tropical coral *Pavona clavus* (Fietzke and Eisenhauer 2006). IAPSO $\delta^{88/86}Sr$ seawater value corresponds to 0.386 ‰ (Liebetrau et al., 2009; Krabbenhöft et al., 2009). The reproducibility of $\delta^{88/86}Sr$ for the JCp-1 measured in the course of this study is ± 0.020‰ (2SD) (n = 10) and is indicated with the grey bar, which covers almost the entire range of $\delta^{88/86}Sr$ values.

In addition, extended the temperature range from Rüggeberg et al., 2008 with *L. pertusa* samples from sites with temperatures >9.6°C, originating from the Mediterranean Sea, the Gulf of Cadiz and the Bay of Biscay. According to our DS-TIMS results the $\delta^{88/86}$Sr values of individual *L. pertusa* samples from the entire European continental margin show no variations within uncertainty over a large range of temperature, salinity and depth. Additionally we observed no compositional variability within the coral skeleton (Fig. VI.2, VI.3, and VI.4).

By now only a few studies have focused on stable strontium isotopes in the marine realm and hence little is know about fractionation processes in marine calcifiers. Different methods have been used to determine natural strontium isotope fractionation (Fietzke & Eisenhauer 2006; Krabbenhöft et al. 2009, Ohno et al. 2008). In this study we employed the DS-TIMS method (Krabbenhöft et al. 2009) with a factor of 2–3 improved precision compared to the standard-bracketing MC-ICP-MS method (Fietzke and Eisenhauer 2006, Rüggeberg et al. 2008).

The observed discrepancy between our results with those from previous studies in the stable strontium isotope fractionation in the scleractinian cold-water coral *L. pertusa* may be explained by the different sample preparation and measurement methods. In particular, the double spike technique also accounts for any fractionation during the ion chromatographic Sr separation and the chemical preparation (Krabbenhöft et al. 2009). Therefore, the use of the DS-TIMS overcomes any matrix related mass bias fluctuations, which probably accounts for most of the variability seen in the $\delta^{88/86}$Sr record of Rüggeberg et al. (2008). Irrespectively from the discrepancies between the bracketing–standard method and the DS-TIMS our findings are further supported by Vollstaedt et al. (submitted) by showing that temperature is not a controlling parameter for stable strontium isotope fractionation in calcitic brachiopods as well.

Moreover, our results display a constant negative strontium fractionation offset of ~0.2 ‰ to the isotopic composition of seawater. Strontium is very conservative in seawater and has a residence time of ~2.5x10^6 years (Hodell et al., 1990). This is very long compared to the mixing time of the oceans (~1000 years) and hence the oceans are well mixed with respect to Sr isotopes (McArthur 1994, Veizer 1989). These findings are supported by first results of Liebetrau et al. (2009) showing that the $\delta^{88/86}$Sr of seawater is homogeneous with 0.386 ± 0.007 ‰ in the North Atlantic, the Gulf of Cadiz and the Mediterranean Sea. However, out results show that coral aragonite records the $\delta^{88/86}$Sr of seawater with a constant offset of $\Delta^{88/86}$Sr = -0.196 ‰ independently from environmental influences(Fig. VI.2). Moreover, the *Porites* standard (JCp-1) shows also a similar offset of $\Delta^{88/86}$Sr = -0.189 ‰ to the IAPSO seawater standard $\delta^{88/86}$Sr value. It remains to be tested if other scleractinian corals also show the same constant $\delta^{88/86}$Sr fractionation. If this is the case, then they might offer an archive of seawater $\delta^{88/86}$Sr, which could extent back to the Triassic period, where the first scleractinian corals in Earth history have been recorded (237 Ma, Stanley & Fautin 2001). The oldest known scleractinian cold-water corals appear in the Cretaceous (<125 Ma, Roberts et al. 2009). With respect to paleoceanographic reconstructions and seawater chemistry the scleractinian cold-water coral *L. pertusa* may serve as promising archive to record the Sr isotopic composition of past water masses and hence provide new insights into the carbonate burial flux and the strontium budget of the ocean (Krabbenhöft et al. 2010, Vollstaedt et al. submitted).

Sr/Ca ratios in *L. Pertusa*

Our results show that Sr/Ca ratios measured in the theca wall of *Lophelia L. pertusa* exhibits a relationship with temperature of 0.08 mmol/mol/°C and no significant relationship to salinity and depth (Fig. VI.3 and VI.7). Unlike other elemental ratios Sr/Ca display less but still significant compositional variability within the entire coral skeleton (Fig. VI.4). As discussed by Gagnon et al. (2007) the compositional variability of Sr/Ca might be different between

different cold-water corals species (see Cohen et al. 2002, 2006) our study supports these findings showing that the Sr/Ca variability throughout the skeleton and the COC is rather ubiquitous.

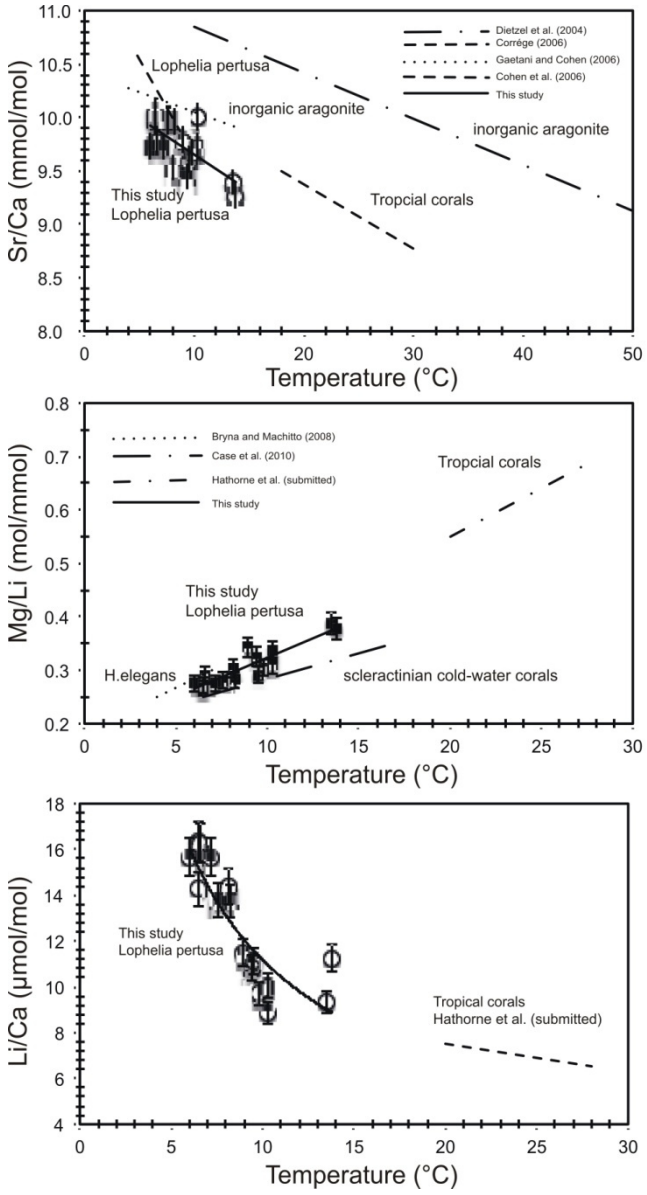

FIGURE VI.7 - Sr/Ca, Mg/Li and Li/Ca ratios measured in scleractinian cold-water coral *L. pertusa* from different locations with seawater temperatures between 6 and 14°C. Sr/Ca-temperature dependence of this study is compared to the Sr/Ca vs. SST calibration of various scleractinian warm water corals (mean: Sr/Ca = –0.0596T (°C) + 10.596; Corrége 2006) and abiogenic aragonite (Sr/Ca = –0.043T (°C) + 11.72; Dietzel et al. 2004) and *L. pertusa* (Sr/Ca = –0.18T (°C) + 11.44; Cohen et al., 2006) as well as another abiogenic aragonite (Sr/Ca = –0.038T + 10.43; Gaetani and Cohen 2006). Mg/Li ratios of *L. pertusa* lie between the slopes of the aragonitic foraminifera *Hoeglundina elegans* (0.0143T (°C) + 0.20; Bryan and Marchitto 2008) and those of scleractinian cold-water corals (0.009T (°C) + 0.19; Case et al., 2010) and of warm-water corals (0.018T (°C) + 0.19; Hathorne et al. submitted). The Li/Ca ratios of *L. pertusa* are plotted together with Li/Ca ratios of the scleractinian warm water coral *Porites (– 0.123T (°C)+ 9.974;* Hathorne et al. submitted).

Strontium to calcium ratios measured in the different genera of cold-water corals (e.g. *Caryophyllia, Flabellum, Stephanocyathus)* suggests that Sr/Ca ratios are related to seawater temperature (Shirai et al. 2005). Moreover, Sr/Ca ratios measured in the theca wall of the deep-sea coral *Desmophyllum dianthus* agree with the expected Sr/Ca of inorganic aragonite precipitated at the temperature of coral growth (Kinsman and Holland 1969, Gagnon et al. 2007). In contrast, Cohen et al. (2006) found a temperature relationship of 0.18 mmol/mol/°C within on single *L. pertusa* polyp and the observed temperature dependency is too large to be solely explained by the temperature control on Sr/Ca in inorganic aragonite (Cohen et al. 2006). Other studies suggested Sr/Ca ratios in scleractinian cold-water corals are also influenced by vital (Montagna et al. 2005, Shirai et al. 2005).

Even though our applied microsampling technique does not provide such high-resolution records as the SIMS (Cohen et al. 2006) our study reveals similar findings as the study of Allison & Finch (2004) in warm-water corals. They showed that the large small-scale Sr/Ca heterogeneity can potentially be calibrated to seawater temperature when the sampling resolution is decreased. This is supported by our Sr/Ca- T dependency analyzed in the theca wall of *L. pertusa* (Fig. VI.7, Eq. VI.1). This Sr/Ca – T dependency is similar compared to that of the zooxanthellate tropical corals showing that the Sr/Ca ratio decreases with increasing water temperature (Fig. VI.7; e.g., Gaetani and Cohen 2006, Beck et al. 1992, Smith et al. 1979). According to our results both azooxanthellate and zooxanthellate corals are controlled by the same processes responsible for the incorporating of Sr/Ca. This is in line with the previous study of Sinclair et al. (2006) showing that Mg/Ca and U/Ca ratios reveal a similar relationship in warm and cold-water corals suggesting, that both corals are controlled by similar biochemical processes. However, although the Sr/Ca ratios measured here with traditional microsampling techniques in *L. pertusa* avoiding the COC is T-dependent the relatively large Sr/Ca-scatter in the overall T calibration severely limits the use for paleoreconstructions. Hence more work is needed to clarify the environmental influence on

Sr/Ca ratios in scleractinian cold-water corals and its compositional variability within the coral skeleton.

Mg/Ca, Li/Ca and Mg/Li in *L. Pertusa*

Unlike, $\delta^{88/86}$Sr and Sr/Ca ratios, the Mg/Ca and Li/Ca ratios do show large variations within the coral microstructure. In particular, we were able to detect the COC by measuring Mg/Ca and Li/Ca ratio both showing extremely elevated values. Such elevated Mg/Ca ratios in COCs of warm water corals were also reported by Meibom et al. (2004, 2008). Moreover, our study reveals that both ratios are significantly correlated within the coral skeleton and throughout the sample set avoiding the corals COC (Fig. VI.5). This behaviour of Mg/Ca and Li/Ca ratios was also shown in the study of Case et al. (2010) of cold-water corals. If we assume that skeletogenesis occurs within the ECF, our observation can be explained by the Rayleigh fractionation as suggested by Gagnon et al. (2007). Both elements have an apparent partition coefficient of <1 and hence a Rayleigh fractionation model would predict a positive correlation between Mg/Ca and Li/Ca. Gagnon et al. (2007) and Case et al. (2010) have though shown that other processes than a Rayleigh fractionation control trace element incorporation into the skeleton of the solitary cold-water coral *D. dianthus*. They found a break in the slope between Li/Ca and Mg/Ca ratios and explained it with either the build up of precursor ACC or Mg-hosting organics within the COC. This is supported by the apparently different slopes of Mg/Ca and Li/Ca ratios from our sample set suggesting that other processes control the incorporation of Mg and Li in the coral skeleton (Fig. VI.5) .The pathways for the incorporation of Mg and Li into the coral aragonite lattice are still poorly understood. While some studies highlight that Mg is directly substituted for Ca^{2+} (Politi et al. 2010) others have shown that Mg is hosted in organic bindings or ACC (Finch and Allison 2008). The incorporation of Li^{+} into biogenic aragonite also is not well constrained, but a recent study on modern aragonitic bivalves by Thébault et al. (2009) showed that it is

influenced by calcification rate. Moreover, the Li/Ca ratios in calcific foraminifera are influenced by growth rate and/or carbonate ion concentration (Lear and Rosenthal 2006). In warm water corals Li/Ca is influences by seawater temperature in (Hathorne et al. submitted). However, similar to the findings of Case et al. (2010) for *Balanophyllidae* corals, our results indicate on the one hand that Mg and Li incorporation are controlled by similar mechanisms. As shown in Figure VI.5 Mg/Ca and Li/Ca ratios within one single polyp appears to be controlled by similar processes, the extensive calibration of all coral samples reveal that Mg incorporation is controlled by different processes in different species. We suggest that the compositional variability of Mg and Li in *L. pertusa* is highly influenced by growth rates as already mentioned by Marriot et al. (2004) for Li and by Cohen et al. (2006) for Mg. Accordingly, the compositional variability of Mg/Ca and Li/Ca ratios do correspond to the coral growth with elevated values within the COC and drastically decreasing values with increasing coral age (Fig. VI.4). Moreover, growth rates of *L. pertusa* from different locations along the European continental margin vary from 5 to 26 mm/y (Roberts et al. 2009), explaining the different slopes in the Mg/Ca - Li/Ca relationship from the sample set (Figure VI.5).

Marriot et al. (2004) suggest that the rate of crystal growth may play an important role on Lithium incorporation. In contrast to the slow growing solitary scleractinian cold-water corals *L. pertusa* is a fast growing cold-water coral that can extend up to 27 mm/y (e.g. Gass and Roberts 2010). Linear extension rates of *L. pertusa* decrease drastically with increasing age and highest growth is associated with the initial growth of coral polyps (Mortensen 2001, Brooke & Young 2009, Gass & Roberts 2010, Maier et al. 2010). The early stage of growth is represented by the COC in the skeletal microstructure (Gass & Roberts 2010). However, Marriott et al. (2004) and Hathorne et al. (submitted) demonstrated that Li incorporation in the warm-water coral *Porites* is also controlled by temperature (Fig. VI.7). The results of Mariott et al. (2004) have shown that Li is more readily incorporated into carbonates at low

temperatures. They concluded that Li incorporation into carbonates is exothermic and hence is less favoured at higher temperatures. This is in line with our results revealing that Li incorporation is more effective at lower temperatures (Eq. VI.2, Fig. VI.7).

The Mg/Li ratio was introduced as a potential temperature proxy by Bryan and Marchitto (2008) showing that it is strongly correlated to temperature in the aragonitic foraminifera *Hoeglundina elegans* (Fig. VI.7). Subsequently, Case et al. (2010) demonstrated a similar temperature-dependency of Mg/Li ratios in scleractinian cold-water corals (Fig. VI.7). Moreover, they showed that neither salinity nor carbonate ion concentration control the Mg/Li ratios. Using traditional sampling techniques Mg/Li correlates with temperature in various scleractinian corals from different ocean basins with r^2= 0.62 for all investigated species and with r^2= 0.82 for the family Caryophylliidae (Case et al. 2010). Our results confirm the potential of Mg/Li ratios as a paleothermometer in cold-water corals (Eq. 3). In particular, most of the temperature sensitivity of Mg/Li appears to be driven by the temperature dependence of Li, although it reveals large variations within skeletal microstructure (Fig. VI.4).

Our dataset is the first extensive examination of *L. pertusa* samples using traditional techniques, revealing a temperature sensitivity of 0.015 mol/mmol/°C for Mg/Li (Eq.3) similar to the Caryophylliidae slope of Case et al. (2010, 0.009 mol/mmol/°C). The scatter in the Mg/Li record of *L. pertusa* is smaller compared to the scatter in Sr/Ca ratios, but may still restrict temperature reconstructions. Using the temperature dependence of 0.015 ± 0.004 mol/mmol/°C and the precision of 5.3% (2SD) temperature variations larger than 2°C can be reconstructed with 95% confidence.

VI.5. Conclusion

This study investigated the potential of the scleractinian cold-water coral *L. pertusa* to serve as an archive for intermediate water temperatures using the geochemical proxies $\delta^{88/86}Sr$, Sr/Ca, Mg/Ca, Li/Ca and Mg/Li. With the higher precision of the Double-Spike-TIMS technique compared to the bracketing standard MC-ICP-MS technique, it was not possible to reproduce the findings of Rüggeberg et al. (2008) by measuring $\delta^{88/86}Sr$ of some of the same samples. Our results show that $\delta^{88/86}Sr$ is not controlled by temperature in *L. pertusa* skeletons. Instead the $\delta^{88/86}Sr$ values display a constant offset of $\Delta^{88/86}Sr$ = -0.196 ‰ from seawater and may thus become useful as an archive to record the Sr isotopic composition of the paleoocean.

Our measurements of the elemental ratios Sr/Ca, Li/Ca and Mg/Li support earlier studies in showing significant temperature relationships that may form the basis for paleotemperature proxies. The sensitivity of Sr/Ca in the *L. pertusa* to temperature, however, severely limits the use as a paleotemperature proxy and further studies are needed to analyse Sr/Ca ratios at micrometre-scale in multiple specimens. The scatter of the Li/Ca and Mg/Li record in *L. pertusa* is small showing the promise of those ratios as a more reliable paleotemperature proxy for new perspectives to reconstruct past intermediate water dynamics. Especially, the strong dependency of Li/Ca at lower temperature highlights this as a paleothermometer for seawater temperature reconstruction of the intermediate ocean. Future studies need to investigate the potential of *L. pertusa* as a high resolution archive for paleoceanographic reconstruction.

VI.6. Acknowledgements

The authors gratefully thank all captains, crews and cruise scientists involved in this study. This manuscript benefited from the remarks and comments of Paolo Montagna. Claudia

Wienberg is gratefully acknowledged for providing some of the coral samples from the Gulf of Cadiz, and Marco Taviani kindly provided the Apulian Bank corals. This work has been made possible thanks to the support from DFG [TRISTAN and ISOLDE (Du 129/37 and Du 129/45 I +II)]. AF and MLC acknowledge funding from the EU-FP VII HERMIONE project (Contract number 226354). Additionally, we would like to thank Folkmar Hauff, Ana Kolevica and Jutta Heinze for their lab-support.

VI.7. Tables

TABLE VI.1 - Meta data, environmental data, stable strontium isotopes and element ratios of *Lophelia pertusa* coral samples.

Cruise	Source	Location	Province	Latitude	Longitude	T [°C]	Salinity	Depth [m]	$\delta^{88/86}$Sr [‰]	Sr/Ca [mmol/mol]	Mg/Ca [mmol/mol]	Li/Ca [µmol/mol]	Mg/Li [mol/mmol]
POS325-433	1	Stjernsund	NNR	70°16.04′N	22°27.37′E	5.9	34.97	295	0.226	9.732	4.312	15.664	0.275
POS325-433	1	Stjernsund	NNR	70°16.04′N	22°27.37′E	5.9	34.97	295	0.191				
PS70/40-4	2	Sotbakken	NNR	70°45.35′N	18°40.04′E	6.6	35.2	265	0.195	9.792	4.720	16.296	0.29
PS70/40-4	2	Sotbakken	NNR	70°45.35′N	18°40.04′E	6.6	35.2	265	0.210				
POS391-552-1	2	Lopphavet	NNR	70°26.80′N	21°10.38′E	6.5	35	230	0.194	10.051	3.809	14.276	0.267
POS391-552-1	2	Lopphavet	NNR	70°26.80′N	21°10.38′E	6.5	35	230	0.209	9.967	4.445	16.316	0.272
POS391-552-1	2	Lopphavet	NNR	70°26.80′N	21°10.38′E	6.5	35	230	0.189				
POS391-552-1	2	Lopphavet	NNR	70°26.80′N	21°10.38′E	6.5	35	230	0.179				
POS325-356/1	1	Trænadjupet	TD	66°58.40′N	11°06.53′E	7.2	35.2	300	0.210	9.732	4.312	15.664	0.275
POS325-356/1	1	Trænadjupet	TD	66°58.40′N	11°06.53′E	7.2	35.2	300	0.224				
POS391-561-1	2	Sula-Reef	SR	64°05.98′N	08°05.86′E	7.6	35.3	290	0.191	9.968	3.850	13.771	0.28
POS391-561-1	2	Sula-Reef	SR	64°05.98′N	08°05.86′E	7.6	35.3	290	0.195				
Røberg #3	1	Trondheimsfjord	TF	63°28.61′N	09°59.72′E	8.1	31.2	240	0.172	9.533	4.357	14.365	0.303
POS391-574-1	2	Oslo Fjord	OF	59°04.01′N	10°44.31′E	8.2	35.2	115	0.179	9.966	3.870	13.743	0.282
POS391-574-1	2	Oslo Fjord	OF	59°04.01′N	10°44.31′E	8.2	35.2	115	0.191				
M61/1-218	1	Little Galway Mound	PSB	51°26.51′N	11°45.43′W	8.96	35.53	881	0.189	9.785	3.941	11.489	0.343
M61/3-551	1	Galway Mound	PSB	51°26.94′N	11°45.16′W	9.54	35.53	837	0.166				
M61/3-551	1	Galway Mound	PSB	51°26.94′N	11°45.16′W	9.54	35.53	837	0.174	9.603	3.242	11.143	0.291
POS265-499 (*)	2	Propeller Mound	PSB	52°08.89′N	12°46.31′W	9.6	35.5	729	0.188	9.445	4.243	10.838	0.325
B10-17b Dive 4	2	Whittard Canyon	WC	48°46.79′N	10°34.20′W	9.79	35.5	835	0.143	9.677	2.963	9.712	0.305
B10-17a Dive 1	2	Guilvinec Canyon	GC	46°56.20′N	05°21.60′W	10.29	35.6	800	0.198	10.054	3.104	10.058	0.309
GeoB12738-1	2	Gulf of Cadiz	GoC	34.59.98′N	07°04.51′W	10.28	---	738	0.179	9.732	2.986	8.857	0.337
M70/1-677	2	Urania Bank	UB	36°50.34′N	13°09.31′E	13.5	38.8	651	0.171	9.393	3.618	9.343	0.387
M70/1-677	2	Urania Bank	UB	36°50.34′N	13°09.31′E	13.5	38.8	651	0.196				
COR2-111	2	Santa Maria di Leuca	SML	39°34.89′N	18°23.00′E	13.65	38.69	496	0.203	9.267	4.263	11.262	0.378

Province: NNR = Northern Norwegian Reefs (Stjernsund, Lopphavet, Sotbakken), TD = Trændadjupet, TF = Trondheimsfjord, SR = Sula Reef, OF = Oslo Fjord, PSB = Porcupine Seabight (Galway Mound, Little Galway Mound, Propeller Mound), WC = Whittard Canyon, GC = Guilvinec Canyon, GoC = Gulf of Cadiz, UB = Urania Bank, SML = Santa Maria di Leuca, Source 1 = Rüggeberg et al. (2008), Source 2 = this study, (*) = Sample represents the mean of four different determinations in one single polyp.

TABLE VI.2 - Intra-individual heterogeneity test of $\delta^{88/86}$Sr, Sr/Ca, Mg/Ca, Li/Ca and Mg/Li ratios in a *Lophelia pertusa* specimen from Little Galway Mound (M61/1-218, Porcupine Seabight; Temperature = 8.96°C, Salinity = 35.53, Depth = 881 m). The Postion corresponds to the cross section along the coral skeleton from 1 (Theca wall) to 7 (COC), see Figure VI.4.

Position	$\delta^{88/86}$Sr	Sr/Ca	Li/Ca	Mg/Ca	Mg/Li
	[‰]	[mmol/mol]	[µmol/mol]	[mmol/mol]	[mol/mmol]
1	0.190	9.98	9.023	2.938	0.326
2	0.188	9.73	9.084	2.678	0.295
3	0.196	9.92	10.868	3.266	0.300
4	0.202	10.03	12.571	3.508	0.279
5	0.179	10.17	13.213	3.677	0.278
6	0.181	10.25	15.222	3.997	0.263
7	0.208	9.85	14.675	3.884	0.265

VI.8. References

Adkins, J., Boyle, E.A., Curry, W.B., Lutringer, A. 2003. Stable isotopes in deep-sea corals and a new mechanism for "vital effects". Geochim. Cosmochim. Acta 67, 1129–1143.

Allison, N., Finch, A.A., 2004, High-resolution Sr/Ca records in modern *Porites lobata* corals: effects of skeletal extension rate and architecture. Geochem. Geophys, Geosys, 5, Q05001. doi:10.1029/ 2004GC000696

Beck, J.W., Edwards, R.L., Ito, E., Taylor, F.W., Recy, J., Rougerie, F., Joannot, P., Henin, C. 1992. Sea-surface temperature from coral skeletal strontium calcium ratios. Science 257 (5070), 644–647.

Böhm, F., Gussone, N., Eisenhauer, A., Dullo, W.-Chr., Reynaud, S., Paytan, A. 2006. Calcium isotope fractionation in modern scleractinian corals. Geochim. Cosmochim. Acta 70 (17), 4452–4462.

Blamart, D., Rollion-Bard, C., Meibom, A., Cuif, J.-P., Juillet-Leclerc, A., Dauphin, Y. 2007. Correlation of boron isotopic composition with ultrastructure in the deep-sea coral *Lophelia pertusa*: implications for biomineralization and paleopH. Geochem. Geophys. Geosyst. 8, Q12001; doi:10.1029/ 2007GC001686.

Brahmi, C., Meibom, A., Smith, D.C., Stolarski, J., Auzoux-Bordenave, S., Nouet, J., Doumenc, D., Djediat, C., Domart-Coulon, I., 2010. Skeletal growth, ultrastructure and composition of the azooxanthellate scleractinian coral *Balanophyllia regia*. Coral Reefs 29, 175–189.

Bryan, S.P., Marchitto, T.M. 2008. Mg/Ca-temperature proxy in benthic foraminifera: new calibrations from the Florida Straits and a hypothesis regarding Mg/Li. Paleoceanogr. 23, PA2220.

Case, D., Robinson, L.F., Auro, M.E., Gagnon, A.C. 2010. Environmental controls on Mg and Li in deep-sea scleractinian coral. Earth Planet. Sci. Lett. 300 (3-4), 215–225.

Cohen, A.L., Owens, K.E., Layne, G.D., Shimizu, N. 2002. The effect of algal symbionts on the accuracy of Sr/Ca paleo-temperatures from corals. Science 296, 331–333.

Cohen, A.L., Gaetani, G.A., Lundälv, T., Corliss, B.H., George, R.Y. 2006. Compositional variability in a cold-water scleractinian, *Lophelia pertusa*: New insights into "vital effects". Geochem. Geophys. Geosys. 7 (12), Q12004.

Cheng. H., Adkins, J., Edwards, R.L., Boyle, E.A., 2000. U-Th dating of deep-sea corals. Geochim. Cosmochim. Acta 64, pp. 2401–2416

Corrége, T., 2006. Sea surface temperature and salinity reconstructions from coral geochemical tracers, Paleogeogr. Palaeoclim. Palaeoecol., 232, 408–428.

Dullo, W.-Chr., Flögel, S., Rüggeberg, A. 2008. Cold-water coral growth in relation to the hydrography of the Celtic and Nordic European continental margin. Mar. Ecol. Prog. Ser. 371, 165–176.

Erez, J., Braun, A., 2007. Calcification in hermatypic corals based on direct seawater supply to the biomineralization site. Geochim. Cosmochim. Acta 71 (15), A260.

Fietzke, J., Eisenhauer, A. 2006. Determination of temperature-dependent stable strontium isotope ($^{88}Sr/^{86}Sr$) fractionation via bracketing standard MC-ICP-MS. Geochem. Geophys. Geosys. 7 (8), Q08009.

Finch, A.A., Allison, N., 2008. Mg structural state in coral aragonite and implications for the paleoenvironmental proxy. Geophys. Res. Lett. 35, L08704

Freiwald, A., Fosså, J.H., Grehan, A., Koslow, T., Roberts, J.M. 2004. Cold-water coral reefs. UNEP-WCMC Biodiv. Ser., Cambridge 22, 84 pp.

Gaetani, G.A., Cohen, A.L. 2006. Element partitioning during precipitation of aragonite from seawater: A framework for understanding paleoproxies. Geochim. Cosmochim. Acta 70, 4617–4634.

Gaetani, G.A., Cohen, A.L., Wang, Z., Crusius, J. 2011. Rayleigh-based multi-element coral thermometry: a biomineralization approach to developing climate proxies. Geochim Cosmochim. Acta 75, 1920–1932.

Gagan, M.K., Ayliffe, L.K., Hopley, D., Cali, J.A., Mortimer, G.E., Chappell, J., McCulloch, M., Head, M.J., 1998. Temperature and surface ocean water balance of the mid-Holocene tropical western Pacific, Science 279, 1014–1018.

Gagnon, A.C., Adkins, J.F., Fernandez, D.P., Robinson, L.F. 2007. Sr/Ca and Mg/Ca vital effects correlated with skeletal architecture in a scleractinian deep-sea coral and the role of Rayleigh fractionation. Earth Planet. Sci. Lett. 261, 280–295.

Gagnon, A.C., Adkins, J.F., Erez, J., 2012. Seawater transport during biomineralization. Earth Planet. Sci. Lett. 150-161, 329–330.

Gass S.E., Roberts, J.M. 2010. Growth and branching patterns of *Lophelia pertusa* (Scleractinia) from the North Sea. J. Mar. Biol. Assoc. UK. 91, 831–835.

Gladfelter, E.H. 1982. Skeletal development in *Acropora cervicornis*: I. Patterns of calcium carbonate accretion in the axial corallite. Coral Reefs 1, 45–51.

Greaves, M., Barker, S., Daunt, C., Elderfield, H. 2005. Accuracy, standardization, and interlaboratory calibration standards for foraminiferal Mg/Ca thermometry, Geochem. Geophys. Geosys. 6, Q02D13; doi:10.1029/2004GC000790.

Hathorne, E., Felis, T., James, R.H., Thomas, A., 2011. Laser ablation ICP-MS screening for coral diagenetically affected areas applied to Tahiti coral from the last deglaciation Geochim. Cosmochim. Acta 75, 1490–1506.

Hathorne, E., Felis, T., Suzuki, A., Kawahata, H., Gabioch, G., submitted.Lithium in the aragonite skeletons of massive *Porites* corals: A new tool to reconstruct tropical sea surface temperatures. submitted to Paleoceanography.

Hodell, D. A., Mead, G. A., and Mueller, P. A., 1990. Variation in the strontium isotopic composition of seawater (8 Ma to present) : Implications for chemical weathering rates and dissolved fluxes to the oceans. *Chemical Geology: Isotope Geoscience section* **80**, 291-307.

Kinsman, D.J.J., Holland, H.D. 1969. The co-precipitation of cations with $CaCO_3$–IV. The co-precipitation of Sr^{2+} with aragonite between 16°C and 96°C. Geochim. Cosmochim. Acta 33, 1–17.

Krabbenhöft, A., Fietzke, J., Eisenhauer, A., Liebetrau, V., Böhm, F., Vollstaedt, H. 2009. Determination of radiogenic and stable strontium isotope ratios ($^{87}Sr/^{86}Sr/\delta^{88/86}Sr$) by thermal ionization mass spectrometry applying an $^{87}Sr/^{84}Sr$ double spike. J. Anal. At. Spectrom. 24, 1267–1271.

Krabbenhöft, A., Eisenhauer, A., Böhm, F., Vollstaedt, H., Fietzke, J., Liebetrau, V., Augustin, N., Peucker-Ehrenbrink, B., Müller, M.N., Horn, C., Hansen, B.T., Nolte, N., Wallmann, K. 2010. Constraining the marine strontium budget with natural strontium isotope fractionations ($^{87}Sr/^{86}Sr^*$, $\delta^{88/86}Sr$) of carbonates, hydrothermal solutions and river waters. Geochim. Cosmochim. Acta 74 (14), 4097–4109.

Liebetrau, V., Eisenhauer, A., Krabbenhöft, A., Fietzke, J., Böhm, F., Rüggeberg, A., Gürs, K. 2009. New perspectives on the marine Sr-isotope record: $\delta^{88/86}Sr$, $^{87}Sr/^{86}Sr^*$ and $\delta^{44/40}Ca$ signatures of aragonitic molluscs throughout the last 27 Ma. Geochim. Cosmochim. Acta 73, A762.

Liu, H-C., You, C-F., Huang, K-F., Chung, C-H. 2012. Precise determination of triple Sr isotopes (δ^{87} and $\delta^{88}Sr$) using MC-ICP-MS. Talanta 88, 338-344.

López Correa, M., Montagna, P., Vendrell, B., McCulloch, M. & Taviani, M., 2010. Stable isotopes ($\delta^{18}O$ and $\delta^{13}C$), trace and minor element compositions of Recent scleractinians and Last Glacial bivalves at the Santa Maria di Leuca deep-water coral province, Ionian Sea.- Deep-Sea Research II, 57 (5/6), 471-486; doi:10.1016/j.dsr2.2009.08.016.

Lutringer, A., Blamart, D., Frank, N., Labeyrie, L. 2005. Paleotemperatures from deep-sea corals: scale effects. In: Freiwald, A., Roberts, J.M. (Eds.), Cold-water Corals and Ecosystems. Springer-Verlag, pp. 1081–1096.

Maier, C., Hegeman, J., Weinbauer, M.G., Gattuso, J.P. 2009. Calcification of the cold-water coral *Lophelia pertusa* under ambient and reduced pH. Biogeosci. 6(8), 1671–1680.

Marriott, C.S., Henderson, G.M., Belshaw, N.S., Tudhope, A.W. 2004. Temperature dependence of δ^7Li, $\delta^{44}Ca$ and Li/Ca during growth of calcium carbonate. Earth Planet. Sci. Lett. 222, 615–624.

Meibom, A., Cuif, J., Hillion, F., Constantz, B., Juillet-Leclerc, A., Dauphin, Y., Watanabe, T., Dunbar, R. 2004. Distribution of magnesium in coral skeleton. Geophys. Res. Lett. 31. p. L23306 http://dx.doi.org/10.1029/2004GL021313

Meibom, A., Cuif, J.-P., Houlbreque, F., Mostefaoui, S., Dauphin, Y., Meibom, K.L., Dunbar, R. 2008. Compositional variations at ultra-structure length scales in coral skeleton. Geochim. Cosmochim. Acta 72 (6), 1555–1569.

McArthur, J.M. 1994. Recent trends in strontium isotope stratigraphy. Terra Nova 6(4), 331–358.

Mienis, F., de Stigter, H.C., White, M., Duineveld, G., de Haas, H. and van Weering, T.C.E., 2007. Hydrodynamic controls on cold-water coral growth and carbonate-mound development at the SW and SE Rockall Trough Margin, NE Atlantic Ocean. Deep Sea Res. Part I: Oceanographic Research Papers, 54: 1655-1674.

Mitsuguchi, T., Matsumoto, E., Abe, O., Uchida, T., Isdale, P.J. 1996. Mg/Ca thermometry in coral-skeletons. Science 274 (5289), 961–963.

Montagna, P., McCulloch, M., Taviani, M., Remia, A., Rouse, G. 2005. High-resolution trace and minor element compositions in deep-water scleractinian corals (*Desmophyllum dianthus*) from the Mediterranean Sea and the Great Australian Bight. In: Freiwald, A., Roberts, J.M. (Eds.), Cold-water Corals and Ecosystems. Springer-Verlag, pp. 1109–1126.

Mortensen, P.B., Rapp, H.T. 1998. Oxygen and carbon isotope ratios related to growth line patterns in skeletons of *Lophelia pertusa* (L) (Anthozoa, Scleractinia): Implications for determination of linear extension rates. Sarsia 83(5), 433–446.

Ohno T., Komiya T., Ueno Y., Hirata T. and Maruyama S. (2008) Determination of $^{88}Sr/^{86}Sr$ mass-dependent isotopic and radiogenic isotope variation of $^{87}Sr/^{86}Sr$ in the neoproterozoicdoushantuo formation. Gondwana Res. 14, 126–133.

Okai, T., Suzuki, A., Kawahata, H., Terashima, S., Imai, N. 2002. Preparation of a new Geological Survey of Japan geochemical reference material: coral JCp-1, Geostandards Newsletter 26, 95–99.

Orejas, C., Gori, A., Gili, J.M. 2008. Growth rates of live *Lophelia pertusa* and *Madrepora oculata* from the Mediterranean Sea maintained in aquaria. Coral Reefs, 27 (2), 255.

Politi, Y., Batchelor, D.R., Zaslansky, P., Chmelka, B.F., Weaver, J.C., Sagi, I., Weiner, S., Addadi, L., 2010. Role of magnesium ion in the stabilization of biogenic amorphous calcium carbonate: a structure-function investigation. Chem. Mater. 22, 161–166.

Raddatz, J., Rüggeberg, A., Margreth, S., Dullo, W.-Chr., IODP Expedition 307 Scientific Party 2011. Paleoenvironmental reconstruction of Challenger Mound initiation in the Porcupine Seabight, NE Atlantic. Mar. Geol. 282, 79–90; doi:10.1016/j.margeo.2010.10.019

Roberts, J.M., Wheeler, A.J., Freiwald, A. 2006. Reefs of the deep: the biology and geology of cold-water coral ecosystems. Science 312, 543–547.

Roberts, J-M., Wheeler, A., Freiwald, A., Cairns, S., 2009. Cold-Water-Corals: The Biology and Geoogy of Deep-Sea coral Habitats. Cambridge University Press. pp. 339

Rollion-Bard, C., Blamart, D., Cuif, J.-P., Dauphin, Y. 2010. *In situ* measurements of oxygen isotopic composition in deep-sea coral, *Lophelia pertusa*: re-examination of the current geochemical models of biomineralization. Geochim. Cosmochim. Acta 74, 1338–1349.

Rosenthal, Y., Field, M.P., Sherrell, R.M. 1999. Precise determination of element/calcium ratios in calcareous samples using sector field inductively coupled plasma mass spectrometry. Anal. Chem. 71 (15), 3248–3253.

Rüggeberg, A., Dullo, C., Dorschel, B., Hebbeln, D. 2007. Environmental changes and growth history of a cold-water carbonate mound (Propeller Mound, Porcupine Seabight). Internat. J. Earth Sci. 96, 57–72.

Rüggeberg, A., Fietzke, J., Liebetrau, V., Eisenhauer, A., Dullo, W.-Chr., Freiwald, A. 2008. Stable strontium isotopes ($\delta^{88/86}$Sr) in cold-water corals - a new proxy for the reconstruction of intermediate ocean water temperatures. Earth Planet. Sci. Lett. 269 (3-4), 569–574.

Shen, G.T., Dunbar, R.B. 1995. Environmental controls on uranium in reef corals. Geochim. Cosmochim. Acta 59, 2009–2024.

Shen, C.C., Lee, T., Chen, C.-Y., Wang, C.-H., Dai, C.-F., Li, L.-A. 1996. The calibration of D[Sr/Ca] versus sea surface temperature relationship for *Porites* corals. Geochim. Cosmochim. Acta 60, 3849–3858.

Shirai, K., Kusakabe, M., Nakai, S., Ishii, T., Watanabe, T., Hiyagon, H., Sano, Y. 2005. Deepsea coral geochemistry: implication for the vital effect. Chem. Geol. 224, 212–222.

Sinclair, D.J., Williams, B., Risk, M. 2006. A biological origin for climate signals in corals - Trace element "vital effects" are ubiquitous in scleractinian coral skeletons. Geophys. Res. Lett. 33 (17). doi:10.1029/2006GL027183.

Smith, S.V., Buddemeier, R.W., Redalje, R.C., Houck, J.E. 1979. Strontium-calcium thermometry in coral skeletons. Science 204 (4391), 404–407.

Smith, J.E., Schwarcz, H.P., Risk, M.J., McConnaughey, T.A., Keller, N. 2000. Paleotemperatures from deep-sea corals: overcoming 'vital effects'. Palaios 15, 25–32.

Smith, J.E., Schwarcz, H.P., Risk, M.J. 2002. Patterns of isotopic disequilibria in azooxanhtellate coral skeletons. Hydrobiologia 471, 111–115.

Stanley, G.D., Fautin, D.G., 2001. The origin of modern corals. Science. 291, 1913–1914.

Strømgren, T. 1971. The vertical and horizontal distribution of *Lophelia pertusa* (Linné) in Trondheimsfjorden on the west coast of Norway. K. Norske Vidensk. Selsk. Skr. 6, 1–9.

Tambutte, E., Tambutte, S., Segonds, N., Zoccola, D., Venn, A., Erez, J., Allemand, D., 2011. Calcein labelling and electrophysiology: insights on coral tissue permeability and calcification. Proc. R. Soc. B. doi:10.1098/rspb.2011.0733.

Taviani, M., Remia, A., Corselli, C., Freiwald, A., Malinverno, E., Mastrototaro, F., Savini, A., Tursi, A. 2005. First geo-marine survey of living cold-water *Lophelia* reefs in the Ionian Sea (Mediterranean basin). Facies 50 (3-4), 409–417.

Thébault, J., B. R. Schöne, N. Hallmann, M. Barth, Nunn, V. E., 2009. Investigation of Li/Ca variations in aragonitic shells of the ocean quahog *Arctica islandica*, northeast Iceland, Geochem. Geophys. Geosyst., 10(12), Q12008.

Veizer, J. 1989. Strontium isotopes in seawater through time. Annu. Rev. Earth Planet. Sci. 17, 141–167.

Vollstaedt, H., Eisenhauer, A., Böhm, F., Fietzke, J., Wallmann, K., Liebetrau, V., Krabbenhöft, A., Farkaš, J., Tomašových, A., and Veizer, J., submitted. Linking marine carbonate burial and long-term anoxia to the end-Permian mass extinctions (Geology)

VII. Chapter

Summary and outlook

VII.1. Summary

This study the first Phanerozoic seawater $\delta^{88/86}Sr_{sw}$ record was reconstructed and interpreted. In summary, we attribute time-dependent changes in $\delta^{88/86}Sr_{sw}$ to imbalances between the Sr input and output fluxes. These imbalances are primarily controlled by changes in carbonate-related Sr fluxes from sedimentation and shelf weathering. In particular, first time reconstructed Sr carbonate fluxes were related to long-term changes in the dominant mineralogy of inorganic carbonates in the ocean and intervals of glaciations and ocean anoxia.

For this, a Sr double spike method for TIMS was developed, which is able to enhance the precision of the bracketing standard technique and to correct for mass-dependent fractionation during the chemical treatment of samples.

This method was applied to modern river waters, hydrothermal solutions, marine carbonates, and seawater to investigate the modern marine Sr budget. Results reveal disequilibrium of the modern ocean with respect to Sr isotopes and fluxes. In particular, glacial/interglacial carbonate shelf weathering rates are considered to change threefold during the last ~20ka, implying the importance of carbonate fluxes to the marine Sr budget.

Modern brachiopod samples have been found to serve as a reliable archive for $\delta^{88/86}Sr_{sw}$, being independent of habitat location, water temperature, and salinity with a mean of 0.176±0.016‰. Extinct belemnites show similar $\delta^{88/86}Sr_{cc}$ when compared to coeval brachiopod samples, implying a fractionation factor of $\Delta^{88/86}Sr_{sw\text{-}cc}$ = -0.21‰ for both species with respect to modern seawater. Major fluctuations in Phanerozoic seawater $\delta^{88/86}Sr_{sw}$ suggest severe changes in the carbonate-related flux of Sr ($F(Sr)_{carb}$). A consequent numerical model approach allows a complete constraint of the Phanerozoic Sr budget of the ocean,

including $F(Sr)_{carb}$ and alteration rates of the oceanic crust. $[Sr]_{sw}$ and $F(Sr)_{carb}$ vary in the range between 25mmol/l and 300mmol/l and $-5x10^{10}$mol/yr and $+1x10^{10}$mol/yr, respectively.

On short-term timescales, these changes are related to carbonate sedimentation, carbonate shelf recrystallization/weathering and dissolution, and ocean anoxia within the Phanerozoic ocean. In particular, massive long-term carbonate burial rates at the Permian/Triassic transition are considered to be a result from increased carbonate alkalinity resulting from BSR in the deep anoxic waters of the stratified P/T ocean. This ~21Myr-lasting ocean stratification is considered to be intermitted by the occasional overturning of anoxic and H_2S-rich deep waters to the surface ocean. These conditions caused a biogeochemical crisis and physiological stress to marine life. Most likely, the combination of short-term surface ocean acidification induced by the Siberian Trap volcanism (SOBOLEV et al., 2011) with long-term seawater anoxia accelerated and amplified the P/T boundary mass extinction, making it the most extreme catastrophe for life on Earth.

On long-term timescales, modeled $\delta^{88/86}Sr_{sw}$, $(Sr/Ca)_{sw}$, and $D(F)_{Sr}$ are in good agreement with literature data and are correlated with times of proposed "aragonite seas" and "calcite seas". This underlines the importance of $F(Sr)_{carb,}$ being the main controlling factor on $\delta^{88/86}Sr_{sw}$, which is in contrast to the $^{87}Sr/^{86}Sr$ system that is controlled by the balance between continental weathering and hydrothermal activity. Further, the considerable changes in modelled Sr residence time (τSr), being in between 1.2Myrs and 19.6Myrs, significantly affects the sensitivity of the two Sr isotope systems. In accordance with modeled τSr, highest rate of change in $\delta^{88/86}Sr_{sw}$ and $(^{87}Sr/^{86}Sr)_{sw}$ is observed during times of low τSr.

With the new Phanerozoic $\delta^{88/86}Sr_{sw}$ record a second isotope reference curve for the Sr isotope system is produced which has the potential to significantly improve the precision of the SIS by applying combined $\delta^{88/86}Sr$-$^{87}Sr/^{86}Sr$ isotope stratigraphy.

VII.2. Outlook

With the reconstruction of carbonate fluxes at the P/T transition, severe long-term changes in the marine carbonate budget and redox chemistry were predicted. These changes in environmental conditions should be also investigated by redox-sensitive proxies like Mo, U, Cr isotopes and/or I/Ca ratios in marine carbonates (JENKYNS, 2010; LU et al., 2010; BRENNECKA et al., 2011). In particular, these studies have to investigate longer time intervals of ~20Myr to determine the duration of the extinction event. However, proposed short-term (~400kyr) P/T ocean acidification as revealed by Ca isotopes (PAYNE et al., 2010; HINOJOSA et al., 2012) should be studied by chemically similar Sr isotopes. In particular, these studies have to find a reliable archive for $\delta^{88/86}Sr_{sw}$ and $\delta^{44/40}Ca_{sw}$, as previous studies investigated unreliable carbonate matrix and biogenic apatite samples (SMALLEY et al., 1994; PAYNE et al., 2010; HINOJOSA et al., 2012). Further, studies on boron isotopes might be able to reconstruct short-term ocean acidification during this event, assuming that further studies will prove the applicability of $\delta^{11}B$ as a paleo-seawater pH proxy in the Phanerozoic.

For the P/T boundary it has been shown that carbonate sedimentation could be linked to ocean anoxia and alkalinity production by BSR. To test if these phenomena are similarly causatively linked during other periods of ocean anoxia, combined $\delta^{88/86}Sr$ and $\delta^{34}S$ could be applied to marine carbonates during Ocean Anoxic Events (OAE) in the Cretaceous. This proposal has been submitted to the Deutscher Akademischer Austauschdienst (DAAD) in July 2012. The experimental approach could be enhanced by a numerical model approach to: i) to explore the effect of ocean anoxia on the carbonate budget in the Early Aptian, ii) to verify and quantify changes in the marine S cycle during the event, iii) to determine the area expansion and intensity of ocean anoxia during OAE 1a, and iv) to assess the timing of these processes to infer feedback mechanisms. The magnitude and timing of these processes will significantly contribute to the understanding of element cycling during anoxic conditions in

the water column. This knowledge could then be transferred to the evolution of modern OMZs to predicted changes in marine biogeochemical changes and global climate.

Long-term reconstructed carbonate fluxes confirm previous hypotheses that Sr seawater chemistry is closely linked to the dominant carbonate mineralogy ("calcite seas", "aragonite seas") (STEUBER and VEIZER, 2002). However, the causative mechanism of similar trends in $(Sr/Ca)_{sw}$, $\delta^{88/86}Sr_{sw}$, $\delta^{44/40}Ca_{sw}$, $(Mg/Ca)_{sw}$, and carbonate mineralogy remains enigmatic. Specifically, the role of MOR spreading and dolomitization rates is still being debated. The investigation of Phanerozoic seawater Mg isotopes, being sensible to dolomitization rates, is thought to significantly contribute to our understanding of the underlying geological processes.

This study showed a Phanerozoic $\delta^{88/86}Sr_{sw}$ record, covering a time interval from the Ordovician period to the Cretaceous period. To investigate seawater chemistry from the Cretaceous to Holocene period, a detailed reconstruction of a $\delta^{88/86}Sr_{sw}$ record for the last ~150Ma would be necessary. In particular, numerical modelling studies for the marine Sr budget would benefit from published MOR spreading rates during this time interval (ROWLEY, 2002), therefore reducing the number of unknowns in the differential equations.

Further applications should take advantage of the combined use of $\delta^{88/86}Sr$ and $^{87}Sr/^{86}Sr$ data. Here, isotope fractionation and mixing processes could be simultaneously investigated and illustrated in three-isotope-plots. Specifically, the weathering of silicate rocks could be studied to examine the processes of incongruent weathering and isotope fractionation during chemical weathering.

VII.3. References

Brennecka, G. A., Herrmann, A. D., Algeo, T. J., and Anbar, A. D., 2011. Rapid expansion of oceanic anoxia immediately before the end-Permian mass extinction. Proceedings of the National Academy of Sciences 108, 17631-17634.

Hinojosa, J. L., Brown, S. T., Chen, J., DePaolo, D. J., Paytan, A., Shen, S.-z., and Payne, J. L., 2012. Evidence for end-Permian ocean acidification from calcium isotopes in biogenic apatite. Geology.

Jenkyns, H. C., 2010. Geochemistry of oceanic anoxic events. Geochem. Geophys. Geosyst. 11, Q03004.

Lu, Z., Jenkyns, H. C., and Rickaby, R. E. M., 2010. Iodine to calcium ratios in marine carbonate as a paleo-redox proxy during oceanic anoxic events. Geology 38, 1107-1110.

Payne, J. L., Turchyn, A. V., Paytan, A., DePaolo, D. J., Lehrmann, D. J., Yu, M., and Wei, J., 2010. Calcium isotope constraints on the end-Permian mass extinction. Proceedings of the National Academy of Sciences 107, 8543-8548.

Rowley, D. B., 2002. Rate of plate creation and destruction: 180 Ma to present. Geol. Soc. Am. Bull. 114, 927-933.

Smalley, P. C., Higgins, A. C., Howarth, R. J., Nicholson, H., Jones, C. E., Swinburne, N. H. M., and Bessa, J., 1994. Seawater Sr Isotope Variations through Time - a Procedure for Constructing a Reference Curve to Date and Correlate Marine Sedimentary-Rocks. Geology 22, 431-434.

Sobolev, S. V., Sobolev, A. V., Kuzmin, D. V., Krivolutskaya, N. A., Petrunin, A. G., Arndt, N. T., Radko, V. A., and Vasiliev, Y. R., 2011. Linking mantle plumes, large igneous provinces and environmental catastrophes. Nature 477, 312-316.

Steuber, T. and Veizer, J., 2002. Phanerozoic record of plate tectonic control of seawater chemistry and carbonate sedimentation. Geology 30, 1123-1126.

VIII. Appendix

VIII.1. Conference abstracts

Goldschmidt Conference 2009, 21.06 – 26.06.2009, Davos, Switzerland

$\delta^{88/86}$Sr record of phanerozoic marine carbonates

H. VOLLSTAEDT[1], A. EISENHAUER[1], A. KRABBENHÖFT[1], J. FARKAŠ[2] AND J. VEIZER[3]

[1]IFM-GEOMAR, Leibniz Institute of Marine Science, Wischhofstr. 1-3, D-24148 Kiel, Germany
[2]Harvard Univ, Dept Earth & Planetary Sci, Cambridge, MA 02138 USA
[3]Carleton University and Ottawa-Carleton Geoscience Centre, Ottawa, ON, Canada K1S 5B6

For the first time we extend and complete earlier application of radiogenic Sr isotopes [1] with a simultaneous measurement of radiogenic and stable strontium (Sr) isotopes [2] ($\delta^{88/86}$Sr[‰]= (^{88}Sr/^{86}Sr$_{sample}$/^{88}Sr/^{86}Sr$_{NBS987}$-1)*1000). Applying a ^{87}Sr/^{84}Sr-double spike we measured paired $\delta^{88/86}$Sr-^{87}Sr/^{86}Sr* ratios of phanerozoic marine carbonates samples which were screened for diagenesis prior to the measurement. For compatibility to earlier measurements ^{87}Sr/^{86}Sr* ratios are also renormalized to $\delta^{88/86}$Sr=0‰ (^{88}Sr/^{86}Sr=8.375209). Data reduction and denormalization is performed using an iterative algorithm closely following the one for Ca-isotopes developed earlier by Heuser et al. [3]. External $\delta^{88/86}$Sr reproducibility based on an internal coral carbonate standard (JCp-1) corresponds to ~0.013‰ (2σ of the mean).

Our data reveal that $\delta^{88/86}$Sr of phanerozoic brachiopods and belemnites samples are in the range of modern marine carbonates (JCp-1 coral standard value: 0.197±0.013‰) but isotopically lighter than modern seawater ($\delta^{88/86}$Sr$_{IAPSO}$= 0.386±0.006‰) being in the range between ~0.081 and ~0.370‰ (mean of 0.189±0.031‰). We observe a constant increase in $\delta^{88/86}$Sr from the beginning of the Paleozoic towards the upper Permian. Highest values (~0.370‰) of $\delta^{88/86}$Sr are reached close to the Permian/Trias boundary. There is no correlation between $\delta^{88/86}$Sr, ^{87}Sr/^{86}Sr* and δ^{18}O on phanerozoic timescale.

Annual Meeting of the Geologische Vereinigung, 05.10 – 07.10.2009, Göttingen, Germany

The Phanerozoic $\delta^{88/86}Sr$ record of marine carbonates – A new dimension for the Sr isotope system

H. VOLLSTAEDT[1], A. EISENHAUER[1*], A. KRABBENHÖFT[1], J. FARKAŠ[2] AND J. VEIZER[3]

[1]IFM-GEOMAR, Leibniz Institute of Marine Science, Wischhofstr. 1-3, D-24148 Kiel, Germany (*correspondence: aeisenhauer@ifm-geomar.de)
[2]Harvard Univ, Dept Earth & Planetary Sci, Cambridge, MA 02138 USA
[3]Carleton University and Ottawa-Carleton Geoscience Centre, Ottawa, ON, Canada K1S 5B6

For the first time we extend and complete the application of the radiogenic Sr isotope system ($^{87}Sr/^{86}Sr$) [1] with a simultaneous measurement of radiogenic and stable strontium (Sr) isotopes [2] ($\delta^{88/86}Sr[‰]=(^{88}Sr/^{86}Sr_{sample}/^{88}Sr/^{86}Sr_{NBS987}-1)*1000$). Taking Sr isotope fractionation into account this opens a new dimension for the Sr isotope system allowing to gain quantitative information about the Sr output from the ocean. Applying a $^{87}Sr/^{84}Sr$-double spike we measured paired $\delta^{88/86}Sr$-$^{87}Sr/^{86}Sr$* ratios of 34 Phanerozoic marine carbonates samples which were screened for diagenesis prior to the measurement. The $^{87}Sr/^{86}Sr$* ratios are renormalized to $\delta^{88/86}Sr$=0‰ ($^{88}Sr/^{86}Sr$=8.375209) in order to be compatible to the radiogenic Sr isotope system values. Data reduction and denormalization follows an iterative algorithm by Krabbenhöft et al. [3]. External $\delta^{88/86}Sr$ reproducibility based on an internal coral carbonate standard (JCp-1) corresponds to 0.008‰ (2SEM).

Our data reveal that the $\delta^{88/86}Sr$ values of Phanerozoic brachiopods and belemnites samples are in the range of modern marine carbonates (JCp-1 coral standard value: 0.192±0.008‰) but isotopically lighter than modern seawater ($\delta^{88/86}Sr_{IAPSO}$= 0.385±0.007‰) being in the range between ~0.080‰ and ~0.370‰ (mean of 0.168). We observe a decrease in $\delta^{88/86}Sr$ from Ordovician (0.200‰) to Silurian period (0.080‰) with a consequent increase in $\delta^{88/86}Sr$

towards the upper Permian period. Highest values (~0.370‰) of $\delta^{88/86}Sr$ are reached close to the Permian/Triassic boundary.

This study examines the main factors that control $\delta^{88/86}Sr$ on Phanerozoic timescale. It was found that temperature is not the main factor that drives $\delta^{88/86}Sr$ of marine carbonates. Rather we suggest that the $\delta^{88/86}Sr$ of Phanerozoic seawater is controlled by changes in the Sr fluxes in and out of the ocean. Modeling of our data allows a quantification of the Phanerozoic imbalance between the Sr input and output fluxes of the ocean.

[1] Veizer et al. (1999) *Chem Geol.* **161**, 59-88 [2] Fietzke and Eisenhauer (2006) *Geochem. Geophys. Geosyst*. **7**, Q08009 [3] Krabbenhöft et al. (2009), *J. of Analytical Atomic Spectr.*, **24**, 1267-1271

AGU Fall Meeting 2009, 14.12 – 18.12.2009, San Francisco, USA

A new dimension to the Sr isotope system - $^{88/86}Sr$ record of marine carbonates in the Phanerozoic

H. VOLLSTAEDT[1], A. EISENHAUER[1*], A. KRABBENHÖFT[1], J. FARKAŠ[2] AND J. VEIZER[3]

[1]IFM-GEOMAR, Leibniz Institute of Marine Science, Wischhofstr. 1-3, D-24148 Kiel, Germany (*correspondence: aeisenhauer@ifm-geomar.de)
[2]Harvard Univ, Dept Earth & Planetary Sci, Cambridge, MA 02138 USA
[3]Carleton University and Ottawa-Carleton Geoscience Centre, Ottawa, ON, Canada K1S 5B6

For the first time we extend and complete the application of the radiogenic Sr isotope system ($^{87}Sr/^{86}Sr$) [1] with a simultaneous measurement of radiogenic and stable strontium (Sr) isotopes [2] ($\delta^{88/86}Sr[‰]=(^{88}Sr/^{86}Sr_{sample}/^{88}Sr/^{86}Sr_{NBS987}-1)*1000$). Taking Sr isotope fractionation into account this opens a new dimension for the Sr isotope system allowing to gain quantitative information about the Sr output from the ocean. Applying a $^{87}Sr/^{84}Sr$-double spike we measured paired $\delta^{88/86}Sr$-$^{87}Sr/^{86}Sr$* ratios of 34 Phanerozoic marine carbonates

samples which were screened for diagenesis prior to the measurement. The $^{87}Sr/^{86}Sr^*$ ratios are renormalized to $\delta^{88/86}Sr=0‰$ ($^{88}Sr/^{86}Sr=8.375209$) in order to be compatible to the radiogenic Sr isotope system values. Data reduction and denormalization follows an iterative algorithm by Krabbenhöft et al. [3]. External $\delta^{88/86}Sr$ reproducibility based on an internal coral carbonate standard (JCp-1) corresponds to 0.008‰ (2SEM).

Our data reveal that the $\delta^{88/86}Sr$ values of Phanerozoic brachiopods and belemnites samples are in the range of modern marine carbonates (JCp-1 coral standard value: 0.192±0.008‰) but isotopically lighter than modern seawater ($\delta^{88/86}Sr_{IAPSO}$= 0.385±0.007‰) being in the range between ~0.080‰ and ~0.370‰ (mean of 0.168). We observe a decrease in $\delta^{88/86}Sr$ from Ordovician (0.200‰) to Silurian period (0.080‰) with a consequent increase in $\delta^{88/86}Sr$ towards the upper Permian period. Highest values (~0.370‰) of $\delta^{88/86}Sr$ are reached close to the Permian/Triassic boundary.

This study examines the main factors that control $\delta^{88/86}Sr$ on Phanerozoic timescale. It was found that temperature is not the main factor that drives $\delta^{88/86}Sr$ of marine carbonates. Rather we suggest that the $\delta^{88/86}Sr$ of Phanerozoic seawater is controlled by changes in the Sr fluxes in and out of the ocean. Modeling of our data allows a quantification of the Phanerozoic imbalance between the Sr input and output fluxes of the ocean.

[1] Veizer et al. (1999) *Chem Geol.* **161**, 59-88 [2] Fietzke and Eisenhauer (2006) *Geochem. Geophys. Geosyst*. **7**, Q08009 [3] Krabbenhöft et al. (2009), *J. of Analytical Atomic Spectr.*, **24**, 1267-1271

AGU Fall Meeting 2010, 13.12-17.12.2010, San Francisco, USA

Revisiting mid-Paleozoic ocean chemistry with the combined measurement of $^{87}Sr/^{86}Sr$ and $\delta^{88/86}Sr$ on Silurian brachiopods

H. VOLLSTAEDT[1]*, A. EISENHAUER[1], A. KRABBENHÖFT[1], V. LIEBETRAU[1], F. BÖHM[1], J. FARKAŠ[2], A. TOMAŠOVÝCH[3] AND J. VÉIZER[4]

[1]Leibniz Institute of Marine Science (IFM-GEOMAR), Wischhofstr. 1-3, D-24148 Kiel, Germany (*correspondence: hvollstaedt@ifm-geomar.de)
[2]Harvard Univ, Dept Earth & Planetary Sci, Cambridge, MA 02138 USA
[3]University of Chicago, Dept of the Geophysical Sciences, 5734 S. Ellis Avenue, Chicago, Illinois 60637 USA
[4]Carleton University and Ottawa-Carleton Geoscience Centre, Ottawa, ON, Canada K1S 5B6

With the extension of the conventional radiogenic Sr isotope system ($^{87}Sr/^{86}Sr$) [1] by a simultaneous measurement of radiogenic and stable strontium (Sr) isotopes ($\delta^{88/86}Sr[‰]=(^{88}Sr/^{86}Sr_{sample}/^{88}Sr/^{86}Sr_{NBS987}-1)*1000$) we are able to add new constraints to Strontium Isotope Stratigraphy (SIS) and the ocean chemistry of the past. By taking Sr isotope fractionation into account we open a new dimension to the Sr isotope system. This allows us to gain quantitative information about the Sr output of the ocean. Applying a $^{87}Sr/^{84}Sr$-double spike (DS) we measured paired $\delta^{88/86}Sr$-$^{87}Sr/^{86}Sr$ ratios of Silurian (444 – 416 Ma) and recent marine brachiopod samples which were screened for diagenesis prior to the measurement [1]. Data reduction and DS denormalization follows an iterative algorithm [2]. External $\delta^{88/86}Sr$ reproducibility based on an international coral carbonate standard (JCp-1) is 0.03‰ (2SD, n=26).

We found that modern brachiopods have similar values independent of habitat location, species and water temperature with a mean of 0.18‰ ± 0.02‰ (2SD, n=13). This provides further support that brachiopods are a reliable carbonate recording phase for $\delta^{88/86}Sr_{seawater}$. Previous studies showed that $\delta^{88/86}Sr$ of Phanerozoic seawater is controlled by changes in the Sr fluxes in and out of the ocean [3]. Our data reveal that Silurian brachiopods are isotopically light in stable Sr isotopes ($\delta^{88/86}Sr_{mean}$ = 0.12‰, n=20) compared to other

Phanerozoic brachiopod and belemnite samples ($\delta^{88/86}Sr$ = 0.07 – 0.36‰ [3]). This follows the foregone mass extinction event and glaciation during late Ordovician period when numerous groups of calcifying organisms disappeared. During the Silurian period both $^{87}Sr/^{86}Sr$ and $\delta^{88/86}Sr$ increase from 0.7081 and 0.07‰ to 0.7088 and 0.18‰, respectively. This might indicate changes in global tectonism (mid ocean spreading rates and continental weathering rates) as well as changes in the Sr fluxes in and out of the ocean. In terms of the Sr output flux of the ocean, isotopically light carbonates represent the most important Sr flux. Therefore, the radiation of mollusks, gastropods, brachiopods along with other calcifying organisms during the Silurian period may be responsible for increasing $\delta^{88/86}Sr_{seawater}$. Furthermore we observe a major shift in $\delta^{88/86}Sr$ during the Silurian period which may be caused by rapid changes in carbonate ocean chemistry and/or changes in the continental weathering regime. This is additionally supported by accompanying major changes in Sr concentrations of the ocean [4].

Ultimately, the combined measurement of radiogenic and stable Sr isotopes enhances our understanding of ocean chemistry of the past and increases the precision of SIS with the addition of a second Sr isotope reference curve.

[1] Veizer et al. (1999) *Chem Geol.* **161**, 59-88; [2] Krabbenhöft et al. (2009), *J. of Analytical Atomic Spectr.*, **24**, 1267-1271; [3] Vollstaedt et al. (2009), *Geochimica and Cosmochimica Acta*, **73**, 13, A1393; [4] Steuber and Veizer (2002), *Geology*, **30**, 1123-1126

EGU General Assembly 2011, 03.04 – 08.04.2011, Vienna, Austria

The Paleozoic $\delta^{88/86}Sr$ record of marine carbonates – Implications to ocean carbonate chemistry and mass extinction events

H. VOLLSTAEDT[1]*, A. EISENHAUER[1], A. KRABBENHÖFT[1], V. LIEBETRAU[1], F. BÖHM[1], J. FARKAŠ[2], A. TOMAŠOVÝCH[3] AND J. VÉIZER[4]

[1]Leibniz-Institut für Meereswissenschaften (IFM-GEOMAR), Wischhofstr. 1-3, D-24148 Kiel, Germany (*correspondence: hvollstaedt@ifm-geomar.de)
[2]Czech Geological Survey, Geologicka 6, 152 00 Praha 5, Czech Republic
[3]University of Chicago, Dept of the Geophysical Sciences, 5734 S. Ellis Avenue, Chicago, Illinois 60637 USA
[4]Carleton University and Ottawa-Carleton Geoscience Centre, Ottawa, ON, Canada K1S 5B6

Within the Phanerozoic Eon stratigraphic boundaries are often associated with the extinction of marine organisms. However, the reasons for these events are still discussed.

Strontium (Sr) is one of the most important divalent cations in calcium carbonate minerals and an important carrier of proxy information. In terms of the Sr output flux of the ocean, isotopically light carbonates represent the major Sr sink. Therefore, the geochemistry and stable Sr isotope composition is strongly coupled to the marine carbonate system. Consequently, variations in [Sr] and $\delta^{88/86}Sr$ becoming a suitable tool to investigate in the global carbonate budget in earth's history including the biotic turnover of calcifying organisms at stratigraphic boundaries which are expected to have a large influence on Sr geochemistry and isotope composition of seawater.

We extended the conventional radiogenic Sr isotope system ($^{87}Sr/^{86}Sr$) by a simultaneous measurement of radiogenic and stable Sr isotopes ($\delta^{88/86}Sr[‰]=(^{88}Sr/^{86}Sr_{sample}/^{88}Sr/^{86}Sr_{NBS987}-1)*1000$). With that we are able to add new constraints to Strontium Isotope Stratigraphy (SIS) and the ocean chemistry of the past. By taking Sr isotope fractionation into account we add an additional dimension to the radiogenic Sr isotope system. This allows us to gain quantitative information about the Sr output of the ocean. Applying a $^{87}Sr/^{84}Sr$-double spike (DS), we measured paired $\delta^{88/86}Sr$-$^{87}Sr/^{86}Sr$ ratios of ~100 modern and Paleozoic marine brachiopod samples which were screened for diagenetic alteration prior to the measurement

[1]. Data reduction and DS denormalization follows an iterative routine [2]. External reproducibility of $\delta^{88/86}Sr$ based on an international coral carbonate standard (JCp-1) is ~0.026‰ (2SD, n=26).

We found that modern brachiopods have similar values independent of habitat location, species and water temperature with a mean of 0.18‰ ± 0.02‰ (2SD, n=13). This provides further support that brachiopods provide a reliable carbonate recording phase for $\delta^{88/86}Sr_{seawater}$. In Paleozoic Eon we observe variations in $\delta^{88/86}Sr_{seawater}$ in the range of 0.25 – 0.45‰. On longterm timescales (~100 Ma) these variations in $\delta^{88/86}Sr_{seawater}$ follow the general distribution of "calcite seas" and "aragonite seas" [3], implying a control mechanism by $Mg/Ca_{seawater}$ ratios and further global spreading rates. On shorter timescales (residence time of Sr in the ocean of ~5 Ma) we observe a positive correlation of $\delta^{88/86}Sr_{seawater}$ and the number of marine genera [4] during mass extinction events in late Ordovician and mid-Devonian. This indicates the strong influence of marine calcifiers on the Sr budget of the ocean and gives us the opportunity of tracing back major extinction events in the Phanerozoic with sudden drops in the $\delta^{88/86}Sr_{sw}$ record. Furthermore, with changes in marine Phanerozoic [Sr] [5] and $^{87}Sr/^{86}Sr$ we are able to correlate these changes in Sr out- or influxes of the ocean.

Ultimately, the combined measurement of radiogenic and stable Sr isotopes enhances our understanding of ocean chemistry of the past and increases the precision of SIS with the addition of a second Sr isotope reference curve.

[1] Veizer et al. (1999), *Chem Geol.* **161**, 59-88; [2] Krabbenhöft et al. (2009), *J. of Analytical Atomic Spectr.*, **24**, 1267-1271; [3] Stanley and Hardie (1998), *P³*, **144**, 3-19[4] Sepkoski (1997), *J. of Paleontology* **71**, 533-539; [5] Steuber and Veizer (2002), *Geology*, **30**, 1123-1126

Goldschmidt Conference 2011, 14.08 – 19.08.2011, Prague, Czech Republic

The Paleozoic $\delta^{88/86}Sr_{seawater}$ record – Quantifying carbonate production rates at mass extinction events

H. VOLLSTAEDT[1]*, A. EISENHAUER[1], F. BÖHM[1], F. FIETZKE[1], A. KRABBENHÖFT[1], V. LIEBETRAU[1], J. FARKAŠ[2] AND J. VÉIZER[3]

[1]Leibniz-Institut für Meereswissenschaften (IFM-GEOMAR), Wischhofstr. 1-3, D-24148 Kiel, Germany (*correspondence: hvollstaedt@ifm-geomar.de)
[2]Czech Geological Survey, Geologicka 6, 152 00 Praha 5, Czech Republic
[3]University of Ottawa, Dept. of Earth Sciences, 140 Louis Pasteur, Ottawa, Canada K1N 6N5

Within the Phanerozoic Eon strata boundaries are often associated with the extinction of marine organisms. However, the reasons for these events are still discussed and quantitative changes in the marine carbonate system are lacking.

Strontium (Sr) is one of the most important divalent cations in calcium carbonate minerals and a carrier of proxy information. In terms of the Sr output flux of the ocean, isotopically light carbonates represent the major Sr sink. Consequently, variations in Sr/Ca and $\delta^{88/86}Sr$ are a suitable tool to investigate in the global carbonate budget throughout earth's history including the biotic turnover of calcifying organisms at stratigraphic boundaries which are expected to have a large influence on Sr geochemistry and isotope composition of seawater. These constraints can be combined with the weathering tracer potential of the $^{87}Sr/^{86}Sr_{seawater}$ ratio.

We measured paired $\delta^{88/86}Sr$-$^{87}Sr/^{86}Sr$ ratios of ~120 modern and Paleozoic marine brachiopod samples which were screened for diagenetic alteration prior to the measurement. Reproducibility of double spike derived $\delta^{88/86}Sr$ basing on an international coral carbonate standard (JCp-1) is 0.019‰ (2SD, n=26).

We observe local minima in $\delta^{88/86}Sr_{seawater}$ at mass extinction events accompanied with decreasing number of marine genera [1], emphasizing the strong coupling of the carbonate system to $\delta^{88/86}Sr$ of seawater. By taking changes in $^{87}Sr/^{86}Sr$, $\delta^{88/86}Sr$ and Sr/Ca we are able to make quantitive statements on the Sr input and output fluxes as well as changes in the

dominant carbonate mineralogy of marine calcifiers at the major Paleozoic mass extinction events, including the Permian/Triassic boundary. We found strong environmental changes at major extinction events with an associated response of marine calcifiers in dominant mineralogy and carbonate production rates.

[1] Sepkoski (1997), *J. of Paleontology* **71**, 533-539

Goldschmidt Conference 2012, 25.06 – 29.06.2012, Montréal, Canada

Marine carbonate burial rates at the Phanerozoic mass extinctions

HAUKE VOLLSTAEDT[1*], ANTON EISENHAUER[1], FLORIAN BÖHM[1], JAN FIETZKE[1], KLAUS WALLMANN[1], VOLKER LIEBETRAU[1], JURAJ FARKAŠ[2,3], ADAM TOMAŠOVÝCH[4], AND JÁN VEIZER[5]

[1] GEOMAR | Helmholtz-Zentrum für Ozeanforschung Kiel, hvollstaedt@geomar.de (* presenting author)
[2] Department of Geochemistry, Czech Geological Survey
[3] Department of Environmental Geosciences, Czech University of Life Sciences
[4] Department of Geophysical Sciences, The University of Chicago
[5] Ottawa-Carleton Geoscience Center, University of Ottawa

Several mass extinctions have disturbed the evolution of life during the Phanerozoic Eon. Information about the past environmental conditions and triggers for the extinctions can be inferred from the geological record and in particular from the analysis of different isotope systems (i.e. carbon, sulfur, and calcium) as well as the extinction selectivity [1].

To extend earlier published mass extinction scenarios we measured radiogenic ($^{87}Sr/^{86}Sr$) and stable strontium (Sr) isotope ratios ($\delta^{88/86}Sr$, [1]) simultaneously on globally distributed brachiopod and belemnite samples to constrain changes in Phanerozoic seawater chemistry. This includes quantitative information about the marine Sr output flux, primarily controlled by the burial of marine carbonates, as the precipitation of calcite and aragonite preferentially incorporates the light Sr isotope [2,3], leaving seawater isotopically heavier.

Our Phanerozoic $\delta^{88/86}Sr$ seawater record shows considerable variability from 0.25‰ to 0.60‰ suggesting major changes of the marine carbonate burial fluxes. To quantify our results we developed a numerical box model to reconstruct changes in the inventory and fluxes of seawater Sr, calcium (Ca), and total alkalinity (TA).

The model results reveal severe disturbances in the marine budgets of Sr (0-300 μmol/l), Ca (0-40 mmol/l), and TA (0-30 mmol/l) at the Phanerozoic extinction events, especially at the Permian/Triassic boundary. These changes in the marine carbonate system are explained by processes including carbonate production rates, (shelf) carbonate dissolution, ocean anoxia associated with bicarbonate production by bacterial sulfate reducers (BSR), and shifts in the dominant carbonate mineralogy (calcite/aragonite). The first time geochemical quantification of these processes is a novelty in the field of Paleocanography and will help to identify the causal processes leading to global mass extinctions in the marine realm.

[1] M. E. Clapham, J. L. Payne (2011), *Geology* **39**, 1059-1062.

[2] J. Fietzke, A. Eisenhauer (2006), *Geochem. Geophys. Geosyst.* **7**. [3] A. Krabbenhöft *et al. (2010)*, *Geochim. Cosmochim. Acta* **74**, 4097-4109.

VIII.2. Conference session proposals

AGU Fall Meeting 2012, 03.12 - 07.12.2012, San Francisco, USA

Reconstructing Phanerozoic seawater chemistry using non-traditional stable isotopes

Hauke Vollstaedt[1], Anton Eisenhauer[1], Christopher R. Pearce[2]

[1] GEOMAR | Helmholtz Centre for Ocean Research, Wischhofstraße 1-3, 24148 Kiel, Germany
[2] The Open University, Dept Earth & Environmental Science, Walton Hall, Milton Keynes, UK

Changes in the chemical and isotopic composition of seawater throughout Earth's history record variations in the biogeochemical processes that have controlled global environmental conditions. Understanding these records consequently enables us to determine the interaction of feedback mechanisms and how they relate to modern ocean processes. This session invites contributions presenting the latest findings using non-traditional stable isotope and multi-proxy approaches in ancient marine deposits. We welcome studies investigating both short- and long-term changes in the chemical evolution of Phanerozoic seawater, as well as those calibrating potential new proxies against existing paleo-records.

VIII.3. Manual for data evaluations of Sr DS TIMS technique

Manual stable Sr data reduction with Excel© (version: 29.05.2012)

EXCEL© spread sheet for stable Strontium data reduction

To ensure a comfortable data processing an EXCEL© spread sheet for data reduction was developed. The aim was to simplify Sr data reduction and to shorten the time needed for evaluation of raw data. Emphasis was put to clarity to prevent input errors. Furthermore, a number of criteria have been established in order to access the data quality. The current version is available at \\leibniz\users\FB2\MG\akolevica\QS-Sr-stabil\aktuelles Makro

Data export from TIMS

The following values have to be exported from the TIMS machine:

^{84}Sr; ^{85}Rb; ^{86}Sr; ^{87}Sr; ^{88}Sr; $^{88}Sr/^{84}Sr$; $^{86}Sr/^{84}Sr$; $^{87}Sr/^{84}Sr$; $^{88}Sr/^{86}Sr$

Here you have to make sure that:

- The "Header" of the files is exported (Export configuration, Fig.VIII.1)
- Invalid values are <u>not</u> marked (Export configuration, Fig. VIII.1)
- Choose only (D_i) in the "View Control" menu (red circle, VIII.Fig.1)

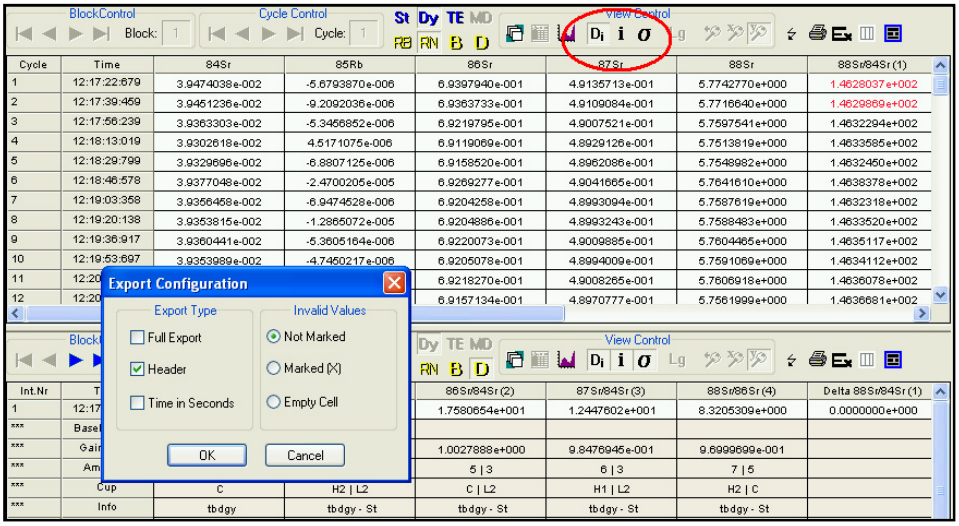

Figure VIII.1 - Data evaluation software

Coose a file on the left hand side and then klick "Ex" on the top right side. The *.dat file is then exported to a *.exp file which can be used for further data processing.

Data reduction with the EXCEL© spread sheet

Overview

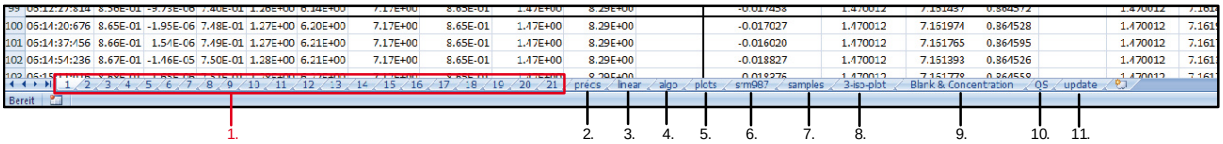

Figure VIII.2 - Worksheets within the EXCEL© spreadsheet for stable Strontium data reduction.

Here a brief overview over the worksheets (Fig. VIII.2) within the stable Strontium evaluation spread sheet is given. Detailed information to every single worksheet is given below.

1. **"1"-"21":** Here the TIMS raw data sets are imported to the EXCEL spread sheet.
2. **"précis":** Here the samples are labeled according to their properties (ic-, id-, standard, sample, blank) to ensure correct evaluation.
3. **"linear":** Here a simple linear fractionation law is used for spike correction (not relevant for users).
4. **"algo":** Here a more appropriate exponential fractionation law is used for spike correction (not relevant for users).
5. **"plots":** Here the development of the $^{88}Sr/^{84}Sr$ isotope ratio during the course of the measurement is plotted (Quality control).
6. **"SRM987":** Here the results for the standard measurements are summarized.
7. **"samples":** Here the results for the samples are summarized.
8. **"3-iso-plot":** Here the $^{88}Sr/^{84}Sr$ is plotted against the $^{86}Sr/^{84}Sr$ for each sample (Quality control).
9. **"Blank and Concentration":** Here the spike/sample ratio and the amount of Strontium in each sample is calculated (Quality control).

10. **"QS":** Here results from linear and exponential evaluation are compared. (Quality control)
11. **"update":** Here the latest updates of the spread sheet are reported.

Data import to Excel©

Worksheet "1" – "21"

This procedure starts in worksheet 1 (left hand side of the red rectangle in figure VIII.2) and is schematically displayed in figure VIII.3.

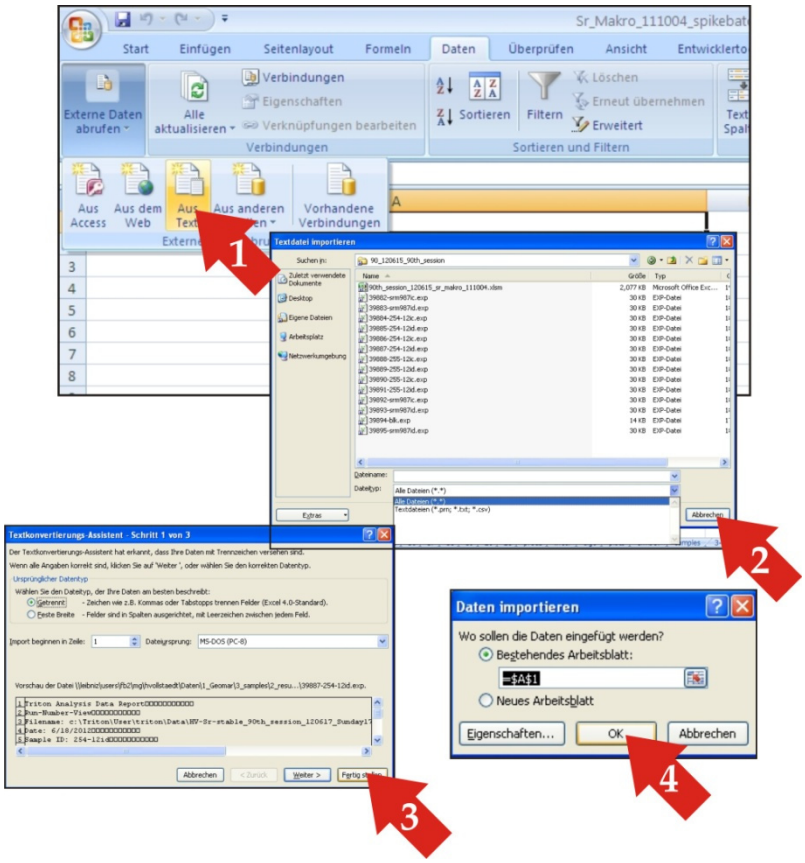

Figure VIII.3 - Data import in Excel©

Import the *.exp- files in the displayed way. This procedure has to be repeated for the 21 export-files of the analyzed samples in worksheet 1 – 21 (Fig. VIII.3). Make sure that data is imported to cell A1 of every worksheet. In worksheet 1, three free parameters are marked in green (Fig. VIII.4).

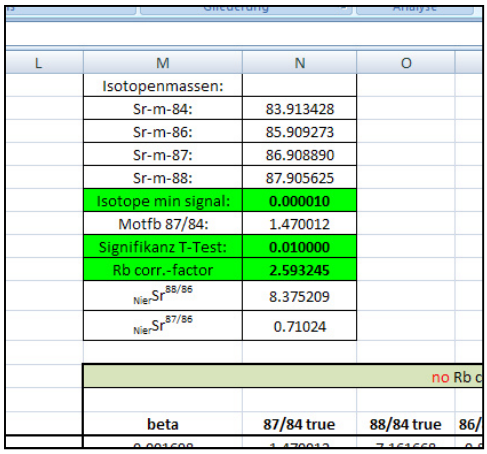

L	M	N	O
	Isotopenmassen:		
	Sr-m-84:	83.913428	
	Sr-m-86:	85.909273	
	Sr-m-87:	86.908890	
	Sr-m-88:	87.905625	
	Isotope min signal:	0.000010	
	Motfb 87/84:	1.470012	
	Signifikanz T-Test:	0.010000	
	Rb corr.-factor	2.593245	
	$_{Nier}Sr^{88/86}$	8.375209	
	$_{Nier}Sr^{87/86}$	0.71024	
			no Rb c
	beta	87/84 true	88/84 true

Figure VIII.4 - Free parameters in worksheet 1-21. The default settings turned out to be reasonable.

- **Isotope min signal:** Represents a lower limit for the output voltage of 84Sr. This value depends on the method chosen for Strontium measurement and is reasonable for maximum voltage of 10 Volts on ^{88}Sr.
- **Signifikanz T-Test:** Here the confidence level of the Rubidium measurement can be adjusted. It is testing if the signal on mass 85 is significant above zero. A value of 0.01 means a confidence level of 99%. When the signal on mass 85 turns out to be significant the ^{87}Sr value will be corrected.
- **Rb-corr. Factor:** This value represents the isotopic ratio $^{85}Rb/^{87}Sr$ and hence is not really a free parameter.

Only these parameters can be changed in worksheet 1. They are taken over to worksheet 2-21 automatically. These worksheets include the traditional radiogenic evaluation (with and without rubidium correction). Invalid values are eliminated by a two sigma test.

Worksheet "précis"

This worksheet represents a summary of the measured isotopic ratios of all analyzed samples. The columns F-H ($_{Motfb}Sr^{88/84}$, $_{Motfb}Sr^{87/84}$, $_{Motfb}Sr^{86/84}$) should be filled with numbers. If not, there might be an error occurred during data import (imported in cell A1? Just imported header + 126 measurements?).

In order to make sure that isotope values are assigned correctly to the algorithm, samples have to be labeled in the following way (Fig. VIII.5):

	SRM987	Sample 1	Sample 2	Sample x	Blank
IC measurement #1	srm-ic-1	1-ic-1	2-ic-1	x-ic-1	
IC measurement #2	srm-ic-2	1-ic-2	2-ic-2	x-ic-2	
ID measurement #1	srm-id-1	1-id-1	2-id-1	x-id-1	Blk-1
ID measurement #y	srm-id-y	1-id-y	2-id-y	x-id-y	Blk-y

Figure VIII.5 - Labelling of samples

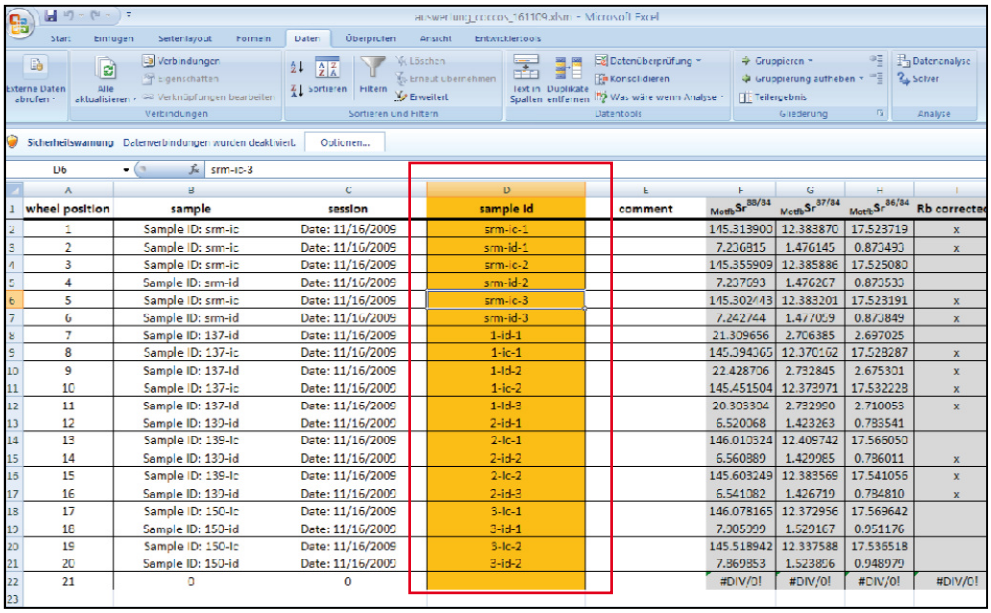

wheel position	sample	session	sample id	comment	$^{88/84}Sr$	$^{87/84}Sr$	$^{86/84}Sr$	Rb corrected
1	Sample ID: srm-ic	Date: 11/16/2009	srm-ic-1		145.313900	12.383870	17.523719	x
2	Sample ID: srm-ic	Date: 11/16/2009	srm-id-1		7.236815	1.476145	0.870490	x
3	Sample ID: srm-ic	Date: 11/16/2009	srm-ic-2		145.355909	12.385886	17.525080	
4	Sample ID: srm-id	Date: 11/16/2009	srm-id-2		7.237093	1.476207	0.870530	
5	Sample ID: srm-ic	Date: 11/16/2009	srm-ic-3		145.302443	12.383201	17.523191	x
6	Sample ID: srm-id	Date: 11/16/2009	srm-id-3		7.242744	1.477009	0.870849	x
7	Sample ID: 137-id	Date: 11/16/2009	1-id-1		21.309656	2.706385	2.697025	
8	Sample ID: 137-ic	Date: 11/16/2009	1-ic-1		145.094065	12.370102	17.529287	x
9	Sample ID: 137-id	Date: 11/16/2009	1-id-2		22.428706	2.732845	2.675301	x
10	Sample ID: 137-ic	Date: 11/16/2009	1-ic-2		145.451504	12.373971	17.532228	x
11	Sample ID: 137-id	Date: 11/16/2009	1-id-3		20.303304	2.732960	2.710053	x
12	Sample ID: 139-id	Date: 11/16/2009	2-id-1		6.520068	1.423263	0.783541	
13	Sample ID: 139-ic	Date: 11/16/2009	2-ic-1		146.010324	12.409742	17.566050	
14	Sample ID: 139-id	Date: 11/16/2009	2-id-2		6.560889	1.429965	0.786011	x
15	Sample ID: 139-ic	Date: 11/16/2009	2-ic-2		145.603249	12.383569	17.541055	x
16	Sample ID: 139-id	Date: 11/16/2009	2-id-3		6.541082	1.426719	0.784810	x
17	Sample ID: 150-ic	Date: 11/16/2009	3-ic-1		146.078165	12.372956	17.569642	
18	Sample ID: 150-id	Date: 11/16/2009	3-id-1		7.305099	1.529167	0.951176	
19	Sample ID: 150-ic	Date: 11/16/2009	3-ic-2		145.518942	12.337588	17.536518	
20	Sample ID: 150-id	Date: 11/16/2009	3-id-2		7.869853	1.523856	0.948979	
21	0	0			#DIV/0!	#DIV/0!	#DIV/0!	#DIV/0!

Figure VIII.6 - Labelling of samples in "précis" worksheet.

Data evaluation

After all turret positions are imported and labelled a summary of isotope ratios are given in the worksheets "srm987" (for standard) and "samples" (for all sample measurements". Here the mean values of all measured samples are given with their corresponding errors.

Standard measurement

A summary of isotope ratios of the standard SRM987 is given in the worksheet "srm987". Please note that all ratios are not normalized (mean $\delta^{88/86}Sr_{SRM987}$ is NOT zero). Every measurement of the standard should be recorded in a srm987 long term table, located at \\leibniz\users\FB2\MG\akolevica\QS-Sr-stabil\Langzeit-Standards.

Sample measurement

A summary of isotope ratios of the samples is given in the worksheet "samples". All isotope ratios are corrected for SRM987 offset to $^{88}Sr/^{86}Sr$ = 8.375209 and $^{87}Sr/^{86}Sr$ = 0.710240. SRM987 offsets are found in columns R+S. All important isotope ratios ($\delta^{88/86}Sr$, $^{87}Sr/^{86}Sr_{corr}$, $^{87}Sr/^{86}Sr_{norm\text{-}corr}$ and $^{87}Sr/^{86}Sr^{*}_{corr}$) are marked with red color in the labeling.

Blank measurement

If a blank measurement was performed the $^{88}Sr/^{84}Sr_{corr}$ and $^{86}Sr/^{84}Sr_{corr}$ ratios are shown in worksheet "Blank & Concentration" in the cells G3 and G4, respectively (Fig. VIII.7). If cell I3 is filled with the net weight of spiked added to the blank (µl spike = mg), the amount of spike is calculated in J3 and K3.

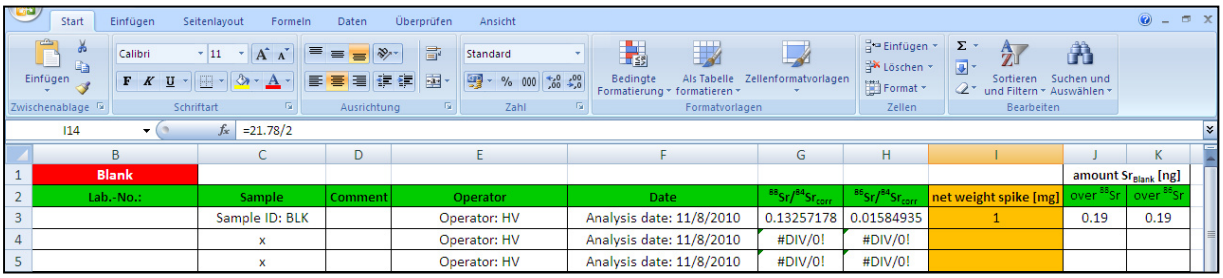

	B	C	D	E	F	G	H	I	J	K
1	Blank								amount Sr_{Blank} [ng]	
2	Lab.-No.:	Sample	Comment	Operator	Date	$^{88}Sr/^{84}Sr_{corr}$	$^{86}Sr/^{84}Sr_{corr}$	net weight spike [mg]	over ^{88}Sr	over ^{86}Sr
3		Sample ID: BLK		Operator: HV	Analysis date: 11/8/2010	0.13257178	0.01584935	1	0.19	0.19
4		x		Operator: HV	Analysis date: 11/8/2010	#DIV/0!	#DIV/0!			
5		x		Operator: HV	Analysis date: 11/8/2010	#DIV/0!	#DIV/0!			

Figure VIII.7 - Calculation of blank amount in worksheet "Blank & Concentration"

Error detection "cook book"

If a sample shows strange isotopic composition (Attention: some natural samples CAN have "strange" isotopic composition without there is a problem with the measurement) you have to check for indications of a bad measurement run. Therefore we give a "receipt" to find eventual errors that may occurred during measurement or sample preparation. When there is a value you wouldn't expect you have to search for the error that may occurred:

a) Check the plots of the single samples in the worksheet "plots". Ideally, the signal should show a continuous increase. If $^{88}Sr/^{84}Sr$ ratios show large variations during different measurement blocks it might be useful to delete some measurement blocks in the corresponding worksheet of the sample ("1" – "21").

b) Check if signal intensity on ^{88}Sr is stable and high enough (should be above 3 V when method intensity aim was 10 V) in worksheets "1" – "21". If signal intensity is

considerable low and produces exceptional isotope ratios (possibly due to consumed sample on the filament) these measurement blocks should be deleted.

c) In the worksheet "3-iso-plot" a $^{86}Sr/^{84}Sr$ vs. $^{88}Sr/^{84}Sr$ for all single IC- and ID-measurements are shown. All IC measurements should fall onto a linear mass fractionation line (more precisely it is an exponential curve, but the extract on the diagram is nearly linear). If deviations from this line are observed, a contamination is likely. In similarity, ID measurements should fall onto a linear line, although they are more separated due to different spike/sample ratios. If a sample is contaminated delete the label on "précis" worksheet.

d) Check $^{87}Sr/^{86}Sr$ values of the IC runs of the sample in "précis" worksheet column "T". Compare these values to excepted values (i.e. $^{87}Sr/^{86}Sr$ = 0.709175 for recent marine carbonates or seawater samples or ~0.704 for basalts). If one of the IC runs show unexceptional values you might delete this measurement in worksheet "précis" by deleting the corresponding label.

e) Look for ^{84}Sr Spike/Sample ratios on worksheet "Blank & Concentration". Fill in the amount of spike added to the ID part of the sample (mg spike = µl spike). Aimed ratio is 20. However samples should fall within a reasonable range of 10-50.

f) In the worksheet "QS" you'll find a plot, showing the difference of $^{88}Sr/^{86}Sr$ ID-ratios calculated from exponential law and linear law (y-axis), respectively. They are plotted against absolute IC $^{88}Sr/^{86}Sr$ from calculated exponential law (x-axis; this gives the "location of fractionation"). Furthermore an empirical function is plotted within the diagram (derived from evaluation of ~200 measurements). If huge deviations from empirical function are observed, mass fractionation during measurement was NOT exponential. Therefore calculated $^{88}Sr/^{86}Sr$ might not be accurate.

Information for the interested user

a. Worksheet "linear"

In this worksheet the spike correction algorithm uses a linear fractionation law. This is valuable when the sample is not fractionated to a large extend during TIMS measurement.

b. Worksheet "algo"

Here the exponential law is used for the spike correction algorithm. When the isotopic composition of one sample seems strange or is far away from reasonable values you can check in the "algo"-sheet whether an ic- or id- measurement has gone wrong. If some values show an indication for bad measurement or contamination the mark of this sample in "précis" has to be deleted (see worksheet "précis"). The result of this single measurement is then not taken into account for further proceedings.

c. Worksheet "SRM987"

Here a compilation of all measures NIST SRM987 standards in your session is given. The results given here are not session offset corrected in order to monitor long term machine drifts.

d. Worksheet "samples"

Here the results of all measured samples are summarized.

e. Worksheet "Blank and Concentration"

In this worksheet the amount of Sr in your sample is calculated. Therefore the amount of spike [mg] per filament has to be written in column "I". Then the Sr amount is calculated through the $^{88}Sr/^{84}Sr$ and the $^{86}Sr/^{84}Sr$ ratio in column "K" and "L". These two calculations should result in approximately the same values. Additionally the $^{84}Sr_{spike}/^{84}Sr_{sample}$ ratio is calculated which should be around 20.

f. Worksheet "update"

Here the latest changes on the Sr evaluation sheet are documented.

Authors: Hauke Vollstaedt hvollstaedt@geomar.de

André Krabbenhöft Andre.Krabbenhoeft@tesa.com

VIII.4. Curriculum Vitae

Personal information

Name	Hauke Vollstaedt
Date of birth	May 27, 1984 in Oldenburg (Oldb), Germany
Nationality	German
Address	Wulfsbrook 6, 24113 Kiel, Germany
Phone	+49 431 3287114
E-Mail	hvollstaedt@geomar.de

Work experience

Gained experience during Ph.D. thesis at GEOMAR | Helmholtz Research Centre for Ocean Research Kiel

- Set-up of the strontium double spike technique
- Development of the data reduction and evaluation method for $\delta^{88/86}Sr$ analysis
- Preparation of different natural samples for isotope and element analysis (e.g. Microtome saw, MicroMill©, wet chemistry)
- Isotope analysis of non-traditional stable isotopes ($\delta^{88/86}Sr$, $\delta^{44/40}Ca$) with TIMS (both MAT 262 and TRITON)
- Element concentrations and ratios with ICP-MS
- Numerical box modeling of marine element budgets with Mathematica

Gained experience as a student research assistant at the University of Göttingen and GEOMAR | Helmholtz Research Centre for Ocean Research Kiel

- Sample preparation and analysis of $^{87}Sr/^{86}Sr$-ratios at TIMS
- Laboratory assistant at the ICP-MS laboratory
- Tutor of the course "Quantitative rock analysis with Excel"
- Managing literature database with Endnote
- Preparation of rock samples for RFA measurements

Internships alongside to my studies

07/2007 – 09/2007 IFM-GEOMAR, Kiel, Germany, Research Unit "Biogeochemical modeling"

04/2007 – 06/2007 Alfred-Wegener-Institute, Bremerhaven, Germany, Research Unit "Marine geology and Paleontology"

Achievements

Conference contributions

Session convener at the AGU Fall Meeting 2012 (Session title: Reconstructing Phanerozoic seawater chemistry using non-traditional stable isotopes)

Conference presentations at AGU 2009, GV 2010, Goldschmidt 2011 and 2012, and EGU 2011

Conference posters at Goldschmidt 2010 and AGU 2010

Education and qualification

Since 11/09	Ph.D. student at the GEOMAR | Helmholtz Centre for Ocean Research Kiel, Germany, Research Unit Marine Geosystems
10/2009	Diploma (M.Sc. equivalent) in Geology/Paleontology at Kiel University, Germany. Overall grade: Excellent with distinction
10/2007 - 10/2009	Studies in Geology/Paleontology at Kiel University, Germany
10/2006	Bachelor of Science in Geosciences at the University of Göttingen, Germany. Overall grade: Good
10/2003 – 03/2007	Studies in Geosciences at the University of Göttingen, Germany
07/2003	Abitur (university entrance qualification)

Scientific Interests

- Isotope Geochemistry (Calibration and application of isotope proxies, fractionation processes)
- Marine Biogeochemistry
- Ocean anoxia
- Marine extinction events
- Biogeochemical modelling

Publications

Articles in international journals

Vollstaedt, H., Eisenhauer, A., Böhm, F., Fietzke, J., Wallmann, K., Liebetrau, V., Krabbenhöft, A., Farkaš, J., Tomašových, A., and Veizer, J., Under review. *Linking marine carbonate burial and long-term anoxia to the end-Permian mass extinctions* Geology.

Raddatz, J., Liebetrau, V., Rüggeberg, A., Hathorne, E., Krabbenhöft, A., Eisenhauer, A., Böhm, F., Vollstaedt, H., Fietzke, J., López Correa, M., Freiwald, A., and Dullo, W.-Chr., Under review. *Environmental influences on the stable Sr-isotope, Sr/Ca, Mg/Ca, Li/Ca and Mg/Li ratios in scleractinian cold-water corals Lophelia pertusa* Earth and Planetary Science Letters.

Krabbenhöft, A., Eisenhauer, A., Böhm, F., **Vollstaedt, H.**, Fietzke, J., Liebetrau, V., Augustin, N., Peucker-Ehrenbrink, B., Müller, M., Horn, C., Hansen, B. T., Nolte, N. and Wallmann, K. (2010) *Constraining the marine strontium budget with natural strontium isotope fractionations ($^{87}Sr/^{86}Sr^*$, $\delta^{88/86}Sr$) of carbonates, hydrothermal solutions and river waters* Geochimica et Cosmochimica Acta, 74 (14). pp. 4097-4109. DOI 10.1016/j.gca.2010.04.009.

Krabbenhöft, A., Fietzke, J., Eisenhauer, A., Liebetrau, V., Böhm, F. and **Vollstaedt, H**. (2009) *Determination of radiogenic and stable strontium isotope ratios ($^{87}Sr/^{86}Sr$; $\delta^{88/86}Sr$) by thermal ionization mass spectrometry applying an $^{87}Sr/^{84}Sr$ double spike* Journal of Analytical Atomic Spectrometry, 24 (9). pp. 1267-1271. DOI 10.1039/b906292k.

Diploma thesis

Vollstaedt, H. (2009) *The Phanerozoic $\delta^{88/86}Sr$ record of marine carbonates*, Christian-Albrechts-Universität, Kiel, 41 pp

Conference contributions – oral presentations

Vollstaedt, H., Eisenhauer, A., Böhm, Fietzke, J., Wallmann, K., F. Krabbenhöft, A., Liebetrau, V., Farkaš, J., Tomašových, A. and Véizer, J. (2012) *Marine carbonate burial rates at the Phanerozoic mass extinctions* In: Goldschmidt Conference 2012, 25.-29-06.2012, Montréal, Canada

Vollstaedt, H., Eisenhauer, A., Krabbenhöft, A., Liebetrau, V., Böhm, F., Farkaš, J., Tomašových, A. and Véizer, J. (2011) *The Paleozoic $\delta^{88/86}Sr$ record of marine carbonates – Implications to ocean carbonate chemistry and mass extinction events* In: EGU General Assembly 2011, 03.-08.04.2011, Vienna, Austria.

Vollstaedt, H., Eisenhauer, A., Böhm, F., Fietzke, J., Krabbenhöft, A., Liebetrau, V., Farkaš, J. and Véizer, J. (2011) *The Paleozoic $\delta^{88/86}Sr_{seawater}$ record – Quantifying carbonate production rates at mass extinction events* In: Goldschmidt Conference 2011, 14.-19.08.2011, Prague, Czech Republic.

Eisenhauer, A., Böhm, F., **Vollstaedt, H.**, Liebetrau, V., Fietzke, J., Kisakurek, B. and Erez, J. (2011) *Strontium isotope fractionation and its application in Earth system sciences* In: Goldschmidt Conference 2011, 14.-19.08.2011, Prague, Czech Republic.

Vollstaedt, H., Eisenhauer, A., Krabbenhöft, A., Böhm, F., Liebetrau, V., Farkas, J. and Veizer, J. (2009) *The Phanerozoic $\delta^{88/86}Sr$ record of marine carbonates - A new dimension for the Sr isotope system* In: Jahrestagung der Geologischen Vereinigung, 05.-07.10.2009, Göttingen.

Krabbenhöft, A., Eisenhauer, A., **Vollstaedt, H.**, Augustin, N., Fietzke, J., Liebetrau, V. and Peucker-Ehrenbrink, B. (2009) *The marine strontium budget derived from paired ($^{87}Sr/^{86}Sr^*$-$\delta^{88/86}Sr$) values of marine carbonates, hydrothermal fluids and river waters* In: 99th Annual Meeting of the Geologische Vereinigung (GV), 05.10.-07.10.2009, Göttingen.

Vollstaedt, H., Eisenhauer, A., Krabbenhöft, A., Böhm, F., Liebetrau, V., Farkas, J. and Veizer, J. (2009) *A new dimension to the Sr isotope system - $\delta^{88/86}Sr$ record of marine carbonates in the Phanerozoic* In: AGU Fall Meeting 2009, 14.-18.12.2009, San Francisco, USA.

Eisenhauer, A., Krabbenhöft, A., Böhm, F., Liebetrau, V., Fietzke, J., Augustin, N., Peucker-Ehrenbrink, B. and **Vollstaedt, H.** (2009) *Strontium isotope fractionation in the marine realm: first application for a $^{87}Sr/^{84}Sr$-double-spike* In: EGU General Assembly, 20.04.-24.04.2009, Vienna, Austria.

Conference contributions – poster presentations

Vollstaedt, H., Eisenhauer, A., Krabbenhöft, A., Liebetrau, V., Böhm, F., Farkaš, J., Tomašových, A. and Véizer, J. (2010) *Revisiting mid-Paleozoic ocean chemistry with the combined measurement of $^{87}Sr/^{86}Sr$ and $\delta^{88/86}Sr$ on Silurian brachiopods* In: AGU Fall Meeting 2010, 13.-17.12.2010, San Francisco, USA.

Vollstaedt, H., Eisenhauer, A., Krabbenhöft, A., Farkas, J. and Veizer, J. (2009) *$\delta^{88/86}Sr$ Record of Phanerozoic Marine Carbonates* In: Goldschmidt Conference 2009, 21.-26.06.2009, Davos, Switzerland.

Krabbenhöft, A., Eisenhauer, A., **Vollstaedt, H.**, Augustin, N., Fietzke, J., Liebetrau, V. and Peucker-Ehrenbrink, B. (2009) *Ocean Sr-budget from paired $\delta^{88/86}Sr$ and $^{87}Sr/^{88}Sr^*$-ratios* In: Goldschmidt Conference 2009, 21.06.-26.06.2009, Davos, Switzerland.

Krabbenhöft, A., Eisenhauer, A., **Vollstaedt, H.**, Augustin, N., Fietzke, J., Liebetrau, V. and Peucker-Ehrenbrink, B. (2009) *Determination of $^{87}Sr/^{86}Sr^*$-$\delta^{88/86}Sr$ values of the oceans Sr sources and sinks to balance the global Sr cycle* In: AGU Fall Meeting, 14.12.-18.12.2009, San Francisco, California, USA.